Petrogenesis and thermal history of the Kunlun Batholith, Northern Tibet

Thesis

Petrogenesis and Thermal History of the Kunlun Batholith, Northern Tibet.

A thesis submitted for the degree of Doctor of Philosophy

by

Cherry Louise Eiluned Lewis B.Sc.

Department of Earth Sciences

The Open University

December, 1988

Author's number : M 7023150

Date of submission : December 1988

Date of award : 20 March 1989

To my parents,

Irene and Wyn;

for my children,

Daniel and Leon.

"..... ever since the dawn of civilization, people have not been content to see events as unconnected and inexplicable. They have craved an understanding of the underlying order in the world. Today we still yearn to know why we are here and where we came from. Humanity's deepest desire for knowledge is justification enough for our continuing quest. And our goal is nothing less than a complete description of the universe we live in."

Stephen Hawking, 1988.

HIGHER DEGREES OFFICE

LIBRARY AUTHORISATION FORM

STUDENT: CHERRY LEWIS SERIAL NO: MT023150

DEGREE: PhD

TITLE OF THESIS: Petrogenesis and thermal history of the Kunlun Batholith, S. Tibet

I confirm that I am willing that my thesis be made available to readers and maybe photocopied, subject to the discretion of the Librarian.

SIGNED: Cherry Lewis DATE: 9 - 5 - 88

ABSTRACT

The Kunlun Terrane is the most northerly of the several microplates that comprise the Tibetan Plateau. Geochronological data from the Kunlun batholith defines three distinct periods of intrusion at 390 Ma, 250 Ma and 190 Ma.

A model is presented whereby the Devonian intrusions are considered to be related to a collision event between the Kunlun and Tarim Terranes, which were part of Gondwanaland and situated in the southern hemisphere at this time. It is proposed that in the region of the 1985 Tibet Geotraverse route, the Golmud Fault represents the Kunlun-Qinling suture line along which the two plates collided. Break-up of this part of Gondwanaland, which proabably also included the Qiangtang, Lhasa and Indian plates, occurred during the Permian along the Zangbo and Jinsha suture lines. Continental rifting was followed by a prolonged period of northward subduction of the Qiangtang Terrane beneath the Kunlun Terrane. This resulted in formation of the Permian batholith, and the massive Songban-Ganzi accretionary prism. Subduction culminated in collision at about 200 Ma. Post tectonic granites were emplaced around 190 Ma.

Initial Sr ratios for the granitoids range from .7074 to .7130, and support the geochemical modelling which suggests that they have been derived from melting mid-crustal sources. Only the Devonian Wanbaogou pluton may have resulted from anatexis of upper crustal sediments.

A reset biotite age of 120 Ma from a pluton cut by the Xidatan Fault, supports sedimentalogical evidence which indicates a major reactivation of thrust faults in the area, as a result of collision between the Lhasa and Qiangtang Terranes during the Cretaceous. Apatite fission track ages from plutons north of the Golmud Fault also document this uplift event. A 100 Ma period of quiescence ensued, during which the Kunlun Terrane cooled extremely slowly until a state of thermal equilibration was reached.

The collision of India with Tibet at 45 Ma thickened the Tibetan crust and resulted in further reactivation of faults in the Kunlun Terrane. Apatites from the granites between the Golmud and Xidatan faults give mixed ages around 20 Ma. It is calculated that uplift in this region, as a result of the Himalayan collision, could have been as recent as 8 Ma.

ACKNOWLEDGEMENTS

If gratitude could be measured on the geological time scale, then what I owe my parents would stretch beyond the age of the dinosaurs and survive the Permian extinctions, only to disappear down the black hole of the Archaean still feeling inadequate. Without them, this thesis would not have been written and some of the mysteries of Tibet would have remained unsolved. I can but say thank you.

I must also take this opportunity to thank everyone who has assisted and encouraged me along the way, particularly Liz Loeffler who first suggested I should do a geology degree, and Doug Robinson who was brave enough to take me on as an undergraduate at Bristol University. Brian Williams who never failed to stimulate an interest in the subject, and Reg Bradshaw who managed to hide his surprise when I passed! My supervisors at the Open University, Nigel Harris and Chris Hawkesworth, have been great fun to work with, and I have very much appreciated being able to go my own way, while being skilfully guided around the pit-holes. In particular I must thank Chris for setting up the project, and Nigel for collecting the rocks and taking the field photographs.

In September 1986 I was very privileged to be able to join the Tibet Geotraverse team at a conference in Beijing, and to be part of the follow-up geotraverse across the Himalayas. This was organised by Robert Shackleton, to whom I am extremely grateful for enabling me to be included, and it was financed by the Royal Society. The Royal Society also partly funded my grant and fully supported my work in Switzerland. I very much appreciate having had those opportunities.

In 1987 I spent three months working with Tony Hurford at Berne University in Switzerland, learning the joys of fission track counting. Special thanks must go to him for being so patient and helpful during that time. There were not really enough hours in the day to get everything done, but somehow we managed. I am very grateful to Emilie Jäger for giving me full use of the facilities there, and to the 'boys in the lab' for their help and advice, especially Marcus Fleisch.

I am particularly grateful to Mark Harrison and Pete Copeland at Albany, New York, for the Ar-Ar data obtained from two of the Kunlun granites. These ages were invaluable in helping to asses the thermal history of the Kunlun Terrane, I only wish there had been time to do more.

Mention must also be made of everyone in the labs at the Open University who keep machinery operative and who see to it that life runs smoothly - Mabs Kunka, Peter Van Calsteren, Nick Rogers, Ian Chaplin and John Watson, to name but a few. Thanks must also go to Stuart Boyd who helped me over innumerable hurdles encountered in 'Word 3', and to Frank Mc Dermott for many a 'granite' discussion. Fiona Mc Gibbon gave me much moral support during the last few trying weeks, and Chris MacLeod kept life in the 'Mac Room' worth living.

Finally I must thank, with all my love, my long-suffering children whom I hope will one day understand why I had to do it.

CONTENTS

List of Figures

List of Tables

List of Plates

CHAPTER ONE

1. INTRODUCTION

"We left England on November 10, 1894, the same party as usual: - Mrs. Littledale, myself, and our dog, accompanied in addition by my nephew, Mr. W. A. L. Fletcher, of Oxford boating renown, who proved himself to be in every respect an admirable travelling companion. My scheme was to strain every nerve to reach Tibet, and, if possible, Lhasa, with plenty of food and animals to carry it. Most of the other expeditions had failed owing to their arriving in a more or less destitute condition, and then, of course, the Tibetans could dictate their own terms. We also relied upon bribery, and went well prepared with the sinews of war for wholesale corruption"

St. George R. Littledale, 1896

1.1 THE ROYAL SOCIETY GEOTRAVERSE

In 1985, almost a century after Mr. Littledale's expedition, a joint Royal Society and Academia Sinica team completed a geotraverse across the Tibetan Plateau from Lhasa in the south, to Golmud in the north, a distance of some 1200 km. At an average elevation of 5000 meters, the Tibetan Plateau is the highest in the world. To the south it is bounded by the Himalayas and India, whilst the northern limit is defined by the Kunlun Shan, a range of mountains that extends from Afghanistan in the west, over 2000km to the east (Fig. 1.1). The objectives of the Geotraverse team were four-fold:

1. To establish the number of microplates Tibet is comprised of and identify the sutures.
2. To discover the provenance of the plates.
3. To constrain the chronology of tectonic events.
4. To investigate how the Tibetan crust was thickened and when it was uplifted.

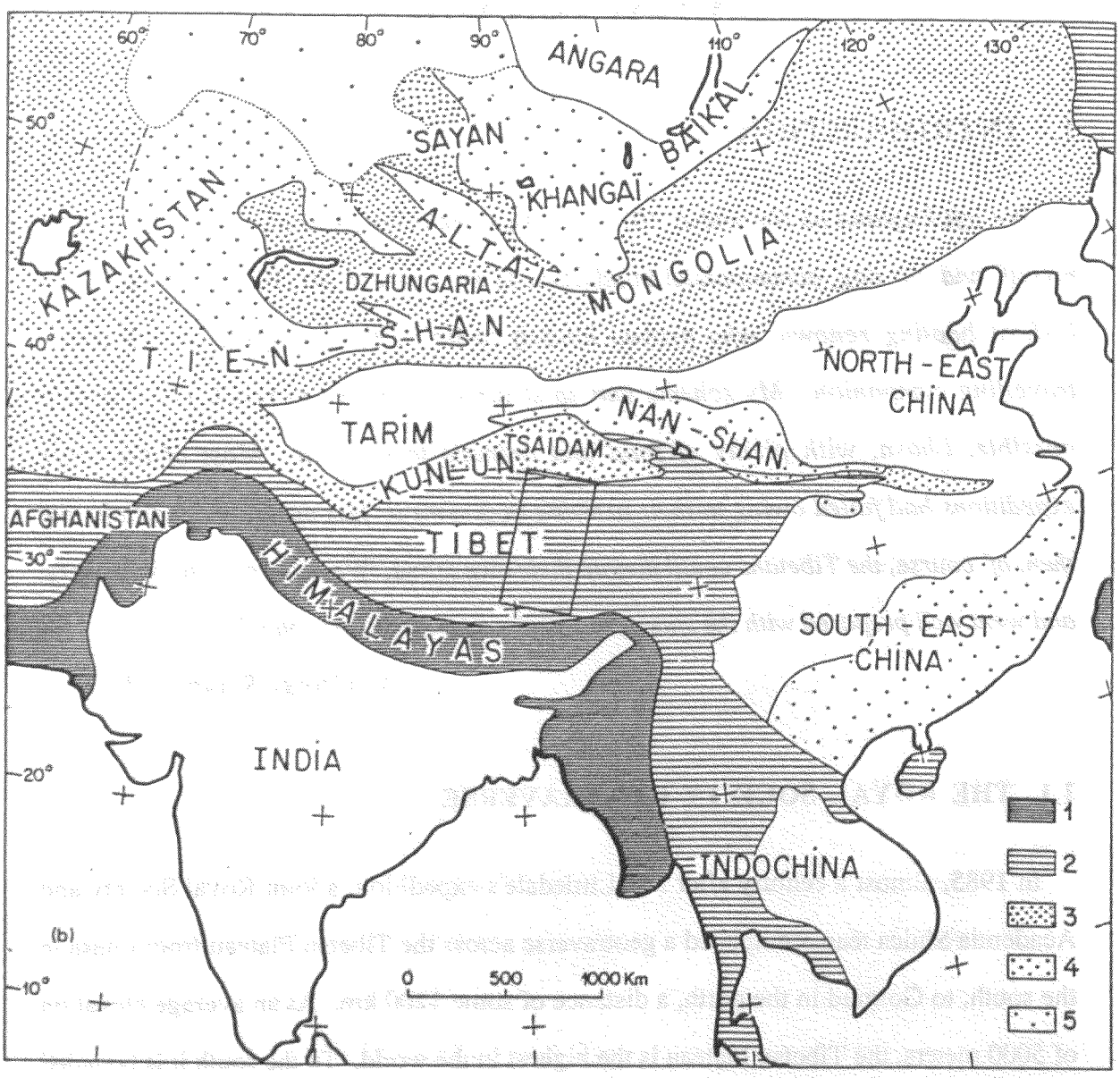

Fig. 1.1 Generalised map of Asia. Boxed area represents region of the 1985 Tibet Geotraverse. 1 = regions with orogenic activity in the Cenozoic due to the Himalayan collision; 2 = regions active in the Mesozoic before the Himalayan collision; 3 = late Palaeozoic; 4 = early Palaeozoic; 5 = presumed Palaeozoic; white areas = Precambrian shields. Redrawn after Molnar amd Tapponnier (1981).

To date, their data show that the plateau is comprised of three or four microplates (Fig. 1.2) believed to have been successively accreted to the southern margin of the Eurasian continent since the Devonian. Although the identification of these plates and positioning of the sutures was a major priority for the Geotraverse team, it proved very difficult in the field to locate them and so the matter remains controversial. The original

interpretation by Chinese geologists (Chang and Zheng 1973; Chang and Pan 1981 and 1984) recognised four plates and four sutures which, from north to south, are termed as follows:

	Terrane	Suture
1	**Kunlun Terrane**	Kunlun - Qinling Suture
2	**Songban - Ganzi Terrane**	Jinsha Suture
3	**Qiangtang Terrane**	Banggong Suture
4	**Lhasa Terrane**	Zangbo Suture

However, on the Geotraverse route no evidence of the Kunlun-Qinling Suture could be seen. There appeared to be both lithological and structural continuity across this zone (Chang *et al.*, 1986), so the area north of the Jinsha suture was subsequently considered as a single tectonic unit, the Kunlun Terrane. But a later interpretation (Dewey *et al.*, 1988) placed considerable significance on the re-instatement of the Kunlun-Qinling Suture and explains how it is obscured in the Geotraverse region by the Xidatan fault (Fig. 1.2). Similarly, the position of the Jinsha Suture is also poorly defined. Believed to have closed during the Triassic it is now overlain in the Geotraverse region by Tertiary red-beds, and the one reported ophiolite outcrop was not reached by the Geotraverse team. However, subsequent mapping by a team of Cambridge undergraduates showed that the ophiolite occurs as numerous angular masses embedded in Triassic sandstones, probably in a mélange. This evidence, coupled with the presence of ophiolite outcrops 200 km both to the east and west of the Geotraverse, and the fact that when Triassic rocks do emerge from beneath the Tertiary cover they are very different north and south of the supposed suture zone, is why it is placed in its current position.

The two southerly sutures are however, much more clearly defined, despite isolated outcrops of thrust bounded ophiolites associated with the Banggong suture being

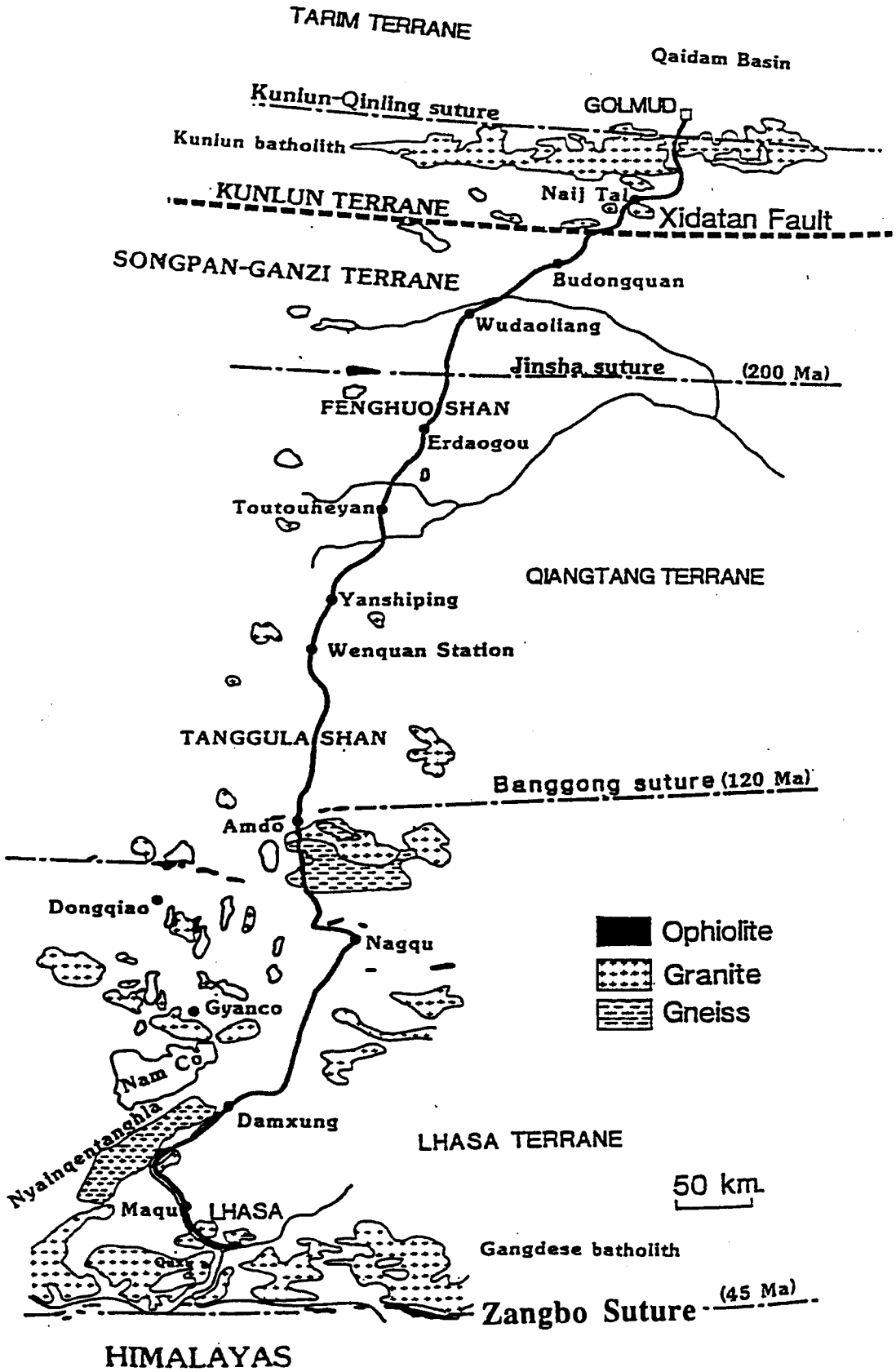

Fig. 1.2 1985 Tibet Geotraverse route from Lhasa to Golmud.

distributed over a 180 km region of the northern half of the Lhasa Terrane . These are now believed to be part of a single disrupted nappe which was obducted at least 180 km from the suture (Girardeau *et al.*, 1984). The Banggong suture is believed to have closed at about 120 Ma whilst collision of the Indian plate with Tibet along the Zangbo suture occurred during the Eocene at about 45 Ma. The interpretation of magnetic anomalies in the Indian ocean show that prior to collision, India was moving northwards at about 10 cm/yr, and even after collision the Indian continent continued to push into Asia at a rate of 4 - 5 cm/yr (Molnar and Tapponnier, 1975; and Mattauer, 1986).

1.2 THESIS OBJECTIVES

This thesis is concerned with the Kunlun Terrane and, primarily, the Kunlun batholith which comprises a large portion of the Kunlun Shan mountains. Despite the huge scale of the batholith and its obvious significance in understanding the evolution of the Tibetan Plateau, a comprehensive study of the rock types had not previously been undertaken. This was due mainly to its physical inaccessibility but also to its political isolation. In 1950 the Chinese invaded Tibet and since then it has been ruled by China as the provinces of Xizang and Qinghai which lie, respectively, to the south and north of the Tanggula Shan (Fig. 1.2). The Xizang-Qinghai plateau has only recently opened up to Westerners and, in the 1980s, co-operation between Chinese and foreign working teams such as those from the Royal Society, have greatly enhanced our understanding of the region, particularly in the more accessible south. At the time of writing (1988) however, there are no continuing scientific studies on the plateau involving groups other than Chinese.

It must be clearly stated that the author of this thesis has not been to the Kunlun Terrane and that samples were collected by my supervisor Dr. Nigel Harris who was a member of the Geotraverse team; the nature of the expedition and the limited time available - two months for the whole 1200 km - did not allow for extensive mapping or large scale sample collecting. Nevertheless, granitoid samples collected from the Kunlun batholith have provided a valuable insight into the evolution of northern Tibet and how it

relates to the region as a whole. Preliminary results of this study were presented by the author at the Beijing conference in 1986, and this was followed by a traverse from Lhasa to Kodai on the Nepalese border, but work done on this traverse will not be presented here. The objectives of this thesis were as follows:

1 To date the age of the Kunlun batholith using Rb-Sr whole-rock and mica techniques.

2 To constrain the timing of collision and establish whether the colliding plate lay to the north or south of the Kunlun Terrane.

3 To evaluate the tectonic environment in which the batholith was emplaced from its geochemical and isotopic signatures.

4 To propose a tectonic model for the evolution of the Kunlun terrane and its relationship to the rest of the Tibetan microplates.

During the course of this work however, a fifth objective presented itself which was to investigate the thermal history of the region and to establish if it was related to the uplift of the Tibetan plateau and the Himalayan collision. To help understand this, three months were spent at Berne University in Switzerland with Dr.Tony Hurford, learning the techniques of fission track dating. The results of this work will be presented in Chapter Four.

1.3 GEOLOGICAL BACKGROUND

Most of the information contained in this section has been extracted from draft versions of chapters for the Tibet Geotraverse volume of the Philsophical Transactions of the Royal Society, London (1988), and compiled here to present a composite picture of geological events in the Kunlun Terrane. In many instances there is confusion over formation/location/fault names etc. or they may not have been named at all and are only referenced by a locality number. This makes for difficult reading and leads to

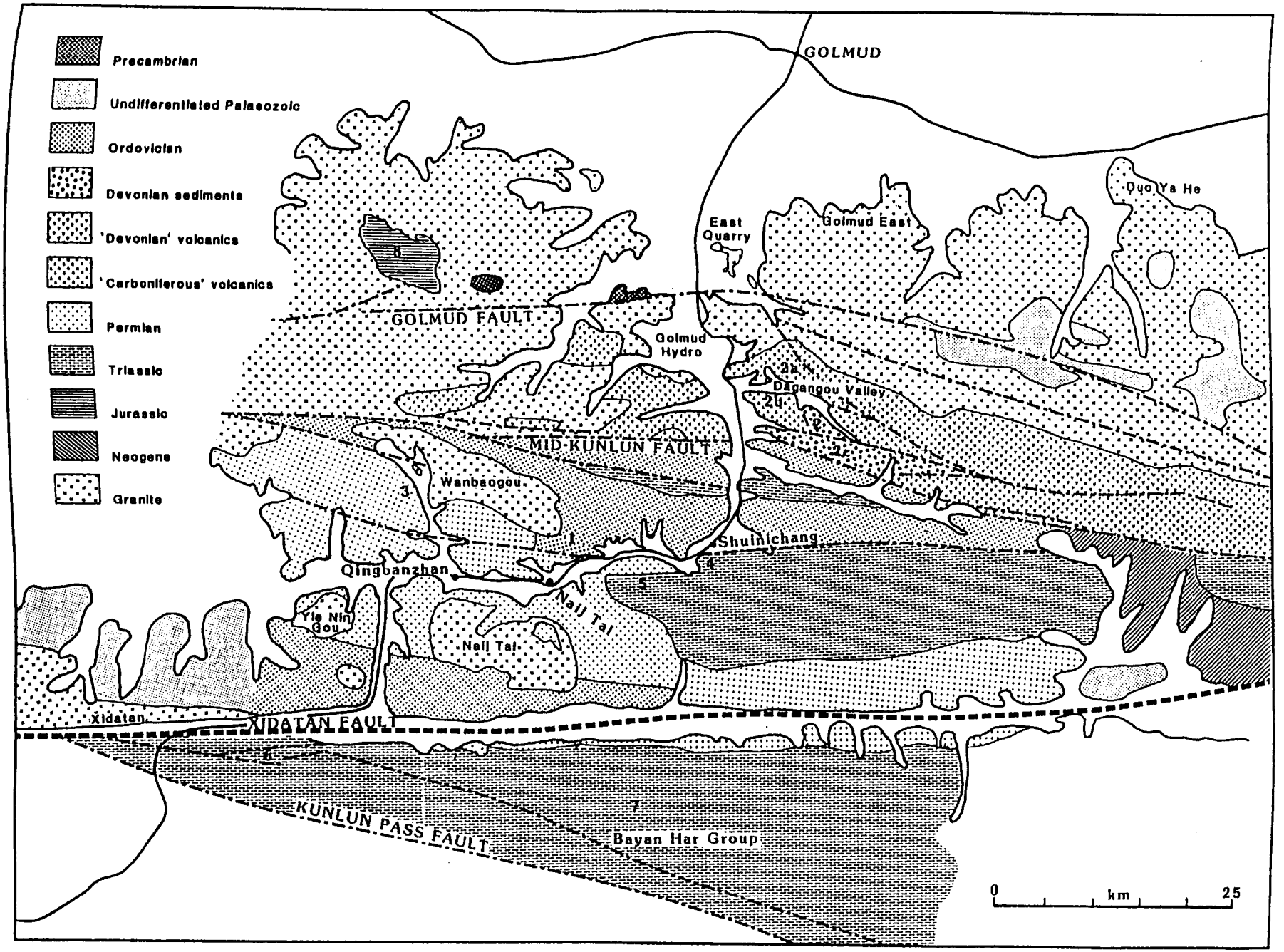

Fig. 1.3 Simplified geological map of the Kunlun Shan north of the Xidatan Fault. Numbers refer to localities mentioned in the text.

misunderstandings, therefore I have tried to be consistent by using either the same terminology as Dewey *et al.*, (1988) for names already in common use, but I have sometimes had to invent my own where none appear to exist.

1.4 STRATIGRAPHY

1.4.1 Ordovician

The oldest dated sediments in the Kunlun terrane are a thick low-grade metamorphic sequence of Ordovician clastics and carbonates (Leeder *et al.*, 1988) - the Naij Tal Group - the best exposures of which were seen just to the north and east of Naij Tal (Fig. 1.3, locality 1). From the presence of a specific trilobite, these beds are dated as early Ordovician at about 500 Ma. Interbedded graphite and quartz schists contain several limestone beds, one of which is oolitic, suggesting a platform margin origin for these facies. Above these lie quartz mica schists containing several major matrix supported conglomerates up to 60 m thick. The coarse clasts which are highly strained and reach 30 cm in diameter are predominatly white limestone and quartz, with subsidiary green and purple sandy phyllites. These horizons suggest debris flow deposits formed around a platform slope.

There then follows a thick succession of poorly bedded, pale green mica schists that grade upwards into a well bedded sequence of dark grey quartz wackes and slates. Due to the considerable tectonic over-printing in this region, much of the primary sedimentary features and fossil content have been destroyed, but this sequence is interpreted as probably of turbiditic origin. The upper-most beds in the succession are thick-bedded fossiliferous micritic limestones of Upper Ordovician age (440 Ma) belonging to the distal portion of a carbonate ramp. A very similar sequence is seen between Xidatan and Wanbaogou, to the south west of Naij Tal, and although no fauna were found with which to determine the age of this succession, it is presumed to correlate with that to the east of Naij Tal. These limestones and shales show tight to isoclinal folding with axial surfaces

dipping steeply to the south. A pronounced cleavage and mineral lineations also dip steeply to the south.

1.4.2 Late Devonian - Carboniferous

In the Dagangou Valley, two volcanic sequences are exposed and termed the Dagangou Volcanics. In the north of the valley (Fig. 1.3, locality 2a) a sequence originally designated by Chinese workers as being Devonian, shows distinct calc-alkaline lavas typical of an active continental margin setting. This then evolves into a high-K shoshonitic spectrum characteristic of a change from subduction to collision environments (Pearce and Mei, 1988). Although there appears to be some confusion, the general consensus expressed by the Geotraverse team at the Beijing conference was that this sequence did stratigraphically underlie, rather than was faulted under, a thick basal sequence of conglomerates of the Dagangou Formation. If this is the case then these volcanics are probably late Devonian to early Carboniferous. In the south of the valley another outcrop of volcanics (Fig. 1.3, locality 2b), hitherto regarded as Carboniferous since they appear to overlie the volcanics to the north, was only seen with faulted contacts by the Geotraverse team. Since the geochemistry of this unit is very similar to that of the lower unit in the volcanics to the north, it is postulated that they may well be a tectonic repetition of the same unit.

In the region of Dagangou, direct field evidence indicates that more than 1500 m of Late Devonian to Early Carboniferous sediments - the Dagangou Formation - are present in the Kunlun Terrane (Fig. 1.3, locality 2). Above the thick basal conglomerate, the sequence coarsens upwards from siltstones and sandstones through to pebbly sandstones, all with a distinctive red colouration. In the lower half, above the thick basal conglomerate, fine grained lithologies predominate and palaeocurrents indicate a north easterly transport direction, the sediment probably being deposited on low gradient alluvial cones by sheet floods. Overlying these, thick sandstones and pebbly sandstones with clasts of basic volcanics, feldspars, marbles and quartz have well developed trough

cross beds of fluviatile origins. Sandstone bodies are separated by up to 13 m of red mudrocks which contain thin calcrete horizons indicating short periods of aerial exposure.

As the system matures, palaeocurrents at first variable later indicate a dispersal system from the south west and clasts are then predominantly quartz pebbles. The upper-most red muds are succeeded by a sequence which rapidly coarsens upwards into a grain-supported, imbricated quartz conglomerate. The well-to-sub-rounded clasts up to 10 cm long clearly represent a major reworking event, probably in a marine shore environment. This is further supported by the overlying 26 m of grey mudrocks and limestones which contain a wide range of shallow water marine faunas. A distinctive shaley coal then appears in the sequence followed by 200 m of cyclically alternating marine limestone, coals and clastics remarkably similar to the 'Yoredale Cycles' that dominated the British and North American continental margin succession of Laurasia during the Lower Carboniferous. The fauna is Late Visean to Early Namurian in age (c 350 - 330 Ma).

This red-bed sequence is interpreted by Leeder *et al.* (1988), as a molassic phase, derived from an unroofing orogenic belt to the north. A major marine transgression, probably of eustatic origin that occurred during the Dinantian, was accompanied by a radical change of drainage system and the establishment of a mature, quartz-rich hinterland in the south west, in complete contrast to that in the lower beds which is from the north east.

The Dagangou red sandstones (Fig. 1.3, locality 2c) show a weak cleavage with moderately tight upward to north-facing folds, that dip steeply northwards in marked contrast to the underlying southward-dipping Ordovician beds, south of the Mid-Kunlun Fault. The volcanics are substantially altered by the later intrusion of the batholith. It is unfortunate that the field relationships of these volcanics are not better understood since their age is critical to the interpretation of the tectonic evolution of the Mid Palaeozoic in the Kunlun Terrane. As will be seen in the following chapter it was also not possible to date them isotopically.

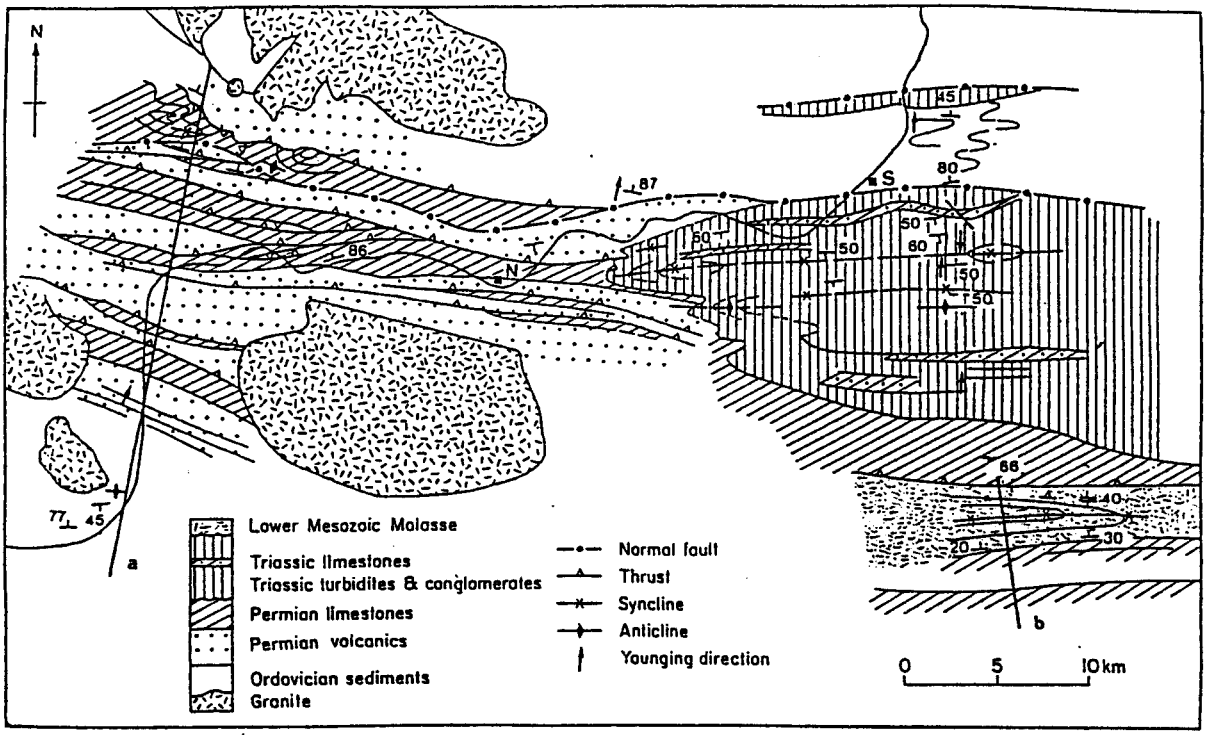

Fig. 1.4 Simplified geological map of the southern Kunlun Shan. Section line (a) is shown in Fig. 1.5 and section line (b) in Fig. 1.8. N = Naij Tal; S = Shuinichang. Redrawn after Coward *et al.* (1988).

1.4.3 Permian

Permian formations seen in the Kunlun Shan include a thick lava sequence at the base which extends for some distance in an east-west direction and is overlain by more than 200 m of tuffaceous sandstones and silts - the Hongshuichan Formation (Fig. 1.3, locality 3; Figs. 1.4.and 1.5). These volcanics lack any subduction component and are of typical intraplate character consistent with an origin either in a continental rift situation during moderate lithospheric attenuation, or in an island chain environment. The presence of sills in the continental basement coupled with the absence of pillow lavas in the lower part of the sequence favours the continental rifting hypothesis (Pearce and Mei, 1988), although Leeder *et al.* (1988) interpret the resedimented tuffaceous sandstones as being the storm deposits on a shelf basin, which is possibly part of a fore-arc sequence. Examples of even greater attenuation are represented east of the Geotraverse region by a series of Permian submarine lavas, sill complexes and basic intrusions that, while not

being strictly ophiolitic, may represent incipient spreading. This clastic Hongshuichan Formation is overlain by 800 m of the Wanbaogou Limestone, typical of a carbonate ramp, with crinoidal debris derived from the south west, and brachiopods that record an upper Permian age. No further volcanism is recorded in this succession.

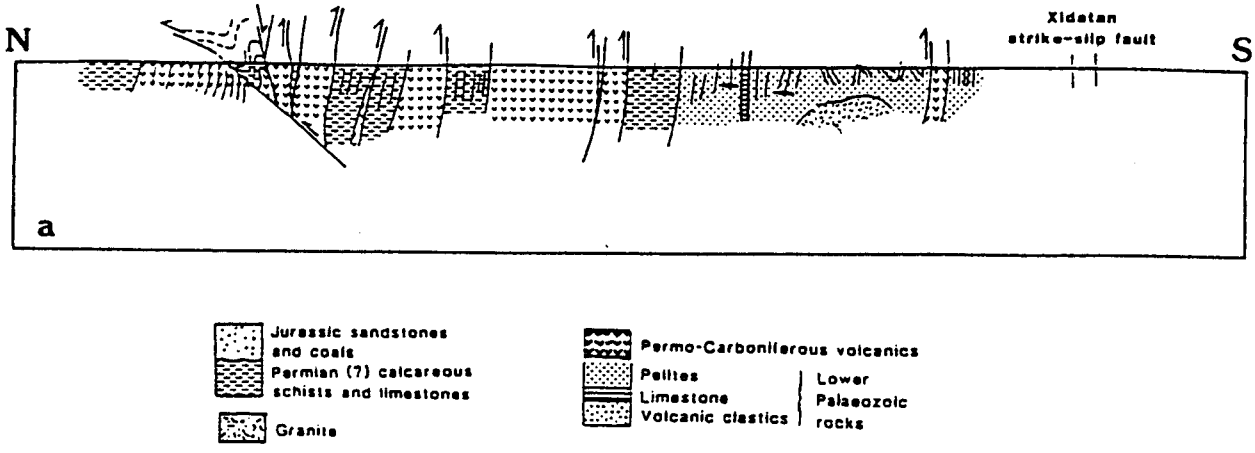

Fig. 1.5 Cross section through the southern Kunlun Shan along the section line (a) indicated on Fig. 1.4.

The Wanbaogou Limestones show upright folds, but deformation increases to the south where the dip is often close to vertical, and a strong cleavage is displayed. They are usually in faulted contact with adjacent rocks. In the Naij Tal valley there are several alternations of mylonitic limestones and metabasite volcanics. It is clear that these rocks have been repeated, probably by thrust imbrication associated with the intense deformation. These lithological repetitions are considered to represent the lateral equivalents of the tectonic mélange zone seen to the south-east (see following section).

1.4.4 Triassic

South of Shuinichang (Fig. 1.3) a thick (200 m) matrix-supported conglomerate (Fig. 1.3, locality 4) which contains clasts (often as large as 1.5m), representing a wide range of rock types including rounded granitoids, quartz porphyry, rhyolites, basic volcanics, gabbros, micaceous wackes, angular limestones, marbles and sandstones. There is an upward change from quartz through limestone to granite dominant clasts.

Overlying this conglomerate is a very thick sequence of quartz sandstones, highly cleaved fine grained wackes, and fine to medium grained sandstones (Fig. 1.3, locality 5). Leeder *et al.*, interpret the environment of deposition to be subaerial alluvial fans and fan deltas draining a hinterland containing Ordovician basement and an unroofing batholith to the north, (although a limited number of palaeocurrent measurements indicate the direction of transport to have been from the south east), and therefore they probably post-date active subduction and collision. Coward *et al.* (1988) suggest that these thick sandstones were deposited by turbidity currents in local basins, but whether they were of extensional or flexural origin is unclear. Folding in these deposits is upright and locally tight with subhorizontal axes trending east to east-north-east. The well developed cleavage is upright and parallel to the fold axial planes. Mineral lineations plunge steeply down dip. A Late Triassic age seems likely for these sediments.

Between the two strands of the Kunlun fault, on the southern margin of the Xidatan fault, several highly thrust sections occur within the Bayan Har Group (Fig. 1.3, locality 6), which represent a wide variety of lithofacies not normally associated with one another (Leeder *et al.*; Kidd *et al.*, 1988). A zone at least 200 m thick, with pebbly horizons, overlies a zone of intensely deformed graded shales to the south that generally young to the north. South of these deformed shales, intensely deformed slates and limestones often occur as discontinuous layers within a shale matrix. This appears to be a tectonic mélange and it seems likely that these thrust slices represent olistolithic masses within a turbidite sequence believed to be Permo-Triassic in age. The mélange is thrust over a series of less deformed red-beds and occasional thin shaley coals that yield a possible Triassic or Lower Jurassic flora. The basal breccia to this section contains angular clasts of acidic volcanics.

The rest of the sequence in this region, from the Xidatan Valley to the Jinsha suture, comprises a highly deformed sequence of clastic Triassic phyllites which is at least several kilometers thick - the Bayan Har Group (Fig. 1.3, locality 7). Due to the repetition produced by tectonic slicing it is difficult to estimate the thickness any more precisely than

this. The majority of these lithofacies are tentatively interpreted as continental rise deposits which were accreted to the southern margin of the Kunlun Terrane as an accretionary prism. Palaeontological evidence places the main phase of flysch deposition as lasting from the middle Lower Triassic to early Upper Triassic (c 245 - 225 Ma).

In general, these intensely deformed sections show steeply dipping beds with cleavage relationships and younging directions that indicate aniticlinal structures to the south, although it was difficult to recognise actual folds. South of Budongquan, fine grained turbidites have been affected by three phases of deformation. South of this to the Jinsha suture most of the features are obscured by Neogene and Palaeogene deposits, as is the suture itself.

1.4.5 Post - Triassic

Very little Jurassic (Fig. 1.3, locality 8), and no Cretaceous sediments are found in the Kunlun Terrane from which it is inferred that this region was an uplifted, non-depositional area throughout this time.

1.4.6 Tertiary

There are many areas of Tertiary outcrop across the Geotraverse route from Lhasa in the south almost to the Kunlun Pass in the north, and in addition there are very thick Tertiary deposits in the Qaidam Basin north of the Kunlun Shan. The largest outcrop occurs in the Fenghou Shan between Erdaogou and Wudaoliang (Fig. 1.2) where they overlie the supposed line of the Jinsha suture. Around Erdaogou itself, more than 1100 m of continental clastic red-beds, with very subordinate lacustrine limestones, make up the sequence. The majority of these sediments are muddy siltstones with interbedded, often lenticular, fine to medium grained sandstone bodies that frequently fine upwards. In the upper part of the succession the fine grained lithofacies contain thin (5-20 cm) limestones that contain Eocene charophytes, fresh-water ostracods and fragmentary plant material indicating that shallow pond conditions developed periodically.

These lithofacies are interpreted by Leeder *et al.*, as the deposits of a large, low gradient alluvial cone, and most of the sequences comprise the fine members of sheet flood origins. Palaeocurrents yield a vector mean towards the north-east. Above these deposits there is a marked change in both palaeoflow and sedimentary facies indicating a major change in basin geography at this time which may have been controlled by the northerly uplift of a growth fold above a new, south-directed thrust complex. It appears that sedimentation, provenance and stratigraphic sequences were being controlled by contemporaneous Tertiary to Recent thrust tectonics subsequent to the collision of India and Tibet. Shortening is estimated to be up to 50 km across this zone (Coward *et al.*, 1988). However, south of Erdaogou where Palaeogene red-beds are thrust across Neogene lake beds, striations on the thrust plane indicate a dominant left-lateral strike-slip component. Therefore, if north-south shortening is occurring within the Tibetan crust it is being accommodated by strike-slip faulting not by thrusting. (Dewey *et al.*, 1988). Unfortunately poor time constraints within the sequences prevent a full interpretation of developments across the whole of the plateau.

1.5 TERRANE PROVENANCE

The provenance of the Tibetan terranes is a question of continual controversy. Palaeontological evidence indicates that the Indian and Lhasa terranes had 'Gondwanan' flora and therefore originated from that region, whilst the Kunlun had 'Cathaysian' affinities and was already accreted to the Asian continent by the Carboniferous. However, a detailed study of the Palaeozoic biota from the Qiadam terrane north of the Kunlun, to the Himalayas in the south, concludes the following (Smith *et al.*, 1987):

1 Climatic fluctuations on a global scale controlled the distribution of the biota of this region during the late Palaeozoic, and that no suture zone can be identified as a consistent boundary between 'Gondwanan' and 'Cathaysian' biotas.

2 The whole region formed one continuous shelf at this time or, under an island terrane model, the terranes formed island platforms spread out across the

region, more or less uniformly. There is no evidence for any consistent dichotomy at one particular suture zone.

3 There is no evidence for any Palaeozoic continental rise or oceanic sediments on the Tibetan plateau. This is contrary to the expectations of an island terrane model and further supports the model of a continuous shelf at this time.

4 That breakup of the region may date from the late Permian.

This suggests that any major ocean in existence during the Carboniferous must have lain to the north of the Tarim Terrane. This model is supported by the palaeomagnetic data presented below.

1.6 PALAEOMAGNETISM

Over a thousand oriented samples for palaeomagnetic analysis were collected from two hundred and fortysix sites along the Geotraverse route. In the Kunlun Terrane, the Dagangou red-bed formation, and dykes from the Triassic igneous province which intrude the batholith, were sampled and the results interpreted as follows (Lin and Watts, 1988).

Using various reference polar wander paths for Eurasia (Irving 1977, Jowet *et al.*, 1987; Westphal *et al* ., 1986), a palaeolatitude was established for a given locality using the present latitude and longitude of the site and the pole position for the appropriate age from the reference compilation. From this is subtracted the palaeolatitude calculated from the mean of the measured palaeomagnetic direction, to give the latitude anomaly. Southern latitudes are considered to be negative, so if the latitude anomaly is positive the location is determined to have been south of the calculated latitude. All measurements had positive anomalies. The errors on the anomaly are found by adding the error of the relevant pole position to the estimated error of the palaeolatitude.

Figure 1.6 plots latitude anomaly against the estimated age of acquisition of the mean direction of magnetism. As can be seen, the Dagangou Formation (Fig. 1.3, locality 2c),

for which the age of deposition is not very well constrained, has a large error on the anomaly in the order of ± 25°. Nevertheless, it still indicates a position for the Kunlun Terrane well south of its present position relative to Eurasia. One of the problems here is that whilst the inclinations from the two samples sites are in close agreement, the declinations differ widely. Values from opposite limbs of a major fold giving 245° and 125° can be reduced to 215° and 168° by correcting for a plunge of 70° to the west, but there is still quite a large discrepancy between the two. However, the alternative scenario of placing the Kunlun Terrane in the northern hemisphere, requires the terrane to be rotated about 180° by the Permian, to account for the observed reversed magnetisation which constrains Carboniferous rocks to the southern hemisphere.

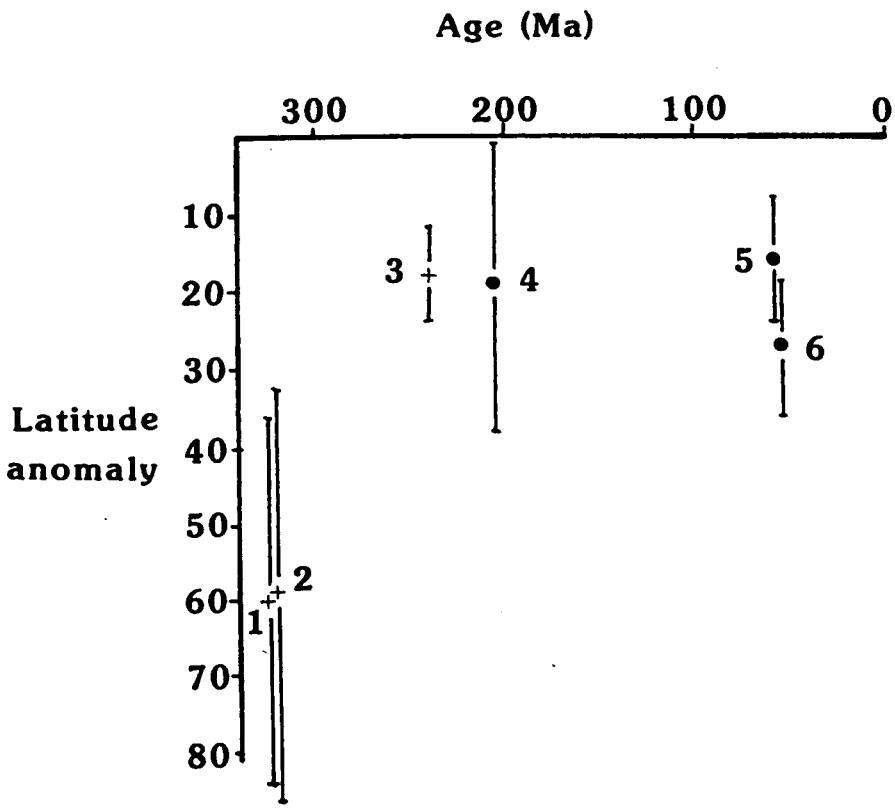

Fig. 1.6 Latitude anomalies for the Tibetan microplates plotted against age of magnetisation. Crosses - Kunlun Terrane, closed circles - Qiangtang Terrane. 1 and 2 Dagangou Formation, 3 Triassic dykes, 4 Batang Group, 5 and 6 Fenghoushan Group. Redrawn after Lin and Watts (1988).

From their data, Lin and Watts conclude that during the Carboniferous the Kunlun Terrane was in moderate southern latitudes, and that the magnitude of the anomaly indicates that an ocean must have existed between the Kunlun Terrane and Eurasia. This interpretation contrasts markedly with previous ideas that the Kunlun Terrane was already sutured to Eurasia by the Early Carboniferous, but is in close agreement with conclusions drawn from the palaeontological data (see previous section). Results from the Triassic dykes that cut the Kunlun batholith (c 240 Ma) show that during the Triassic, the terrane had a latitude anomaly of only 20°, requiring the terrane to have travelled north a distance of some 5000 km in about 100 Ma (Dewey *et al.*, 1988).

Figure 1.7 presents the Lin and Watts palaeogeographic reconstruction for the Carboniferous. Note in particular, that the Qiangtang and Kunlun Terranes are still in the same relative positions as they are today, as inferred from palaeontological evidence (Smith *et al.*, 1988), but are separated from the Tarim and Qaidam Terranes (which now border the Kunlun Terrane to the north) believed to be accreted to Eurasia by the Carboniferous.

Palaeomagnetic data also indicate a latitude anomaly of about 20° for the Batang Group of volcanics in the Qiangtang Terrane, (Fig. 1.2, south of the Jinsha Suture and to the east of Erdaogou), which are dated at about 205 Ma (early Jurassic). Whilst it is not possible to directly compare these data with those from the Triassic dykes in the Kunlun because of the age difference, it does imply that both terranes were in the same latitude belt during the Triassic. Furthermore, data from the Fengoushan Group indicates that this 20° anomaly for the Qiangtang Terrane, and therefore presumably the Kunlun, persisted until at least the Palaeocene, which is the age of these deposits. Clearly then, if the Carboniferous palaeomagnetic reconstruction is correct, and the Jinsha suture is accurately positioned, then separation of the Qiangtang and Kunlun Terranes must have occurred post-Carboniferous, probably during the Permian, only for them to be re-united again by the late Triassic. Recent palaeomagnetic work from the Tarim Terrane (McFadden *et al.*, 1988) suggests that infact the Tarim Terrane was not sutured to Eurasia until the Permo-Triassic. If this is the case, it could resolve many of the problems

associated with the positioning of the Kunlun Terrane during the Carboniferous. This will be further discussed in the concluding chapter.

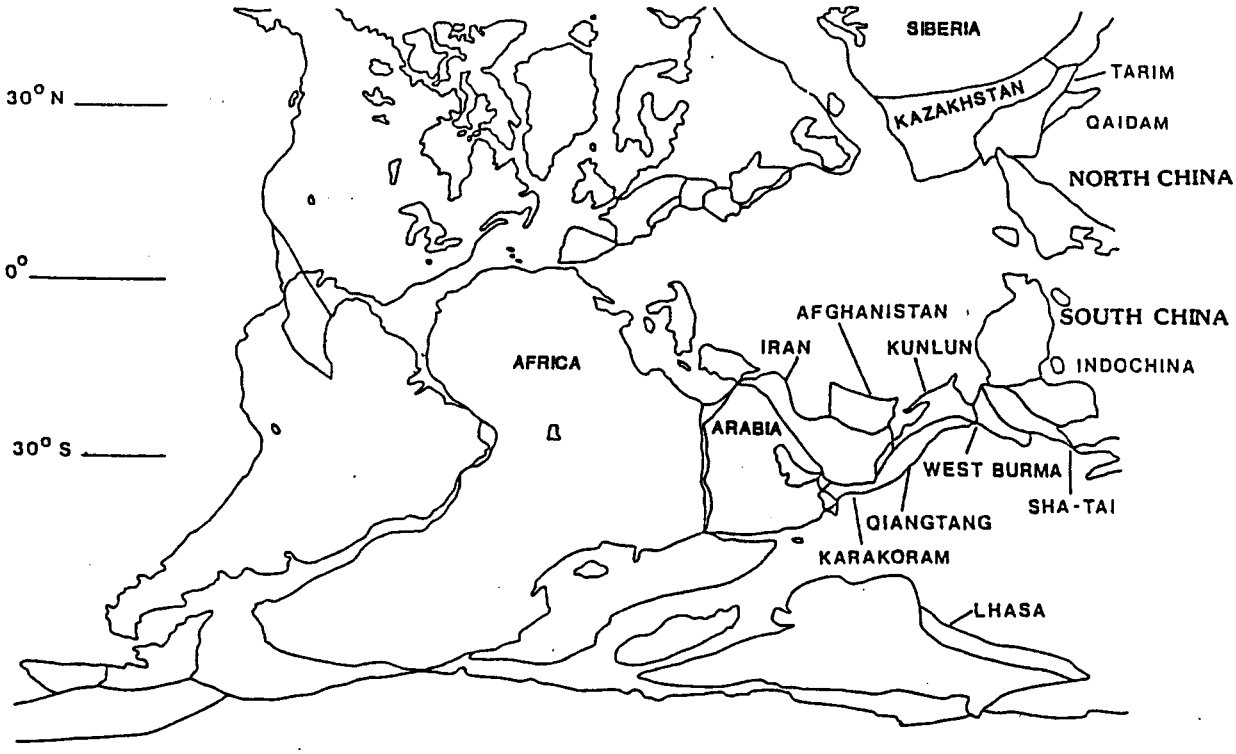

Fig. 1.7 Carboniferous palaeogeographic reconstruction for southern Asia (after Lin and Watts, 1988).

1.7 STRUCTURE

Structurally the Kunlun Terrane is complex. Having been subjected to multiple tectonic events it is difficult to unravel one event from the overprint of the next, but undoubtedly there is one major feature that dominates the region - the Kunlun Fault. It trends east-west through the Kunlun Shan, and in the Geotraverse area splits into two strands, the more northerly of which is known as the Xidatan Fault (Fig. 1.3), whilst the southerly branch trends south east and is known as the Kunlun Pass Fault. From here on the Kunlun Fault will be discussed under the local name of the Xidatan Fault. This region was extensively examined by the Geotraverse team and a summary of their results are presented here.

The Kunlun Fault can be traced for many hundreds of kilometers both east and west of the Geotraverse region. It dips steeply to the north and there is a clear north-side-up thrust component to it bringing Permian limestones south over Triassic red-beds. The dominant structure here is of an inclined south verging syncline with an over-turned northern limb beneath the footwall to a major thrust - the Xidatan Fault - which carries the tectonic mélange on its footwall (Fig. 1.8). However, recent left lateral slip has been inferred from the displacement of once adjacent structures seen on the Landsat imagery. This has then been backed up by the identification of outcrops on the ground. In particular, a moraine containing boulders of a pyroxenite is separated by 30 km from the nearest outcrop of such a rock on the other side of the fault. This implies a rate of slip since the late Pliocene (c. 2.4 Ma) of 10 - 20 mm/yr, probably averaging about 13 mm/yr (Kidd *et al.*, 1988). Fault plane solutions of two earthquakes, one of which occurred as recently as April 1963, also infer left lateral slip. The total displacement along the Xidatan Fault has been deduced from the position of a 'pale unit' seen on the Landsat imagery on the north side of the Xidatan fault, some 75 km west of a unit of truncated phylonites observed in the field. If this pale unit is the phyllonite and not limestone or marble, then the minimum total offset on the Xidatan strand of the Kunlun Fault is 75 km. At rates of displacement deduced by the Quaternary offsets, it has been calculated that this total displacement must have occurred during the last 7 Ma.

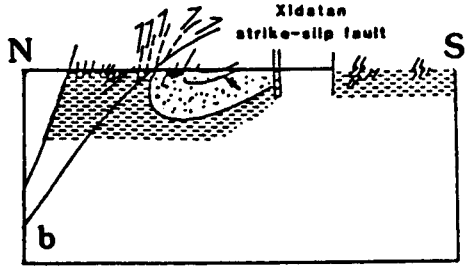

Fig.1.8 Cross section through the region of the Xidatan strike-slip fault. Section line (b) as shown on Fig. 1.4, and key as shown on Fig. 1.5. Redrawn after Coward *et al.*, (1988).

Somewhat suprisingly, considering its pronounced geomorphological expression on the satellite image (Plate 1.1), the total displacement on the Kunlun Pass Fault is determined not to be greater than 3 km, but this could be explained by the fact that it may not have been initiated until the Holocene. Kidd *et al.* (1988) conclude that the large rate

of slip seen on the Xidatan during the last few million years probably occurred in discrete jumps of 15 - 20 meters during rare earthquakes every 500 - 1000 years. This resulted in the area south of the fault being rapidly extruded eastwards as a direct consequence of the continued penetration of India into Eurasia.

In the centre of the Kunlun Shan, the Mid-Kunlun Fault forms part of a zone of discontinuous fault segments and splays, and its less continuous nature suggests that the overall strike-slip displacement is small compared to the Xidatan. Unfortunately these faults were only examined in detail for evidence of recent faulting associated with the neo-tectonics of Tibet, and little attention was paid to their likely age. The Mid-Kunlun Fault clearly separates the less deformed, uncleaved Dagangou Formation to the north, from the strongly cleaved Ordovician and Permo-Triassic rocks to the south (Coward *et al.*, 1988). It dips steeply southwards and thrusts Ordovician limestones and shales over Carboniferous red-beds. Further north again, an un-named fault, that also dips south, is considered by Kidd *et al.*, to be a northerly strand of the Mid-Kunlun Fault system. However, geochemical and fission track data indicate that this fault is a significant and long-lived lineament in the Kunlun Shan, and it is here termed the Golmud Fault.

Overall, the structures in the Kunlun Terrane are of north verging folds in the north Kunlun; upright folds in the centre and intensely deformed south verging folds in the south. The total area covered by these highly deformed sediments and their associated structures, which are considered to have resulted from the accretion of deep water sediments on to a magmatic arc, is about 100 km. The amount of shortening is unknown, but from comparison with other accretionary prisms it could be at least 50%. From the steepness of the beds and faults, and the intensity of the cleavage Coward *et al.*, (1988) consider the shortening in the Kunlun Terrane to be in excess of 75% . The dominant overthrust directions are south-south-east and north-north-west suggesting that this was the main plate convergence vector.

Plate 1.1 Landsat image of the Geotraverse route in the Kunlun Terrane. The Xidatan and Kunlun Pass Faults are pronounced features.

1.9 THE BATHOLITH

To the north of the Mid-Kunlun Fault, granitoid plutons intrude the Dagangou volcanics which are openly folded, but often steeply dipping. A swarm of dykes that cut the batholith, the volcanics and the surrounding sediments (Fig. 1.3, locality 10) are not deformed. This therefore constrains the folding of the volcanics to a period prior to the intrusion of the dykes which are 250 Ma . To the south of the Mid-Kunlun Fault, small individual plutons intrude Permian limestones. These granitoids are believed to be Permo-Triassic in age. The geochronology of the granites will be discussed in detail in Chapter 3 and their geochemistry in Chapter 5.

1.10 METAMORPHISM

Considering the apparent complex collision history of the Kunlun Terrane (Zhang et al, 1984; Watson et al, 1987; Dewey et al, 1988 and Chapter 6, this study), there is remarkably little metamorphism associated with it. South of the Xidatan Fault a thick zone of dark, grey - black phyllonites is intensely deformed, and within 10 km north of the fault a garnet isograd strikes north-east (Harris *et al.*, 1988b). However, this

amphibolite grade metamorphism soon dies out northwards, and just north of the Yie Nin Gou pluton pelites contain a greenschist assemblage of chlorite - quartz ± sericite ± biotite ± magnetite. The peak metamorphic grade determined from the garnet-bearing sediments records pressures of 4.3 ± 1.5 kbar at 470 ± 30°C. The metamorphic isograds determined by Harris *et al.* (1988b) are shown in Fig. 1.9.

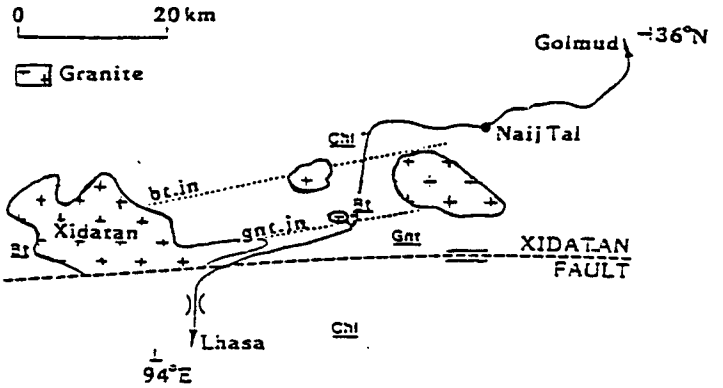

Fig.1.9 Sketch map showing the metamorphic isograds determined for the Kunlun Terrane. Chl = chlorite; Bt = biotite; Gnt = garnet. Redrawn after Harris *et al.*, (1988b).

That the plutons in the Southern Region were emplaced subsequent to regional greenschist metamorphism is seen in their discordant contacts across the fabric in the country rocks (Coward *et al.* 1988), and it is significant that the Yin Nin Gou, Naij Tal and Xidatan plutons all straddle major thrust faults (Fig. 1.4) which may have acted as conduits for the escaping melts. Further evidence that the granites were intruded post regional metamorphism is seen in the contact aureoles around the Yie Nin Gou X and Xidatan plutons where thermal metamorphism is superimposed on the regional facies. Harris *et al.* (1988b) suggest that the metamorphic assemblages seen in these thermal aureoles indicate that emplacement depths were no greater than 10 km, and they conclude that the regional metamorphism is synchronous with emplacement of the batholith at 250 Ma. Coward *et al.*, (1988) imply that the metamorphism is related to the accretion of deep water sediments on to a magmatic arc prior to collision of the Qiangtang and Kunlun Terranes which could also have been synchronous with batholithic emplacement. The inferred north-easterly trend of the metamorphic isograds, which may be expected to

parrallel the plate boundaries, concurs well with the main plate convergence vector indicated by the dominant overthrust directions that are towards the north-north-west and south-south-east. Both Coward *et al.* and Harris *et al.* agree that the strong penetrative fabric seen in the Xidatan orthogneiss supports evidence for a later deformational event.

A full regional summary of the Kunlun Terrane is presented in the final chapter .

CHAPTER TWO

2 FIELD RELATIONS and PETROLOGY

2.1 INTRODUCTION

Along the Geotraverse route, the Kunlun batholith is exposed in the north of the Kunlun Shan whilst in the south of the range individual, probably post-tectonic, plutons occur. All the eleven granitoid localities sampled for this project lie north of the Xidatan Fault and south of the Qaidam Basin (Fig 2.1), and because the granites fall into three separate groups associated with three distinct regions within this area, it has been divided up as summarised in Table 2.1.

XIDATAN FAULT	
Region	**Pluton**
Southern	**Xidatan**
	Yie Nin Gou
	Naij Tal
	Wanbaogou
MID-KUNLUN FAULT	
Central	**Golmud Hydro Group**
	Central
	Pink
	Little
	Golmud Junction
GOLMUD FAULT	
Northern	**East Quarry**
	Duo Ya He
	Golmud East

Table 2.1 Summary of pluton names and regions in which they are exposed.

Fig. 2.1 Sample location map of the Kunlun batholith granites.

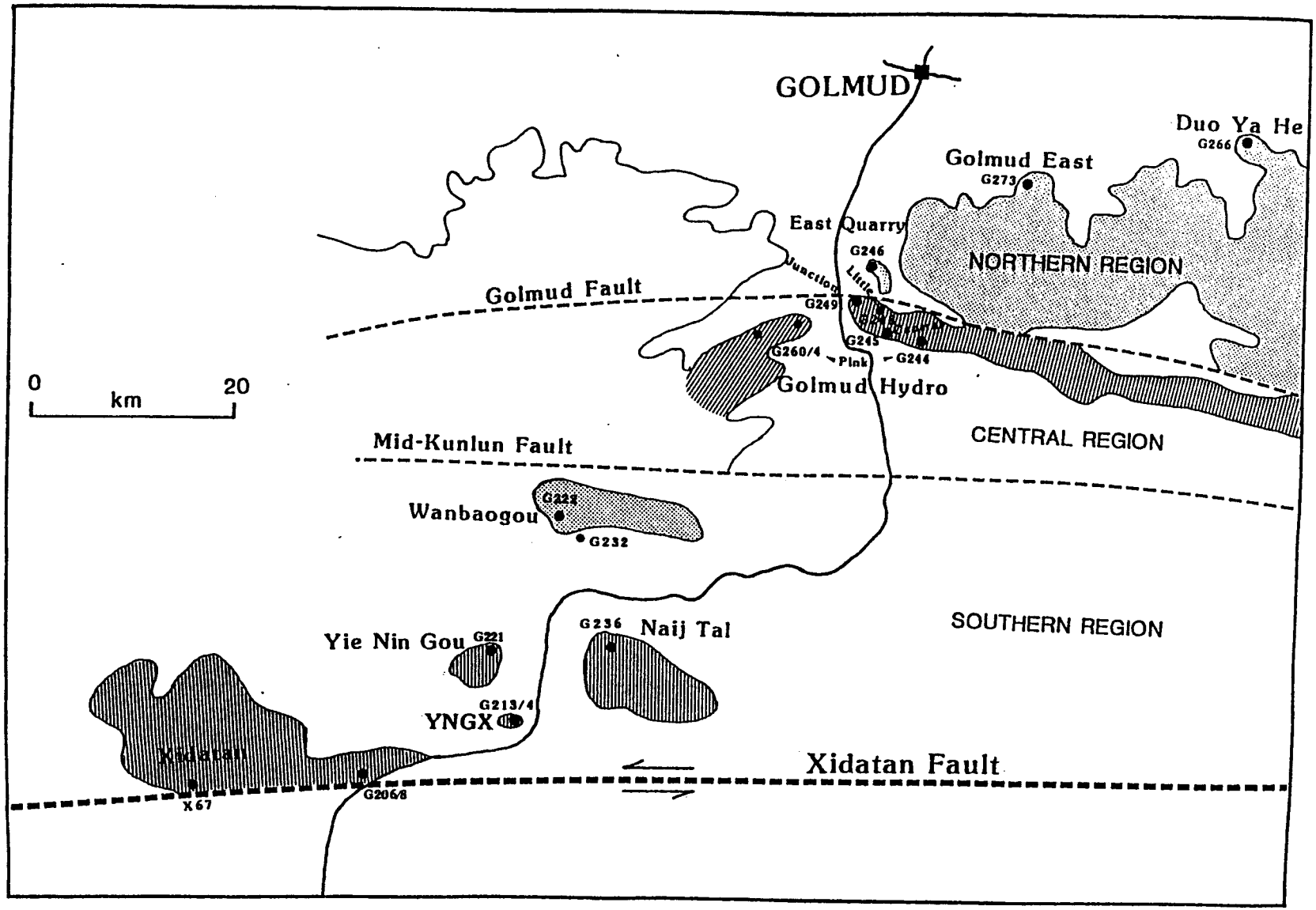

The Southern Region extends from north of the Xidatan fault to the Mid-Kunlun Fault which defines the southern boundary of the main batholith. The Central Region lies between the Mid-Kunlun and Golmud Faults (Fig. 1.3), and the Northern Region extends beyond this to the northern edge of the batholith. Starting in the south, the field relations and petrology of each pluton will be discussed in turn. Some microprobe data has very kindly been provided by Chinese colleagues and, where relevant, is included in this section.

2.2 SOUTHERN REGION

2.2.1 Xidatan

The most southerly of the individual, post tectonic plutons is the Xidatan orthogneiss. The original granite was emplaced into phyllites which are probably Ordovician in age. (Leeder *et al.*, 1988). Immediately north of the Xidatan fault (Fig. 2.1), from where the samples were collected, the granite has a strong gneissic fabric (Plate 2.1) that strikes at 90°, which is parallel to the fault . The dominant rock type is a foliated biotite granite (G206a,b, G207, G208 and X67) cut by bands of a much more leucocratic granite (G206c,d,e and f). Within the body is a leucocratic garnet-muscovite granite dyke about 1m in width which also shows an E-W foliation parallel to the fault (Jin pers. comm.). In thin section the two groups are primarily distinguished by the percentage of biotite present. The Fe-rich biotite ($FeO_t/FeO_t + MgO = 0.72$) comprises between 3 and 10% for the first group but is less than 3% in the more leucocratic samples that contain up to 5% muscovite, although this is considered to be a secondary development. Quartz is totally recrystallised and 'flows' around the larger plagioclase porphyroblasts which contain many biotite inclusions and have begun to develop 'augen' characteristics. Typically the groundmass contains microcline and myrmekitic intergrowths.

Accessory phases also differ in the two groups with the presence of large, euhedral allanites, often with idioblastic clinozoisite coronas (Plate 2.2), being a distinctive feature of the less evolved group. The clinozoisite corona is more fully developed when in

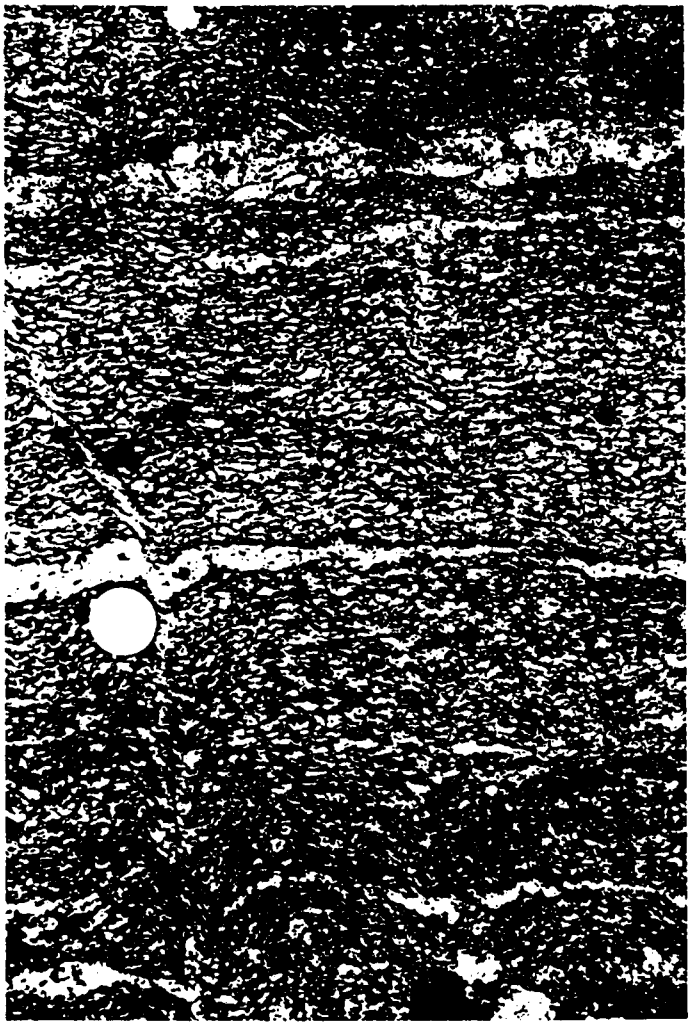

Plate 2.1 Kink bands in the Xidatan orthogneiss.

contact with biotite and these crystals appear to cut across the penetrative fabric, indicating that the growth of the corona occurred during metamorphism. Apatite, zircon, and sphene are seen in all samples, although in much lower abundances in the leucocratic group where sphene is almost totally altered to rutile. Clinozoisite is also seen in all samples replacing biotite and plagioclase. Sample X67 was collected from the south-western edge of the pluton, almost on the fault line. It is highly altered and contains up to 10% of various epidote minerals. However, the speckled saussuritisation of feldspars normally associated with epidote alteration is not seen here to any great extent.

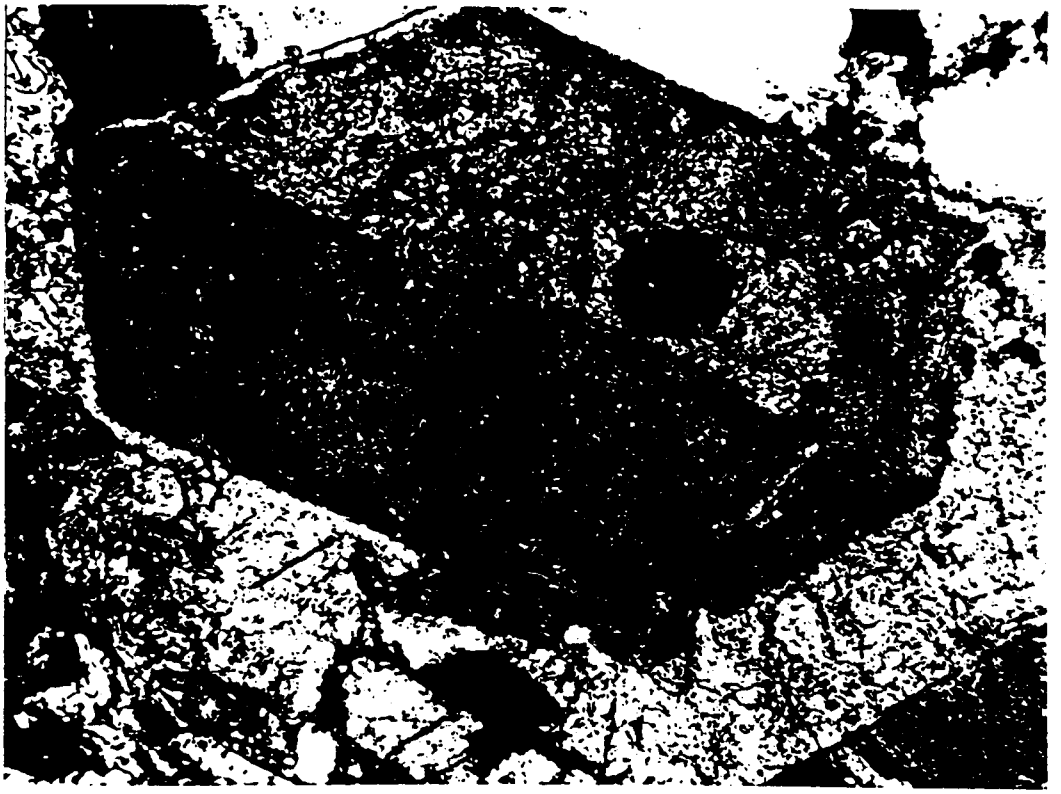

Plate 2.2 Large euhedral allanite with corona of clinozoisite from the Xidatan pluton. Dark patch in the allanite is a basal section of apatite, and a large zircon shows high interference colours. Field of view = 0.9 mm. All plates are with crossed polarised light unless otherwise stated.

2.2.2 Yie Nin Gou

Two kilometers north of the Xidatan Valley, to the west of the Lhasa-Golmud Highway (Fig. 2.1), a small (2.5 km diameter) undeformed circular pluton also intrudes the Ordovician phyllites. This intrusion, (G214) previously known as the Xiaonanchuan pluton, but now believed to be another exposure of the Yie Nin Gou pluton, is a high level, post-tectonic granitoid with sharp, steep contacts dipping at 60 - 70° around which cordierite-bearing hornfels is developed, and many granitic tongues and veins penetrate the country rock. From here on this pluton will be known as the YNG X (Yie Nin Gou - Xiaonanchuan) pluton. YNG X is a homogeneous, medium-grained, peraluminous biotite granite, which is again associated with a leucocratic phase (G213) where biotite occupies less than 3% of the total volume. Secondary epidote forms euhedral but poikiloblastic crystals within plagioclase, and idiomorphic clinozoisite mantles the occasional allanite. Four kilometers to the north-west, a second outcrop of the Yie Nin

Gou pluton (G221) is slightly less evolved, coarser grained and metaluminous (Plate 2.3). This outcrop is also homogenous and undeformed containing biotite-rich enclaves (G221h) and calc-silicate xenoliths.

Plate 2.3 Granite boulders from the Yie Nin Gou pluton .

Distictive features seen in thin section are the oscillatory zoned plagioclases (An 30 - An 35 - An 21, from core to rim) and the extensive poikolitic microcline (Or 90 Ab 8.5 An 1.5) which is obviously the last crystallising phase (Plate 2.4). Accessory minerals include siginificant amounts of sphene, usually euhedral but also as inclusions in biotites; apatite as profuse inclusions in the very dark green Fe-rich biotites ($FeO_t/FeO_t + MgO$ = 0.75); some zircon, allanite and opaques. Epidote and clinozoisite are present as large subhedral crystals always in close association with biotite suggesting primary cystallisation. However, since they are clearly seen as a secondary phase replacing plagioclase, the nature of the epidote phase remains equivocal. Saussurite alteration is quite extensive whilst sericitisation is seen here as relatively large muscovite flakes within the feldspars.

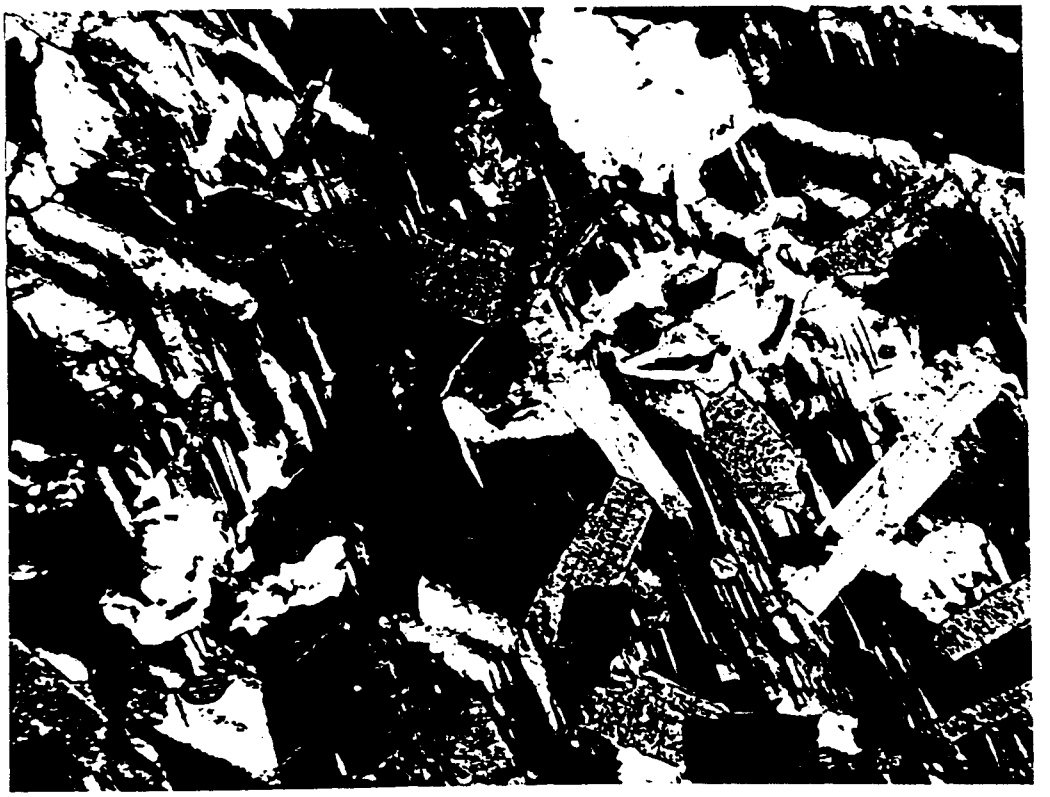

Plate 2.4 Poikilitic microcline in sample G221b from the Yie Nin Gou pluton. Field of view = 3.5 mm.

The enclave (G221h), is similar in texture and composition to its host, although of a smaller grain size, with poikolitic microcline and perthite encompassing laths of plagioclase, biotite and some hornblende. The most noticeable feature of this enclave is the large amount (> 1%) of slightly stubby, prismatic apatite grains which appear to be randomly scattered, cross-cutting all grain boundaries regardless of composition. It is clearly a very early crystallising phase. This is a common feature of dioritic enclaves in granites and may represent rapid growth within a quench environment (Holden, *et al.*, 1987; Wyllie and Cox, 1962) such as might occur when a hot, more basic magma becomes entrained into the cooler granitic melt (Frost and Mahood, 1987; Sparks and Marshall, 1986). Other accessory minerals include clusters of large anhedral zircons (up to 1mm in length, Plate 2.5), considerable amounts of allanite, euhedral opaques and trace amounts of sphene. Substantial epidotization resulted in the presence of both epidote and clinozoisite.

Plate 2.5 Zircon clusters (centre) and stubby apatite grains (bottm right) from an enclave (G221h) found in the Yie Nin Gou pluton. Field of view = 0.6 mm.

2.2.3 Naij Tal

Due south of the village of Naij Tal, and to the east of the Lhasa-Golmud Highway (Fig. 2.1), the Naij Tal pluton (20 x.10 km) is emplaced into the Permian limestones and shales of the Wanbaogou Group. It is cut by aplites, and contains xenoliths of marble and dioritic enclaves. A near horizontal upper contact with the country rock indicates that the intrusion has been uncovered close to the roof of the chamber. All the Naij Tal samples (G236 and G237) are biotite granites, with the exception of G236D which is a granodiorite and contains minor amounts of hornblende. In thin section, this pluton is similar to Yie Nin Gou but with less zoning in the plagioclase (An 30 - An 31 - An 20 from core to rim), and the poikolitic microcline and perthite are not so common (Or 90 Ab 7 An 3). However, where plagioclase is enveloped in microcline, myrmekite is developed. The brown Mg-rich biotites ($FeO_t/FeO_t + MgO = 0.71$) are altering to chlorite which frequently shows brilliant Berlin blue interference colours. Quartz has a shadowy extinction and is partially recrystallised, but no fabric is developed. Primary allanite, a feature of all these southerly plutons, is usually rimmed by secondary clinozoisite and is

often seen to have apparently nucleated around a single crystal of apatite. As in the other plutons, sphene, apatite and minor amounts of zircon comprise the remaining accessory minerals, whilst the ubiquitous clinozoisite suggests that all these plutons have been subjected to the same type of alteration which is probably a result of low grade regional metamorphism.

2.2.4 Wanbaogou

Fourteen kilometers north of Qingbanzhan, the southern margin of an apparently post-tectonic porphyritic biotite granite (G222) is exposed (Plate 2.6). To the south of the main body in the Wanbaogou Valley lies a leucocratic, muscovite-tourmaline stock (G232) but it is not clear from field evidence whether this is an integral part of the Wanbaogou pluton since it is in faulted contact with the main body. However, geochemical and isotopic evidence indicate that it is and so it will be considered as such here. Similarly, three boulder samples (G225) found in a stream in the Wanbaogou Valley, presumed to have been eroded from the Wanbaogou pluton, will also be included in the Wanbaogou group, although geochemical and isotopic evidence indicate that this assumption is somewhat equivocal.

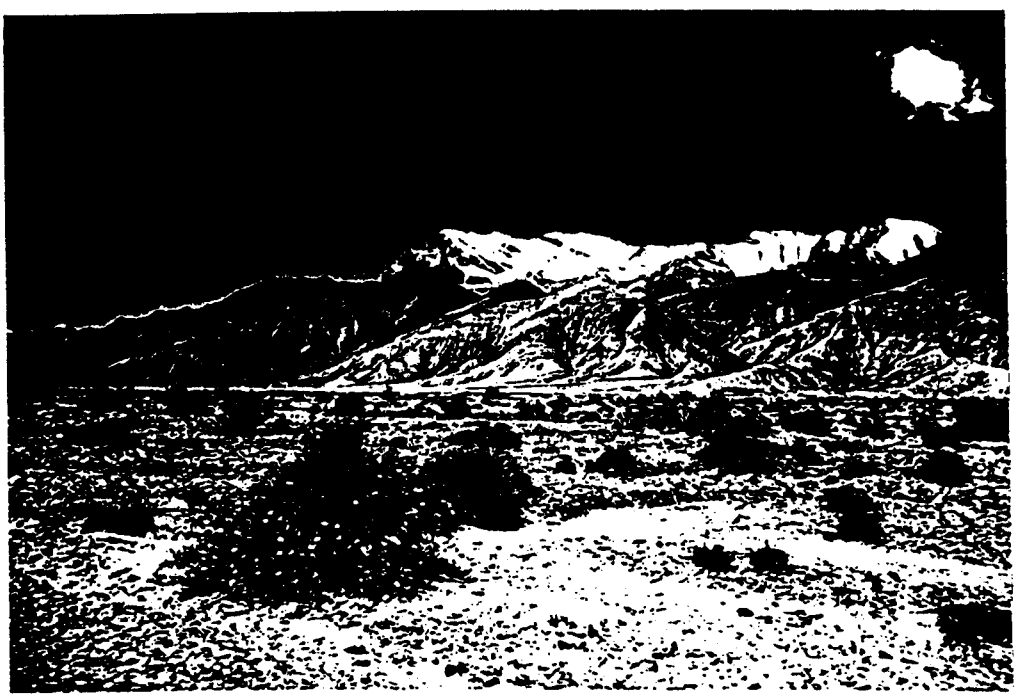

Plate 2.6 The Wanbaogou granite seen from the Wanbaogou Valley.

In this porphyritic granite, the white phenocrysts, up to 4 cm in length, are predominantly microcline (Or 95.7 Ab 4.3) traversed by perthitic lamellae. These phenocrysts are presumed to have formed early in the crystallisation history of the melt. The matrix consists of medium grained microcline; plagioclase that is rarely zoned and has a composition ranging from An 25 - 30; quartz and green, Fe-rich biotite (FeO_t/FeO_t + MgO = 0.84) with the usual accessory phases of zircon, apatite and infrequent but large allanites up to 2mm in length (Fig. 2.7). Hornblende is sometimes seen in the less evolved samples and occasionally it is found to mantle biotites. Alteration of plagioclase is manifest in the considerable 'cloudiness' of saussuritisation as well as in large flakes of muscovite as a result of sericitisation.

Plate 2.7 Large allanites from the Wanbaogou granite show very different crystal habits from those seen in the Xidatan granite (Plate 2.2). Field of view = 2.8 mm.

The enclave (G222h), is fine grained and equigranular with plagioclase laths showing no zoning. The mafic portion comprises biotite and hornblende in almost equal proportions and, as in the previous enclave (221h), large prismatic apatite needles (Plate 2.8) are in random profusion throughout the sample. Large zircons over 1mm in length are stubby and rounded indicating that they may be inherited rather than primary

Plate 2.8 A long prismatic apatite needle from the enclave in the Wanbaogou granite. Field of view = 0.9 mm in ppl.

The presence of tourmaline (Plate. 2.9) seen in the leucocratic stock (G232) suggests a late stage granite affected by boron rich fluids. It is often seen in symplectic intergrowth with plagioclase, never shows an euhedral form, and appears to be interstitial. Muscovite is also found as an interstial phase. The small amount of biotite present is almost completely chloritised and associated with a considerable amount of opaques which are probably magnetite as a result of the break-down of Fe-rich biotites.

Plate 2.9 Tourmaline (yellow) in a leucocratic stock sample of the Wanbaogou pluton. Field of view = 2.5 mm.

The G225 boulder samples analysed in an attempt to acquire a more mafic representative of this pluton, are substantially saussuritised, particularly the plagioclase phenocrysts, although these still retain a reasonable euhedral outline. The biotite content is very low having almost completely been replaced by chlorite and opaques. The incipient deformation is seen in the recrystallisation of quartz. Allanite is quite common but the smaller accessory minerals such as zircon and apatite are difficult to see due to the heavy saussuritisation. A little secondary epidote is present. If these samples are from the Wanbaogou pluton, it seems likely that they have been derived from the northern edge which is close to the Mid-Kunlun Fault, since none of the other samples examined show any signs of deformation.

2.3 CENTRAL REGION

The Golmud Hydro Group is comprised of three granitic groups (see Table 2.1) which, from isotopic evidence, were intruded at slightly different times, although their chemistry is very similar. The Central Granite (G245a-f) is a biotite granite cut by biotite pegmatites and aplites indicating that it was possibly the last of the three phases to be intruded. At the southern and western margins it becomes strongly porphyritic with pink perthitic K feldspar crystals up to 1.5 cm in length (G244 and G260-264), and veins of this Pink Granite are seen to cut the sub-porphyritic Little Granite (G248) which mantles the Central Granite to the north. Here the phenocrysts are less than 1 cm in length and more commonly only 0.5 cm. Clearly the Little Granite has to be the oldest of the three. All facies contain enclaves of dioritic or granodioritic material and are cut by abundant mafic dykes (Plate 2.10) that have a north-easterly trend. Along its southern margin, the Golmud Hydro Group intrudes Devonian andesites and basalts (G250 and G253) of the Dagangou Volcanics. These are strongly hornfelsed at the contacts which dip sharply to the south. The northern edge of the pluton appears to intrude a hornblende granodiorite, the Golmud Junction granodiorite (G238 and G249), that shows a pronounced schistosity where it is adjacent to the Golmud Fault.

2.3.1 Golmud Hydro Group

This group includes the Central Granite core and the porphyritic margins around it (Little and Pink plutons). All samples show some deformation and recrystallisation suggesting that these may be syn-collision granites. The Little Granite is the least affected, while those closest to the Mid-Kunlun Fault have a distinct gneissic appearance. The porphyritic crystals are pink perthite which have a higher Ab content (15.4%) than those in the much finer granular matrix (Ab 5 - 8%). The green biotites of the porphyritic phase have a higher Fe content than the brown ones in the Central Granite at $FeO_t/FeO_t + MgO$ = 0.84 and 0.75 respectively. The composition of the zoned plagioclases however varies little (An 30 - 27). Hornblende is a minor phase in the more mafic samples. Allanite is also quite common but is not present in the more highly fractionated Central Granite. In these, muscovite is a minor phase although probably results from secondary alteration.

Epidote, clinozoisite and chlorite are also alteration products, and all samples are saussuritised and sericitised to varying degrees. Zircon and apatite are in very low abundances in the Central Granite.

The four G248 samples are all very similar in thin section and hand specimen. Medium grained, granular and anhedral with small phenocrysts of perthite, they display an incipient fabric with partially recrystallised quartz and myrmekitic intergrowth in the matrix. Biotite is interstitial and substantially chloritised, and a small amount of apatite is seen both as inclusions in biotite and, less commonly in these plutons, also in the matrix. Allanite is present as well as large zircons whilst epidote is here considered to be secondary. There is a noticeable absence of sphene in all the Golmud Hydro Group.

Plate 2.10 Basalt dykes cut the Golmud Hydro Group granites.

2.3.2 Golmud Junction

The relationship of the Golmud Junction pluton (G238 and G249) to the others of the Golmud Hydro Group is not so clear. Being that much closer to the Golmud Fault it has a pronounced fabric and has clearly been substantially recrystallised. However, in the less altered samples this granite is very similar to the Little Granite to which it is adjacent. Small pink phenocrysts of perthite are aligned within the fabric but in the more altered

samples, boundaries around the phenocrysts are breaking down to a fine granoblastic groundmass and myrmekitic intergrowth is common in the matrix. Internal shearing has off-set albite twins which have very fine lamellae typical of low grade metamorphism. Poikiloblastic hornblende shows idioblastic crystal faces. Allanite, previously not seen in the metamict state in granitoids to the south, displays a pleochroic halo when in contact with biotite. Coronas of clinozoisite mantle the opaques, whilst zircon, apatite and a very little sphene make up the other accessory minerals. Sample G249e is considerably more mafic than the others from this intrusion which suggests that it may be an enclave.

2.4 NORTHERN REGION

North of the Mid-Kunlun Fault, plutonic rocks are continuously exposed for 30km to the northern edge of the Kunlun Shan and for some several hundred kilometers both east and west of Golmud. Immediately north of the Golmud Junction intrusion, some 25km south of Golmud, lies the small East Quarry stock (G246/7); a biotite-hornblende tonalite with dioritic enclaves (G246f). It is cut by abundant garnet bearing pegmatite veins some 5cm in width (Jin, pers. comm.). A biotite-hornblende granodiorite with hornblende-rich enclaves (G273a-e) is quarried in the Golmud East intrusion 20 km south east of Golmud. Twentyfive kilometers east of this, the Dou Ya He granodiorite (G266a-e) is slightly foliated, intruded by a hornblende granite, and contains biotite-rich autoliths.

2.4.1 East Quarry

In thin section, deformation not visible in the hand specimen, is clearly seen to be affecting the fabric of this rock. Mg-rich biotites ($FeO_t/FeO_t + MgO = 0.70$) that had begun to flow around the larger grains are often chloritised and flanked by comminuted sphene, while quartz displays a shadowy extinction and the classic metamorphic mosaic of recrystallisation. Zoned plagioclase shows the only measured example of reverse zoning seen in the whole batholith (An 31.2 - 32.3 - 34.7 from core to rim). Epidote replaces hornblende and biotite to such an extent that it often appears primary, and here mantles the ubiquitous allanite in place of the more usual clinozoisite. Apatite and zircon are the other accessory minerals.

The dioritic enclave is characterised by cores of clinopyroxene that are mantled by a zone of colourless amphibole which grows greener towards the edges, eventually becoming common hornblende (Plate 2.11). Clearly the amphibole is secondary after clinopyroxene as the more basic magma becomes hydrated with the breakdown of biotite. Lamallae of orthopyroxene are seen within the clinopyroxene cores. The feldspar is almost exclusively plagioclase laths which have multiple inclusions of, and are frequently zoned by, flecks of green hornblende. The only biotite seen in the sample is a couple of large poikolitic crystals which encompass plagioclase laths and a symplectic intergrowth of hornblende and plagioclase. Large zircons, allanites and apatites are present in considerable abundance, and the whole section is peppered with opaques.

Plate 2.11 Clinopyroxene cores in hornblende seen in enclave G246f from the East Quarry stock. Field of view = 0.9 mm.

2.4.2 Golmud East

This greyish white granodiorite (G273) looks very fresh in hand specimen. The brown, Mg-rich biotites ($FeO_t/FeO_t + MgO = 0.63$) are much more abundant than hornblende and have quite large inclusions of secondary prehnite (Plate 2.12). Zoned plagioclase (An 38.6 - 42.5 - 36.5) is often seen in myrmekitic intergrowth, and the alkaline feldspar is not twinned (Or 95.8 Ab 4.2). Sphene is the major accessory phase in these northerly plutons accompanied by, in order of decreasing abundance, apatite, zircons (which are large and of a rounded appearance), and only the occasional allanite.

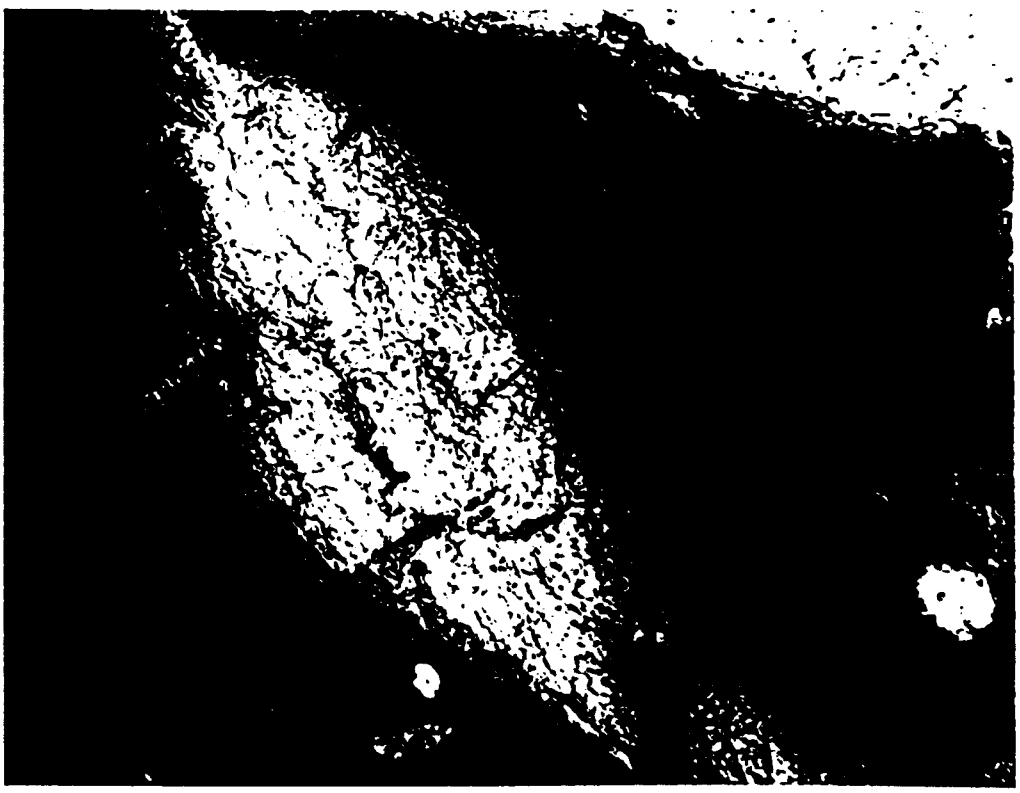

Plate 2.12 Prehnite in biotite from the Golmud East pluton. Field of view = 0.6 mm.

2.4.3 Duo Ya He

The feature of this pluton is the completely different crystal habit of the epidote mineral which has been difficult to specifically identify. Amorphous in outline and pale brown in colour, it displays a faint pleochroism and planar twinning, but the interference colours are always of the lowest order such as those seen in zoisite (Plate 2.13). It has a

pleochroic halo when in contact with biotite and therefore contains radioactive elements such as uranium or thorium commonly found in allanite. It seems likely therefore that this is a partially metamict form of allanite which may explain the anomolously low birefringence. This pluton displays a distinct fabric of re-organised biotites and recrystallised quartz. Large crystals of plagioclase show very fine lamellae of albite twins and the occasional symplectite structure. The accessory phases are the same as in the Golmud East pluton with large rounded zircons again being a distinctive feature.

Plate 2.13 Amorphous allanite (centre) shows planar twinning and anomalously low birefringence colours. Field of view = 3.5 mm.

2.5. METAMORPHISM OF THE GRANITES

The formation of epidote marks the boundary between greenschist and epidote-amphibolite, with clinozoisite as the high pressure phase (Holdaway, 1972). In the Xidatan pluton, large allanites, considered to be a primary phase, are frequently present with extensive rims of clinozoisite that have nucleated around the allanite as the pressure

increased during a secondary event. These often form spectacular euhedral crystals, particularly when in contact with biotite, that cross-cut the fabric formed by recrystallisation of the biotites Zoisite and epidote are also present but in minor amounts. Away from the Xidatan fault in the other post-tectonic plutons where there is no pronounced deformational fabric, epidote predominates over clinozoisite and zoisite, and the euhedral rims of clinozoisite become patchy and poikiloblastic. However, the epidote crystals are often large (1mm) and when in contact with biotite frequently appear magmatic. In their work on magmatic epidote in granites, Zen and Hammarstrom, (1984) describe occurrences of epidote that correspond to those described above, and conclude that it crystallises at moderately high pressures equivalent to depths of at least 25 km, which would place them in the middle to lower crust. However, this is not in agreement with the metamorphic work which proposes emplacement at depths (presumably as a melt phase) at about 10 km (Harris *et al.* 1988b). Undoubtedly some, if not all, of the epidote is secondary as it is seen to be replacing plagioclase. All plutons show substantial alteration of biotite to sphene particularly at crystal boundaries and along fractures and cleavage planes, and hydrothermal alteration of the feldspars.

Several authors, (Dempster, 1986; Verschure *et al.*, 1980) report a colour change in biotites from brown to green with recrystallisation and alteration, suggesting a change in composition with metamorphism. This is not seen here and both brown biotites, as in the Naij Tal pluton, and green biotites, from the Yie Nin Gou pluton, have similar compositions (see previous section for probe analysis) which do not appear to be related to degree of metamorphism. The large green Ti and Fe-rich biotites in the Wanbaogou pluton contain very small amounts of sphene and epidote suggesting little alteration, but the feldspars have been rendered almost indistinguishable due to alteration by hydrothermal fluids.

Samples from the Golmud Hydro Group show patchy recrysallisation of quartz but no real fabric is developed and both sphene and epidote are virtually absent. In the Golmud Junction samples close to the Golmud Fault however, shearing appears to have been almost as intense as on the Xidatan Fault. Some sphene is present in little aggregates,

while a small amount of clinozoistie mantles the opaques that appear to be being exsolved from the Ti and Fe-rich biotites. The hydrothermal alteration of feldspars is quite substantial, but is probably related to a late magmatic phase of volatile fluxing rather than a metamorphic event.

Metamorphic minerals in the Northern Region granitoids are restricted to minor amounts of prehnite and some secondary sphene. Clearly the metamorphic grade is less intense with increased distance north of the Xidatan Fault..

2.5.1 Reaction Mechanisms During Alteration

The mineralogical changes that occurred during alteration of the feldspars and micas involved the conversion of microcline, plagioclase and biotite to epidote, chlorite, sphene and muscovite. The change is unlikely to have occurred as a single reaction but would have taken place at different reaction sites in the individual minerals involving a fluid that contained both molecular and ionic species. This would result in several reactions proceeding simultaneously (Ferry, 1979). Mineral reactions which represent the observed phase changes can be written as seen below and are based on the work of Ferry (1979). Since compositional data for epidote and sphene are not available, it is assumed that chemical balance is preserved by ionic species in the fluid phase.

Where biotite is converted to chlorite and sphene, the following reactions approximate the observed mineral changes:

$$3 \text{ biotite} + 9\ H_2O + H^+ + Mg^{2+} + Fe^{2+} + Mn^{2+} + Ca^{2+}$$
$$= 1.5 \text{ Chlorite} + 0.5 \text{ Sphene} + 3\ H_4SiO_4 + K^+ + Na^+ \qquad (1)$$

For the alteration of micocline to muscovite:

$$3 \text{ microcline} + 10\ H_2O + 1\ H^+ + Fe^{2+} + Ti^{4+}$$
$$= 1 \text{ muscovite} + 5\ H_4SiO_4 + K^+ + Na^+ \qquad (2)$$

Where plagioclase is converted only to muscovite, such as in the Naij Tal pluton where epidote is relatively rare, then:

$$1\ \text{Ca plagioclase} + H_4SiO_4 + H^+ + K^+ + Na^+ + Mg^{2+} + Fe^{2+} + Ti^{4+}$$
$$= 1\text{muscovite} + H_2O + Ca^{2+} \qquad (3)$$

but where epidote is present, then a second reaction is required that proceeds simultaneously with (3):

$$2\ \text{Ca plag} + 1\ H_4SiO_4 + H_2O + K^+ + Na^+ + Mg^{2+} + Fe^{2+} + Ti^{4+} + Fe^{3+} + Mn^{2+}$$
$$= 1\ \text{epidote} + 0.5\ \text{muscovite} + H^+ \qquad (4)$$

Reactions (1) and (2) produce SiO_2, but where these are not observed as small grains in the altered biotite or microcline, it is likely that the silica left the sites dissolved in the fluid (H_4SiO_4) and was involved in other reactions, or precipitated elsewhere in the rocks. That no calcite is seen in these granites suggests that the rocks were in equilibrium with an essentially CO_2 free, H_2O fluid. The difference in metamorphic assemblages found in the sheared Xidatan and Golmud Junction plutons may be accounted for by differences in fluid composition and availability. The Golmud Hydro plutons are intruded into volcanics whilst the post -tectonic plutons intrude mainly Permian limestones.

CHAPTER THREE

3 GEOCHRONOLOGY

"How immeasurable would be the advance of our science could we but bring the chief events which it records into some relation with a standard of time!"

W.J.Sollas, 1900

3.1 INTRODUCTION

In an attempt to put the Kunlun batholith into the evolutionary context of the Kunlun Terrane and its relationship to the development of Tibet, it is important to have well constrained ages of intrusion, so that the timing of significanct tectonic events such as the collision of continents and subsequent uplift and unroofing can be understood. Here the geochronology of the batholith is considered fundamental in building up this tectonic picture, not so much for the absolute age of intrusions but more in terms of how the plutons relate to each other. For example, it is pointless trying to relate two adjacent plutons through petrogenetic modelling if 200 Ma separates them in time, although such a relationship does allow a comparison between their source regions and melting regimes.

Rb-Sr whole rock age determinations have been carried out on samples representing all eleven granitoid intrusions already examined petrologically in Chapter Two. Two outcrops of the Dagangou volcanic suite have also been analysed, as well as some granitoid pebbles from two conglomerate horizons that could not be dated stratigraphically, but were important in constraining periods of rapid uplift which would post date a collision event. Sample locality numbers are shown in Fig. 2.1, and analytical techniques are described in Appendix A. The isotopic ratios of $^{87}Sr/^{86}Sr$ were determined to better than ± 0.01%, 2 standard errors on the mean, whilst errors on the Rb-Sr elemental ratios determined by XRF are calculated to be ± 2% at the 2 sigma level. For all isochron calculations the isochron regression line was calculated using a computer programme written by D.W. Wright using the least squares approximation method of

York (1969). This formally defines an isochron as having an MSWD less than one. If however, the MSWD is greater than one then the correct definition is errorchron.

In a few cases it was found that one point on an isochron would greatly increase the MSWD and the error on the age, so in these instances it was left out of the age calculation but is still included on the diagram as a cross to distinguish it from the other points. It was considered that many points falling directly on the line were more likely to be representative of the true age than an age biased by one sample that is clearly anomalous. A scatter of points can be attributed to several causes that are considered below.

3.1.1 Scatter

One of the main causes of scatter has to be related to the fact that the region has been tectonically active for a long time (Kidd and Molnar, 1988), and is transected by many major and minor faults which may have acted as pathways for fluids. Low grade regional metamorphism and hydrothermal alteration to a greater or lesser extent can be seen in all plutons, as evidenced by saussuritised feldspars and the presence of secondary epidote, while samples in close proximity to faults display gneissic characteristics. Rubidium, a highly mobile element, may well have been mobilised by these fluids - in some cases perhaps only on the grain boundary scale - but in other instances it may have been substantially removed from the system. In other words, the assumption of a 'closed system' which is essential for the development of a perfect isochron is in reality, unrealistic.

Wickham (1987) showed that when melting sediments to form granites it may only be necessary to melt 40% before a melt is totally mobilised and Huppert and Sparks (1988) have calculated that up to 30% may remain as restite material in the melt. This would lead to an inhomogeneous melt which may be reflected in varying initial Sr ratios on the hand specimen scale. On the other hand, low degree crustal melts such as the High Himalayan leucogranites seldom provide whole rock isochrons (Deniel *et al.*, 1987).

Due to the nature of the geotraverse it was necessary to restrict the amount of material brought back, and therefore the granite sample sizes were usually less than 1 kg and may not always have been truly representative of the rock.

3.2 SOUTHERN REGION

3.2.1 Xidatan

Seven samples from this, the most southerly of all the plutons examined, define a well constrained isochron that gives an age of 190 Ma ± 7 (Fig. 3.1). Samples are shown to be a reasonable fit about the line due to the low MSWD of 3. Sample numbers prefixed by an X indicate those collected by someone other than Dr. N. Harris and there is often little information regarding field relations. Sample X67 was collected from the south-western edge of the Xidatan pluton, some 10 km away from the other collection site where it is truncated by the Xidatan Fault. It is considerably altered, containing at least 10% epidote, suggesting substantial fluid interaction. However, the low $^{87}Rb/^{86}Sr$ ratio is consistent with values obtained from other similarly less evolved granites in the region

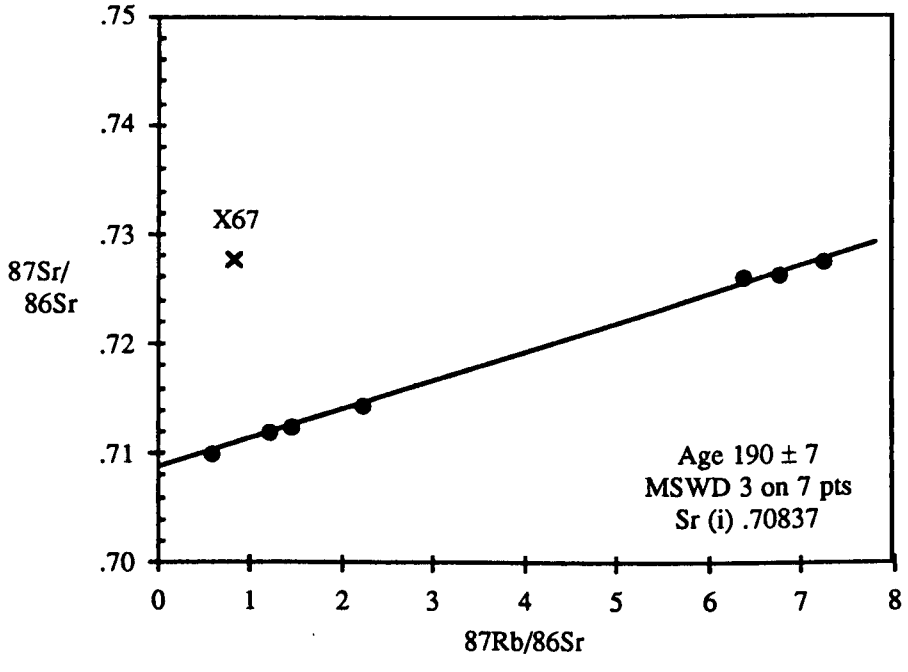

Fig. 3.1 The Xidatan pluton isochron gives an age of 190± 7 Ma

It is therefore considered likely that, rather than removing Rb, these fluids were from a more radiogenic source resulting in this sample having such a high $^{87}Sr/^{86}Sr$ ratio.

3.2.2 Yie Nin Gou and Naij Tal

Because of their petrographical similarities and close spatial proximity, it was considered that these two plutons may have been derived from the same source. However, although they are very similar both mineralogically and chemically, clearly the fact that they lie on two parallel isochron lines in Fig. 3.2 indicates that they must have had different initial ratios. This suggests that they were not co-magmatic, even allowing for the fairly large error on the initial ratio of Yie Nin Gou. The ages however, at 187 ± 21 Ma and 178 ± 10 Ma respectively, are within error both of each other and the Xidatan pluton .

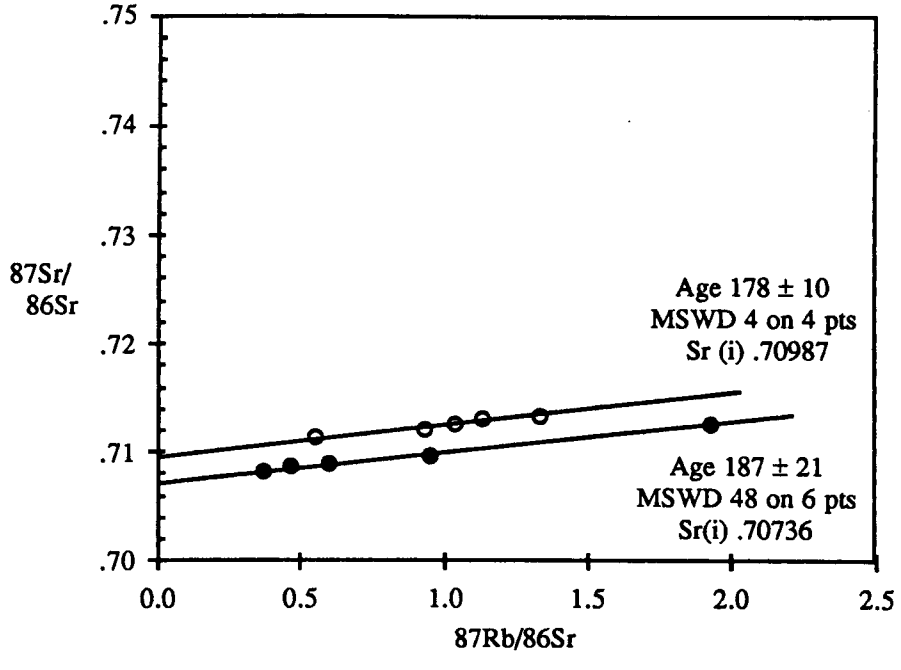

Fig. 3.2 The Yie Nin Gou (closed circles) and Naij Tal (open circles) isochrons give ages within error of each other, but the different initial ratios suggest separate, although similar, sources.

3.2.3 Wanbaogou

At 388 ± 10 Ma, the age of this pluton is in marked contrast to the others in the Southern Region, being some 200 Ma older (Fig 3.3). Clearly however, neither the boulders from the stream in the Wanbaogou Valley nor the small leucocratic stock fall on the isochron line defined by the 8 samples from the main body. That the mafic enclave does fall on the isochron line is evidence to suggest that it forms part of an earlier fractionate rather than being representative of the source or a restite fraction.

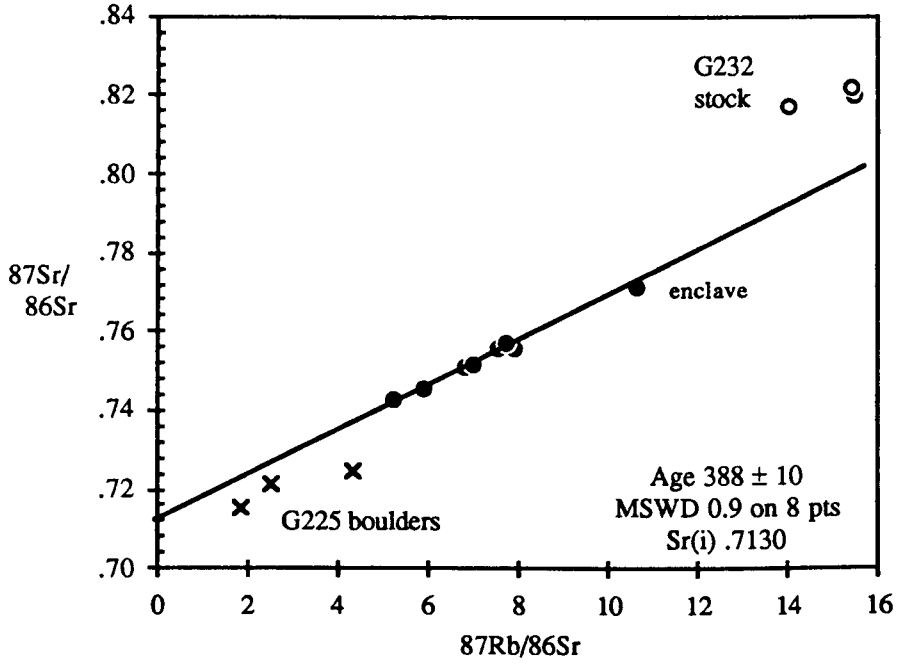

Fig. 3.3 The Wanbaogou isochron gives an age of 388 ± 10 Ma.

Taken on their own, the boulders define a very poor three point isochron at 267 ± 30 Ma with an MSWD of 22. For this reason they are not considered as part of the Wanbaogou suite, and although the age is close to that of the main batholith it is not clear which pluton they may have been derived from and therefore will not be considered in further discussions. The leucocratic stock on the other hand was subjected to the passage of hydrothermal fluids, as evidenced by the presence of tourmaline, at a late stage in its development and these fluids may well have removed Rb rendering the $^{87}Rb/^{86}Sr$ ratio lower than would be expected. Alternatively, the fluids may have been from a more radiogenic source thereby increasing the $^{87}Sr/^{86}Sr$ ratio with respect to the other samples.

The geochemical relationship of these samples to the main pluton will be examined in further detail in the geochemistry chapter.

3.3 CENTRAL REGION

3.3.1 Golmud Hydro Group

Samples were collected from both east and west of the Lhasa-Golmud Highway in this region and appear to define 3 ages of intrusion, although these are all very similar. Since field evidence indicates that the Little Granite is cut by the Central Granite, and intruded by porphyritic veins from the Pink Granite, it is concluded that the Little Granite was the first of the group to be emplaced. Indeed, the isochron defines an age of 261 Ma on four samples, which makes it the oldest of the group, but because the Rb-Sr spread is so small, the large error of ± 56 Ma, despite the low MSWD of 2, indicates a high degree of uncertainty. Both the Pink and Central Granites at 254± 2 and 248 ± 3 Ma have very similar initial ratios and isochron ages that are almost within error of each other (Fig. 3.4 a and b), and for this reason it is considered that they may well be co-magmatic. The

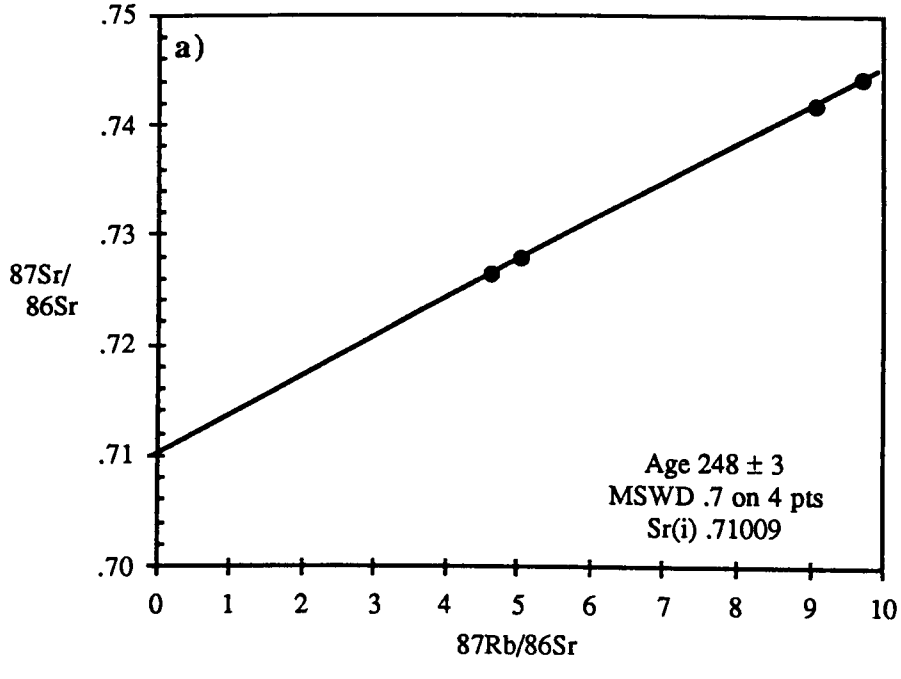

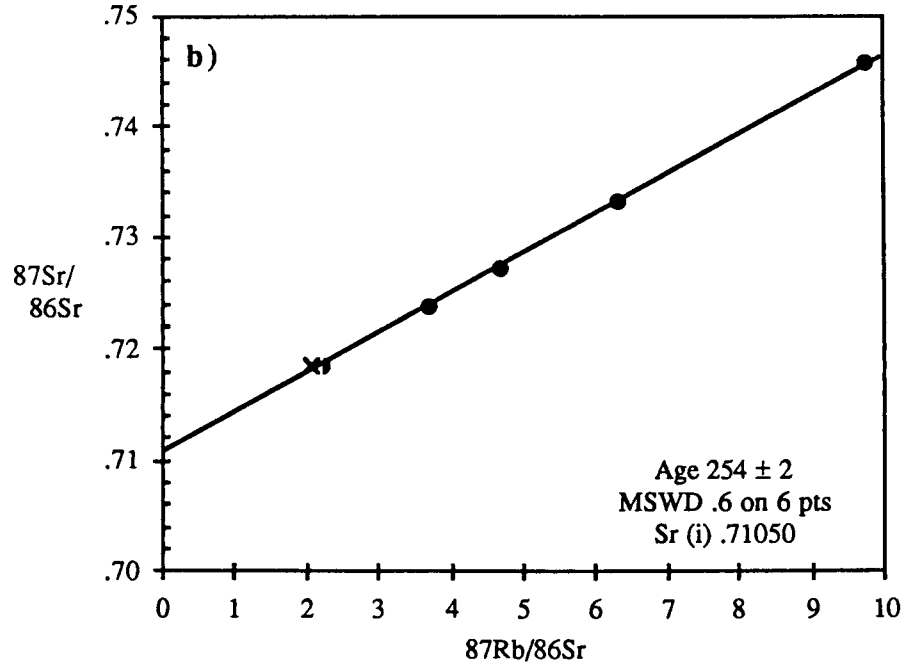

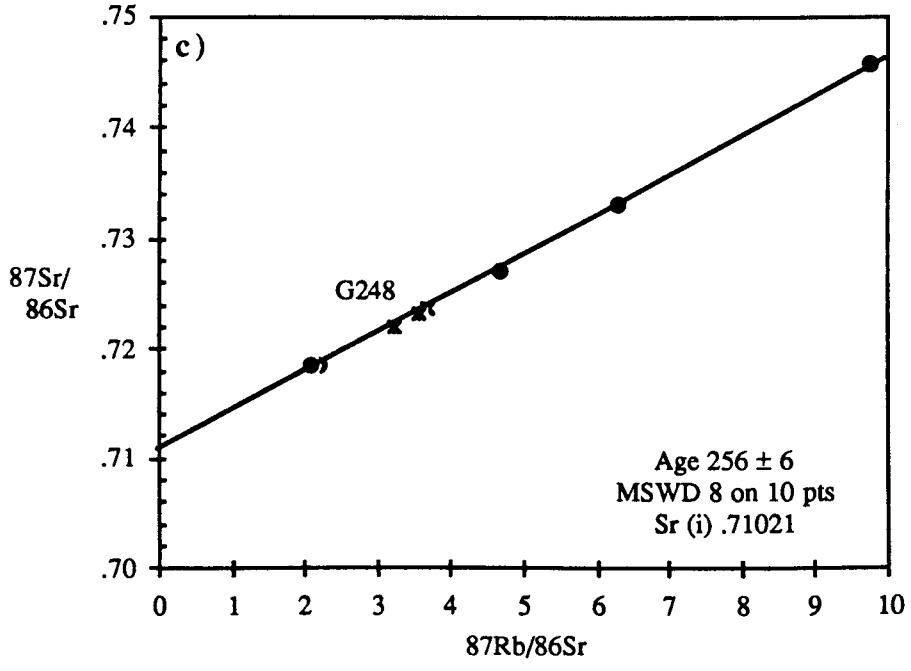

Fig. 3.4 The Golmud Hydro Group isochrons a) Central Granite, b) Pink Granite, c) Pink and Little Granites.

large error on the initial ratio of the Little Granite (.70974 ± 140) suggests it could be co-magmatic with the others. If it is included on the Pink Granite isochron (Fig. 3.4c) then this reduces the age to that within error of the Pink Granite, although increases the MSWD to 8 which implies a rather poor fit. It is hoped that geochemical modelling will

resolve this problem, but the age of 256 ± 6 for the Little Granite is considered more realistic and is within error of that obtained originally for these samples on their own.

3.3.2 Golmud Junction

A somewhat ambiguous age of 217 ± 20 was obtained from the 6 considerably altered samples representing this pluton (Fig. 3.5). The upper limit on the error is really still too low for it to be classified with the Golmud Hydro Group, as would be expected from its close proximity to them, and although the lower limit does place it just within the error boundaries for the Southern Region post-tectonic plutons, it did not have the field characteristics of a post-tectonic pluton and no others have been identified north of the Mid-Kunlun Fault. The Golmud Fault cuts the northern boundary of the Golmud Juction pluton and since this age of 217 Ma is actually closer to cooling ages obtained from biotites to the north of the fault (see Chapter 4), it is possible that this pluton was emplaced at more or less the same time as the others in the Golmud Hydro Group but has subsequently been reset.

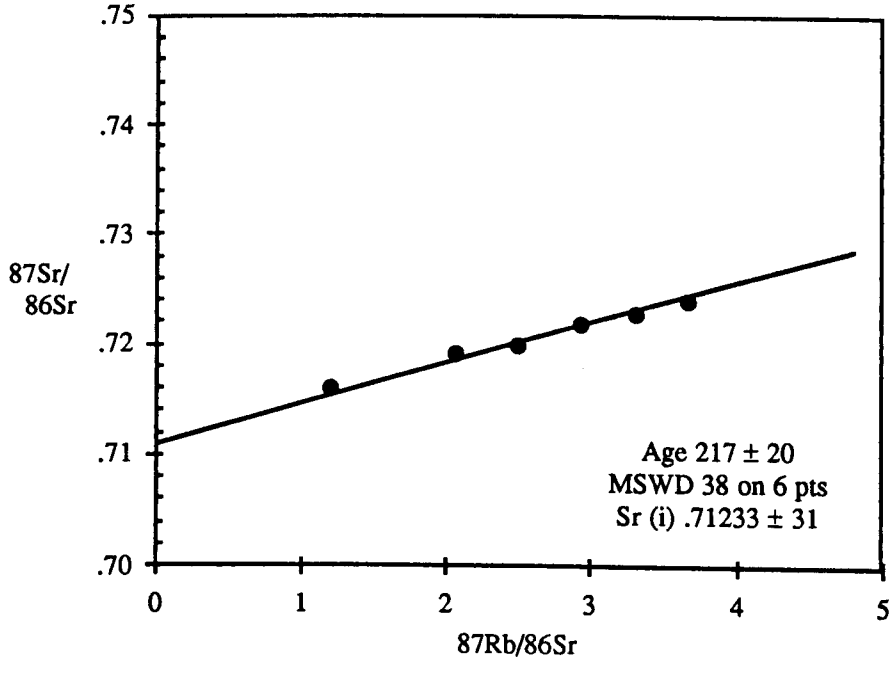

Fig. 3.5 The Golmud Junction isochron gives an ambiguous age of 217 ± 20 Ma.

If all the Golmud intrusions are plotted on the same isochron line they give an anomolously low age of 234 ± 8 with a very high MSWD of 63 (Fig. 3.6). However, it appears that the Central, Pink and Little Granites may have been derived from the same source, but have different evolutionary trends having fractionated from the melt at different times.

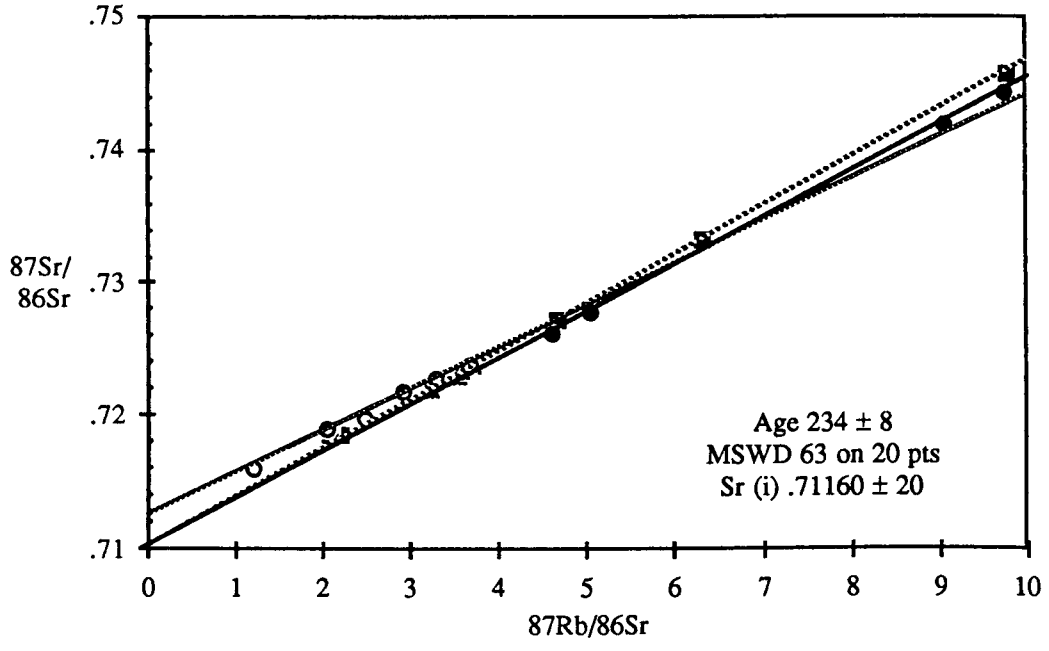

Fig. 3.6 Isochron lines for all the Golmud plutons. Closed circles = Golmud Central; closed squares = pink pluton; crosses = Little pluton open circles = Golmud Junction;

3.3.3 Dagangou Volcanics

The age of the Dagangou Volcanics has been a critical problem in establishing the provenance of the Kunlun Terrane. As described in Chapter One, samples for palaeomagnetic work were taken from the red-beds of the Dagangou Formation which apparently overlies the volcanics stratigraphically. However, the age of these red-beds is poorly constrained and only inferred to be earlier than middle Carboniferous from limestone fauna found much higher up in the sequence. It would have placed much greater constraints on this age if one could have been established for the underlying volcanics. Furthermore, the age of the volcanics is also significant in terms of

interpreting which phase of granitoid intrusion they are related to and it was hoped, despite both the regional metamorphism and hydrothermal alteration, that it would be possible to at least establish a greater degree of probability for either a Devonian or a Permian age.

Twelve samples represented in Fig. 3.7 were chosen from both north and south of the Dagangou valley to try and establish whether the two outcrops represented two different age groups as inferred by the Chinese geological maps. Samples included a rhyolite so

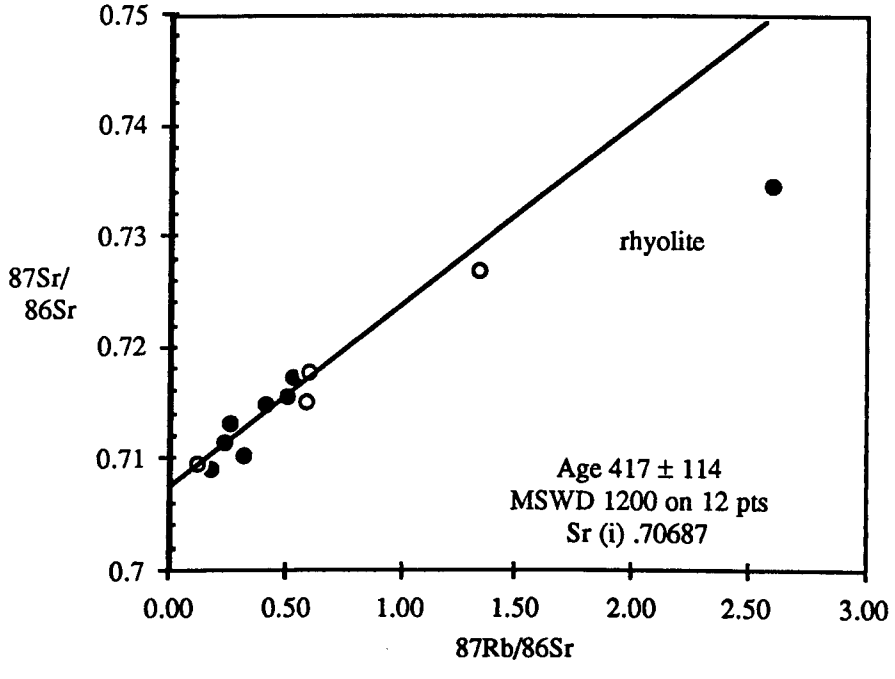

Fig. 3.7 The Dagangou Volcanics errorchron. Open circles = 'Devonian' samples from the north of the valley; closed circles = 'Carboniferous' samples from the south.

that a reasonable Rb-Sr spread was obtained. Unfortunately, as anticipated, the enormous MSWD of 1400 renders the calculated age of 417 ± 140 Ma almost meaningless, and there does not appear to be any distinct difference between the two groups north and south of the valley. The rhyolite, collected some 10km to the south of the valley and some distance from the other collection site, appears not to be related to all the others. However, it could be argued that being on top of the volcanic pile (Pearce

and Mei, 1988) and apparently furthest away from the batholith, the rhyolite is likely to have leen less affected hydrothermally and therefore represents a more accurate trend. Unfortuntely at this stage it is not possible to establish the age of this volcanic pile any more precisely. It should be noted however, that despite the large MSWD, the age obtained for the volcanics is within error of that given by the isochron of the Devonian plutons (Wanbaogou and Duo Ya He) at 414 ± 6 Ma (see section 3.4). This, coupled with the field evidence, does tend to suggest that a Devonian rather than a Permian age is more realistic for these volcanics.

3.3.4 Conglomerate Clasts

Several granite clasts from two conglomerate sequences north east of Naij Tal (G242 and G262) were analysed isotopically in an attempt to constrain the age of the plutons being eroded, and so to establish a minimum age of deposition for the conglomerate. Again this facies could not be dated palaeontologically and it was important to see which period of intrusion the clasts were related to since the conglomerate clearly represented an unroofing event resulting from uplift. Fig. 3.8 shows how the clasts analysed relate to isochrons from other plutons in the area that have established ages. Two of the clasts define an isochron with X67 to give an age of 760 ± 70. Knowing that X67 is related to the Xidatan pluton this seems coincidental. These samples could either represent reworked Precambrian basement that has become involved in the conglomerate, or they may have been affected by fluids in the same way as sample X67.

Two other clasts (G242 c and d) from the more northerly site fall on the isochron line of the Xidatan pluton. The G242 conglomerate lies some 50 km north east of the Xidatan pluton, and was probably much further away during deposition before extensive shortening occurred across this region. This is a considerable distance for 1.5 m boulders to travel. Furthermore, biotite cooling ages from the Xidatan pluton reveal that it was still at depth until at least the Early Cretaceous. Field evidence from the Naij Tal pluton suggests that the roof is still visible and since all these post-tectonic plutons appear to have been emplaced at much the same time and probably at much the same level, it seems

unlikely that the Xidatan intrusion was exposed as early as the Triassic, which has been the assumed age for this conglomerate. This leads one to conclude that either the conglomerate is post-Early Cretaceous and that the boulders have travelled at least 50 km from the south, or that it is coincidental that they fall on the Xidatan isochron and that infact they were derived from some unsampled pluton closer to the area of deposition. Despite the good fit on the isochron and the similar model Nd ages, the latter suggestion seems more likely. Unfortunately this does not constrain the age of the conglomerate, however, since both Permian and Devonian plutons are exposed today, it seems highly probable that both ages were being eroded when the conglomerate was formed, and it would be suprising if the age could have been determined any better.

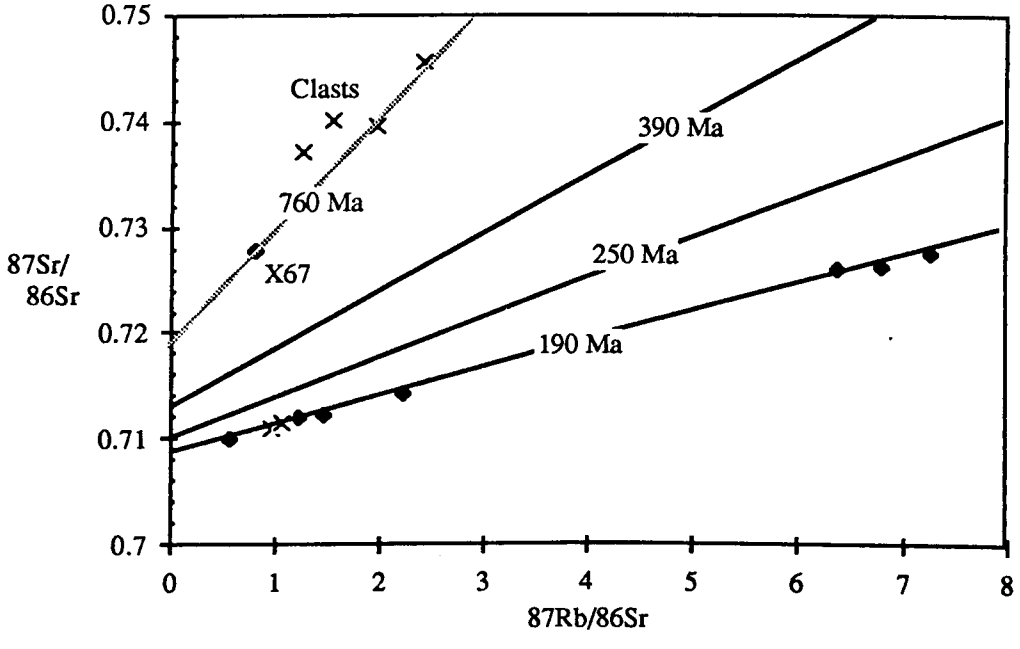

Fig. 3.8 Isochron lines for the three main age groups seen in the Kunlun Terrane. Crosses indicate the 6 conglomerate clasts analysed. The 760 Ma line is a hypothetical age line through X67. See text for discussion.

3.4 NORTHERN REGION

North of the Golmud Fault, all three localities sampled were tonalite or granodiorites with such low and consistent Rb-Sr values that it was impossible to obtain reliable whole rock isochrons from them. The East Quarry stock revealed a biotite-whole rock age of

258 ± 3 Ma, which is consistent with intrusion at the same time as the Golmud Hydro Group, but there is a pronounced fabric to this pluton and it would not be suprising if this was a reset age as a result of intrusion of the main batholith at this time.

From the Golmud East intrusion three populations of zircons were analysed by Xu Ronghua (Harris *et al.* 1988) and were found to give virtually concordant ages falling around 240 ± 6 Ma which is within error of the main period of intrusion. Finally, the age of the Duo Ya He pluton is again highly ambiguous. Due to the low Rb-Sr spread, the error of ± 160 Ma on an age of 382 Ma allows it to fall into any of the three age groups so far established. However, the fact that it also falls on the Wanbaogou isochron (Fig.3.9), and that samples from both plutons have similar model ages somewhat older than the younger groups, argues for an Early Devonian period of intrusion for the Duo Ya He pluton.

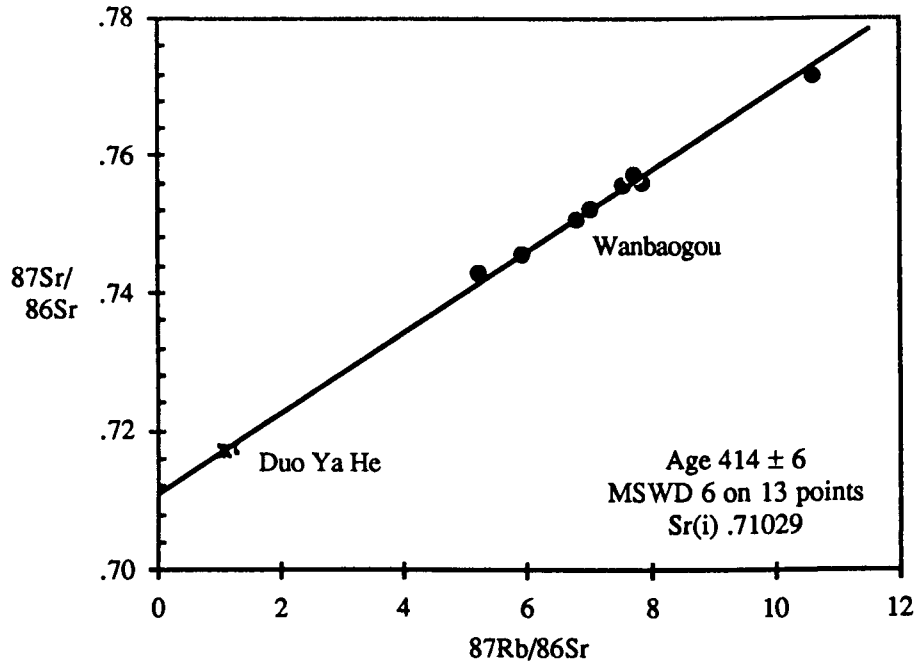

Fig. 3.9 The Duo Ya He pluton on the Wanbaogou isochron.

3.5 SUMMARY

From Table 3.1 it can be seen that three phases of intrusion have been indentified in the Kunlun batholith. The earliest of these occurred during the Early Devonian around 390 Ma and is represented by the Wanbaogou and probably the Duo Ya He plutons. The second phase started during the mid Permian and extended into the Earliest Triassic spanning a period of some 20 Ma in the geotraverse region from 260 - 240 Ma.

Pluton	Age	MSWD	Sr(i)	Method
SOUTHERN REGION				
Xidatan	190 ± 7	3	.70837 ± 7	whole rock
Yie Nin Gou	187 ± 21	48	.70736 ± 11	whole rock
Naij Tal	178 ± 10	4	.70987 ± 7	whole rock
Wanbaogou	388 ± 10	0.9	.71300 ± 52	whole rock
WBG boulders	267 ± 30	27	.70823 ± 67	whole rock
CENTRAL REGION				
Golmud Hydro Group				
Central Granite	248 ± 3	0.7	.71009 ± 13	whole rock
Pink Granite	254 ± 2	0.6	.71050 ± 8	whole rock
Little Granite	261 ± 56	2	.70974 ± 140	whole rock
Golmud Junction	217 ± 20	38	.71233 ± 31	whole rock
NORTHERN REGION				
East Quarry	258 ± 3		.71242	biotite
Duo Ya He	382 ± 160	11	.71078 ± 134	whole rock
Golmud East	240 ± 6		.70960	zircon

Table. 3.1 Summary of granitic emplacement ages in the Kunlun Terrane.

It appears that this represents the main period of batholithic emplacement although a very small area has been sampled and further work may reveal a wider age range such as that represented by the Gangdese batholith in southern Tibet. There, intrusion along the

2000 km length spans some 70 Ma (Deitrich and Gansser,1981; Harris *et al.*, 1988). To the south of the Mid Kunlun Fault, plutons are post-tectonic and range in age from 190 - 180 Ma representing the final period of intrusion. These constrain the timing of collision to a period between 240 and 190 Ma. Palaeontological data suggest it would have been about 200 Ma.

CHAPTER FOUR

4 THERMAL HISTORY OF THE KUNLUN TERRANE

"The total generation of heat from one gram of uranium when in equilibrium with all its products amounts in one year to 6.5 calories. In itself this is a trifling quantity . Its real meaning can only be grasped when the total amount of uranium in the earth is taken into account, and when it is realised that out of 7,000 million atoms of that uranium, only one disintegrates during a single year. What is the effect of this slow but never failing supply of heat on the earth?"

A. Holmes, 1915

4.1 INTRODUCTION

The uplift and thickening of the Tibetan Plateau is one of the more controversial subjects in geology today. At an average elevation of 5000 m, it is the highest plateau in the world, and beneath it lies some of the thickest crust. Seismic data show that the crust along the Himalayan Front is 45 km thick and that it sharply increases in thickness up to the Zangbo suture (Fig. 4.1). North of the suture the thickness remains at a fairly constant 70 km up to the Kunlun Shan, where it drops to approximately 56 km north of the Xidatan Fault (Zhao and Morgan, 1985; Zhang *et al.*, 1984). From our knowledge of the northward movement of the Indian plate it appears that more than 1500 km of crust needs to be accounted for by subduction or intracontinental compression since the initial collision at 45 Ma (Achache *et al.*, 1984; Searle *et al.*, 1987). Many theories claim to account for this, which broadly fall into three categories:

1 Shortening and stacking of the Tibetan crust due to collision with India (England and Houseman, 1986), resulting in the extrusion of Tibet to the east along massive strike -slip faults (Molnar and Tapponnier, 1975 and 1978; Burke and Sengor, 1986; Tapponnier *et al.*, 1982 and 1986).

2 Underthrusting of India below Tibet resulting in isostatic uplift (Bird,1978; Powell and Conaghan, 1979; Powell, 1986).

3 Injection of magma into or at the base of the crust (Zhao and Morgan, 1985 and 1987; Zhao and Yuen, 1987).

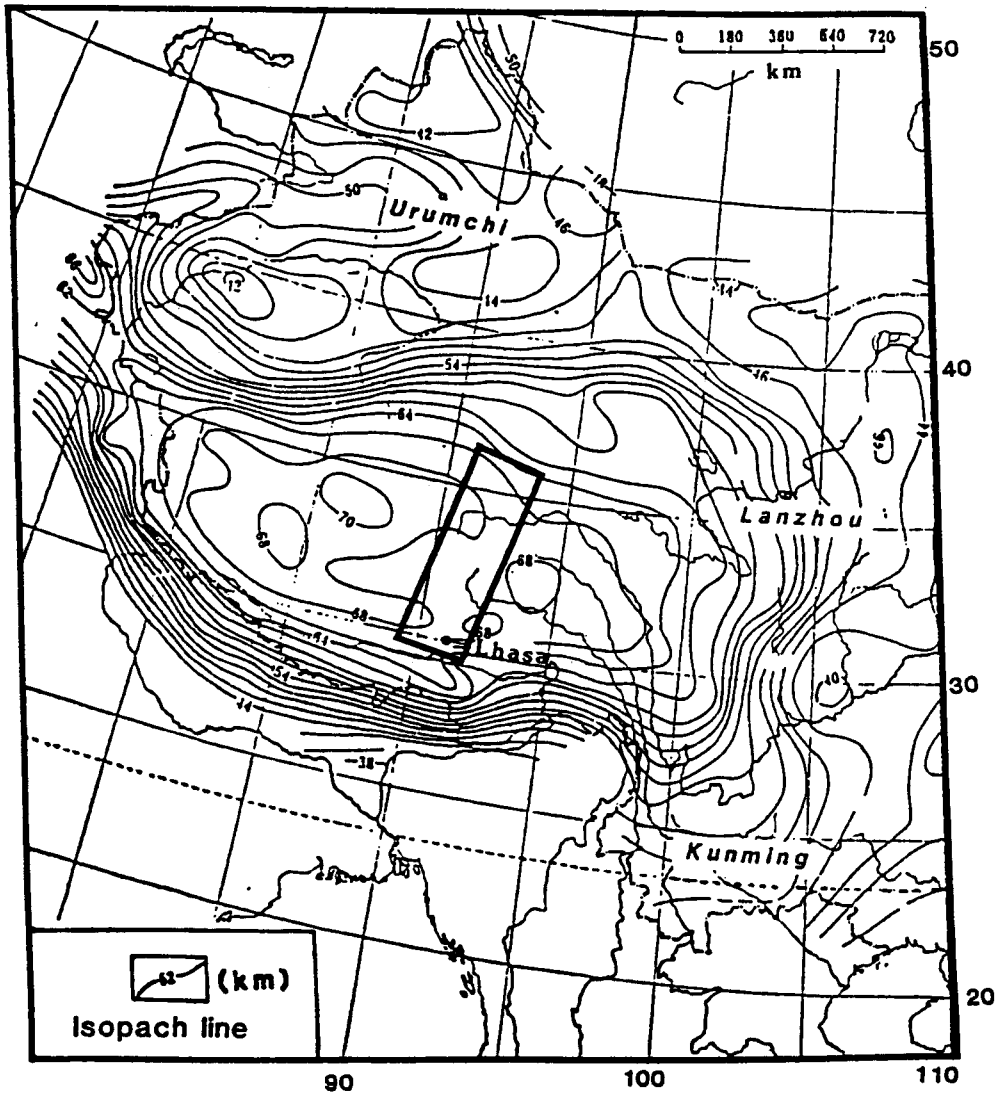

Fig. 4.1 Isopach map showing crustal thicknesses in Tibet. Boxed area represents the region covered by the Tibet Geotraverse route. Redrawn after Zhang *et al.* (1984).

From palaeo samples of flora and fauna collected in Tibet, Li *et al.* (1981) and Xu (1981) claimed that the elevation of Tibet could not have been greater than 1 km up until the end of the late Pliocene, and that consequently the uplifting to its current altitude of some 5 km must have occurred during the last two million years. Other workers however, believe that the uplift process was a more gradual one and that it has been occurring since the collision with India some 45 Ma ago (Dewey and Burke, 1973; Hirn

et al., 1984 a and b; Chang *et al.*, 1986;, Molnar *et al.*, 1987; Copeland *et al.*, 1987). Undoubtedly, accurate information on the timing of this uplift across the plateau would be of great value, since this would help to constrain the mechanism by which uplift occurred - the time available for uplift being itself a limiting factor. All previous uplift studies have so far concentrated on the southern edge of the plateau (Zhao and Morgan, 1985; Zeitler 1982 and 1985; Copeland *et al.*, 1987). In particular, the work by Copeland *et al.* showed that the section of the Gangdese batholith examined by them uplifted in discrete pulses, with the most rapid phase occurring between 20 and 17 Ma when uplift rates approached a peak of 4.4 mm/yr (Fig. 4.2).

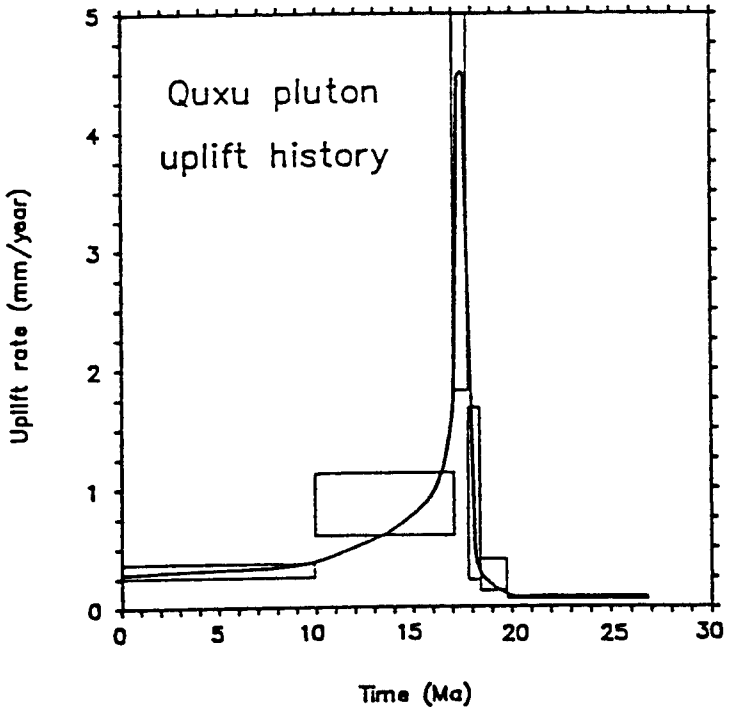

Fig. 4.2 Uplift history of the Quxu pluton for the last 30 Ma. Uplift rate for the interval 17.8 to 17 Ma is 4.4 mm/yr. After Copeland *et al.* (1987).

Unfortunately there is so little exposure of suitable granitoid material for this type of dating in the centre of Tibet, that a complete examination of the whole plateau was not possible. However, it was considered that a similar study carried out on granites from the Kunlun Terrane would allow uplift comparisons to be made with data from the south. In particular, an investigation into whether effects of the Indian collision with Tibet could be

identified in the granites of the Kunlun Shan, some 1200 km to the north, was considered worthwhile.

The techniques applied were the Rb-Sr method on whole rocks and separated biotites, and the fission track method on separated zircons and apatites. Some K-Ar data were already available from Chinese colleagues (Harris *et al.*, 1988) and Peter Copeland (pers. comm.) subsequently provided invaluable Ar-Ar data on feldspars and biotites from two of the Kunlun plutons. The fission track work was done at Berne University, Switzerland under the guidance and continual encouragement of Dr. Tony Hurford. The granitoids, which were not originally collected with this study in mind were less than ideally suited for such work, the main problem again being that of small sample sizes. Nevertheless this study gives an important preliminary insight into the thermal history of the Kunlun Terrane.

The data are presented as age information where the age of a mineral is calculated from the accumulated products of radioactive decay. Radioactive parent isotopes decay to radiogenic daughter products, and the resulting age represents the point in time at which the daughter product becomes 'immobile' when the term 'mobility' refers to the rapid diffusion from the lattice site at which the radiogenic isotope was formed. There is a strong dependence of diffusion rate upon temperature. At high temperatures the daughter escapes as soon as it is formed, but at low temperatures the rate of escape under normal conditions is negligible and so it can accumulate undisturbed. The temperature at which a particular mineral starts to accumulate daughter products is termed the 'closure' or 'blocking' temperature. It will depend on the exact cooling history of a particular system, but will be independent of the starting temperature as long as the latter is sufficiently high. However, if during subsequent tectonic events, such as metamorphism, the temperature of the system is raised above the closure temperature, then the element in question will again become mobile, fully or partially resetting the apparent ages.

The range of techniques applied allowed access to information over a wide range of closure temperatures, which are generalised in Table 4.1 below. As mentioned above, the

exact closure temperature of a mineral is dependent upon its cooling history. Rapid cooling leads to higher closure temperatures, while very slow cooling may result in the mineral closing at much lower temperatures. This will be assessed in more detail as each technique is discussed in the following sections.

Mineral	Method	Closure T °C
Biotite	Rb/Sr	300
Biotite	K/Ar	260
K Feldspar	Ar/Ar	250
Zircon	Fission track	200
Apatite	Fission track	100

Table 4.1 Approximate closure temperatures for the range of minerals and techniques used in this study.

4.2 THE RUBIDIUM - STRONTIUM METHOD

Of all dating techniques, the Rb-Sr method is the most versatile because it can be applied to total rock samples and isolated minerals for the dating of magmatic intrusions, mineral crystallisation and metamorphism. As seen in Chapter 3, this technique has already been successfully applied to determining the intrusion age of many of the plutons from the Kunlun Shan. In this study it is applied to the biotites from these plutons in an attempt to place high temperature constraints on the fission track work (which utilizes the fact that certain minerals have low closure temperatures to fission tracks), and to identify any high temperature metamorphic episode seen in the biotites that would not be overprinted by later lower temperature events which may reset the fission tracks.

Previously the technique had not been run routinely at the Open University. On the occasions when it had been investigated the problems encountered with high Rb interference made it difficult to reproduce results. The extremely wide variation of Rb-Sr ratios ranged from as low as 12 in biotites from the less evolved granodiorites, to an order

of magnitude larger at 130 in biotites from the more highly evolved 'S' type granites. The latter in particular proved very difficult to run as Rb values were often in excess of 1000 ppm and tended to swamp the low levels of Sr. Several months were therefore spent investigating these problems and improving the techniques used until acceptable levels of reproducibility were achieved. Discussions with Marcus Flisch at Bern University where the technique has been routinely run for many years, proved very helpful. Details of the technique can be found in Appendix A. After analysis a two-point isochron is obtained using the Rb/Sr and $^{87}Sr/^{86}Sr$ ratios from both the whole rock and biotites to calculate the age at which the biotite reached its closure temperature.

Closure temperatures are strongly dependent upon the rate of cooling. Theoretical closure temperatures for biotites with a 1mm diameter range from 311°C at a cooling rate of 30°C/Ma, to 250°C at 3°C/Ma (Hofmann & Giletti, 1970). Alpine biotites with known ages of 10 and 20 Ma have calculated closure temperatures of 288°C and 268°C respectively (Dodson, 1979), the difference being a result of their different cooling rates. However Dodson warned against applying his calculations to Mesozoic or older orogenic belts, within which rocks being sampled today may have spent considerable periods of time at depths of several kilometres. This may result in the body cooling to a steady temperature, at which diffusion is significant over the life of the system, as is clearly likely to be the case in the Kunlun Shan granites.

4.3 THE POTASSIUM - ARGON METHOD

The K-Ar values presented here were analysed by Dai Tong-mo at the Academia Sinica, Beijing. Details of the exact analytical techniques are unknown but assumed to follow conventional methods, as described by Hunziker (1979). One of the common problems associated with this technique is that of inherited argon, which may give $^{40}Ar/^{36}Ar$ ratios quite different from the atmospheric ratio of 295.5 with which ages are normally calculated. This is particularly common in polymetamorphic terranes, in which the radiogenic argon from a former metamorphic event is partially or completely released by subsequent metamorphism. This then either finds its way into the atmosphere or

becomes trapped in minerals. High pressure low temperature terranes in particular suffer from inherited argon, and the calculated ages are then without geological significance. Alternatively, large intrusions being emplaced into cold crust may release substantial amounts of radiogenic argon from the wall rocks, which becomes incorporated into the magma and hence the crystallising minerals. This will induce an apparent age that may be much older than the actual closure age of the mineral to ^{40}Ar or even than the intrusive event itself (Hebeda *et al.*, 1980).

4.4 THE $^{40}Ar/^{39}Ar$ METHOD

The theory and analytical techniques are generally similar to those used for conventional K-Ar dating. The main difference is that no direct chemical analysis of K is required, since it is measured as a function of ^{39}Ar, which is produced from ^{39}K by neutron activation. Consequently, only the measurement of the ratio of ^{40}Ar to neutron-produced ^{39}Ar is required for age determinations. Following irradiation a sample may be totally fused and all the liberated argon analysed in a single experiment, thereby obtaining an age roughly analogous to a conventional K/Ar age. However, the great advantage of the Ar-Ar technique is through the step-wise (incremental) heating of the irradiated samples. At each temperature increment an apparent age can be calculated from its $^{40}Ar/^{39}Ar$ ratio; thus a series of ages can be generated which are expressed as an accumulative percentage of the ^{39}Ar released. Characteristics of the age spectrum can then be evaluated and a more complete geochronological picture may be obtained. In particular, the probability of excess Ar in the system can be more readily assessed. Two Kunlun Terrane plutons were analysed in this way by Peter Copeland at Albany, New York.

4.5 THE FISSION TRACK METHOD

Fission tracks are formed as the original nucleus of a heavy element such as U breaks up, by spontaneous fission, into 2 lighter nuclei of approximately equal mass liberating about 200 Me V of energy. Due to the Coulomb repulsion between the two highly charged fragments, the two fission nuclei fly apart at 180° to each other creating a single

fission damage track in the enclosing atomic lattice. Although the exact way this happens is not completely understood, the Ion Explosion Spike Mechanism (Fleischer *et al.*, 1965) is a widely accepted model. The two fragments are highly positively charged and are driven apart with great force, stripping electrons from the atoms of the host lattice which lie in their path in an attempt to restore their charge balance. This leaves a zone of positively charged ions which mutually repel each other forcing themselves into the lattice interstices thereby creating a damaged zone or fission track which is typically 10-20μm long and a few angstroms wide (Fig. 4.3). The numerical density of these tracks is related 1) to the rate of fission decay and consequently to the time that they have had to accumulate; 2) to the original uranium content of the host and 3) to the track length,which determines the probability of a track cutting a given plane.

A number of different types of charged particle tracks exist and the length and shape of these tracks are dependent upon the type of particle forming them. In terrestrial samples however, there is only one common, naturally occurring track: the uranium fission track. Most of the other types of natural tracks are found in meteorites and lunar materials caused by cosmic-ray interactions. But, because the earth's atmosphere absorbs most of the cosmic rays capable of forming a track, these tracks are not seen in terrestrial material. Three naturally occurring isotopes fission spontaneously: ^{232}Th, ^{235}U and ^{238}U, but only ^{238}U produces a significant number of fission events because the other two have such

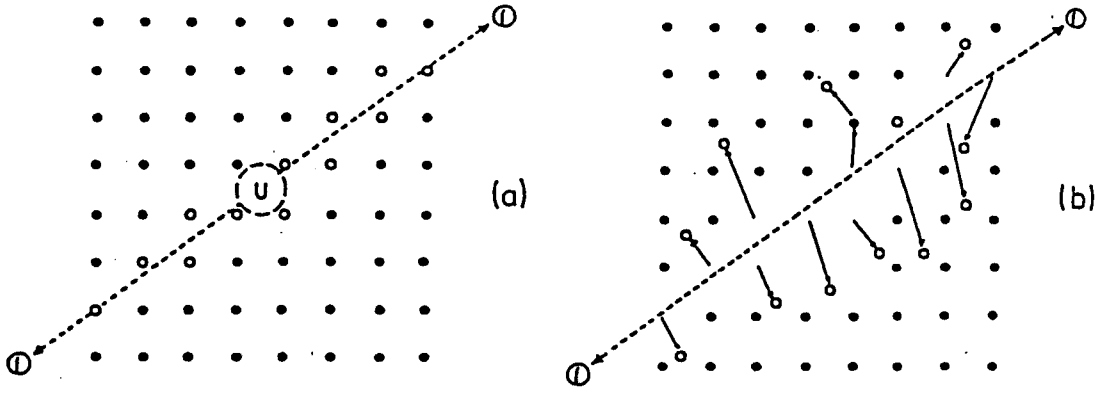

Fig.4.3 Ion explosion spike model for the formation of fission tracks. Redrawn after Fleischer *et al.* (1965).

long half lives for spontaneous fission that for all practical purposes, observed fission tracks can be assumed to be produced only from ^{238}U.

The three most common minerals in which tracks are counted are zircon (Plate 4.1), apatite and sphene, although when the uranium content is high enough garnet, epidote, micas and volcanic glasses can also be used. A given mineral can then be dated if uranium is present in sufficient quantities and if enough time has elapsed since its formation for it to have accumulated a significant number of tracks. Tracks in their normal state are too small to be seen except with an electron microscope, but by choosing the right chemical etchant it is possible to enlarge the tracks without dissolving the crystal, so that they can be seen under an optical microscope at magnifications as low as 200. For counting purposes 1000 - 1500 x is generally used.

There are a bewildering number of methods described in the literature as to how to handle and process samples for fission track dating, but only two are now commonly in use - the population and external detector methods. In this study, due mainly to the small amount of sample available, only the external detector method (EDM) was used and therefore only this technique is described in Appendix B. After preparation of the sample, a small sliver of mica with a very low uranium content is placed up against it - this is the external detector - and sample and detector are sent to the reactor to be irradiated.

The object of irradiating the samples is to induce a second set of tracks in the sample, which will allow the calculation of the uranium content. It is important therefore to realise that thermal neutron irradiation, i.e. irradiation with low energy neutrons ($\sim$ 0.025eV), causes only ^{235}U to fission. Using the external detector method this second set of induced tracks is registered in the mica adjacent to the sample; these will then be etched and counted. The geometry factor assumes that tracks are revealed equally, both in the sample and in the mica, an assumption which is valid if crystals are selected for counting according to a set of strict criteria (Gleadow, 1978 and Naeser *et al.*, 1980). A second set of tracks will also have been induced in the sample, but since they are not

etched after irradiation these are not seen and do not interfere with the original set produced by the spontaneous fission of ^{238}U. By knowing the isotopic abundance ratio of $^{235}U/^{238}U$ (7.2527×10^{-3}) the U concentration can then be calculated.

As for other radioisotopic systems, the age equation for fission track dating presents a ratio of the number of parent atoms (ρ_i) still remaining to the number which have already undergone radioactive decay (ρ_s), and its expression has a very similar format:

$$t = \frac{1}{\lambda_D} \ln \left\{ 1 + \frac{\lambda_D \phi \sigma I \rho_s}{\lambda_f \rho_i} \right\} \qquad (1)$$

where

λ_D = the total decay constant of ^{238}U = (1.55125×10^{-10} yr $^{-1}$)

λ_f = the spontaneous fission decay constant of ^{238}U (anything between $6.85 - 8.42 \times 10^{-17}$ yr $^{-1}$)

I = the isotopic abundance ratio of $^{235}U/^{238}U$ (7.2527×10^{-3})

σ = the nuclear cross section of ^{235}U for fission induced by thermal neutrons = 580.2×10^{-24} cm^2 or 580 barns)

ϕ = the thermal neutron fluence (time intergrated flux or the no. of neutrons per cm^2 that pass through the sample per unit time = n cm^{-2})

ρ_s = the spontaneous track density

ρ_i = the induced track density

However, whilst ages may be calculated this way, problems immediately arise because the spontaneous fission decay constant of ^{238}U is unknown and the neutron fluence is very difficult to measure accurately by conventional methods. Using these techniques the neutron-induced gamma activity in a metal foil placed in the reactor is counted electronically and the results are used to calibrate the system. But Hurford and Green (1982 and 1983) found this to be a potential source of systematic errors, which could result in poor age determinations.

Although the total decay constant of ^{238}U is well defined, it includes the decay of ^{238}U by alpha emission to form ^{206}Pb, which is 6 orders of magnitude more frequent than spontaneous fission (and Arthur Holmes has already pointed out how infrequent that is!). Suggested values for the spontaneous fission decay constant are 6.85 $x10^{-17}$ yr^{-1} (Fleischer and Price, 1964), 7.03 x 10^{-17} yr^{-1} (Roberts *et al.*, 1968) and 8.42 x 10^{-17} yr^{-1} (Spadavecchia and Halm, 1967; Wagner *et al.*, 1975). Clearly there is a significant difference between the three values and little agreement in the literature as to which is the more acceptable. Furthermore, since many experiments to determine the value for the decay constant have employed thermal neutron irradiation procedures to evaluate the uranium content of the fission source, the two values are clearly interdependent and cannot be considered separately, so that it is not simply a matter of declaring which value for the decay constant has been used. Therefore, a procedure that circumvents the need for an explicit evaluation of the spontaneous fission decay constant, or an absolute determination of the thermal neutron fluence, must be advantageous.

4.5.1 Zeta Age Calibration

In 1982 Hurford and Green first tested the concept of zeta age calibration originally proposed by Fleischer and Hart (1972). It is now widely used and involves the technique of glass dosimetry. Here a glass with a precisely known U concentration is included at intervals in the irradiation package along with standards of an accurately known age determined by alternative isotopic methods. An external detector is placed against both the glass dosimeter and the age standard, and registers the tracks produced by the induced fission. These tracks are then etched and counted in the same way as the sample, so that by knowing the track density in the dosimeter mica for a given amount of U, the neutron dose can be evaluated. As for the irradiation of Ar-Ar samples, the neutron flux is inhomogeneous over short distances and therefore must be calculated from several dosimeter glasses placed at regular intervals along the irradiation package. Once the induced and spontaneous tracks in the standard and the induced track density of the relevant dosimeter glass have been counted, then the zeta factor for that glass can be evaluated using the following equation:

$$\zeta = \frac{\exp(\lambda_D t_{std}) - 1}{\lambda_D \, (\rho_s/\rho_i)_{std} \; g \; \rho_d} \qquad (2)$$

where

λ_D = total decay constant of ^{238}U

t_{std} = known age of the standard

$(\rho_s/\rho_i)_{std}$ = ratio of spontaneous to induced tracks in the age standard

g = geometry factor = 0.5

ρ_d = track density of relevant dosimeter glass now representing the neutron flux

The simplified age equation can now be written in terms of three track densities and a proportionality factor - zeta (ζ):

$$t = \zeta \left(\frac{\rho_s}{\rho_i} \right) \rho_d \qquad (3)$$

Over a period of time, each worker will acquire a unique zeta value for each type of dosimeter glass used. It will also vary according to the mineral being examined and the counting conditions. Table 4.2 shows my apatite zeta factors for dosimeter glass SRM 612 compared to Tony Hurford's taken from published data in 1983 (Hurford and Green, 1983), when he already had considerable counting experience. Since then however, his value has decreased to a constant 339 ± 5, where it has remained for several years. Beginners tend to have high values reflecting their lack of experience in recognising tracks and inaccurate counting. Ideally, many zeta values are determined before unknown samples are counted. However, it should be borne in mind that for this study time was very limited and it was not possible to count as many zetas as I could have wished. It is significant though, how my average zeta had improved after counting my samples, compared to the inexperienced value obtained before counting. Nevertheless the combined average of 376 ± 19 was used for age determinations. In an attempt to reduce bias when counting, samples were not labeled with recognisable sample numbers and ages not calculated until all samples of each mineral type had been counted. This required sustained will-power over several weeks!

ZETA VALUES

LEWIS 1987	HURFORD 1983
370 ± 30	378 ± 29
358 ± 26	361 ± 17
405 ± 46	340 ± 16
392 ± 51	345 ± 15
397 ± 34	341 ± 32
Average (Before samples counted) **384 ± 20**	321 ± 20
349 ± 35	398 ± 26
372 ± 47	317 ± 12
359 ± 39	352 ± 16
382 ± 35	342 ± 16
Average (After samples counted) **366 ± 15**	**Average 350 ± 24**
Total average 376 ± 19	**Average now 339 ± 5**

Table 4.2 Zeta values before and after counting samples compared to Hurford's 1983 results for dosimeter glass SRM 612.

Zircons from the Kunlun samples were small, strongly zoned and with an uneven distribution of uranium making for difficult counting. Track densities were frequently as high as 20 x 10^6 tracks/cm^2 so it was often possible to count only small regions of each crystal. Ideally, 20 crystals are counted per sample but the small quantity and poor quality of these samples rarely made this possible. Nevertheless, the calculated ages fit well on the age curve between the higher and lower temperature constraints obtained from the biotites and apatites and are therefore considered to be reasonable estimates. The apatites had the opposite problem, with the uranium content being so low and the ages relatively young, so that many crystals contained very few tracks. Consequently a misidentification could make a large difference to the track ratio. However, four apatite samples were recounted, and all were found to be within error of the first count, so confidence in the apatite ages is high.

Ages are calculated for each individual crystal within a sample, and the results subjected to a chi-squared test, which statistically analyses the spread of data (Galbraith,

1981). When a sample fails the test, the age is calculated using the mean track ratios of the individual crystals (ρ_s/ρ_i). When the test is passed, the age is calculated using the total track ratio (N_s/N_i) from all crystals.

4.5.2 Closure Temperatures

The principles of track accumulation are identical to all other isotopic decay systems. Tracks will only start to accumulate once the mineral has closed below its closure temperature and, as with other systems, this appears to be strongly dependent upon the cooling rate. If the temperature is subsequently raised above the closure temperature, the tracks will start to anneal or fade. Track annealing occurs progressively over a temperature range termed the annealing zone or zone of partial stability. Annealing experiments with apatite give some idea of the track stability for different annealing times and temperatures. For example, the temperatures required to reduce the track density in an apatite by 50% for different heating times extrapolated from experiments (assuming a constant activation energy at all temperatures) are (Wagner, 1968):

Duration of heating	Temperature °C
1 hour	336
10 yr	196
10^6 yr	122
10^9 yr	69

For a cooling rate of 10°C/10^6 yr Wagner and Reimer, (1972) calculated that no tracks are stable above 190°C, 50% are stable at 125°C and all tracks are stable below 70°C. By 1977, however, Wagner *et al.* suggest for that cooling rate that the upper and lower thresholds are 150°C and 55°C respectively, while for rates as fast as 1°C/10yr the limits are as high as 230°C and 125°C respectively. Theoretical treatment of experimental data by Dodson (1979) from Naeser and Faul (1969) suggests the following closure temperatures for various cooling rates of apatites:

Cooling rate°C/Ma	Closure temperature°C
30	105
10	98
3	92

and similar values were computed by Haack (1977):

10	94
1	78

while somewhat higher values at

3	105

have been extrapolated from observations made on naturally annealed tracks in the Eielson borehole (Naeser and Forbes, 1976). Note, however, that although this provides a general picture of the relation of time and temperature to annealing, new extensive laboratory annealing studies clearly indicate that a constant activation energy at all temperatures is an invalid assumption (Green *et al.*, 1988).

Results of laboratory annealing are usually presented in the form of an Arrhenius plot that relates the logarithm of time to the reciprocal of the absolute temperature required to produce a certain degree of track density reduction (Green *et al.*, 1986). In these plots straight lines, denoting conditions which produce an equal annealing effect, normally give a fanning array (Fig. 4.4) increasing in slope from total track retention to total track loss (Hammerschmidt *et al.*, 1984; Laslett *et al.*, 1987). These straight lines are interpreted in terms of activation energies (Fleischer *et al.*, 1965), which increase with the degree of annealing. The data are then extrapolated from laboratory to geological time scales. However, this usually predicts a wider range of temperatures over which annealing should be observed than is actually the case when boreholes samples are examined, as shown in Fig. 4.5 (Naeser, 1981; Gleadow and Duddy, 1981; Gleadow *et al.*, 1983). From the investigation of boreholes Gleadow *et al.* (1986) define the annealing zone to be between 70°C and 125°C. However, Green *et al.*, (1988) suggest the range is much greater at 20 - 130°C, while Green (1988) concludes that "there are no geological conditions in which tracks can be regarded as stable". Recent work by Crowley (1988),

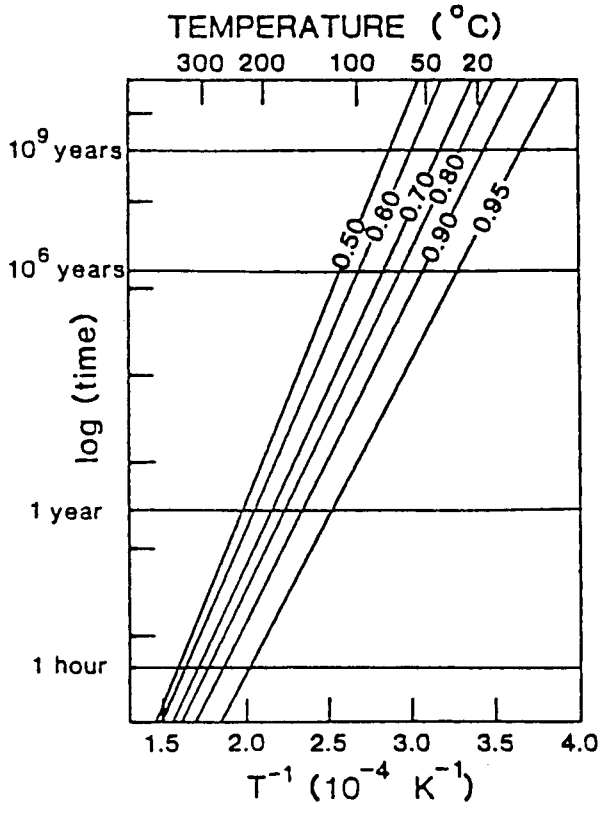

Fig. 4.4 A fanning Arrhenius plot using laboratory data extrapolated to geological time scales. Each line represents a specific degree of track retention. After Laslett *et al.*, (1987).

shows that annealing behaviour is highly dependent upon apatite composition and that chlorapatite is much more resistant to annealing than fluorapatite (Fig. 4.6), therefore future work on annealing experiments must take this effect into account.

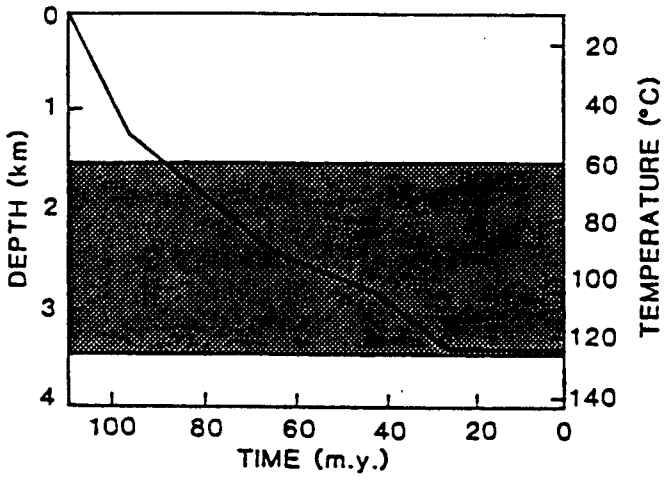

Fig. 4.5 An example of how fission track ages decrease with depth in a borehole. The shaded area represents the apatite fission track partial stability zone. After Gleadow *et al.*, (1981).

Data on zircon closing temperatures are much less abundant, but have to be constrained between about 300°C for the Rb-Sr closure temperature in biotite and 100°C for fission

tracks in apatite. Using this method Hurford (1986) interpolated a closure temperature for zircon to be 240 ± 50°C, but Harrison *et al.* (1979) place it much lower at 175 ± 25°C, although this may reflect a difference in cooling rates.

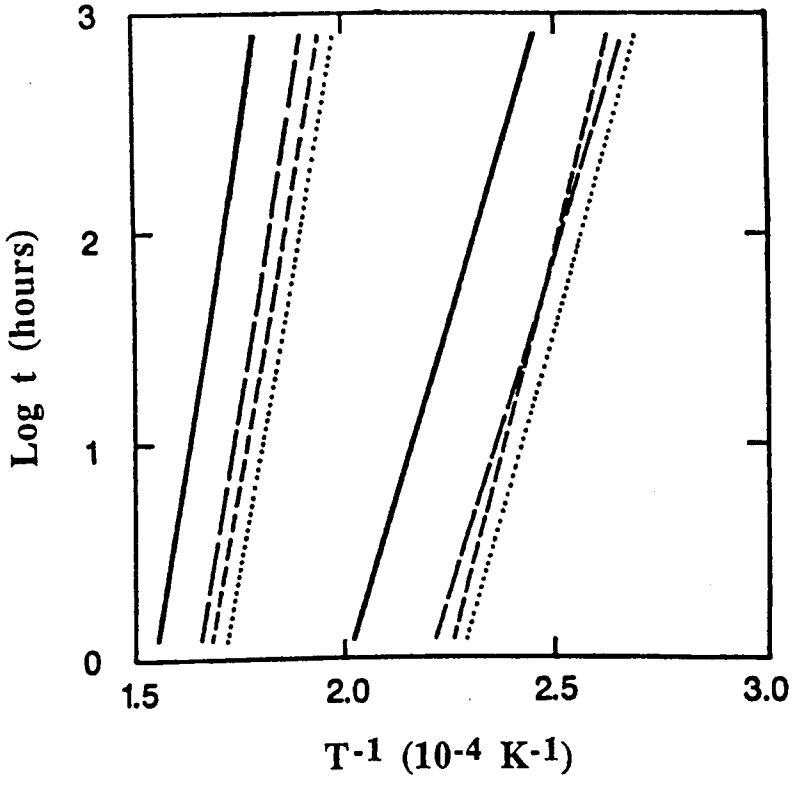

Fig. 4.6 Arrhenius diagram showing the zone of partial track stability for several apatite varieties. Solid lines, Cl-OH apatite; long dashed lines, Sr-F apatite; short dashed lines, F apatite; dotted lines, OH apatite. Redrawn after Crowley *et al.*, (1988).

From these studies it can be seen that there is as yet no conscensus on the 'closure temperature' of apatites and that when the term is used in reference to fission track samples, it has a somewhat different connotation to that in other isotopic systems.Generally, therefore, when a temperature is quoted as being a closure

temperature for fission tracks, it is assumed that this refers to the temperature at which 50% of the tracks became stable. Clearly, ages calculated from samples that have only been reheated into the annealing zone will be a mix of the original age and the reset age, and will therefore be geologically difficult to interpret. In this study the cooling rate and the closure temperature of apatite are assumed to be constant. Since cooling rates from biotite closure are very slow, this seems a reasonable assumption to make and facilitates the handling and modelling of data. The closure temperature of zircon is interpolated between biotite closure at 300°C and temperatures calculated either from the low temperature portion of the $^{40}Ar/^{39}Ar$ age spectra or from apatite closure, which is assumed to be 90°C.

4.5.3 Uplift rates?

Before examining the data the question must be asked as to what is represented geologically by fission track ages. Assuming the ages do not represent mixed ages as a result of having been partially annealed, a fission track age simply reflects the last time that the relevant mineral cooled through its closure geotherm. In this study this age will be referred to as the 'cooling age' (after Zeitler, 1985).

Once the cooling age has been determined, 'apparent' uplift rates (Parrish, 1983) can then be calculated in several ways. If rocks are sampled at different altitudes in areas of large differential vertical relief, ages at the top will be older than those at the bottom. The height difference divided by the age difference will give an apparent uplift rate. Alternatively the mineral-pair method, which is the method used in this study, obtains an apparent uplift rate by making assumptions both about the geothermal gradient during cooling, and about the closure temperatures of the mineral-pair concerned. The temperature difference between the closure of the two minerals divided by the geothermal gradient will give the distance that the body has moved towards the surface in the time between the closure of the two systems. But ,as the term implies, 'apparent' uplift rates do not necessarily represent true uplift of the rocks relative to sea level or some other baseline. Prolonged erosion may eventually bring the rocks to the surface passing them through the closure geotherms as they move upwards, and geotherms will move

downwards with respect to a stationary rock column as a region cools. Uplift, erosion and the movement of geotherms are all highly interdependent. Therefore true uplift will only occur when the erosion rate is equal to the uplift rate and when the closure geotherms are horizontal and stationary throughout the period of uplift. Obviously it is difficult, if not impossible, to recognise whether these conditions have been met in the geological past; therefore extreme caution should be used when interpreting uplift rates.

In this study even the modified expression of 'apparent' uplift rates is considered misleading, because of the uplift implication, and the term 'surface approach rate' (SAR) is preferred. But, even when the uplift or surface approach rate has been established, it is clear, particularly in regions where the rates are very slow, that this is only an average rate between the closure temperatures of the mineral-pair. What is not revealed is whether there has been a thermal heating event during the period in question.

4.5.4 Track Lengths

At the time of formation all tracks will have a relatively constant initial length, which is controlled by the energy released during the fission decay and by the nature of the registering medium (Gleadow *et al.*, 1986). During thermal annealing, existing tracks become progressively shorter and will eventually disappear, while new tracks are being formed and themselves annealed if temperatures are still sufficiently high. In the temperature range over which apatite fission track dates give useful information, it is possible, by examining the distribution of track lengths in apatite, to differentiate between slow cooling and overprinting as a result of a thermal event. Lengths are measured only on horizontal internal or 'confined' tracks that do not cut the surface, but which are intersected either by another track or by a fracture in the mineral that does intersect the surface. In this way when the tracks are etched, acid has access to the confined track via the track or fracture that is exposed at the surface (Fig. 4.7), and the full length of the confined tracks

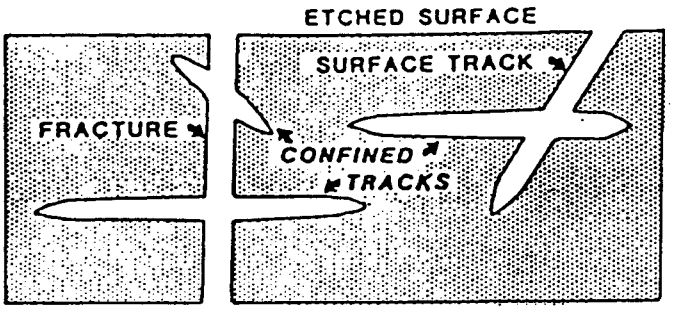

Fig.4.7 Diagram illustrating the etching of confined fission tracks used to measure track lengths. Such tracks are etched from fractures or other tracks which provide a pathway for the acid.

can be etched and then measured. If the measured track is not confined and almost horizontal then the true length cannot be fully assessed and the track distribution will be misleading. Ideally a hundred such confined tracks are measured in each analysis, but, where track density is very low, this is often not possible.

Gleadow *et al.* (1986) showed convincingly how the form of track length distribution in naturally annealed borehole samples depends upon the down-hole temperature. Tracks near the top of the annealing zone had a narrow distribution of long tracks, but with increasing depth and temperature there was a steady decrease in the track lengths and an increase in the length variation. The deepest parts revealed a broad, flat distribution with a mean length value of 50% of the initial unannealed lengths (Fig. 4.8).

Laboratory experiments showed very similar results, and a bimodal distribution was induced by annealing samples at 350°C for 1 hour. Fig. 4.9 shows a comparison of natural and induced track distribution in slowly cooled and overprinted samples. In reality though, a well-resolved bimodal distribution will only occur if the thermal event was fairly intense but of relatively short duration. If the period of heating is too long or short, a second peak will not be defined and the two distributions will merge. Nevertheless, a bimodal length distribution is clear evidence of a two-stage thermal history: a steady slow cooling thermal history will produce a broad, asymmetrical,

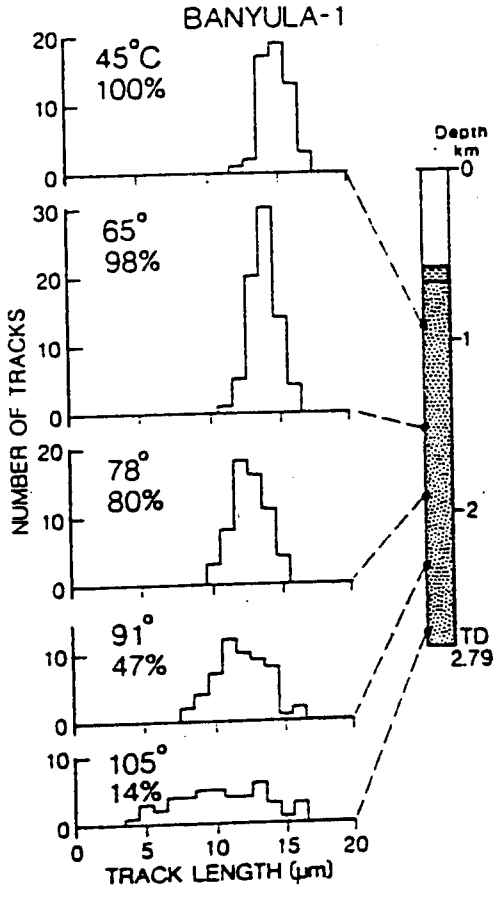

Fig. 4.8 Track length distributions observed in apatites from a hydrocarbon exploration well. The estimated formation temperature and the percentage to which the apparent fission track age has been reduced is also shown for each length distribution. Ater Gleadow *et al.*, (1986).

unimodal distribution of track lengths characterised by a declining tail toward shorter lengths, whilst rapid uplift will be represented by a narrow distribution of long tracks. However, since the shortening of track lengths will result in a reduction in the track density, it will also result in a reduction in the apparent age. Consequently it is now becoming common practice to 'normalise' sample ages to the mean track length of age standards, which is 15mμ, using the following equation:-

$$\frac{\text{Track length of standard}}{\text{Track length of sample}} \times \text{Measured age of sample}$$

Green (1988) however, suggests that age corrections of this type should be used with extreme caution. In this study no age correction is used mainly because the number of identified confined tracks was so small that a normalised age may have been more misleading than the uncorrected measured age. Nevertheless, it should be borne in mind that the mean track lengths of the Kunlun samples have been reduced by 10-15% compared to age standards.

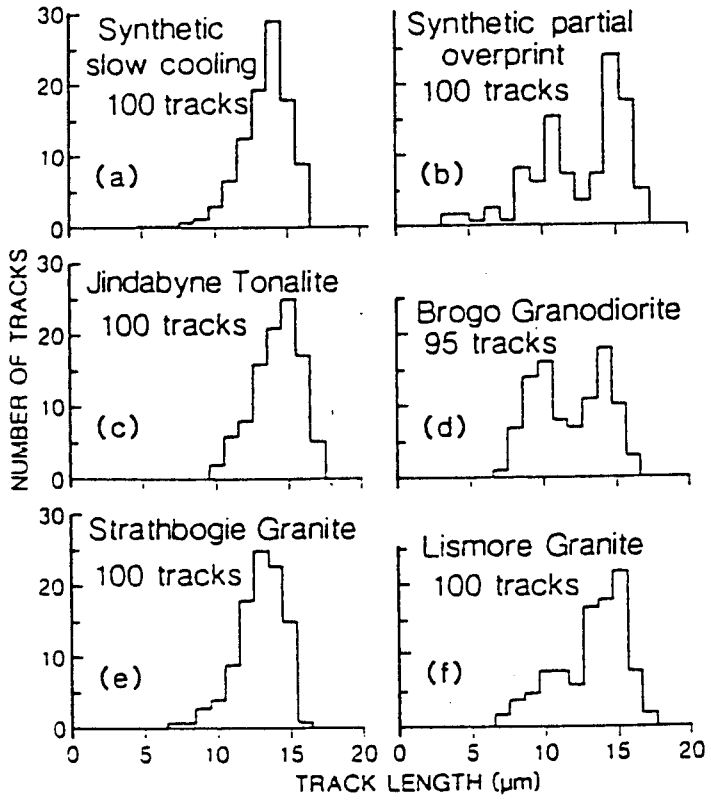

Fig. 4.9 Synthetic and actual track length distributions corresponding to rapid uplift (a,c and e), and partial overprint (b,d and f) thermal histories. Redrawn after Gleadow *et al.*, (1986).

4.6 DIFFUSION

Factors considered to influence diffusion rates are almost as numerous as authors who discuss the problem, although arguments tend to centre around whether isotopic exchange occurs almost exclusively as a result of thermally activated volume diffusion, or whether other factors, such as fluids and the extent of physical deformation, have an important role to play.

Dodson (1979) reports identical ages from adjacent biotites in Alpine fissures ranging in size from 1 mm - 30 cm, which suggests that the diffusion geometry is independent of physical grain size and is being controlled by the distribution of cleavage fractures, planes of dislocation or other imperfections in the crystal lattice. Deformation may therefore reduce the 'effective' grain size of a mineral by increasing these imperfections. This is

further supported by Deutsch and Steiger (1985), who demonstrate that K-Ar ages in the Lepontine Alps were not fully reset until the rocks were completely recrystallised. Other evidence also suggests that alteration during fluid migration decreases the effective grain size and that regions of alteration, which may be on the sub-microscopic scale, act as 'sinks' down which the radiogenic element disappears (Hofmann, 1979; Dodson, 1981; Onstott and Peacock, 1987 and Brodie, in press). Dempster (1986) however, in another examination of Alpine metamorphism showed a clear correlation of age with grainsize in the Mittagfluh granite with coarser fractions giving the older ages.

Further evidence to suggest that diffusion is not entirely temperature dependent is shown by Verschure *et al.* (1980), who demonstrate that at temperatures as high as 400°C radiogenic Ar and Sr were not lost as a result of volume diffusion and that the systems remained virtually closed up to the breakdown of minerals due to recrystallisation. Chopin and Maluski (1980) went even further and caused a riot in the literature (Desmons *et al.*, 1982; Chopin and Maluski, 1982) by suggesting that thermally activated diffusion processes are geologically insignificant. They also make the very valid point that a distinction should be drawn between closure and opening temperatures, since the latter will be much more variable, being affected by many more processes. They consider that the primary controls are pervasive deformation and the related behaviour of fluids, with chemical reactivity and starting mineralogy playing significant roles. Harrison (1981), however, showed that the ^{40}Ar diffusivity in hornblendes was not strongly dependent upon the Mg/Fe ratio and that diffusion radius was a fundamental control. The importance of fluids in the system is further highlighted by Hebeda *et al.* (1980) who show that the local absence of fluid phases in regional metamorphism prevent not only the occurrence of metamorphic reactions, but also the redistribution of radiogenic Sr between the constituent minerals. In contrast to that, but still emphasising the importance of fluids, Hayatsu and Carmichael (1970), reported that volcanics and sediments over a 30 km section trapped excess argon of the same $^{40}Ar/^{39}Ar$ ratio during a mild metamorphic event, thereby demonstrating the extreme mobility of argon in the crust which was probably being carried in a fluid phase.

Clearly, a wide range of factors affects rates of diffusion, many of which are not yet fully understood, although fluid migration and chemical reactions are unlikely to be triggered without some increase in the temperature. However, in dry environments where there is an absence of hydrous minerals, it is possible to significantly raise the temperature before chemical reaction and breakdown occurs. It is of course now widely accepted that the presence of fluids greatly facilitates metamorphic reactions. It therefore seems more realistic to assume that the factors involved are all highly interdependent, but that in different environments one process may prevail over the others. It is then encumbent upon each study to ascertain which factor is considered to have dominated in that particular case.

4.7 Rb - Sr AND ARGON RESULTS

4.7.1 Southern Region - Post-tectonic Granites

Fig. 4.10 plots biotite age against whole rock age and Table 4.3 presents the Rb-Sr data for all biotites analysed in this study. From these and Fig. 4.11 it can be seen that in the post-tectonic plutons of the Southern Region there is an increase in biotite age with increasing distance north of the Xidatan Fault, with the highly deformed Xidatan orthogneiss, which is cut by the fault, giving the youngest age at 120 Ma. Some 4 km to the north, the Yie Nin Gou X pluton records an age of 130 Ma whilst the Naij Tal pluton, 8 km further north again, gives a biotite age of approximately 140 Ma. Only the main body of the Yie Nin Gou pluton with a biotite age of 183 ± 1 Ma is within error of the emplacement age of 187 ± 21 Ma and in fact, in this instance, the biotite age is probably a more realistic age for emplacement than the whole rock age. Since it was demonstrated in Chapter Two (section 2.5) that emplacement of the plutons post-dates the Triassic regional metamorphism, then it is clear that these young biotite ages cannot date that metamorphic event and must be related to a later event.

The P-T data discussed in the metamorphic section (see chapter 2.5) indicate that the plutons were emplaced into fairly high levels in the crust, having been generated from crustal melts at lower levels, probably during or towards the end of the Triassic

metamorphic event. At 183 Ma the Yie Nin Gou pluton in particular has retained a biotite age that implies very rapid cooling subsequent to intrusion. Zeitler (1985) shows how steep cooling curves between hornblende and biotite cooling ages are diagnostic of rapid cooling following intrusive emplacement, and Wagner *et al.* (1977) record similar results from the Central Alps where temperatures dropped from 670°C to 300 °C in 2 Ma, resulting in a cooling rate greater than 150°C/Ma. Unfortunately the emplacement ages of these southerly plutons are not so well constrained, but even allowing 10 Ma between intrusion at about 670°C and biotite closure at 300 °C still implies a cooling rate of 40-50°C Ma, suggesting that uplift may have been a contributory factor to that rate.

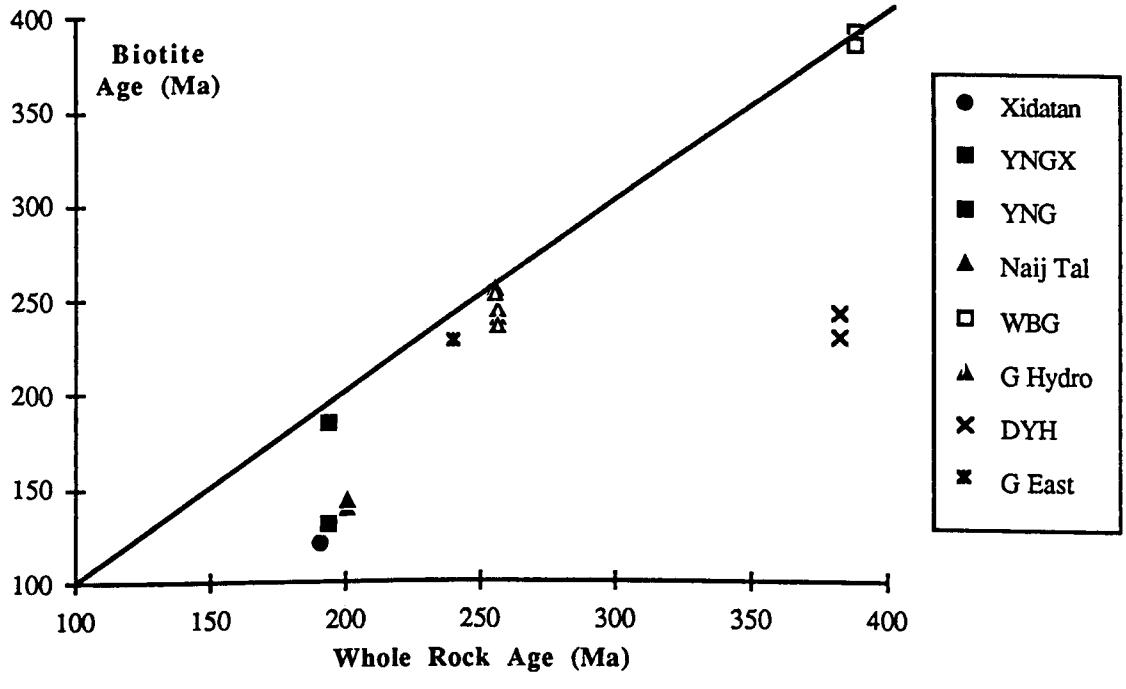

Fig. 4.10 Biotite/whole rock ages for the Kunlun Terrane granitoids. Biotite ages that fall off the line have been fully or partially reset.

As discussed in Chapter 1 (section 1.10), the Naij Tal pluton is exposed close to its roof, and it is therefore suprising that it too does not show a similar cooling history to the Yie Nin Gou, with a rapid cooling event immediately subsequent to intrusion. The geochemistry, mineralogy and age of all these plutons are so similar that it is difficult to argue convincingly that they were not all intruded at much the same level in the crust.

From the stratigraphy (Chapter 1, Fig. 1.4), it appears possible that they may have been ponding at the unconformity between the Permian limestones and volcanics, and the overlying Triassic conglomerates and turbidites. It is therefore highly unlikely that the 140 Ma biotite age of the Naij Tal pluton represents slow cooling from intrusion, since this would require a significantly greater depth of intrusion for this granite than for the Yie Nin Gou. An alternative model would be to invoke differential uplift for each pluton but that would necessitate a complicated fault pattern which is not substantiated in the field. Whilst the plutons do sit astride thrust faults, there is no evidence that these have been active since the emplacement of the granites.

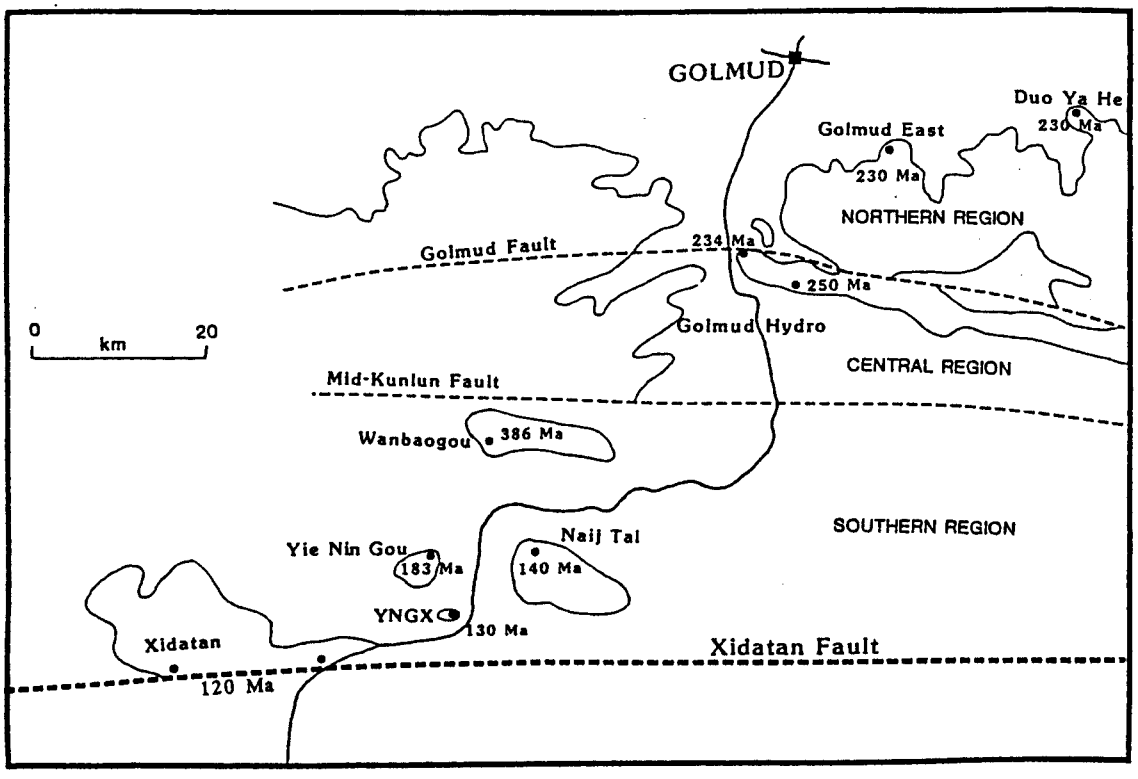

Fig. 4.11 Sketch map showing location of biotite ages from the Kunlun Terrane

It is far more consistent with the data to suggest that all the granites have been derived from a very similar source and been emplaced at much the same high levels in the crust within a few million years of each other, and that a subsequent event has reset the younger biotite ages. This is further supported by the deformational fabric, recrystallised

Sample	Rb ppm	Sr ppm	Rb/Sr	87Sr/86 Sr	Age
Southern Region					
XIDATAN					
206b	726.7 ± 0.31	11.06 ± .0097	65.71	1.0492 ± 11	121.6 ± 0.9
206d	1048.4 ± 0.57	10.73 ± .0045	97.7	1.2192 ± 6	119.5 ± 0.8
YIE NIN GOU					
221b	442.8 ± 2.3	20.48 ± .0055	21.62	0.8728 ± 2	183.3 ± 0.7
221b	438.5 ± 0.21	20.37 ± .0056	21.52	0.8726 ± 4	183.7 ± 0.7
YNG X					
214c	588.5 ± 2.7	19.90 ± .0059	29.57	0.8593 ± 3	122.6 ± 0.5
214c	561.7 ± 0.2	19.89 ± .0053	28.24	0.8604 ± 4	129.4 ± 0.5
NAIJ TAL					
236d	568.4 ± 0.43	37.14 ± .0210	15.3	0.8014 ± 5	143.3 ± 0.9
236e	730.4 ± 0.27	18.49 ± .0051	39.5	0.9508 ± 3	139.9 ± 0.5
WANBAOGOU					
222c	1103 ± 1.5	9.98 ± .0023	110.52	2.8650 ± 9	392.0 ± 2.3
222c	1107 ± 0.66	9.93 ± .0033	111.48	2.2762 ± 12	386.3 ± 2.
Central Region					
Little					
244a	918.4 ± 3.2	6.858 ± .0130	133.92	2.2282 ± 10	239.6 ± 1.5
263	787.7 ± 0.58	9.802 ± .0023	80.36	1.5539 ± 5	235.1 ± 1.5
Central					
245a	1136.0 ± 0.57	27.81 ± .0110	40.84	1.1563 ± 6	254.9 ± 1.9
245f	900.9 ± 0.52	18.21 ± .0059	49.47	1.2507 ± 5	252.3 ± 1.7
Junction					
249b	590.1 ± 0.58	30.40 ± .0047	19.41	0.9026 ± 3	233.9 ± 1.7
Northern Region					
EAST QUARRY					
246d	387.4 ± 0.28	12.55 ± .0037	30.87	1.0515 ± 4	258.5 ± 1.8
GOLMUD EAST					
273a	620.9 ± 0.26	11.26 ± .0039	55.14	1.2557 ± 5	227.9 ± 0.8
273e	473.0 ± 0.46	40.27 ± .0120	11.75	0.8202 ± 3	226.5 ± 1.0
273e	513.2 ± 0.18	18.24 ± .0051	28.14	0.9792 ± 3	226.8 ± 0.8
DUO YA HE					
266a	694.6 ± 0.41	6.36 ± .0030	109.21	1.8624 ± 12	229.8 ± 0.8
266a	715.6 ± 0.68	12.84 ± .0039	55.73	1.2671 ± 5	229.0 ± 0.8
266e	628.5 ± 0.41	21.12 ± .0075	29.76	1.0190 ± 5	242.6 ± 0.9

Table 4.3 Measured biotite ages from the Kunlun Terrane

biotites, exsolved sphene and extensive epidotization seen in the Xidatan orthogneiss all of which are evidence for greenschist facies metamorphism (Verschure *et al.*, 1980 and Dempster, 1986). It seems unlikely that under these conditions the Rb-Sr isotopic system would have remained undisturbed. Therefore it is considered that the 120 Ma biotites from the Xidatan pluton represent rejuvenation of the system at that time, as a result of thrusting on the Xidatan Fault, and that ages become older to the north because they have only been partially reset.

Kinematic indicators in the Xidatan granite suggest overthrusting to the south on the Xidatan fault (Coward *et al.*, 1988), which at this time may have been a significant thrust fault evolving only recently into the major strike-slip fault seen today. This is known to have occurred in the High Himalayas, where Quaternary and Recent neotectonics have reactivated and transformed many of the thrust faults into strike-slip faults (Searle *et al.*, 1987). In their study of heat transfer in regions of thickened continental crust, England and Thompson (1984) suggest that frictional heating during deformation does not contribute significantly to the overall heat budget of a thermally metamorphosed region. However they do recognise that locally it may be important if stresses on the fault are high enough. The distance (l) that such metamorphism would extend from the fault is related to the thermal diffusivity (k) of the medium, and the duration (t) of the deformation, by:

$$l = \sqrt{t\ k} \qquad \text{(Graham and England, 1976)}$$

and they calculate that deformation for 1 Ma could result in metamorphism up to 5 km away from the fault. Brewer (1981), also calculated simple models for overthrust sheets in crystalline basement rocks and showed that significant thermal effects may result from their movements, when the rates of movement are reasonably high, the thrust sheets some 5 - 15 km thick and the distances moved sufficiently large. He demonstrates that temperatures may rise as high as 300°C above the normal geothermal gradient, and that prograde metamorphic reaction zones will be seen near the fault and inverse reaction zones below it. The leucocratic dykes and pods seen within the Xidatan orthogneiss suggests that temperatures were sufficiently high to generate partial melting, indicating

they must have been around 650 - 700°C. From Brewer's temperature profiles, assuming a depth of intrusion at 10 km and no significant erosion between emplacement and thrusting, it can be calculated that the amount of southward horizontal displacement on the Xidatan fault must have been in the region of 100 - 200 km.

Dehydration reactions will release H_2O that can percolate through the rocks, and England and Thompson (*op.cit.*) stress the significant role played by these convecting pore fluids, which can transport heat very efficiently. Brewer (*op. cit.*) also emphasises their importance, especially in generating melting. Convecting fluids will occur particularly in shallow level environments (< 10 km), where the overburden is insufficient to close all microfractures and where permeabilities have been inferred to be in the millidarcy range for crystalline rocks (Brace, 1980), which is close to the permeability of many sandstones. Calculations by Walther and Orville (1982), show that H_2O and CO_2 produced during devolatilization will occupy 12 vol % of the rock at 500°C and 5 kb. The escape of this fluid can be accommodated by a single fracture 1 cm long and 0.2μ wide per cm^2. So whereas thermally activated diffusion as a result of frictional heating may have a limited range over which it can be effective, the presence of fluids could extend the possibility of isotopic exchange over much greater distances, as shown by Brewer (1969); Hayatsu and Carmichael (1970) and Roddick and Farrar, (1971).

Whilst not showing a penetrative metamorphic fabric, the Naij Tal and both Yie Nin Gou plutons contain substantial amounts of secondary sphene and epidote, suggesting that they too have been affected by secondary fluid activity. However, the Yie Nin Gou pluton still retains a biotite emplacement age but is distinguished by coarse biotites which at >2mm in diameter, are more than twice the size of those in the other plutons. Clearly this size difference not only reflects the lesser degree of alteration to which this pluton has been subjected, but the increased grain size must play a significant role in controlling diffusion in these biotites. Coupled with a dissipation of the heat supply as a result of increased distance from the heat source in the fault zone, these factors could well account for the fact that the age has not been reset in the Yie Nin Gou. Whereas for the smaller sized biotites in the Naij Tal pluton the thermal supply, and associated fluid activity may

just have been sufficient to allow some escape of radiogenic Sr thereby partially resetting the age. The closer to the fault the greater the resetting. This model implies that diffusion geometry, fluid activity and temperature have all acted as controls in the radiogenic exchange which has fully reset the biotite age of the Xidatan pluton but only partially rejuvenated those to the north.

Rocks overlying the thrust plane will cool rapidly after the heating event and the cessation of thrusting (Graham and England, 1976; England and Thompson, 1984) and this will effectively 'freeze in ' the age at which the event occurred, which in this case is inferred to be movement of the Xidatan Fault at 120 Ma. This Cretaceous age is coincident with the age of collision between the Lhasa and Qiangtang Terranes (Dewey *et al.*, 1988), the impact of which may well have reactivated thrust faults to the north of the collision.

K-Ar biotite data is available for the Xidatan and Naij Tal plutons (Table 4.4). At 130 ± 2 Ma and 169 ± 3 Ma respectively, these ages, whilst retaining the same pattern of increasing age away from the Xidatan Fault, are considerably older than the Rb-Sr biotite ages. This is despite evidence to suggest either that both systems have very similar closure temperatures around 300°C (Armstrong and Jäger, 1966; Wagner *et al.*, 1977) or even that the K-Ar system closes at lower temperatures (Harrison *et al.*, 1979), which would imply that the K-Ar ages should be younger rather than older than the Rb-Sr ages. However, this relationship of older K-Ar ages is commonly seen in metamorphic terranes (Kulp and Engles, 1962; Foland 1979; Vershure *et al.*, 1980; Roddick *et al.*, 1980; Dempster, 1986) and is usually explained as being due to trapped excess Ar in the system. During metamorphism Ar becomes mobile within the rock, perhaps advancing from depth (Roddick *et al.*, 1980), which increases both the argon pressure (P_{Ar}) and the $^{40}Ar/^{36}Ar$ composition of the ambient argon. Minerals may be only partially degassed before the area cools below the relevant closure temperature. The diffusive loss of radiogenic Ar will then be modified by isotopic exchange as the ambient argon is incorporated into the sites where diffusion has taken place.

For the Naij Tal biotites (Table 4.4), it is difficult to determine whether the 169 Ma age represents partial resetting by a small amount of argon loss, which would apparently reduce the age of intrusion, or excess Ar trapped subsequent to a more complete degassing phase which resulted in an age older than that given by the Rb-Sr systematics. But given that temperatures and fluid activity were sufficient to reset Rb-Sr, and that P_{Ar} was high, as inferred from excess argon in the Xidatan, then the latter possibility seems the most plausible. This type of problem can be much better resolved by looking at the $^{40}Ar/^{39}Ar$ age spectra data, which are available for the Xidatan orthogneiss.

Pluton	K wt %	^{40}Ar * x 10^{-9} mol/g	$^{40}Ar/^{40}K$ x 10^{-10}	Age ± 1 σ
Xidatan	7.48	1.7510	0.7843	130.1 ± 2
Naij Tal	7.10	2.1716	1.0248	169.3 ± 3
Wanbaogou	6.35	5.3593	2.8276	430.9 ± 7
Pink Granite	6.77	3.4121	1.6887	269.5 ± 4
Little Granite	7.09	3.3045	1.5616	250.5 ± 4
East Quarry	7.48	3.4122	1.5284	245.6 ± 4

Table 4.4 K-Ar data for the Kunlun Granitoids kindly supplied by Chinese colleagues.

Fig. 4.12 shows the age spectra obtained both from biotites and K-feldspars separated from sample X67 and analysed by Pete Copeland at Albany, New York. Apart from the first step, which represents less than 10% of the ^{39}Ar released, the biotite displays an unusually well defined plateau at about 120 Ma. There is no evidence of excess argon and only the low temperature step indicates loss perhaps as a result of some mild metamorphic event at that time. This age of 120 Ma agrees very well with Rb-Sr ages obtained from the G206 samples some 10 km to the east along strike of the Xidatan Fault, although these samples have a K-Ar age of 130 Ma (Table 4.4). That X67 has been subjected to a higher degree of alteration than the others is evident from the very extensive deformation and epidotisation (10% of mineral content) seen in this sample

which may account for the greater resetting of Ar, although it is not clear why this area should escape the effects of excess Ar as seen in all other samples. Perhaps argon expelled from this region has been incorporated within other plutons.

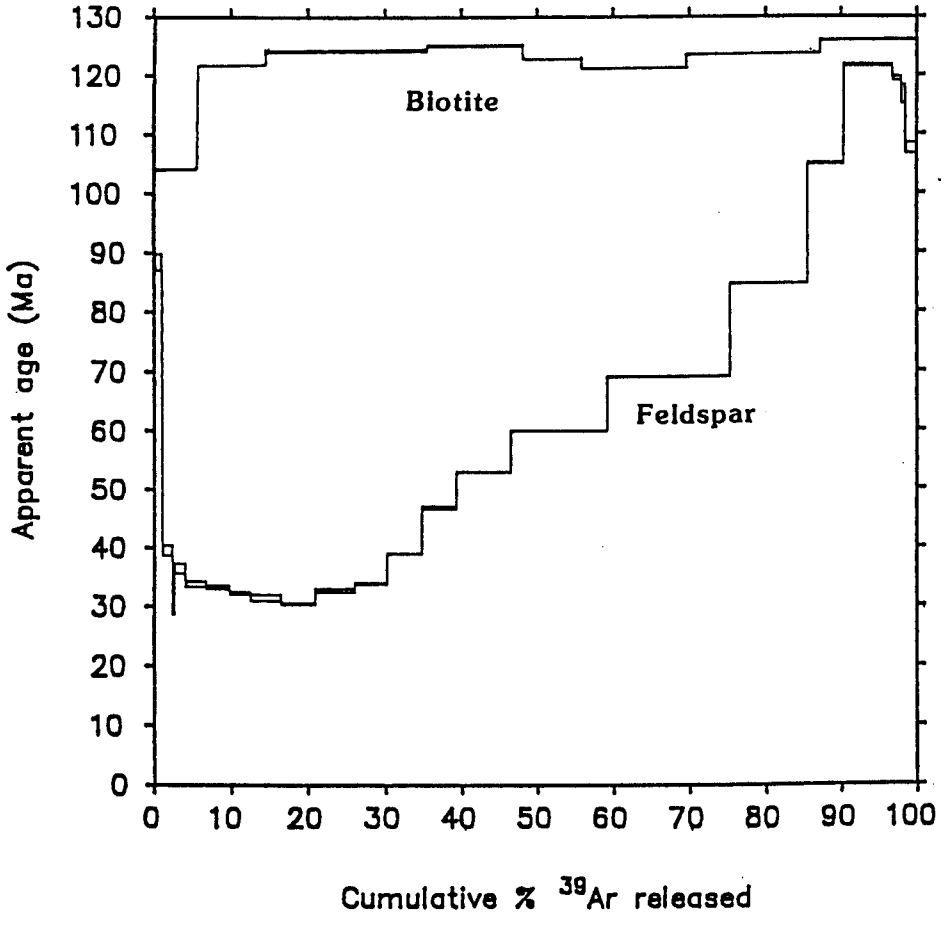

Fig. 4.12 $^{39}Ar/^{40}Ar$ age spectra for the Xidatan Granite as shown by biotite and feldspar mineral separates.

The feldspars reveal a very different picture. Only when the highest temperature steps are reached and 90% of the ^{39}Ar has been released does the apparent age reach that of the biotite. The middle range of the spectra appears to represent mixing between 120 Ma and 35 Ma, when the plateau flattens out again. Closure temperatures for the high temperature portion are about 250°C, whilst those for the low temperature portion are around 155°C (Harrison, pers.comm.). This may simply reflect very slow cooling at a rate of slightly more than 1°C/Ma over this period, or there may have been a low temperature event at 35 Ma. Roddick *et al.* (1980) convincingly demonstrate how in their

samples the initial steps actually represented the resetting age, and they emphasised how these should not be ignored. It is interesting to note that the first step of the biotite indicates Ar loss whilst the first step of the feldspar appears to contain excess Ar. This could indicate a very local low temperature event around 100 Ma where Ar was lost from the biotite and incorporated into the feldspar, but what is less evident is whether the low temperature plateau at 35 Ma has any real significance.

4.7.2 Southern Region - Wanbaogou Granite

The Wanbaogou pluton has a well defined whole-rock age of 388 ± 10 Ma and the two Rb-Sr biotite ages of 392 Ma and 386 Ma (Table 4.3) are within error of the emplacement age, again indicating very rapid cooling to the wall-rock temperatures, probably as a result of intrusion at fairly high levels in the crust coupled with some uplift. The K-Ar biotite age of 431 ± 7 Ma is again much older, and is clearly a result of trapped excess argon since this apparent cooling age is even older than that of intrusion. It is not suprising that this pluton contains excess argon since, by looking at the age spectra from the $^{40}Ar/^{39}Ar$ data (Fig 4.13), it is evident that it has been subjected to several metamorphic events during the 400 Ma of its history.

The $^{40}Ar/^{39}Ar$ age spectra show that the oldest age from the biotite is similar to the K/Ar age at about 430 Ma, further confirming the presence of excess Ar, but although the steps either side pass through the Rb-Sr biotite age, they do not clearly define it. However, the low temperature portion of the biotite and the high temperature section of the feldspars together create a significant plateau at about 250 Ma, which undoubtedly represents a reheating of the region at this time as a result of emplacement of the Permian batholith. The low temperature portion of the feldspar spectra, considered to have a closure temperature equivalent to about 120°C (Kidd, pers.comm.), is very disturbed which indicates a resetting event perhaps around 75 Ma rather than slow cooling. Alternatively it may represent argon loss during a metamorphic event such as thrusting on the Xidatan Fault at 120 Ma.

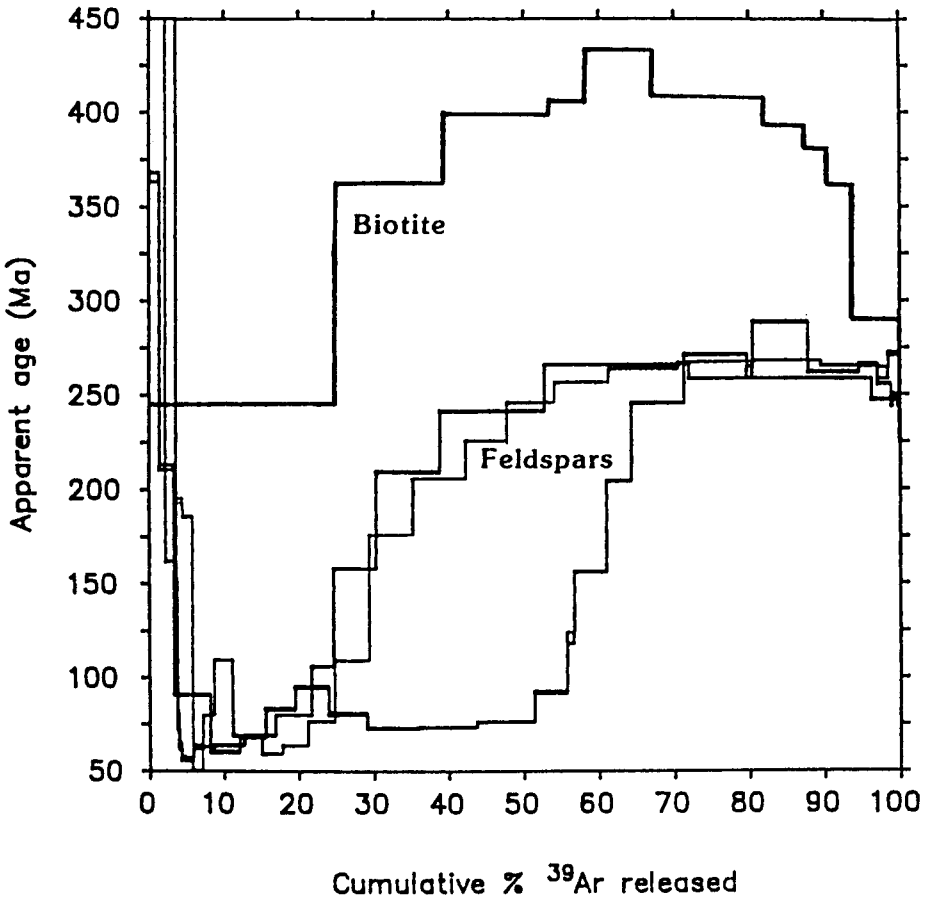

Fig. 4.13 $^{39}Ar/^{40}Ar$ age spectra for the Wanbaogou granite obtained from biotite and feldspar mineral separates.

4.7.3 Central Region

North of the Mid Kunlun Fault there is a wide range of biotite ages from the Golmud plutons spanning a period of some 20 Ma (Fig.4.11 and Table 4.3). Biotite ages from the Central Granite (253 ± 3 Ma) are the only ones from the Golmud Group to give ages indistiguishable from emplacement ages. This rapid cooling again implies that the depth of intrusion was quite shallow, although it could have been greater if intrusion was accompanied by uplift. Biotite ages from the Little Granite are somewhat younger between 244 and 235 Ma, which implies either a resetting event at this time, or a much longer period of cooling, perhaps as a result of the wall rocks having been heated up during previous batch emplacements, so that conductive heat dissipation did not occur so rapidly.

The age of 234 Ma from the Golmud Junction biotites supports the earlier suggestion that 217 Ma obtained from the whole-rock isochron (Chapter 3, section 3.3.2) is geologically meaningless. It is reasonable to assume therefore, that this batch was intruded at much the same time as others in the Central Region. Being so close to the Golmud Fault, many of the Golmud Junction samples are significantly altered, and so biotites from G249b were specifically analysed because they displayed a pronounced penetrative fabric. It was hoped that the age of this deformation could be dated. Rather disappointingly it gave an ambiguous age of 234 ± 2 Ma. This similarity in age to those from the Little Granite suggests either that it represents a fully or partially reset age as a result of deformation due to movement on the Golmud Fault (and that possibly the Little Granite has also been reset), or that the formation age of the fabric has not been recorded and that this age simply reflects slow cooling. Given the extent of the deformation, however, and the proximity of these samples to the fault where, at least locally, temperatures would have been high, it seems probable that this represents an age of movement on the Golmud Fault.

K-Ar data for this region show the same pattern of excess Ar giving an anomalously old age for the Pink Granite at 270 ± 4 Ma (Table 4.4) which, although meaningless in itself, at least supports the suggestion of a metamorphic event having affected this region. Unfortunately no $^{39}Ar/^{40}Ar$ data are available to confirm this.

4.7.4 Northern Region

North of the Golmud Fault, the East Quarry stock gives a biotite age of 259 ± 2 Ma, which again supports rapid cooling subsequent to emplacement. This is the only sample analysed where the K-Ar age at 246 ± 4 Ma is lower than the Rb-Sr age, and probably reflects argon loss at some time.

It is interesting that both the most northerly plutons, although some 25 km apart, show identical biotite ages, within error, around 228 Ma. The exception is one biotite sample from the Duo Ya He pluton which gives an age of 243 ± 1 Ma consistent with a zircon emplacement age for the Golmud East intrusion at 240 ± 6 Ma. With the limited structural

data available for this region and no argon information it is difficult to interpret these ages with any degree of certainty. If, as postulated earlier (Chapter 3.4), the Duo Ya He pluton is Devonian, then these biotites have clearly been reset either in response to intrusion around 240 Ma (this body is intruded by another granite) or by a metamorphic event that rejuvented both plutons at 228 Ma. However, the presence of prehnite in these samples indicates that the metamorphic grade is dying out northwards and therefore this age may well be the result of resetting during the Triassic metamorphic event.

4.8 FISSION TRACK RESULTS

4.8.1 Southern Region

Table 4.5 presents apparent age data for all fission track results, but full fission track data are presented in Appendix B. Figure 4.14 plots apparent ages against assumed closure temperatures for the post-tectonic granites of the Southern Region, and curves can be drawn through these points to give an average cooling rate and surface approach rate for each pluton. However, information from this type of plot is only given at the point of mineral closure. What is not revealed is what may have happened to the curve between points. For example, the increase in biotite ages away from the Xidatan Fault is clearly shown in Fig. 4.14, and this results in an apparent difference in cooling rates for the different plutons between emplacement and biotite closure temperatures. However, it has now been clearly demonstrated that this effect is the result of a resetting event at 120 Ma, and that the intrusion age of the post-tectonic plutons has been affected. But, were it not for the constraint provided by the Yie Nin Gou pluton, which still retains its emplacement age of 183 Ma, it would not have been clear that ages from the other plutons did not simply reflect differential cooling rates from emplacement temperatures. In fact, probably all the plutons intitally cooled at the same rate as the Yie Nin Gou and were subsequently reheated to much the same temperatures, although this is not apparent from the curves. Furthermore, it also seems probable that since temperatures were sufficient to partially reset biotites in all the plutons, both zircon and apatite fission tracks would have been totally annealed at this time. This problem of the unknown shape of the curve between known points must be continually borne in mind when assessing these types of data. If

only data from the Yie Nin Gou X pluton were available for example, slow cooling to biotite closure would have been inferred and the resetting event at 120 Ma would have remained undisclosed.

ZIRCON				
Pluton	Age (Ma)	(±) 1σ	No. crystals	Chi-square %
215b	120.6	11	9	58
Xidatan	81.3	3	15	32
Xidatan (X67)	76.7	8	12	fail
Wanbaogou	83.1	3	12	96
Pink Granite	103.1	10	7	fail
Duo Ya He	162.0	7	15	30
Golmud East	136.1	13	11	10
APATITE				
Xidatan	12.8	2	9	100
Yie Nin Gou	17.4	3	11	100
YNG X	20.8	2	18	58
Wanbaogou	20.1	3	10	99
Pink Granite	19.4	3	10	100
Duo Ya He	119.0	9	8	12
Golmud East	106.0	8	14	100

Table 4.5 Zircon and apatite fission track ages. Chi - square % is the probability of obtaining the measured chi - squared value, or an indication of how good the count was.

Following the Cretaceous thrusting event at 120 Ma and resetting of the biotites, the cooling curve for the Xidatan granite is well constrained in having both a zircon age (81± 3 Ma), and a calculated low temperature feldspar age (155 ± 20°C at 34 Ma) between the biotite and apatite ages. Assumption of a constant rate of cooling between

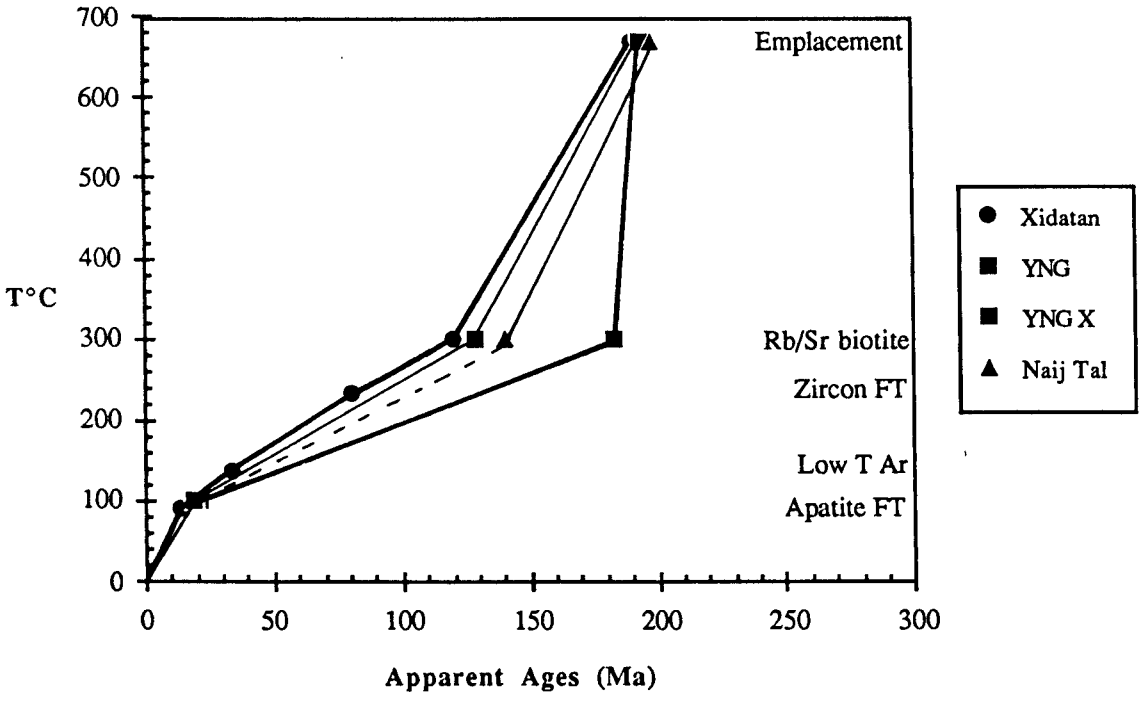

Fig. 4.14 Cooling curves for the Southern Region post-tectonic granites.

biotite closure at 120 Ma and feldspar closure at 34 Ma allows for interpolation of the zircon closure temperature between these two points which, at 234 ± 5°C, is close to the value of 240°C obtained by Hurford (1986). Alternatively, interpolation between biotite and apatite closure leads to values of 222 ± 5°C for zircon, but then the interpolated low temperature argon value of 130°C falls just outside the calculated range of 155 ± 20°C. An error for the age was not provided. However, given the uncertainties on the ages and, in particular the wide range of closure temperatures suggested for both zircon and apatite, it is perhaps suprising that the ages and temperatures agree as well as they do. The very slow cooling rates from biotite resetting to apatite closure at 13 ± 2 Ma, are calculated to be in the region of 2°C/Ma.

Since there is no evidence to the contrary, it is assumed that the other post-tectonic granites followed a very similar pattern of slow cooling to give observed apatite ages around 20 Ma. If the Xidatan granite was disturbed at 34 Ma, this may have delayed apatite closure for slightly longer in this pluton as a result of a moderate heat increase, and hence may explain the younger age in this pluton of 13 ± 2 Ma. It is likely however, that

the temperature increase was not very great, since the zircon fits well on the cooling curve and does not appear to have been disturbed. This suggests that any thermal increase was well below 200°C and that the apatites may only have been partially annealed, which would result in a mixed age. It was hoped that confined track lengths would clarify this point. However, the small sample size available, coupled with the very low track density in these apatites owing to low uranium concentrations and young ages, resulted in a very small probability of finding either two tracks that crossed each other or a fracture in the mineral, so that the confined length could be measured. In fact only 9 confined tracks were found in the Xidatan pluton, which gave a mean track length of 13.82 ± 1μm, and this is far too small a distribution to draw any meaningful conclusions from.

That both the Yie Nin Gou and the Yie Nin Gou X plutons give apatite cooling ages within error of each other around 19 Ma, lends futher support to the suggestion that temperature was not the primary control in resetting biotites from the Yie Nin Gou X, since it seems probable that the temperature differences between them at that time were not significant and that the region soon equilibriated thermally to close all apatites at much the same time. This reinforces the argument that deformation, fluid activity resulting in chemical alteration and, perhaps most important of all, diffusion radius played significant roles in resetting the biotites.

4.8.2 Central Region and Wanbaogou Pluton

For the purposes of comparison, the Wanbaogou pluton has here been included with the Central Region granites, since its cooling history is more similar to the granites in this region than those to the south (Fig.4.15). At 250 Ma the feldspars in the Wanbaogou pluton were apparently reset by circulating hydrothermal fluids resulting from intrusion of the Permian batholith. From a calculated high temperature closure of 250°C for these feldspars it is suggested that this pluton was at a depth of about 8 km at this time. Alternatively, this temperature may be independent of depth and could simply reflect a cooling of the hydrothermal fluids to this temperature at this time. However, although the

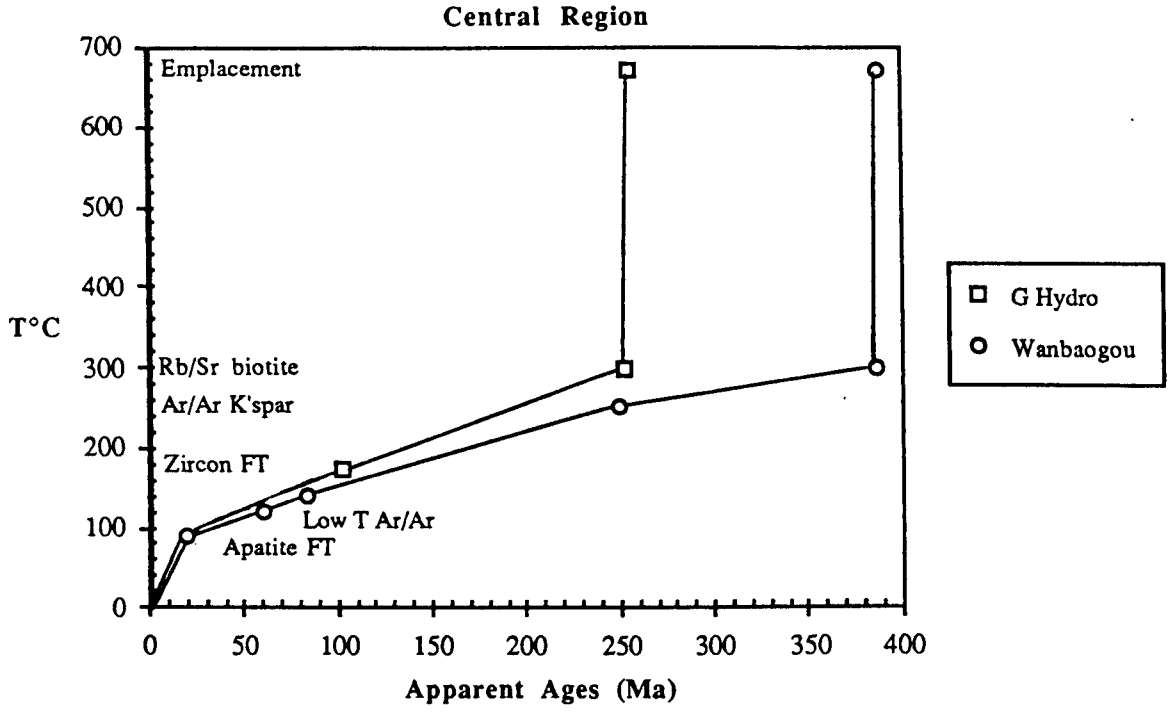

Fig. 4.15 Cooling curves for the Wanbaogou pluton (WBG) and Pink Granite from the Golmud Hydro Group.

depth cannot be precisely defined, the Wanbaogou pluton is likely to have been at shallower levels than the intruding Permian batholith, which was only closing to biotites at this time (250 Ma) and was therefore likely to have been at least 10 km deep.

The Wanbaogou granite gives a zircon cooling age of 83 ± 3 Ma, although if a cooling temperature for this age is interpolated in the same way as for the Xidatan pluton between the high and low temperatures calculated from the $^{40}Ar/^{39}Ar$ age spectra, a very low closure temperature of 136 ± 5°C is inferred for the zircon. However, if the curve is extrapolated to apatite closure at 90°C it passes, within error, through the measured age of 20 ± 3 Ma which acts as a further control on the curve and supports interpolation of the zircon cooling temperature in this way. It may be that the very slow cooling rates seen in this pluton result in very low closure tempertures. Alternatively, since the Wanbaogou zircon cooling age of 83 ± 3 Ma is within error of the Xidatan zircon cooling age at 81 ± 3 Ma, it may be that the zircons, with a lower closure temperature, may well have been partially or fully annealed by the Cretaceous thrusting event at 120 Ma, although temperatures were insufficient to reset the biotites. If this is the situation then the age of

the zircons represents either a mixed age as a result of partial annealing or a cooling age from 120 Ma. But, since it is the same age as the Xidatan it is more likely to be the latter. In this case then it is clearly invalid to interpolate a closure temperture for the zircons from the Permian resetting of the feldspars at 250 Ma, and caution should be used in accepting such a low closure temperature for the zircons.

North of the Mid-Kunlun Fault a rather poorly constrained zircon cooling age of 103 ± 10 Ma indicates that ,by this time, the Pink Granite was at shallower levels than the Wanbaogou, which does not pass through the zircon closure temperature until some 20 Ma later. The implication from these relative depth differences is that movement on the Mid-Kunlun Fault must have brought up the Pink Granite relative to the Wanbaogou between 244 and 100 Ma and, although this gives rather a wide choice of available time, it is likely to have been either during the Triassic metamorphic event - perhaps 234 Ma as inferred by movement on the Golmud Fault to the north - or at 120 Ma when there are known to have been compressional movements in the region. If the Central block was uplifted during the Jurassic, it could account for the slightly younger zircon cooling ages found in this region. Apatites in the Pink Granite give an age of 19 Ma ± 3, which is again within error of those in the Southern Region .

4.8.3 Northern Region

North of the Golmud Fault there is a pronounced increase in both zircon and particularly apatite ages, which are some 100 Ma older than those in the south. Fig 4.16 shows that there must have also been differential rates of movement between the two intrusions for the Duo Ya He to have closed to both minerals so much earlier than Golmud East, although both were clearly at the same temperature at 228 Ma when the biotites closed simultaneously. What is more significant is that apatite closure around 120 - 110 Ma indicates that, unless there has been significant movement on the Golmud Fault between the Northern and Central Regions, then approximately the same amount of material has been eroded from the Northern Region since apatite closure at 120 Ma, as has been removed from the Central and Southern Regions since apatite closure only 20 Ma ago. If this is the case then a model to explain this data must be investigated.

been removed from the Central and Southern Regions since apatite closure only 20 Ma ago. If this is the case then a model to explain this data must be investigated.

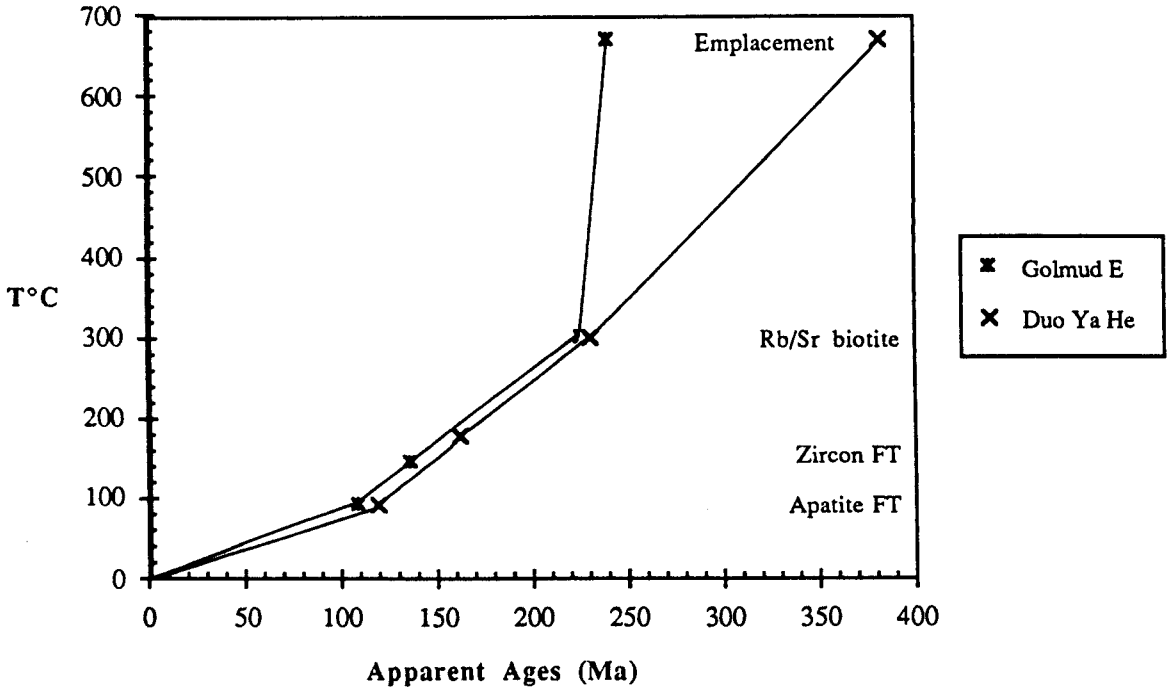

Fig. 4.16 Cooling curves for the Northern Region plutons.

4.8.4 Zircon closure temperatures

Fig. 4.17 plots interpolated zircon closure temperatures against the apparent age difference between biotite and zircon cooling for all plutons. The data appear to fall into 2 parallel trends which define different rates of cooling. The post-tectonic and northern plutons which have the same cooling pattern (see Fig. 4.23) and a cooling rate of approximately 2°C/Ma define one trend, whilst the Central and Wanbaogou plutons which apparently cooled at < 1°C/Ma fall on the other trend. However, the data base is very small so it is not clear whether these trends have any real meaning.

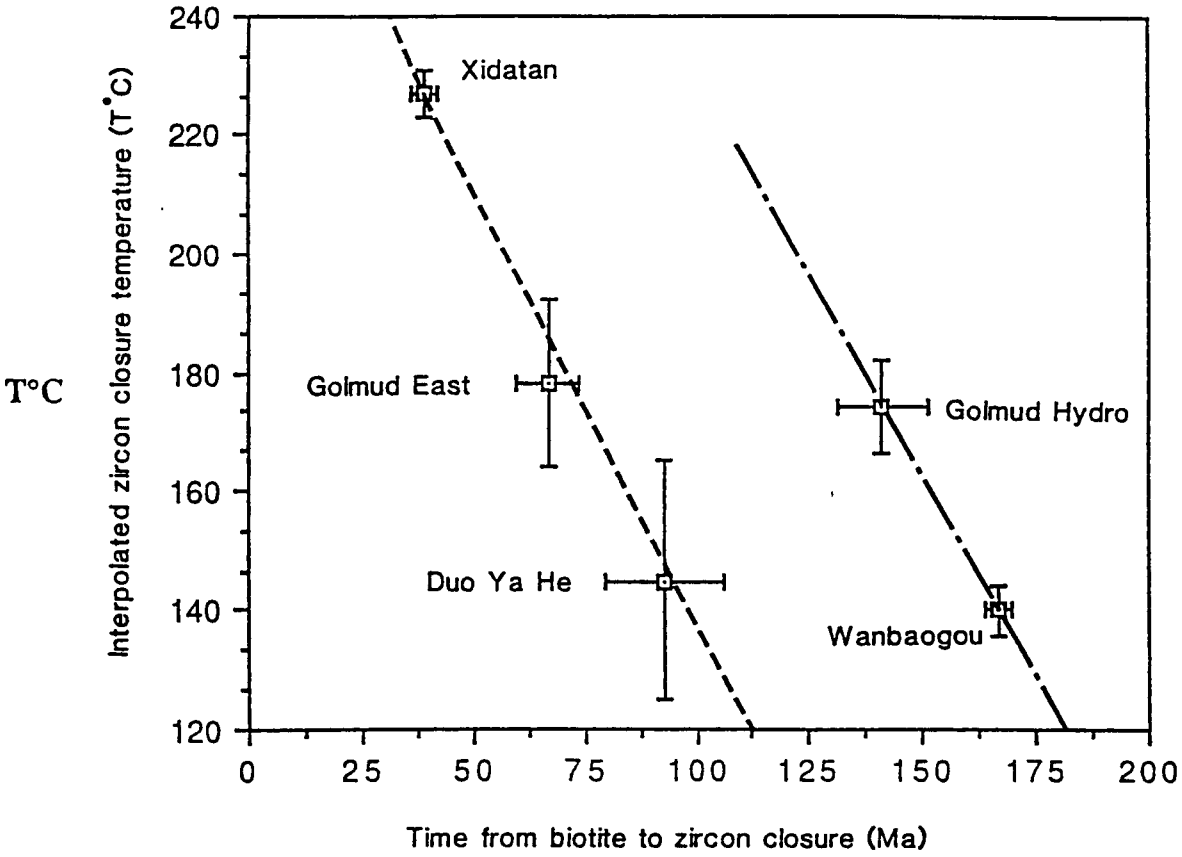

Fig. 4.17 Interpolated closure temperatures for zircons from the Kunlun granitoids define two parallel trends. Short dashes, 2°C/Ma and long dashes, < 1°C/Ma.

4.9 DISCUSSION

The five isotopic analytical techniques applied to the Kunlun granitoids provide a thermal history for the region stretching back 400 Ma, and the data are presented graphically against distance from the Xidatan Fault in Figure 4.18. From this it can be seen that significant events occurred around 390, 250, 120 and 20 Ma and that thermal equilibration occurred in the region south of the Golmud Fault during the 100 Ma between 120 and 20 Ma. At 250 Ma, intrusion of the batholith thermally disturbed a region that had been relatively stable for some 150 Ma, since collision of the Kunlun with the Tarim Terrane and intrusion of the Devonian plutons. That the crust was relatively cold prior to the Permian intrusion is evidenced by rapid cooling of the early plutons, coupled with uplift, (as indicated by the basal conglomerates seen in the Triassic), and a resetting of ^{40}Ar in the Wanbaogou feldspars, which must have previously cooled below 250°C. This episode of subduction followed by collision with the Qiangtang Terrane appears to

have been followed by a period of very slow cooling to zircon closure of both the Golmud Hydro and the Wanbaogou plutons. Emplacement of the post tectonic granites some 50 Ma later (190 Ma) at the end of the Triassic metamorphic event (Harris *et al.*, 1988b) is again into crust that has cooled sufficiently for biotite closure to appear geologically instantaneous.

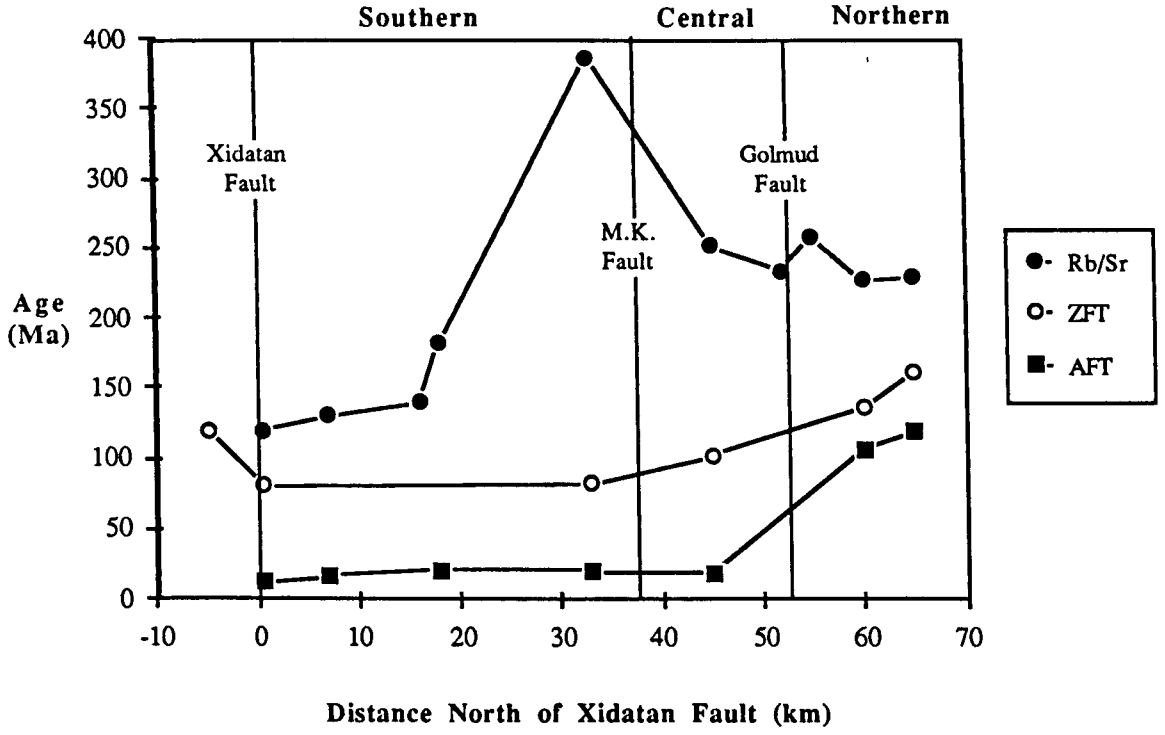

Fig. 4.18 Summary plot of all age data against distance north of the Xidatan Fault. Rb/Sr = biotite ages, ZFT = zircon fission track ages, AFT = apatite fission track ages.

At 120 Ma, collision of the Lhasa Terrane with the Qiangtang had a major impact in the Kunlun, overthrusting the post-tectonic granites perhaps several hundred kilometers to the south, causing partial melting in the Xidatan orthogneiss and partially resetting biotites in the other plutons. But, by 80 Ma the perturbations caused by the thrusting event appear to have flattened out and the whole region south of the Mid-Kunlun Fault has thermally equilibriated to temperatures between that of zircon and apatite closure. By 20 Ma the Mid-Kunlun Fault is no longer a thermal barrier and all apatites south of the Golmud Fault closed at about the same time. Figure 4.18 also shows one data point south of the

Xidatan Fault. This is from zircons in a quartz porphyry, which on its own is not very meaningful, but it has been included since it does give a zircon closure age of 120 Ma which may be related to movement on the fault.

But what was happening north of the Golmud Fault? That the apatites closed within error of each other around 115 Ma intuitively links them to the known thrusting event at 120 Ma, which may have caused sufficient uplift of the Northern Region for the apatites to pass through the closure temperature. The problem with this argument is that an uplifted region would be expected to erode faster and therefore have younger, not older, ages exposed at the surface compared to a static region. In fact, the Northern Region appears to have taken 100 Ma years longer than the Central and Southern Regions to bring samples to the surface which were presumably at similar depths when they passed throught the apatite closure temperature.

Alternatively, differential uplift of the block between the Xidatan and Golmud Faults (Central and Southern Regions) may not have brought that block through the closure temperature until 20 Ma, but this implies a period of fairly recent uplift which is not immediately recognised either in the cooling curves of the granites, or in the track length measurements (Fig.4.19) which, although admittedly of a rather limited number, do not show the small distribution of long tracks expected from rapidly uplifted regions. These two alternative models will now be examined and discussed in the following sections.

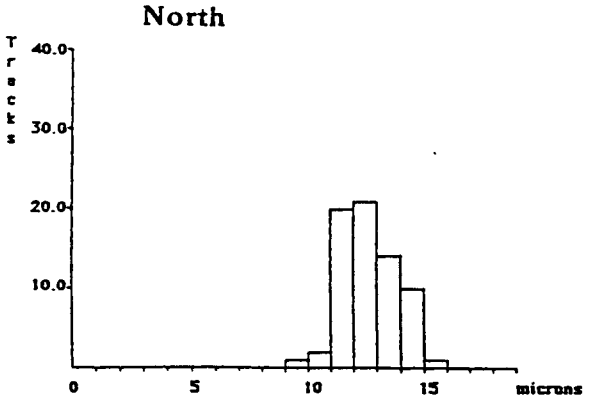

No. of tracks: 69

Mean track length: 12.62±1.21 microns

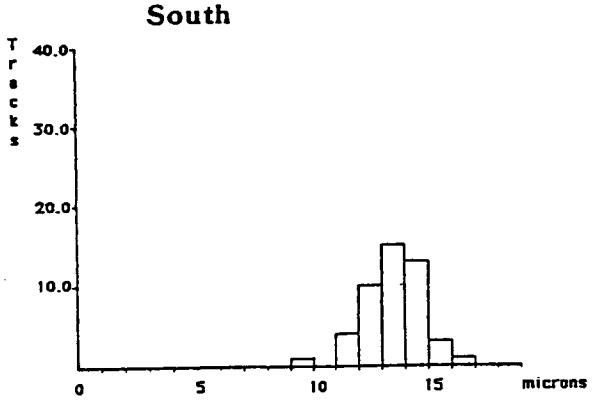

No. of tracks: 47

Mean track length: 13.52±1.35 microns

Fig.4.19 Confined track lengths for samples north and south of the Golmud Fault. Due to small sample sizes few confined tracks were found so the number has been summed from each region. Compared to mean track lengths in standards the distribution from the south indicates there has been about 10% annealing while in the north it is up to 15 %.

4.9.1 Geothermal Gradient Model

A curve for the evolution of apatite fission track ages with depth in the Earth's crust, in areas of recent uplift under normal geothermal gradients (Fig 4.20) has been calculated by Van den Haute (1986). He constructed it from the stepwise approach for calculating track accumulation as outlined by Haack (1977), and from the Arrhenius diagram for fission track retention in apatites published by Hammerschmidt *et al.* (1984). It shows that at rates of uplift of 1 km/Ma, an age of 3.4 Ma will be registered at the surface, corresponding to the time when the rocks passed the closure geotherm of 112°C at a depth of 3.4 km. This also corresponds to a time when approximately 50% of tracks will have become stable. However, the total time that has elapsed since the onset of track accumulation is 5.2 Ma which is the minimum amount of time for uplift to last to allow

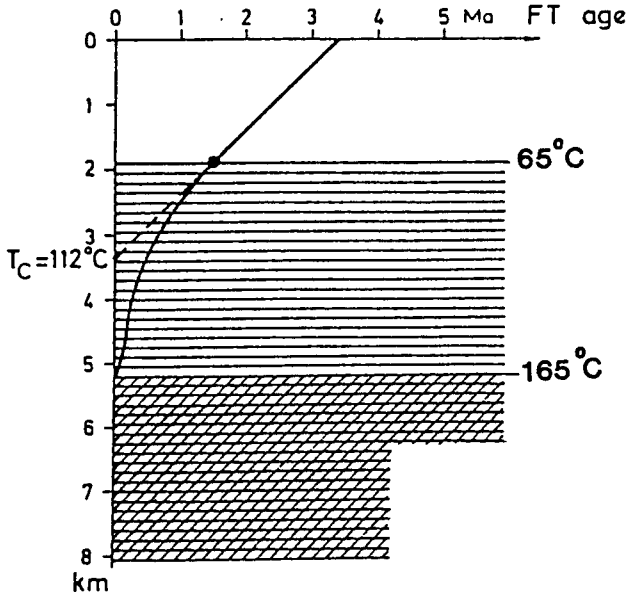

Fig. 4.20 A curve for the evolution of apatite fission tracks with depth assuming a geothermal gradient of 30 °C/km and an uplift rate of 1 km/Ma. Region above point on curve (65°C) = zone of full track stability; region of horizontal lines (65 - 165°C) = zone of partial stability. In the hatched region no tracks are retained. The closure temperature (T_C) is extrapolated to be 112°C. Redrawn after Van den Haute (1986).

full development of the curve. From this it should be clear that only apatites situated in the top 2 km of the total track stability zone will yield true uplift ages. If, during rapid uplift, erosion exceeds uplift then samples from lower altitudes such as valley floors may well give ages that have penetrated the partial annealing zone, and these will consequently not be true uplift ages. When taking this into account, along with assumptions made about consistent and parrallel geotherms, even in areas of recent orogenesis, calculated uplift rates can at best only be crude estimates. So, when attempting to extrapolate these types of calculations over hundreds of millions of years during which cooling and uplift rates have been very slow, the errors become multiplied and the calculated surface approach rates virtually meaningless. It then becomes much more meaningful to turn the interpretation approach around and, instead of looking for periods of uplift which probably represent a very small percentage of the time scale involved, to interpret the data in terms of defining periods of crustal stability which are occasionally punctuated by orogenies. If the data are viewed in this way, then it becomes apparent that the reduction in mineral ages with time does not necessarily reflect a rise of the rock towards the surface, but a relaxation of the geothermal gradient in an essentially static and equilibrating continental block coupled with normal erosion rates.

Figure 4.21 shows the variation of apatite ages with crustal depths in regions of slow cooling (10 m/Ma) calculated by Van den Haute (1986) using the same parameters as for the calculation of Figure 4.20. Here however, two different geothermal gradients are

considered, a normal one at 30°C/km and a low one of 15°C/km, which represents the extreme case of a geothermal gradient in a cratonised block. From this it is apparent that a sample on the normal gradient will pass into the zone of total track stability some 200 Ma later than one on the lower gradient. Thus the large difference in apatite ages across the Golmud Fault could be explained in terms of different geothermal gradients either side of the Golmud Fault, with the gradient to the north being lower than that in the south. In particular, this allows for both ages to be exposed at the surface at the present day, without having to invoke differential uplift or erosion rates across the fault in a region that appears to have been essentially stable for 100 Ma.

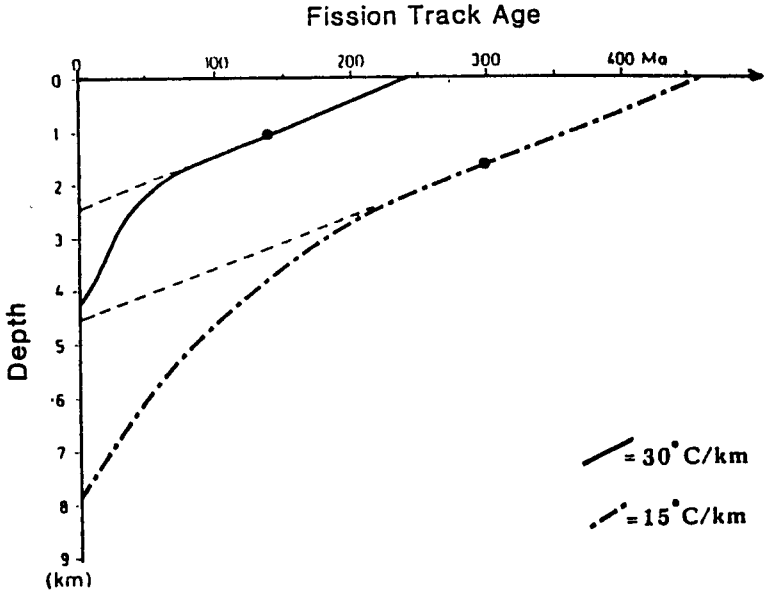

Fig. 4.21 Variation of fission track ages with crustal depth for cases of slow cooling, assuming two different geothermal gradients. Dots on lines represent points above which tracks are stable. Redrawn after Van den Haute (1986).

However, Fig. 4.22 shows the calculated values for the different geothermal gradients north and south of the Golmud Fault at 120 Ma, assuming that biotites in the south were closing at 300°C at approximately the same time and depth as apatites were closing at less than 100°C in the northern block. During the Jurassic thrusting event 50°C/km seems a reasonable value for the south but results in a very low calculated gradient of 15°C/km for the northern region. Furthermore, this large difference in gradients across a relatively small present-day distance of about 25 km, seems geologically unrealistic. However, if both plutons are placed on the same average geothermal gradient of 30°C/km (Fig 4.22) then at 120 Ma the northern block is at a depth of only 3 km, whilst the southern block is

at 10 km. This would require almost 7 km of differential uplift to be accounted for between the two blocks, since 120 Ma.

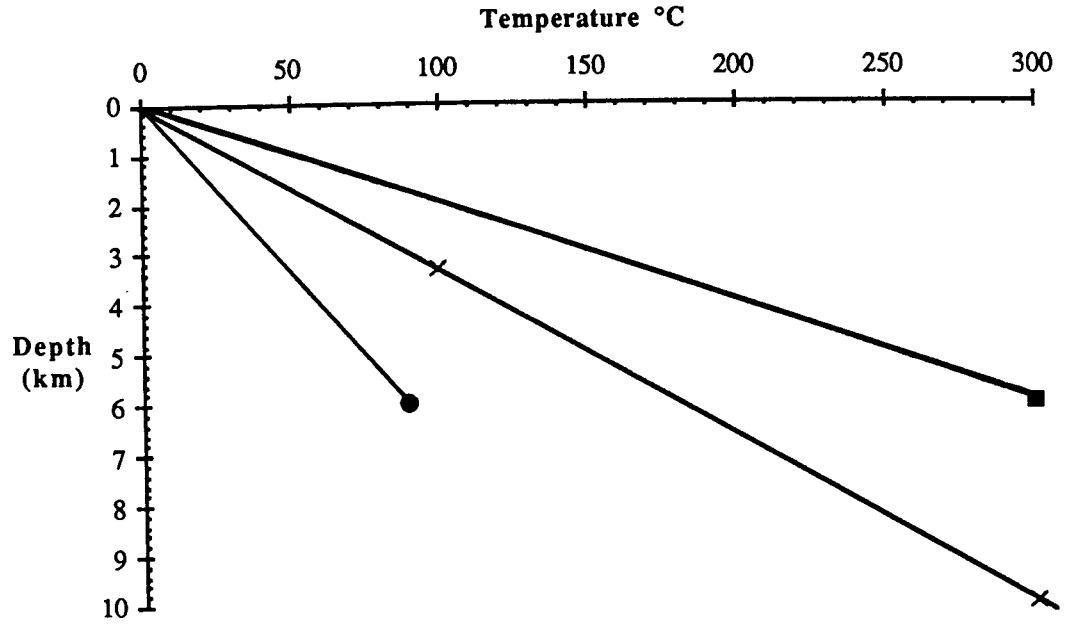

Fig. 4.22 Possible geothermal gradients north and south of the Golmud Fault at 120 Ma. Closed circles = 15°C/km; crosses = 30°C/km; closed squares = 50°C/km.

4.9.2 Differential Uplift Model

Conventionally it is believed that fission track ages decrease with depth as tracks enter the zone of partial annealing and become shortened. Classic examples are to be found in the fission track analysis of deep boreholes (Gleadow and Duddy, 1981 Gleadow *et al.*, 1983 and Hammerschmidt *et al.*, 1984). As a result of partial annealing the track density becomes reduced, which in turn reduces the measured age. However, in regions such as the Kunlun Terrane where slow cooling over a prolonged period of time may have been followed by a phase of uplift, it is possible for the zone of partial annealing associated with this slow cooling, to become uplifted and eroded. The measured ages will then be a mixture of shortened tracks accummulated prior to uplift while sitting in the annealing zone, and new longer tracks formed since uplift into the stability zone. This will result in a mixed age that is older than the actual onset of uplift. Ideally this will result in a bimodal distribution of confined track lengths which can then be identified, but in reality

the two distributions often merge and overlap. Fig. 4.23 shows a generalised curve for the fission track depth profile in the period prior to uplift, in a region that has been static for about 100 Ma (Fitzgerald and Gleadow, 1988).

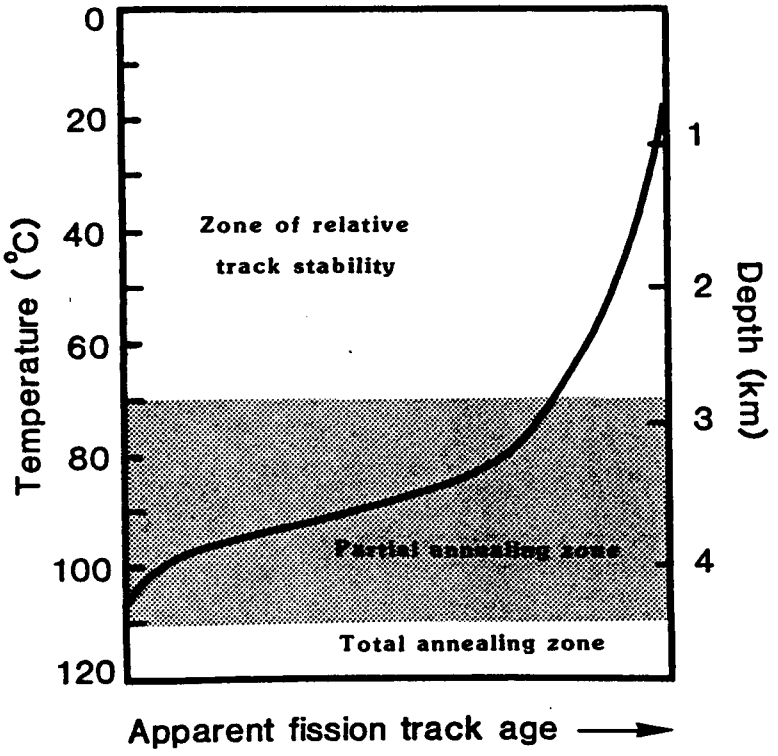

Fig. 4.23 Apparent fission track ages decrease with depth as track lengths become reduced in the partial annealing zone. This curve was calculated for a continental block that has been essentially static for 100 Ma, using the apatite annealing models of Laslett *et al.*, (1987) and Green *et al.*, (1988), and redrawn after Fitzgerald and Gleadow (1988). It assumes a geothermal gradient of 25 °C/km.

If the static region subsequently experienced a period of rapid uplift, then collection of a suite of samples from a vertical section through the region, should reveal a pattern of fission track ages that defined a pronounced break in slope at the point where uplift began (Fig. 4.24). Samples from the slow cooling annealing zone would have a wide range of track lengths and record ages that were older than the onset of uplift, while samples that lay below the break in slope would record younger ages that were closer to the real time of uplift, and have a narrow distribution of long track lengths.

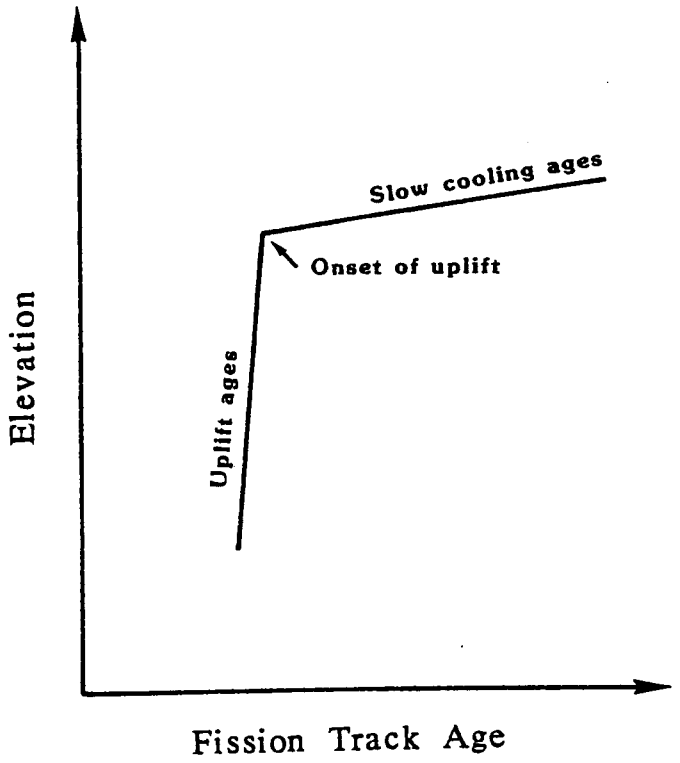

Fig. 4.24 Anticipated fission track age distribution with height in a region that had experienced a long static period followed by rapid uplift.

Typical distributions of confined track lengths from the Southern and Northern Regions show a fairly broad range of tracks with a mean length of 13.52 ± 1.35 μm and 12.62 ± 1.21 μm respectively (Fig. 4.19). Compared to average track lengths of 15 μm from age standards, tracks from the Southern block show a reduction in the mean track length of only 10%, suggesting they are from the upper region of the partial annealing zone (Fig. 4.25) Those from the Northern Block have been reduced by about 15% and are therefore from a slightly lower level in the annealing zone. For this reason it is considered that the Kunlun samples lie on the upper part of the slope in Fig. 4.24.

Examination of Fig. 4.26 confirms a long period of slow cooling in the Kunlun Terrane, with surface approach rates not exceeding 60m/Ma between 120 and 20 Ma. However, the marked increase of surface approach rates in the period subsequent to an apparent age of 20 Ma, suggests there may have been substantial uplift in the Southern block at this time. Also included on Fig. 4.26 is an 'averaged' uplift rate over the last 20 Ma from the Quxu pluton in southern Tibet, to demonstrate how these cooling curves can

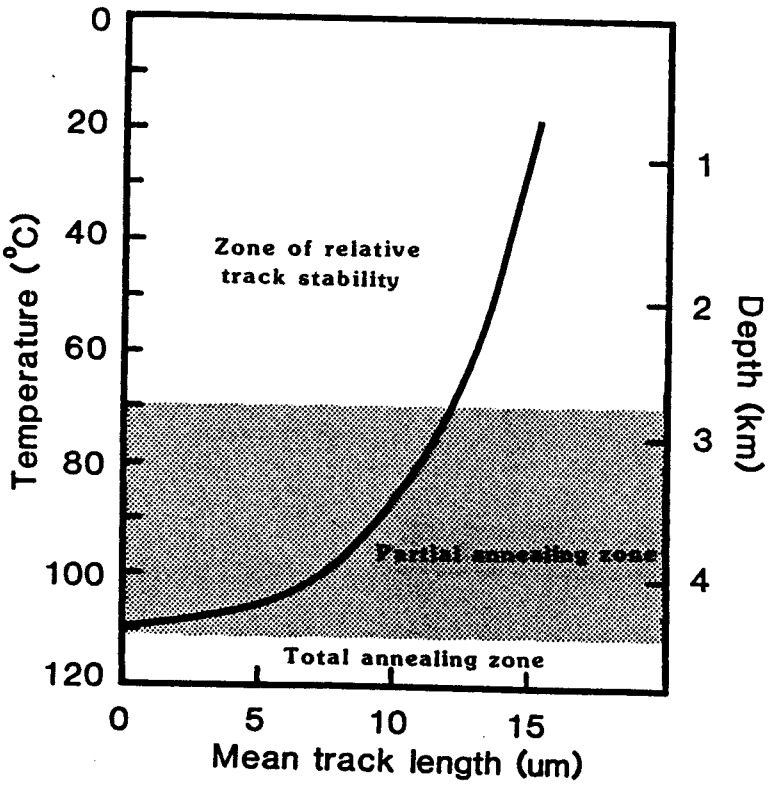

Fig. 4.25 Mean track lengths calculated for samples from a continental block that has been essentially static for 100 Ma, using the models sited in Fig. 4.23. Samples with mean lengths of 12.5 - 13.5 μm, such as those found in the Kunlun Terrane, appear to reside in the upper portion of the partial annealing zone.

hide peaks of uplift such as the period between 20 and 17 Ma, from which it is known that rates accelerated to as much as 4 mm/yr. Clearly, without further constraints it is not possible to be more specific about when periods of acceleration occurred in the Kunlun Terrane.

Nevertheless, since the onset of uplift, 3-4 km must have been removed to expose at the surface today, samples from the top of the partial annealing zone. Had the onset of uplift occurred as long ago as 20 Ma then it is to be expected that even moderate erosion rates would have penetrated to the base of the partial annealing zone to reveal true uplift ages. For example, assuming erosion rates equal uplift rates, even at a moderate erosion rate of 0.5 mm/yr, only 8 Ma would be required to penetrate to the base of the partial annealing zone to reveal true uplift rates. Since these do not appear to be revealed, it must be concluded either that uplift has been relatively recent, or that erosion rates are

unusually slow. That there is no evidence for a major escarpment at the Golmud Fault suggests that the latter is not the case. Thus from these data it appears that the maximum age for the onset of uplift in the Southern block can be constrained to 20 Ma, and the minimum age could be as recent as 8 Ma.

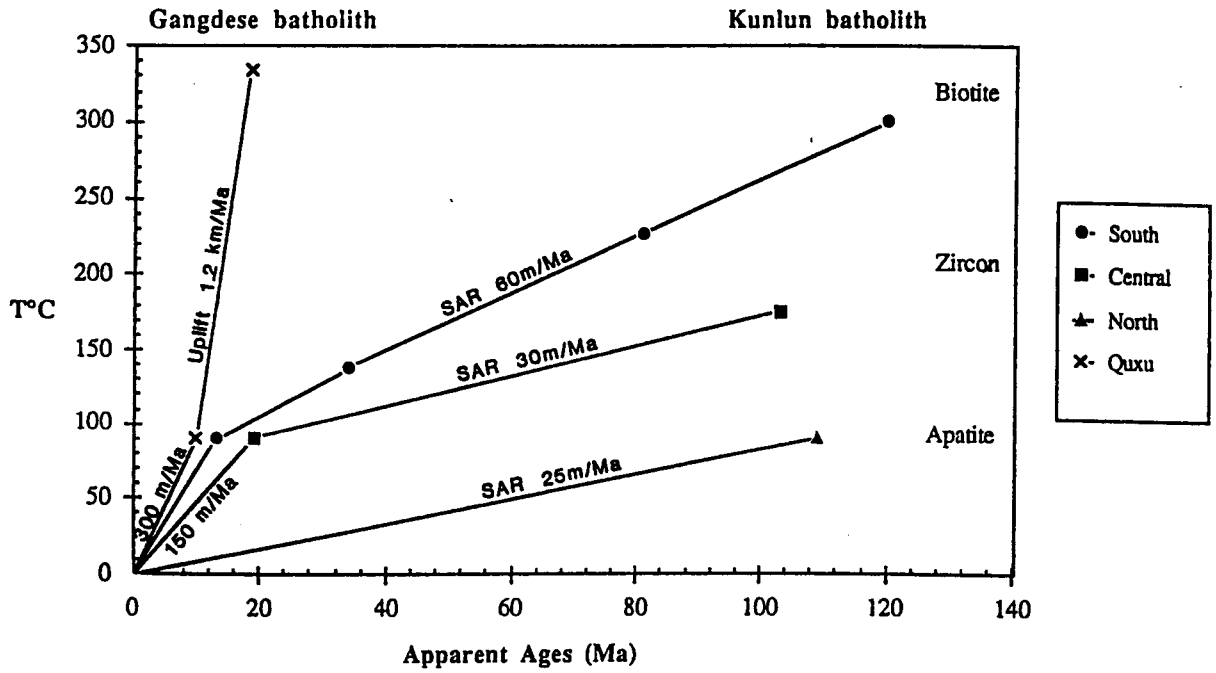

Fig. 4.26 Surface approach rates (SAR) for plutons in the Kunlun compared with averaged rates from the Quxu in Southern Tibet, assuming a geothermal gradient of 30°C/km.

4.9.2 Summary

In summary there are five major features which arise from the fission track data:

1 All apatites south of the Golmud Fault give the same ages around 20 Ma, although present day outcrops are distributed over a horizontal distance of 50 km and a vertical height difference of about 1.5 km.

2 There is a major break in apatite ages across the Golmud Fault with those to the north being 100 Ma years older.

3 Surface approach rates for all plutons between biotite and apatite closure are extremely slow, never approaching more than 60 m/Ma, assuming a geothermal gradient of 30°C/km .

4 Track length distributions suggest that the zone of partial annealing has been penetrated by erosion and that therefore at least 3 km have been eroded from the Southern and Central Regions so this block must have been uplifted relative to the Northern Region.

5 Any rapid uplift in the Kunlun probably occurred between 20 and 8 Ma.

Plate 4.1 Uranium fission tracks in a zircon. Sharp polishing scratches indicate that this face is parrallel to the c axis, and well etched.

CHAPTER FIVE

"Whence came all the granite? How was it formed? For decades this has been a hotly debated subject in geology, and the controversy has recently reached a high pitch."

Tuttle, 1955.

5 GEOCHEMISTRY OF THE KUNLUN GRANITOIDS

5.1 INTRODUCTION

Major element, trace element and isotope geochemistry of all the Kunlun granitoids described in previous chapters will be presented here, so that an integrated approach to the petrogenesis of these granites can be achieved. As defined in Chapter 2, and maintained throughout subsequent chapters, the Kunlun Terrane, north of the Xidatan Fault, is divided into 3 regions by the Xidatan, Mid-Kunlun and Golmud Faults (respectively from south to north) as seen in Fig. 2.1 and Table 2.1. Within these 3 regions the granites show geochemical differences that distinguish one region from another, so for this reason these divisions will be maintained in this geochemistry chapter. However, the Devonian Wanbaogou pluton, although situated in the Southern Region, has geochemical similarities to the Permian Golmud Hydro Group in the Central Region. In this chapter therefore, it will be discussed with this group.

5.2 CLASSIFICATION OF GRANITES

The classification of granitoid rocks has long proved to be problematic and up until the mid-seventies there was not even a widely recognised scheme for naming the plutonic rocks. However, in 1975 Streckeisen published his classification based on the normative proportions of quartz, alkali feldspar and plagioclase, which has now become more or less universally accepted, although the term 'adamellite' is still frequently used instead of monzogranite. In this thesis the Streckeisen classification is adhered to with the addition of monzo and syeno granite fields as being useful sub-divisions within the granite field. Fig. 5.1 clearly demonstrates that the large proportion of Kunlun granitoids are either

monzogranites or granodiorites. Only a few spill over into the syenogranite field while the East Quarry pluton is the only one as basic as a tonalite. Three enclaves fall into the monzodiorite and diorite fields. The calculated normative mineral proportions are given on page 254 of the index.

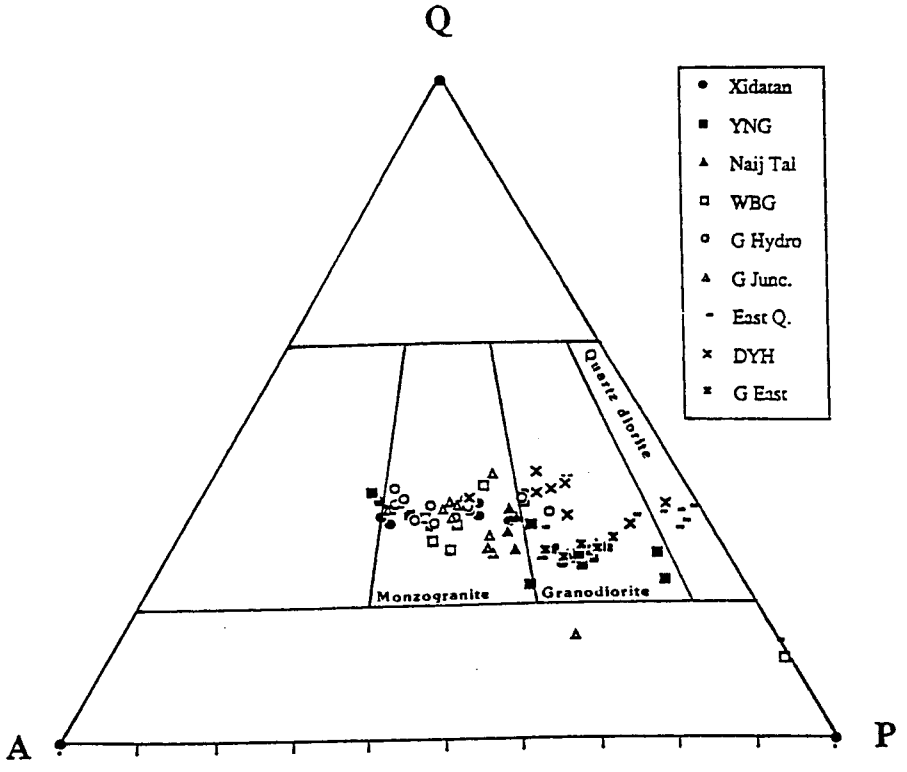

Fig. 5.1 Streckeisen triangular plot for the Kunlun granitoids. Q = quartz; A = alkali feldspar; P = plagioclase feldspar.

Many classification schemes have been used in an attempt to identify the criteria that answer questions regarding the petrogenesis of granites, and the tectonic regime operating at the time of emplacement. Over 60 years ago Shand (1927) used the degree of alumina saturation (A/CNK) to quantify as molecular oxide percent, the peraluminous ($Al_2O_3 > Na_2O + K_2O + CaO$), metaluminous ($Na_2O + K_2O < Al_2O_3 < Na_2O + K_2O + CaO$) and peralkaline ($Al_2O_3 < Na_2O + CaO$) granites. Fig. 5.2a demonstrates the region of the triangle where the Kunlun granites fall along the peraluminous/metaluminous boundary, such that it is necessary to expand the field (Fig. 5.2b) in order to identify exactly which side of the line plutons actually lie. Clearly even at this scale there is little variation, but in general the Central Region and Wanbaogou plutons are peraluminous, along with the Xidatan granite from the Southern Region and the Duo Ya He granodiorite and East

Quarry tonalite from the Northern Region. The only pluton that is totally metaluminous is the Golmud East intrusion; the others straddle the peraluminous/metaluminous boundary.

In 1931 Peacock used the ratio of calcium to alkaline oxides to determine the calc-alkaline series. This scheme was then modified by Brown (1982) to classify granitoids from magmatic arcs in terms of arc maturity as defined by crustal thickness. A further division placed on the Shand triangular plot at 65% CaO identifies the gradation of these magmas from calcic to calkalkaline affinities. It is interesting to note that the high SiO_2 (73-75%) Duo Ya He granodiorite is both calcic and yet peraluminous, as is the far less evolved (65-67% SiO_2) East Quarry stock. These differences must reflect not only different degrees of melting and fractionation, but possibly also different source compositions.

Based on a range of geochemical and mineralogical criteria Chappell and White (1974) produced their now much abused classification of granites from the Lachlan fold belt, Australia. They divided them into two groups, based on inferred source characteristics, which were considered to be either igneous, producing 'I' type granites or sedimentary, producing 'S' type granites. However, this classification proved difficult to impose on granites outside the type area in Australia since many others, such as those from the Kunlun, appear to have characteristics ascribed to both 'I' and 'S' types and did not fall clearly into either group. One of the main criteria extracted from this classification and now frequently used to distinguish 'S' types is whether the granite is strongly peraluminous and has an A/CNK ratio greater than 1.1, which is taken as evidence for a sedimentary source. The A/CNK > 1.1 line has also been added to diagram 5.2b, and it can be seen that only a few Kunlun samples plot above it suggesting that they may be true 'S' types, i.e. that they have been derived entirely from mature sedimentary sources (Chappell and White, 1974; Miller, 1985; White *et al.*, 1986).

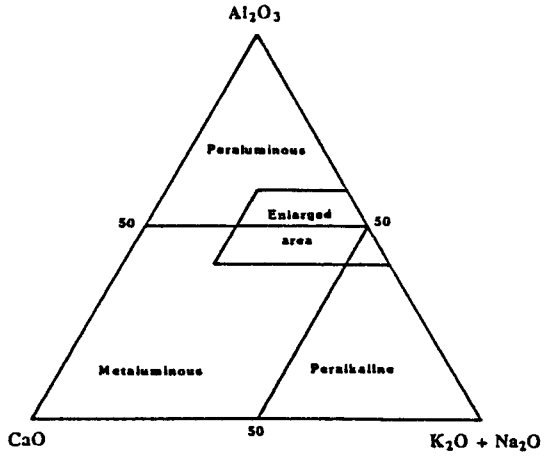

Fig. 5.2a The full Shand triangular plot shows the area expanded in Fig. 5.2b.

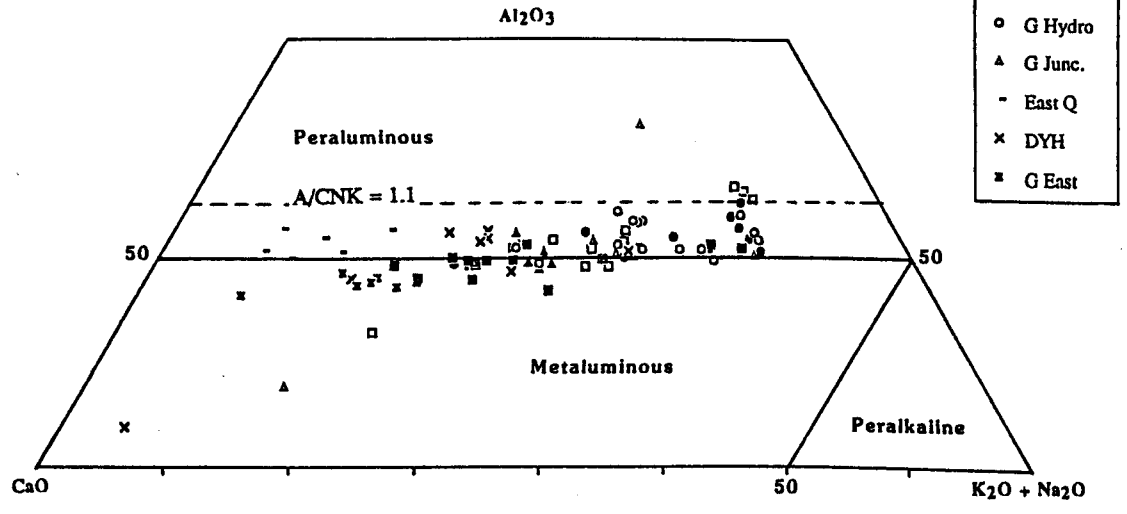

Fig. 5.2b The Shand triangular plot determines the degree of alumina saturation in granitoid rocks. All the Kunlun granitoids fall around the metaluminous/peraluminous boundary. Only a few samples are sufficiently peraluminous to lie above the A/CNK = 1.1 line. Legend as in Fig. 5.1.

However, this definition can often be misleading, and Miller (1985) shows how strongly peraluminous granites, frequently equated with 'S' types, can be derived from a wide variety of sources including a) the melting of intermediate to felsic crust of both immature sedimentary rocks and meta-igneous rocks, and b) the partial melting of metaluminous mafic (crustal or subcrustal) sources. Cawthorn and Brown (1976) have also shown that calc-alkaline magmas as a whole grade with increasing silica from strongly metaluminous through weakly to strongly peraluminous. They attribute this

effect to the fractionation of hornblende which they suggest may persist until the liquids are strongly peraluminous. Zen and Hammerstrom (1982) demonstrate that epidote fractionation can also drive liquid compositions into the strongly peraluminous field and Miller (*op. cit.*) suggests that sphene may have the same effect. It is interesting to note that the more strongly peraluminous samples from the Kunlun are devoid of sphene. In particular, the Xidatan pluton shows how the partial melting of an already weakly metaluminous igneous body can result in a peraluminous melt. The peraluminous leucocratic pods in this orthogneiss (samples 206 c,d,and e) represent partial melts formed during the Jurassic thrusting event when temperatures on the Xidatan fault must have exceeded 700°C (see Chapter 4) and are in no way related to the melting of a sedimentary source. Fractionation may then have enhanced the peraluminous nature of the melt.

Miller, (1986) in his comment on White *et al.* (1986) makes the point that if strictly defined, 98% of granites become 'I' types and only 2% 'S' types. If the definitions are more loosely applied then the classification becomes meaningless, but clearly a classification that only distinguishes 2% of its members is equally useless. It seems reasonable therefore to propose that since the term 'S' type has become entrenched in the literature, it is worth retaining to define a granite with geochemical and isotopic characteristics inherited through the partial melting of a mature crustal sedimentary source. However, further classification must be sought for the remaining 98%.

In 1984 Pearce *et al.* proposed a series of discrimination diagrams that used trace elements in an attempt to assign granitic rocks to 4 tectonic settings. Based on 600 samples from known tectonic environments, the systematic differences seen in the trace element ratios were used to identify these groups. Whereas this classification worked well for extreme types such as ocean ridge and within plate granites, it was much harder to distinguish volcanic arc from syn-collision granites unless the latter had exceptionally high Rb, and post-tectonic granites fell into almost any field.

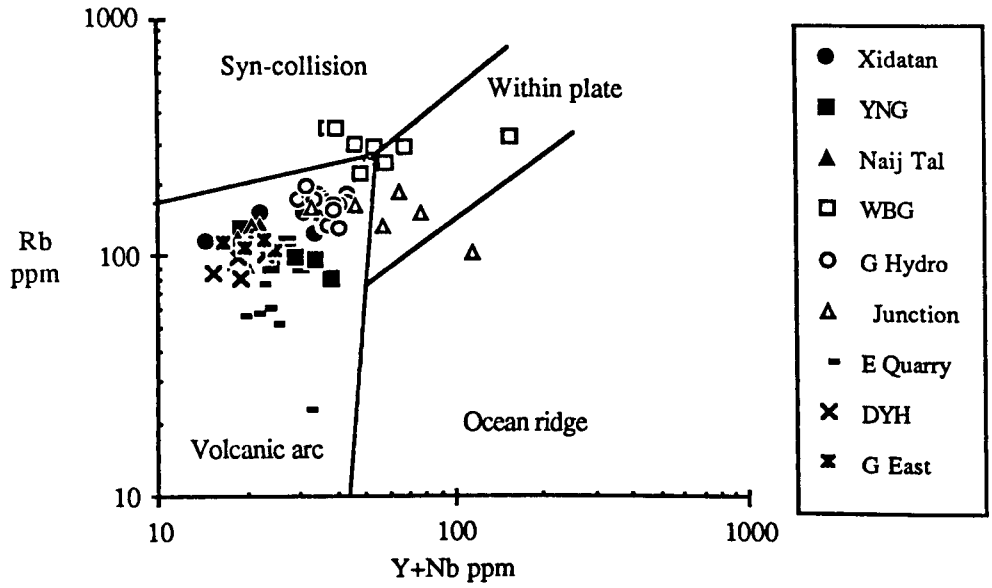

Fig. 5.3 Trace element diagram of Rb/Y+Nb used to discriminate between magmatic emplacement of granites into different tectonic environments. After Pearce *et al.*, (1984).

In the Kunlun granites, Fig 5.3 shows that all samples except for the Wanbaogou pluton fall into the volcanic arc field. Despite this it can be seen that samples from the Kunlun Central Region have increased Rb values, which separates them from the others. The post-tectonic granites from the Southern Region however, and the Northern Region granodiorites are virtually indistinguishable. Furthermore, it is not clear whether granites from the Central Region represent Rb-poor, syn-collision granites, or if they are simply more highly fractionated and evolved equivalents of the granodiorites to the north. Similarly, the Wanbaogou pluton may be a syn-collision granite since it plots in this field, but the field relations are consistent with it being a post-tectonic granite, possibly similar to the Grandes Rousses post-collision granite which Pearce *et al.* show also falls into the syn-collision field. The high Nb and Y values seen in the Golmud Junction pluton are believed to be the result of them predominantly representing a restitic phase of the Golmud Hydro group, and not because they have been derived in a within plate environment as inferred by Fig. 5.3.

Syn-collision granites are typically represented by High Himalayan leucogranites such as the Manaslu granite (Denielle *et al.*, 1987), which fall into the syn-collision field on Fig. 5.3, due to their high Rb contents. Partial melting will fractionate Rb and Sr due to

the greater incompatibility of Rb during this process. Sedimentation processes however, also fractionate Rb and Sr since Rb tends to remain in clay minerals while Sr is more easily dissolved and washed away. This results in mature sediments having a high Rb content which, when subjected to partial melting, will be increased even further. The Himalayan leucogranites have been shown to have been derived from such sources but it is probable that melts of immature sediments will not show such highly fractionated Rb values, especially if the melt volumes are large, and they will therefore not necessarily fall into the syn-collision field even though they have been generated in the type of tectonic regime that this implies.

Clearly, while many of these classifications are useful as a first order interpretation, it is still necessary to look in detail at individual suites to examine why they do (or why they do not) fit the classification.

5.3 MAJOR AND TRACE ELEMENT VARIATIONS

Silica variation within any one pluton is extremely limited and in the sampled plutons the total range is only between 65% and 76%. The full major and trace element data set is given in Appendix D. Harker variation diagrams are presented here for each of the 3 regions from the Kunlun Terrane and the Wanbaogou pluton. Inherent in these diagrams is the assumption that if the major and trace elements depicted behave in a coherent manner and define linear trends, then they are likely to reflect primary igneous processes. Included on the diagrams are values from the enclaves found in association with the host granites in an attempt to constrain the relationship between them.

5.3.1 Southern Region

For comparison, all the Permian post tectonic granites from the Southern Region are shown on the same diagrams and, except for Na_2O, the major elements define tight linear trends (Fig. 5.4a). The scatter seen in Na_2O may reflect the slight amount of feldspar alteration seen in these plutons. The enclave (61% SiO_2), from the Yie Nin Gou intrusion, falls on an extrapolation of all the major element trends, except CaO, Na_2O and

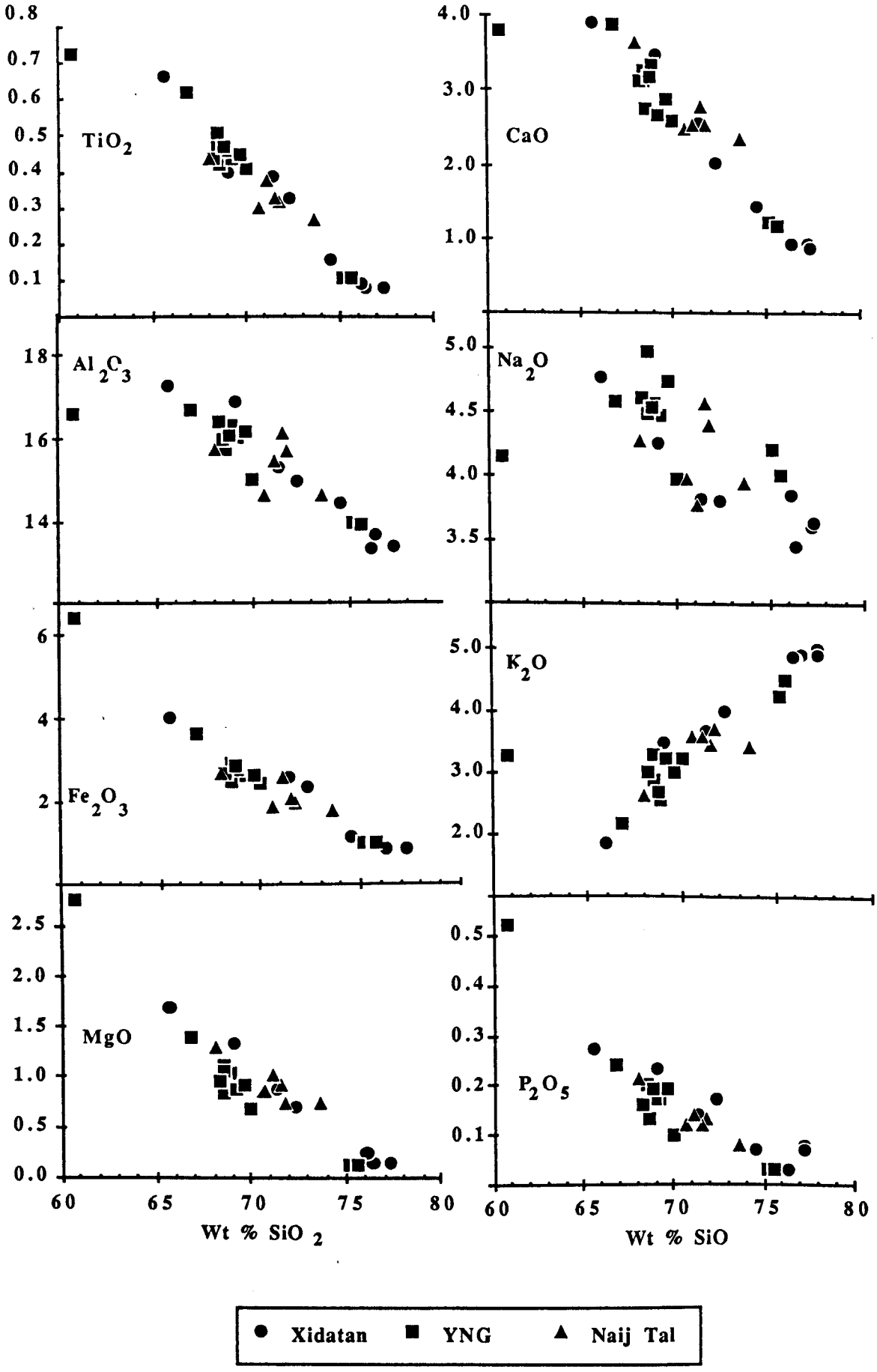

Fig. 5.4a Harker diagrams for major elements from the Southern Region plutons.

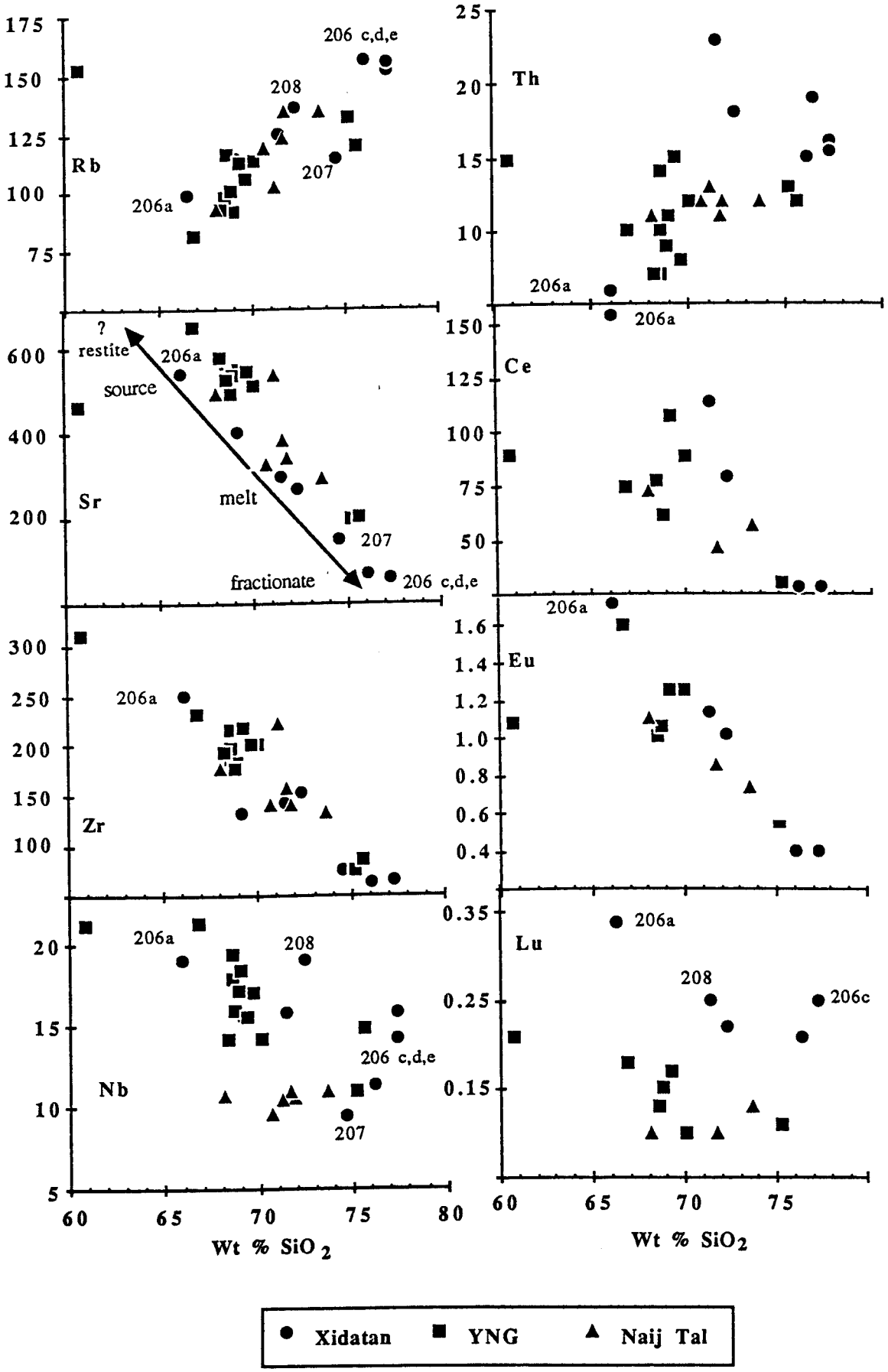

Fig. 5.4b Harker diagrams for trace elements from the Southern Region plutons.

K_2O, indicating that it may represent an earlier, less evolved fraction of the granite and be related by simple fractionation. However, that the enclave values consistently fall below the highest value for the strongly compatible elements (Ca, Na, Sr and Eu) and that the reverse is true for the incompatible elements, suggests that there is an inflexion point in the data at about 65% SiO_2 which corresponds to the appearance and disappearance of liquidus minerals carrying these elements.

Of the trace elements, only Sr and Eu define good trends (Fig. 5.4b), undoubtedly reflecting feldspar fractionation. Rb and Zr show limited scatter but the remaining trace elements and REE appear to be fairly random, although on closer inspection the grouping within each pluton is noticeably consistent, if in no way linear. As mentioned in Chapter 2 (section 2.2) a feature of these plutons is the accessory phases of apatite, zircon, sphene and, in particular, allanite. These minor phases appear to be variously influencing the behaviour of the trace elements in these plutons causing the considerable scatter seen here. This difference in behaviour of the trace elements in the different plutons suggests that they are not cogenetic and have experienced separate fractionation histories, although the melts could have originated from similar sources.

5.3.2 Xidatan Pluton

As already mentioned in previous chapters, the biotite age of the pluton has been totally reset at 120 Ma and the leucocratic dykes and pods within it indicate that incipient melting occurred during the resetting event. If this interpretation is accepted, then the trace elements must be viewed as defining a partial melting trend rather than a fractionation trend. In fact the data are best explained by considering that sample G206a represents the original, relatively unaffected source from which varying degrees of melt have been extracted, leaving a residue or restite phase that has not been sampled. Due to the difficulty of separating such small degree melts from their source, a representative sample of the restite is unlikely to exist. Samples G208 and G206b can then be interpreted as representing melt plus restite, while G207 is mostly melt from which G206c,d, and e have fractionated (see Sr box on Fig. 5.4b).

Chappell and Stevens (1988) argue that the composition of a granite source must lie on a linear trend between restite and melt. In this suite however, trends are complicated by fractional crystallisation of the extracted melt. Sr for example shows a linear trend from G206a, which most closely represents the restite phase, through to the fractionated extremes of the melt, that is almost impossible to distinguish from a fractionation trend. Nb and Th however, have elemental abundances in the restite and melt-mix samples that are much the same as in the source. Extraction of the melt (G207) leaves it severely depleted in these compatible elements while fractionation increases them again to the same or higher abundance levels than in the source.

5.3.3 Wanbaogou pluton

TiO_2, Fe_2O_3, MgO, CaO and trace elements from the Wanbaogou pluton show reasonably well defined trends that can often be extrapolated back to the enclave (Fig. 5.5.a and b), although the alkalis display some scatter which may have resulted from the hydrothermal alteration discussed in section 3.2.3. That the three G232 samples from the leucocratic stock also fall on the trends is a good indication that they are cogenetically related and part of the same evolutionary suite. From their high $^{87}Sr/^{86}Sr$ ratios which caused these samples to fall above the isochron line, and the fact that they are in faulted contact with the main body, it was not clear whether these were part of the same sequence. The major and trace elements allow a cogenetic origin for the two suites and lend futher support to the suggestion that boron-rich, late-stage hydrothermal fluids may have contained a high $^{87}Sr/^{86}Sr$ component .

Although the major and trace element data are limited, the enclave (SiO_2 55%) is considered to represent an earlier phase of the fractionation trend and an inflexion point could be imposed on the data set at about 65% SiO_2. As such, this is evidence for a liquid magma, the evolution of which was controlled by fractional crystallisation. Further support for the enclave being part of the fractionation trend is seen in the fact that the enclave falls on the isochron line (section 3.2.3).

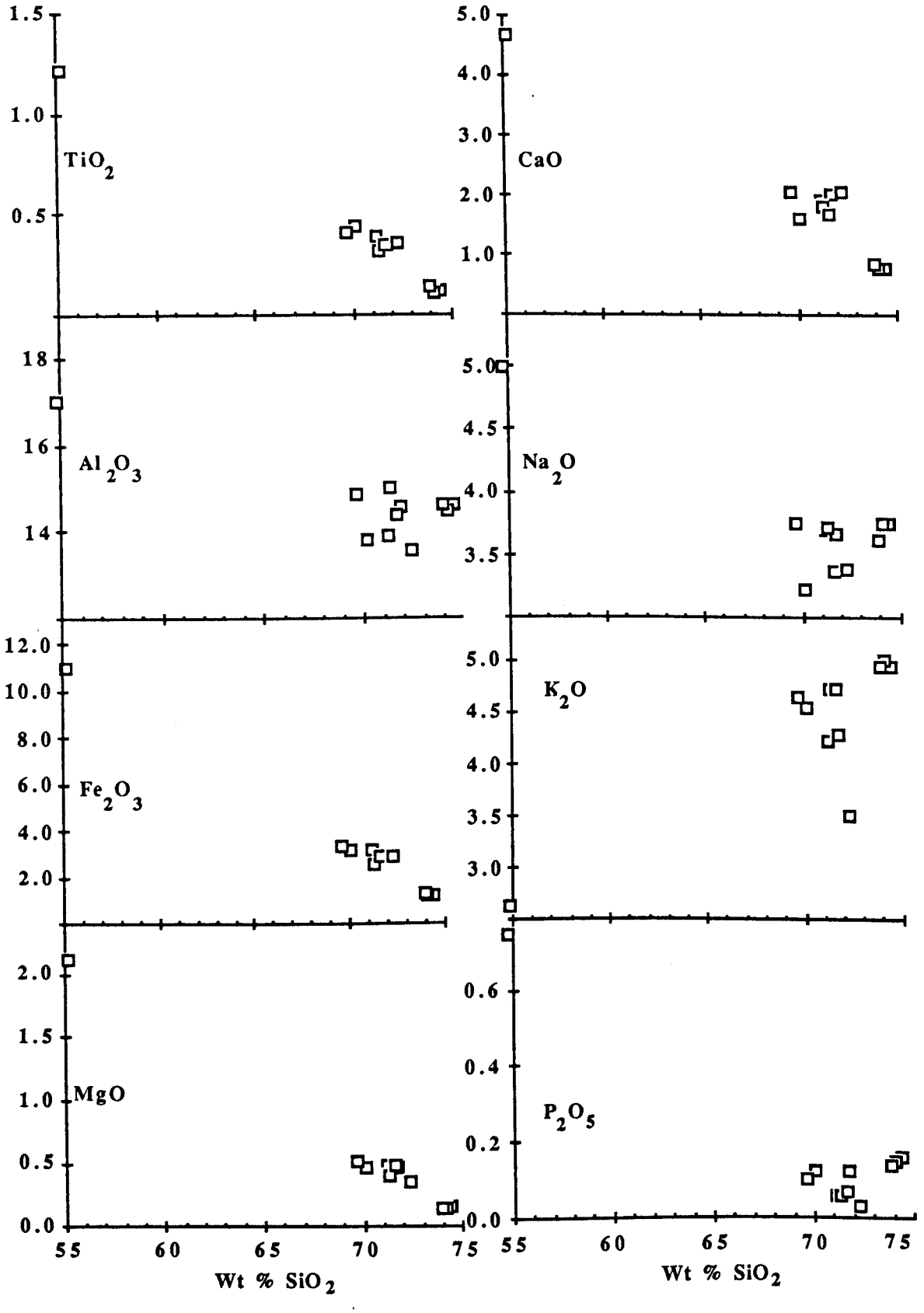

Fig. 5.5a Harker diagrams for major elements from the Wanbaogou pluton.

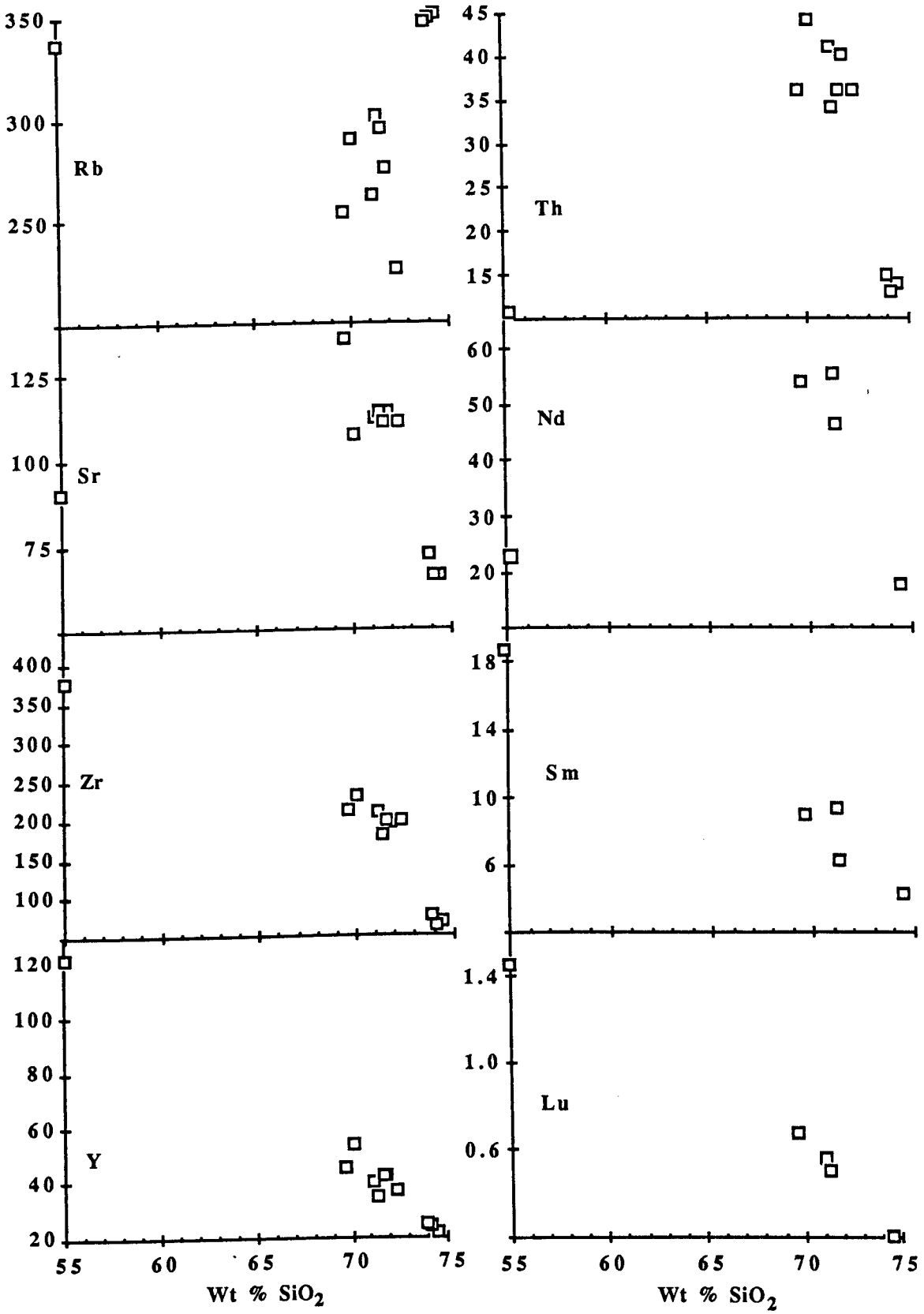

Fig. 5.5b Harker diagrams for selected trace elements from the Wanbaogou pluton.

5.3.4 Central Region

Reasonably well defined trends, that can also be extrapolated to the enclave from the Golmud Junction intrusion, are found in most of the major elements from this group although the alkalis again show some scatter (Fig. 5.6a). Sr and Eu (not shown) again reflect feldspar fractionation. As in the Southern Region, the crystallisation of minor phases appears to be strongly controlling the trace elements (Fig 5.6b) so it is significant that the absence of sphene and allanite, coupled with a marked reduction in the amount of zircon and apatite seen in the highly evolved Golmud Central granites, is reflected in low abundances of trace and rare earth elements. The high Y + Nb values demonstrated on Fig 5.3 which cause the Golmud Junction suite to fall in the 'within-plate' field could be explained if this group is considered to primarily represent restite material from which varying degrees of melt have been extracted, resulting in enrichment of compatible elements in these samples. This seems more realistic than trying to argue for a significant difference in tectonic environment during the emplacement of this pluton which is clearly related geochemically to the rest of the Golmud Hydro Group. On the other hand, Zr, usually a good indicator of cogenetic relationships, does not show a clear trend between the Golmud Hydro and Golmud Junction groups. This indicates that the suggestion of two trends seen in many of the major element plots (MgO, K_2O and Fe_2O_3) is real and that although the magmas may have been related at source, they again represent different melting events which have been subjected to different fractionation histories. Significant in this suite is the marked compatibility of all trace elements. Only Ta and Rb in the Golmud Hydro suite show an incompatible trend.

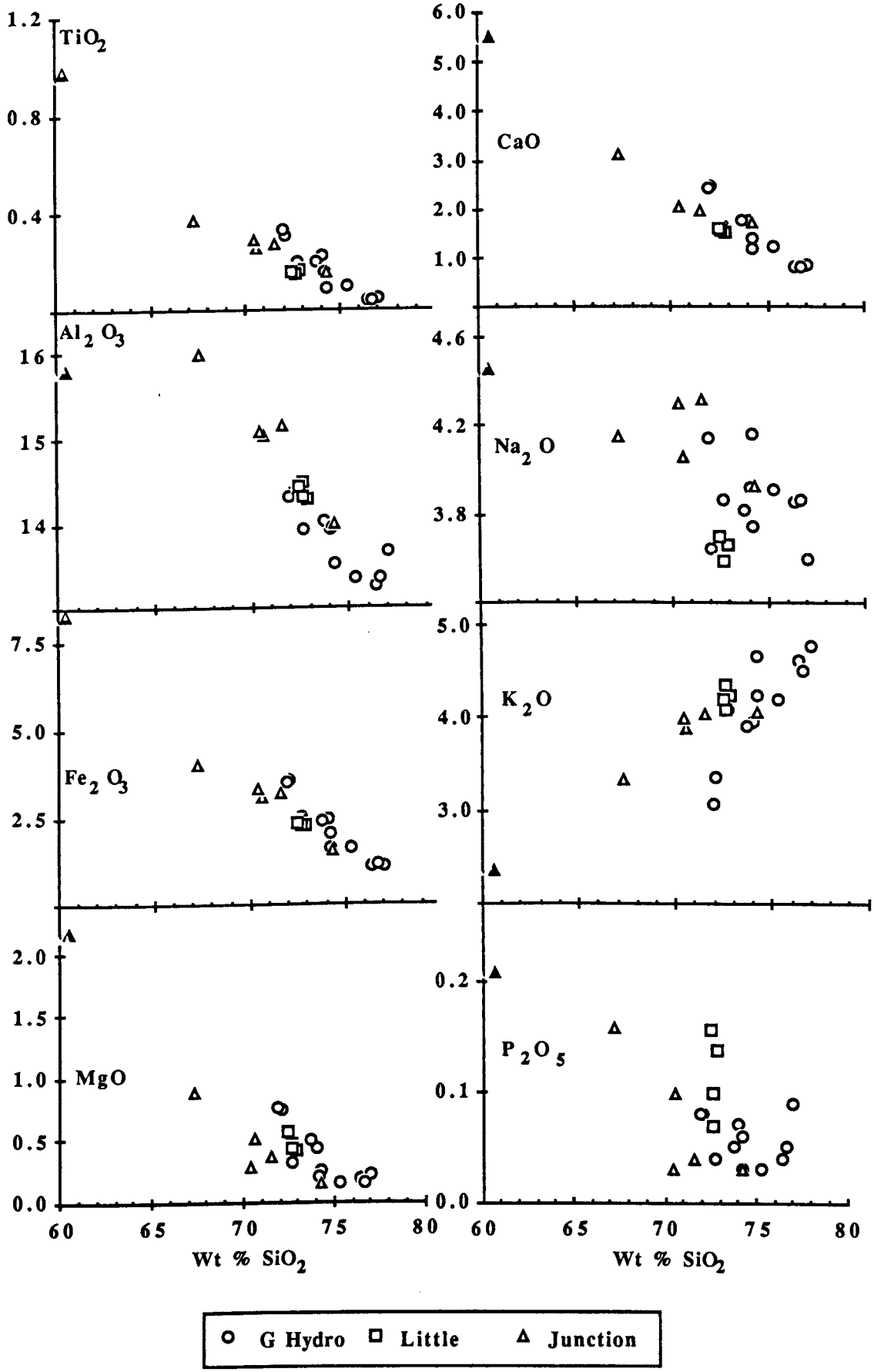

Fig. 5.6a Harker diagrams for major elements from the Golmud Hydro Group.

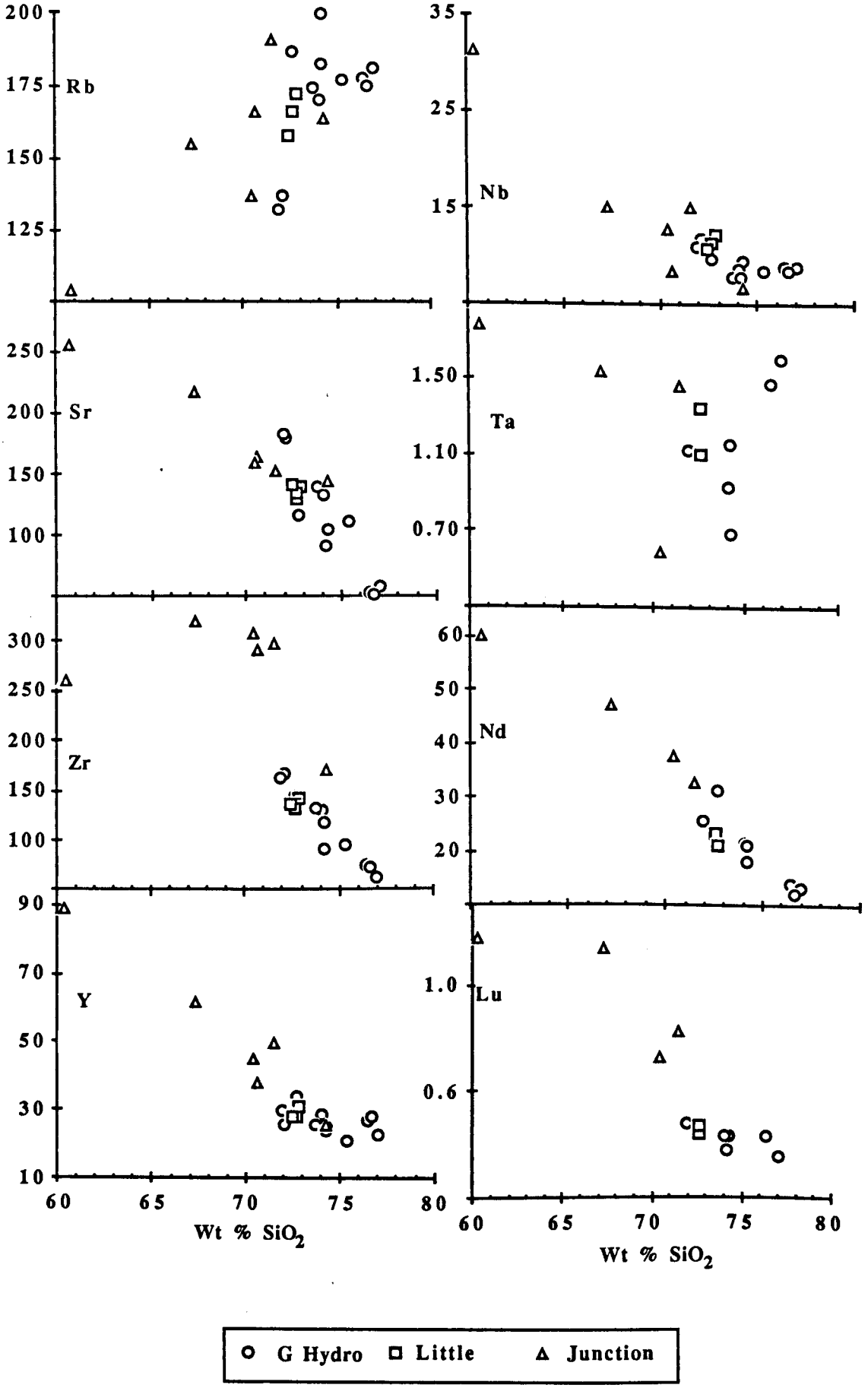

Fig. 5.6b Harker diagrams for trace elements from the Central Region plutons.

5.3.5 Northern Region

The East Quarry stock is well constrained in having both an enclave (SiO_2 = 53%) and a pegmatite (SiO_2 = 75%) with which to mark the extremities of magmatic evolution. Most of the major elements define a tight linear trend on which samples from the Golmud East pluton also fall, although K_2O shows the 2 plutons group very differently. Trace elements again indicate that the enclave is part of the fractionation trend but most of the elements are severely depleted in the pegmatite. The small spread of SiO_2 values from the main body of the pluton does not give a clear indication of an elements compatibility, but the indications are that even in these considerably more mafic melts, only Rb is obviously incompatible.

Clearly these three Northern Region plutons are not related cogenetically, although the East Quarry stock and Golmud East intrusion may be derived from the same source and have similar fractionation histories. The Duo Ya He pluton however, appears to have originated from a more silicic source.

5.4 TRACE ELEMENT GEOCHEMISTRY

Although trace element modelling is generally considered to be a powerful technique for identifying the source of granitoid melts (Arth and Hanson, 1975; Barker *et al.*, 1976; Condie and Hunter, 1976; Hanson, 1978; Foucarde and Allègre, 1981, and Pearce *et al.*, 1984), many problems arise as a result of the high silica contents and consequent high viscosity of granitic melts. Due to this high viscosity, most granitic magmas can be considered to be crystal 'mushes' from which separation of the melt phase is probably very inefficient. This results in no clear division between cumulate and liquid fraction, and Miller and Mittlefehldt (1982) suggest that small accessory phases can only separate from the magma if they are incorporated as inclusions in larger crystals such as biotite.Mahood and Hildreth (1983) argue that when the silica content is greater than 75% SiO_2, then the partitioning of trace elements is no longer controlled by the ease with which they can enter the lattice of a crystallising phase. Instead, the dominant control

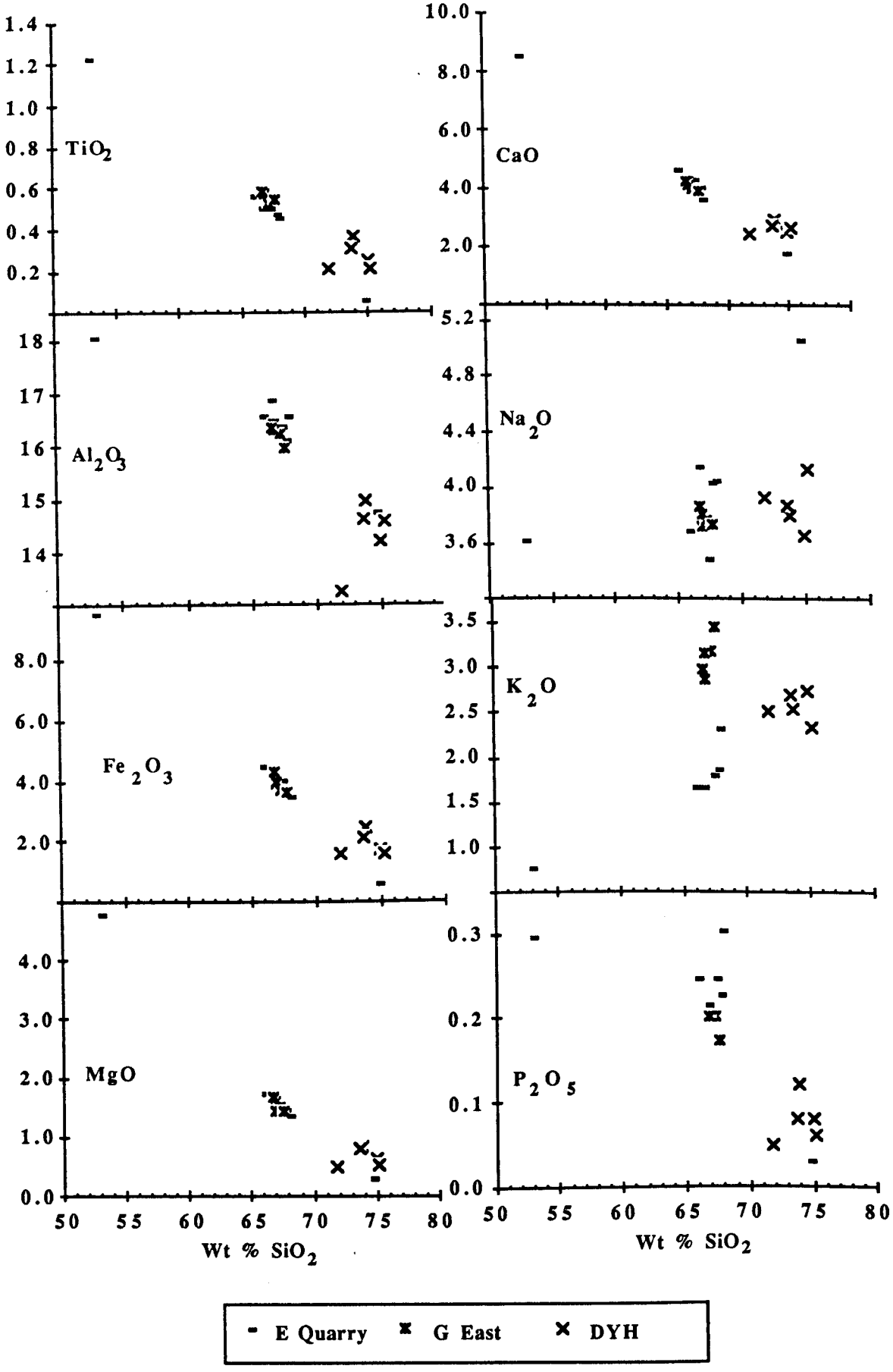

Fig. 5.7a Harker diagrams for major elements from the Northern Region plutons.

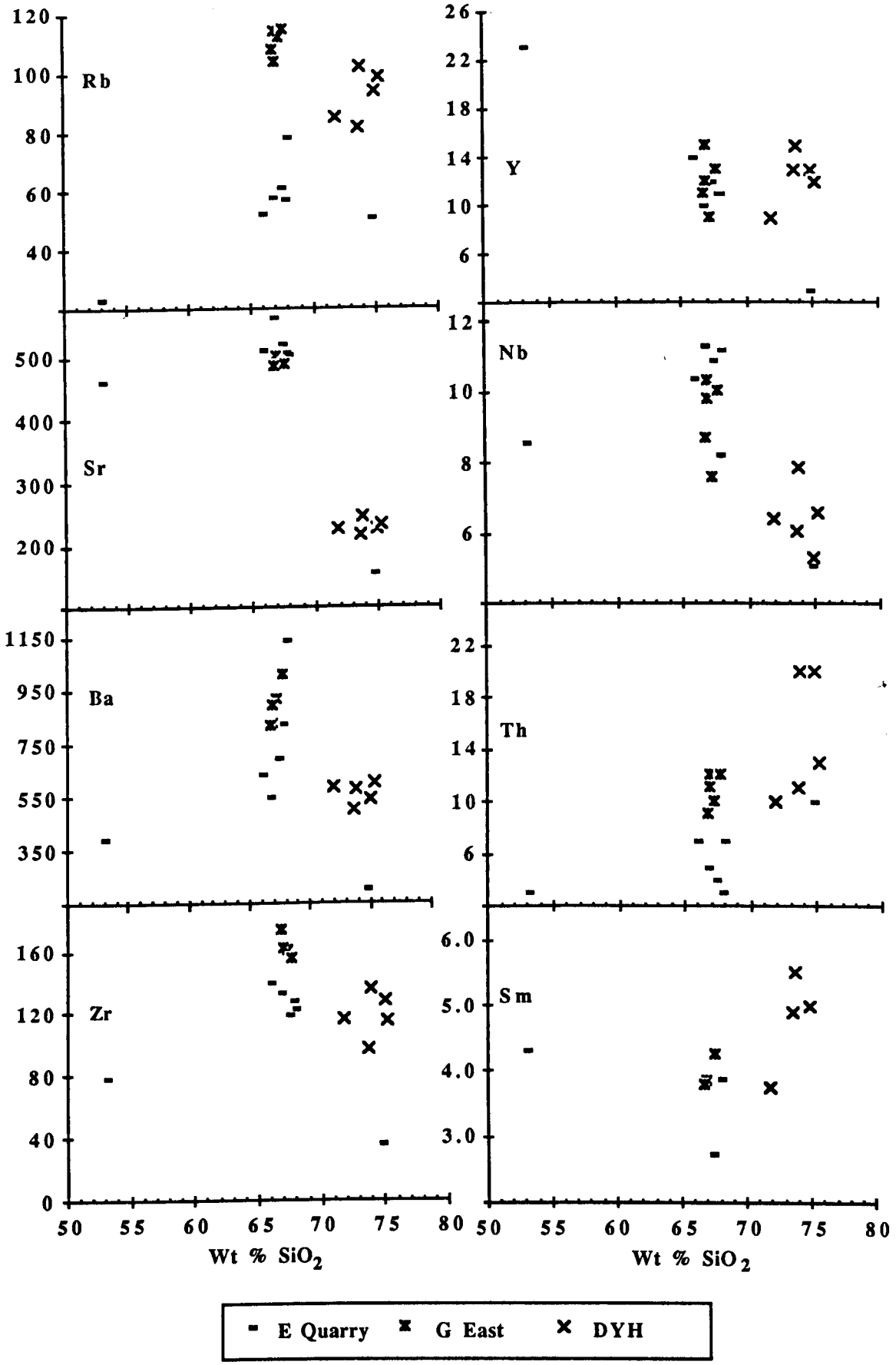

Fig. 5.7b Harker diagrams for trace elements from the Northern Region plutons.

becomes the 'liquid structure' of the melt which can greatly alter the distribution coefficients of trace elements. In less silicic melts the distribution of many trace elements, particularly the LREE, Hf, Zr, Th, U and Ta, is now generally accepted to be strongly controlled by the crystallisation of minor phases such as sphene, allanite, zircon, apatite and, in some granites, xenotime and monazite. These last two phases were not identified in the Kunlun granitoids although the similarity in thin section of zircon and monazite often precludes identification of the latter. Miller and Mittlefehldt (1982) suggest that the LREE are stochiometric constituents of allanite, comprising about 20% of the mineral. This results in allanite having an effective KD_{LREE} in the range of 10^3 to 10^4.

Zircon solubility is lower in highly silicic melts than in more intermediate melts at the same temperature (Watson and Harrison, 1983) and in peraluminous melts the saturation concentration of the melt is between 25 ppm Zr (Watson and Harrison *op. cit.*) and 70 ppm Zr (Harrison *et al.*, 1987). Therefore, peraluminous melts that contain higher values than that in the least evolved member of a fractionation suite, should contain a significant proportion of inherited zircons. Support for the presence of inherited zircons in the Kunlun granitoids is seen not only in their high Zr concentrations, but also in samples which contain large (up to 1mm), but rounded zircons. It seems likely that the rounding effect is due to partial dissolution of the zircon as a result of reaction with the melt as they were being entrained. All zircons polished and etched for fission track analysis showed strong zonation of U implying several stages of growth. Large, rounded zircons are particularly a feature of the mafic enclaves and the less evolved Northern Region plutons, and is strong evidence that these were derived from crustal, rather than mantle, melts.

Apatite is generally considered to be largely residual during crustal melting (Harrison and Watson, 1983) and Chappell (1978) found that it occurred as inclusions in all mineral phases, but was concentrated in biotite and hornblende by a factor of 20 or more relative to alkali feldspar. These data suggest that apatite was a restite phase and since most of the Kunlun enclaves contained approximately 1% apatite it suggests that these early fractions still contained a high proportion of restite. However, along with sphene, apatite has

KD_{REE} in the range of 20 - 60, so large quantities would need to be removed by fractionation from the melt to significantly deplete the liquid in REE. Fig 5.8 shows typical REE patterns for the accessory mineral phases found in the Kunlun granitoids (data from Taylor and Mc Lennan, 1985).

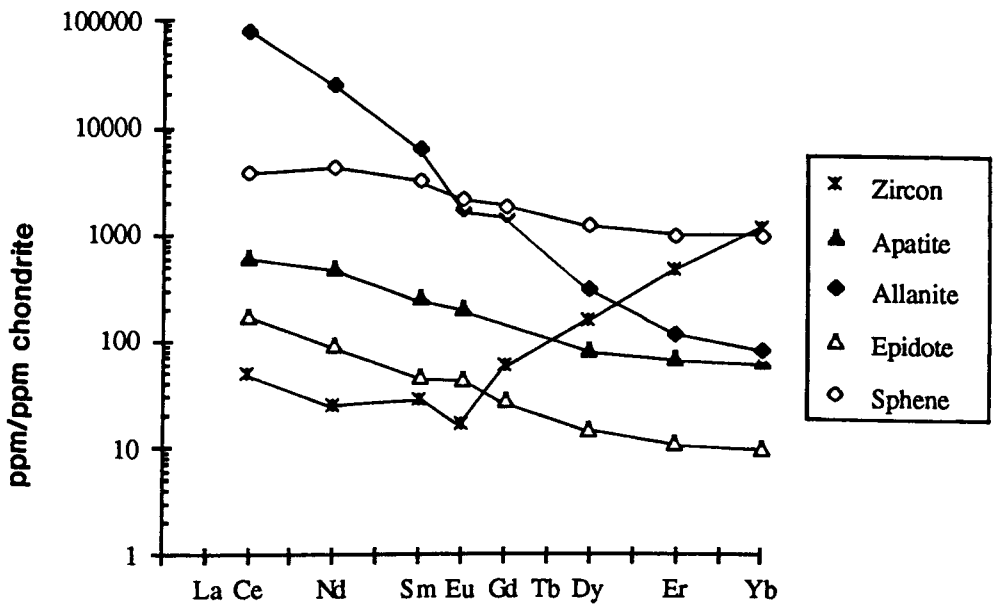

Fig. 5.8 REE patterns for the accessory mineral phases found in the Kunlun granites. Redrawn after Taylor and McLennan (1985).

Volatile components can also play a major role in controlling the behaviour of trace elements in granitic melts. Harris (1981) demonstrated that F tends to concentrate in the residual fluid while Cl is concentrated in the volatile phase. F in the melt greatly decreases the K_D values of HFS elements through the stability of fluoride complexes.

5.4.1 Large Ion Lithophile Modelling

The LIL elements Rb, Sr, and Ba have been used for petrogenetic modelling in granitic systems (e.g. McCarthy and Hasty, 1976; McCarthy and Groves, 1979, and Tindle and Pearce, 1981) because they are found almost entirely within the major silicate phases. The data are presented as logarithmic plots of Ba against Rb and Sr, and superimposed on

the diagrams are vectors for the Rayleigh fractionation of the three LIL element bearing phases of plagioclase feldspar, alkali feldspar and biotite.

Problems with this type of modelling are associated with assumptions regarding the accuracy of the distribution coefficients used in the calculations, which can change considerably as the melt becomes progressively more acidic, so the values used can only be an average or an approximation of the real values. Assumptions inherent in the Rayleigh crystal fractionation model are also somewhat simplistic in that it presumes a closed system in which crystals are removed from the liquid as fast as they are formed. Nevertheless, the modelling does appear to give a reasonable estimation of the dominant mineral phases involved during crystallisation and the amount of liquid remaining after fractionation. The equation is given below and the distribution coefficients used in the calculations are shown in Table 5.1.

$$C_l^e = C_o^e F^{(D-1)} \qquad (5.1)$$

where

C_l^e = concentration of the element in the final liquid

C_o^e = concentration of the element in the initial liquid

F = weight fraction of liquid remaining

D = bulk distribution coefficient of the element

	Plagioclase	K-feldspar	Biotite
Ba	0.36	6.12	6.36
Sr	2.94	3.87	0.12
Rb	0.05	0.34	3.26

Table. 5.1 Distribution coefficients used in LIL element modelling. (Values after Arth and Hanson, 1975 and Hanson, 1978.)

In the Southern Region the Yie Nin Gou granodiorite shows limited fractionation dominated by alkali feldspar crystallisation (Fig 5.9), particularly for the highly evolved 213 samples from the YNG X pluton.

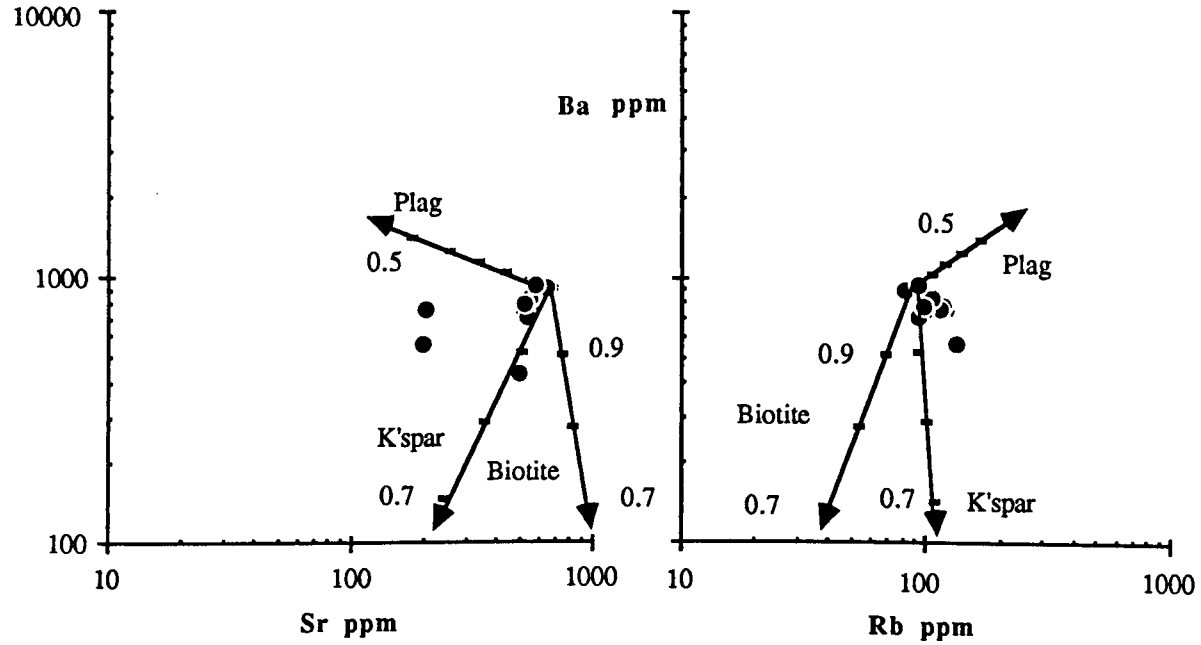

Fig. 5.9 LIL element models for the Yie Nin Gou pluton.

The LIL elements in the Xidatan pluton (Fig 5.10) also appear to be strongly controlled by alkali feldspar crystallisation, if G206a is considered to represent the least evolved sample, and the degree of fractionation required to produce the final liquid as represented by sample 206c is much higher than in the Yie Nin Gou. Modelling showed that it was not possible however, to relate the two trends by fractionation from the same initial liquid, supporting the earlier suggestion that whilst these plutons are of a very similar age and composition , they represent discrete melting events and are therefore not cogenetic. In the light of discussions in section 5.2.1 however, if sample G207 from the Xidatan suite is considered to represent the least evolved sample of the later melt, then clearly the degree of fractional crystallisation has been considerably less than that indicated in Fig. 5.10.

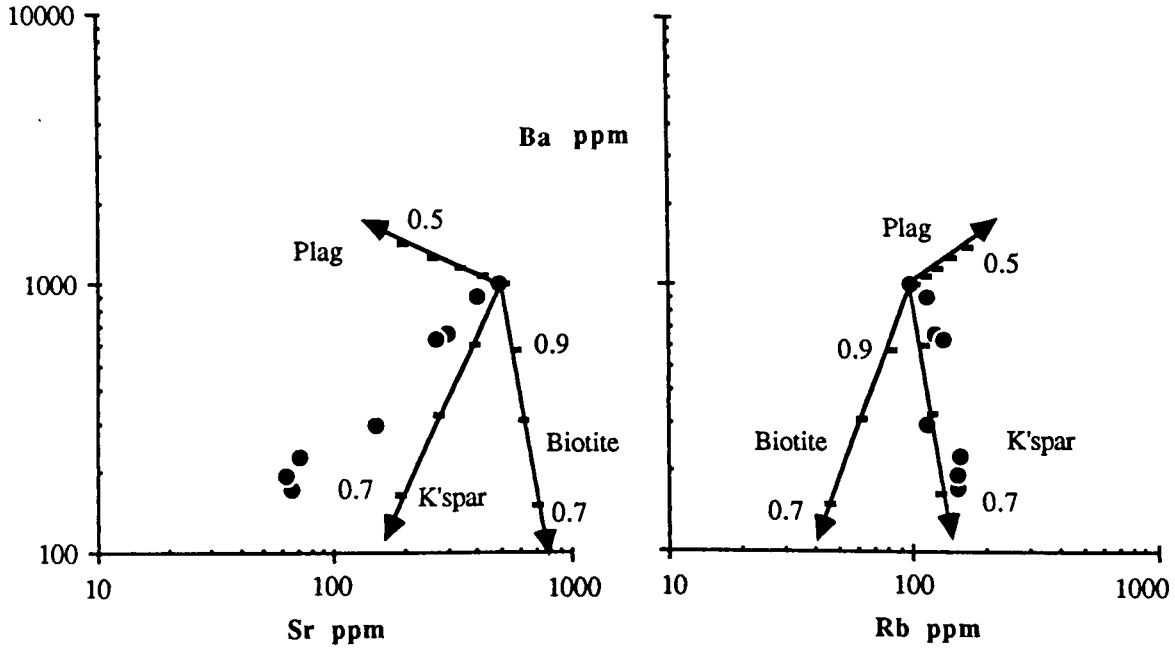

Fig. 5.10 LIL element models for the Xidatan pluton.

Samples from the Wanbaogou pluton show 2 distinct trends, one for the main body of the pluton which appears to be controlled by biotite fractionation, while the leucocratic stock (G232 samples) is dominated by alkali feldspar fractionation although they have clearly originated from the same initial liquid (Fig. 5.11). The degree of fractionation

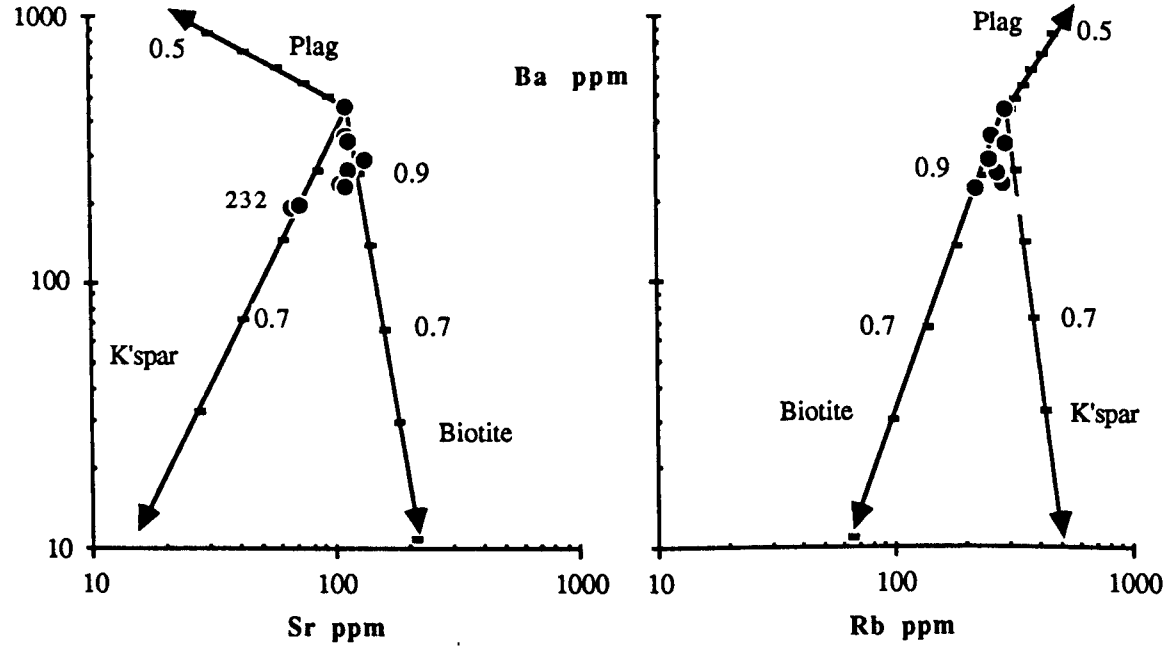

Fig. 5.11 LIL element models for the Wanbaogou pluton. Note the lower values used for the Ba scale in this pluton

is surprisingly small considering the highly evolved nature of the pluton and this must reflect a significant difference in the source composition compared to that of the post-tectonic plutons to the south.

In the Golmud Hydro Group it is unclear whether sample G249a is representative of the least evolved liquid from which all pulses of magma have been derived, (as seen in Fig 5.12a); whether the Golmud Junction suite represents restite material, or if the two trends have originated from different liquids. If G244a is assumed to represent the primary liquid for the Golmud Central and Pink plutons (Fig 5.12b) then the main difference is seen in the degree of fractionation required to crystallise the most highly evolved samples. The main trend is still controlled by alkali feldspar crystallisation, while in the Golmud Little and Junction plutons biotite crystallisation plays a greater role. The two samples (G260 and G261) that fall off the main trend of the Golmud Hydro group (Fig. 5.12b) are considered to represent restite material and are therefore not part of the fractionation trend.

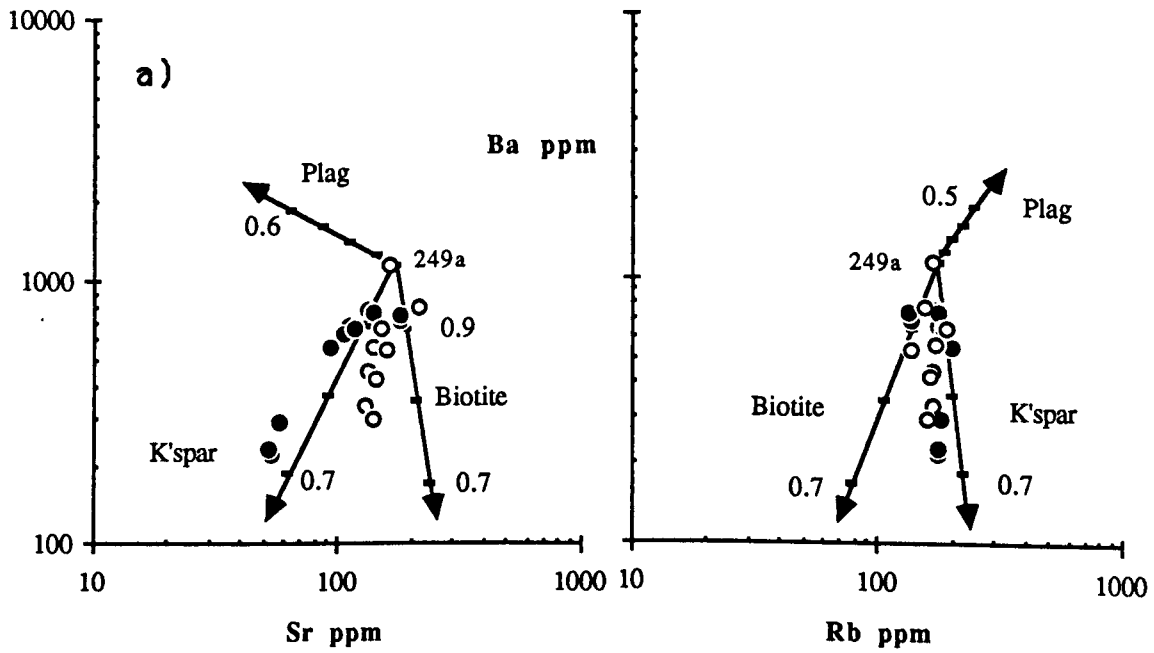

Fig. 5.12a LIL element models for the Golmud Hydro Group. a) shows all Golmud Hydro samples assuming sample 249a represents the original liquid. Open circles, Golmud Junction and Little plutons, closed circles, Golmud Hydro and Pink plutons.

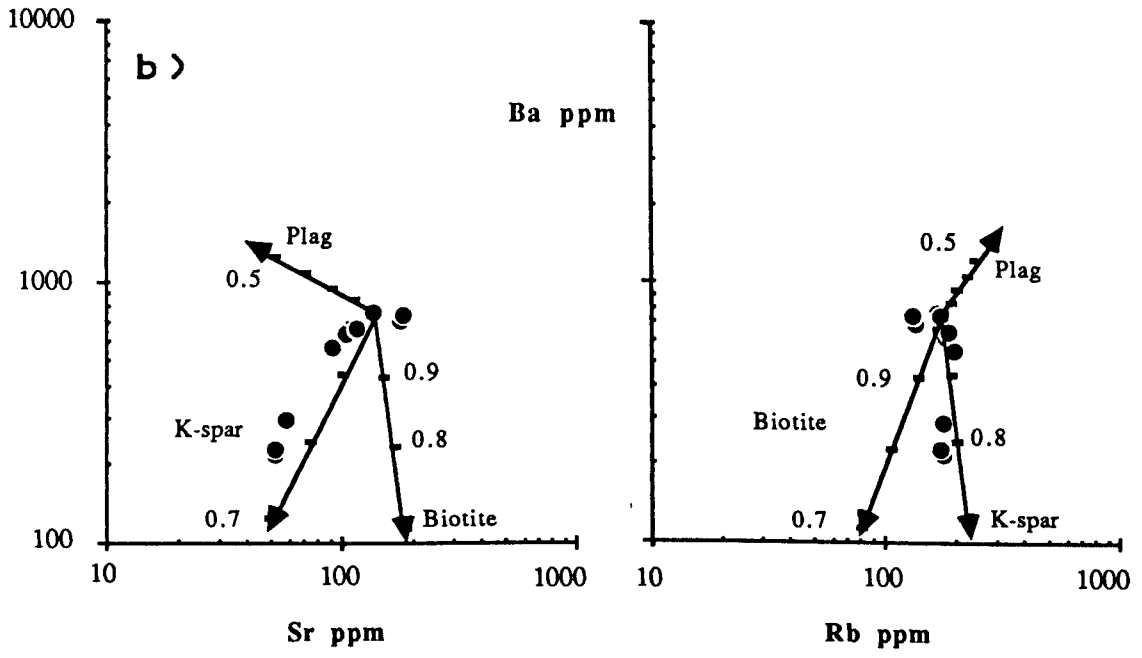

Fig. 5.12b This shows the lesser amount of crystallisation required to fractionate the more evolved samples in the Golmud Central and Pink plutons if sample 244a is the assumed original liquid for this group. Symbols as for Fig. 5.12a.

Fig 5.13 shows LIL element modelling of both the East Quarry and Golmud East plutons, and assumes the same original liquid composition for both plutons. However, whereas the liquids may have been very similar in terms of Ba and Sr, and both plutons

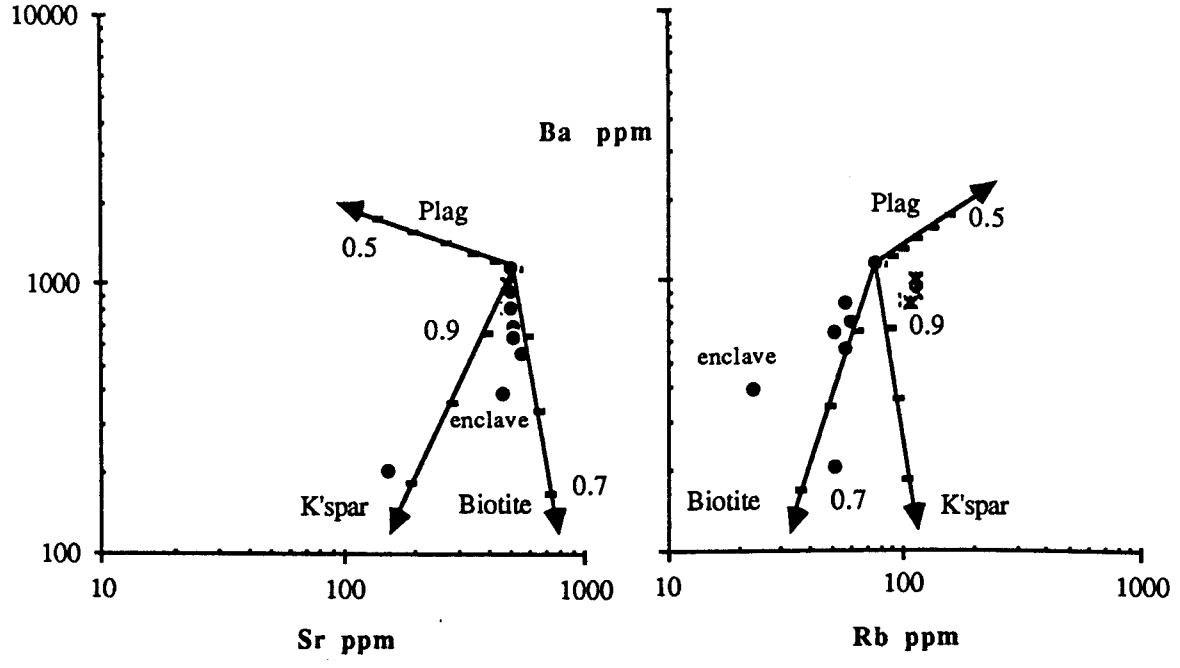

Fig. 5.13 LIL element models for the East Quarry pluton. Also included on the diagram are samples from the Golmud East pluton which clearly have not been derived from the same initial liquid.

were strongly controlled by biotite fractionation, the higher Rb contents in the Golmud East pluton clearly indicate a different trend. Consequently the two plutons could not have evolved from the same liquid, although the source was probably very similar. As was to be expected, the East Quarry pegmatite was strongly influenced by alkali feldspar crystallisation. The fractionation range seen in the Duo Ya He pluton was too small to be modelled.

5.4.2 Fractional Crystallisation Modelling

The LIL element modelling shows that Rayleigh fractionation is a reasonable model to explain the observed LIL element variations, and therefore it should also be possible to justify trace element variations in general, using the same principles.

Allègre *et al.*, (1977) used the Rayleigh equation to estimate bulk distribution coefficients during fractional crystallisation for a range of trace elements. Basing their technique on hygromagmatophile (incompatible) element systematics (Treuil and Varet, 1973), they showed that the Rayleigh fractionation equation could be solved to give the bulk distribution coefficient of a compatible element providing one element behaved incompatibly.

In equation 5.1, the Rayleigh fractionation equation for any element is given by:

$$C_l^e = C_o^e F^{(D-1)} \qquad (5.1)$$

However, since a hygromagmatophile (H) element will have $D << 1$, then $D - 1$ will approximate to -1, or 1/F. Equation 5.1 can then be simplified to:

$$C_l^H = C_o^H/F \text{ or } F = C_o^H/C_l^H$$

This can then be substituted back into equation 5.1, so it can be solved for a more compatible element (e) then the bulk D value for that element can be estimated so:

$$C_l^e = C_o^e \left(C_o^H / C_l^H \right)^{(D^e-1)}$$

$$\log\ C_l^e = \log C_o^e + \log \left(C_o^H - C_l^H \right)^{(D^e-1)}$$

$$\log\ C_l^e = \log C_o^e + (D^e-1)\ (\log C_o^H - \log C_l^H)$$

therefore:

$$D^e = (\log C_l^e - \log C_o^e / \log C_o^H - \log C_l^H) + 1 \qquad (5.2.)$$

The major problem with applying this technique is in finding a suitably hygromagmatophilic element. The assumption of total incompatibility always causes an under-estimation of the volume of residual liquid (F) and so an over-estimation of the calculated bulk distribution coefficient (Miller, 1988). Results can therefore only be an approximation. Furthermore, these are only average bulk D values since they are based on the assumption that D remains constant throughout the entire fractionation process. However, once D has been estimated for the range of trace elements it is possible to estimate the amount of fractional crystallisation that can account for the observed element trends using equation 5.3 given below and the calculated D value for the given element:

$$\log F = (\log C_l^e - \log C_o^e) / D^e - 1 \qquad (5.3)$$

For example, assuming G222g to represent the original liquid and G232a the final liquid in the Wanbaogou pluton, it is possible to calculate the amount of residual liquid (F) left after fractional crystallisation. Inspection of Table 5.2 shows Ta to be the most incompatible element in this suite therefore D values calculated using Ta are used to estimate F. Taking Sr as an example gives:

$$\log F = (\log 66 - \log 135) / 1.18$$

so $F = .54$ or 46% fractional crystallisation.

Using this method, the degree of fractional crystallisation was calculated for most plutons. The results and H element used in the calulations are given in Table 5.2. Table 5.3. gives the least and most evolved samples from each suite, and the average bulk D values for all trace elements calculated, using 2 or 3 hygromagmatophile elements. The value obtained for bulk D using the calculated least compatible element, is then used to calculate F for all suites.

Pluton	Degree of fractional crystallisation	H element used
Yie Nin Gou	38%	Rb
Wanbaogou	46%	Ta
Golmud Hydro	37%	Ta
East Quarry	16%	Cs

Table. 5.2 Fractional crystallisation values calculated for the Kunlun granites. Final column gives the hygromagmatophile (H) element used in the calculations.

Kidatan	Cs	Rb	Sr	Ba	Zr	Hf	Nb	Ta	Y	Th	U	La	Ce	Nd	Sm	Eu	Tb	Yb	Lu
206a	4	99	495	1023	253	7	18	0.96	14	19	4	79	154	48	7.1	1.67	0.8	1.2	0.21
206c	3	152	65	171	63	3	16	1.63	23	16	3	13	28	11	3.0	0.40	0.7	2.0	0.25
Ta	1.51	0.19	4.84	4.38	3.63	2.84	1.29	0.00	0.06	1.31	1.45	4.40	4.21	3.70	2.61	3.70	1.19	0.04	0.67
Rb	1.63	0.00	5.74	5.17	4.24	3.27	1.36	-0.23	-0.16	1.39	1.56	5.20	4.96	4.33	2.99	4.33	1.23	-0.19	0.59
Yb	1.53	0.16	4.99	4.51	3.73	2.91	1.30	-0.04	0.02	1.33	1.47	4.54	4.33	3.80	2.67	3.81	1.19	0.00	0.66
YNG	Cs	Rb	Sr	Ba	Zr	Hf	Nb	Ta	Y	Th	U	La	Ce	Nd	Sm	Eu	Tb	Yb	Lu
221b	2	82	649	904	233	6	21	1.80	17	10	1	37	75	34	5.8	1.60	0.7	1.2	0.18
213a	2	132	198	562	77	3	11	0.99	8	13	2	17	30	16	3.0	0.56	0.3	0.6	0.11
Rb	1.52	0.00	3.49	2.00	3.33	2.65	2.41	2.26	2.58	0.45	-0.23	2.62	2.88	2.55	2.38	3.20	2.78	2.42	2.03
Th	1.95	-0.82	5.53	2.81	5.22	4.00	3.55	3.28	3.87	0.00	-1.22	3.93	4.42	3.81	3.50	5.00	4.23	3.58	2.88
WBG	Cs	Rb	Sr	Ba	Zr	Hf	Nb	Ta	Y	Th	U	La	Ce	Nd	Sm	Eu	Tb	Yb	Lu
222g	20	254	135	291	211	7	13	1.48	45	36	4	54	110	44	9.0	1.24	1.2	3.8	0.68
232a	33	351	66	196	69	2	15	2.71	22	14	3	18	37	18	4.3	0.52	0.6	1.2	0.21
Ta	0.14	0.47	2.18	1.65	2.85	2.85	0.76	0.00	2.18	2.56	1.51	2.82	2.80	2.48	2.23	2.42	2.14	2.87	2.96
Nb	-2.63	-1.26	6.00	3.76	8.82	8.84	-0.03	-3.24	6.00	7.61	3.17	8.72	8.60	7.25	6.21	7.02	5.81	8.92	9.30
Rb	-0.61	0.00	3.21	2.22	4.46	4.46	0.55	-0.87	3.21	3.92	1.96	4.41	4.36	3.76	3.30	3.66	3.13	4.50	4.67
Gol II	Cs	Rb	Sr	Ba	Zr	Hf	Nb	Ta	Y	Th	U	La	Ce	Nd	Sm	Eu	Tb	Yb	Lu
244a	6	170	132	767	129	4	9	0.93	29	22	3	29	62	22	3.9	0.70	0.8	2.7	0.43
245a	6	178	53	219	74	3	9	1.47	27	21	3	19	40	14	3.5	0.29	0.8	2.7	0.43
Rb	0.43	0.00	20.81	28.22	13.07	7.21	0.26	-8.94	2.55	2.01	1.00	10.40	10.63	10.25	3.23	20.14	2.33	0.84	1.00
Ta	0.94	0.90	2.99	3.74	2.21	1.62	0.93	0.00	1.16	1.10	1.00	1.95	1.97	1.93	1.22	2.93	1.13	0.98	1.00
EQ	Cs	Rb	Sr	Ba	Zr	Hf	Nb	Ta	Y	Th	U	La	Ce	Nd	Sm	Eu	Tb	Yb	Lu
246e	1.24	78	504	1135	123	3.54	11.20	0.67	11	7	1	39	68	26	3.9	1.03	0.4	0.9	0.13
246a	1.48	61	519	695	119	4.10	10.90	0.62	12	4	1	12	26	14	2.7	1.01	0.4	0.8	0.13
Cs	0.00	2.39	0.83	3.77	1.19	0.17	1.15	1.44	0.51	4.21	2.39	7.44	6.48	4.35	2.98	1.11	1.55	1.67	1.00
Hf	-0.20	2.67	0.80	4.34	1.23	0.00	1.18	1.53	0.41	4.86	2.67	8.75	7.60	5.04	3.38	1.13	1.66	1.81	1.00
Y	-1.03	3.82	0.66	6.64	1.38	-0.69	1.31	1.89	0.00	7.52	3.82	14.09	12.13	7.81	5.02	1.23	2.12	2.37	1.00

Table 5.2 Bulk D values for a range of trace elements calculated using the H elements given in the left hand column.

5.4.3 Rare Earth Elements

Chondrite-normalised REE patterns of all the granitoid suites are shown in the following figures. They fall into two distinct groups with those from the Southern Region displaying steep trends with LREE enrichment around 200x chondrite, small negative Eu anomalies and HREE depletion at 10x chondrite. The Wanbaogou pluton and Central Region intrusions display a somewhat flatter over-all pattern with lower LREE, a pronounced negative Eu anomaly and significantly higher HREE around 50x chondrite. North of the Golmud Fault the Northern Region plutons all have steep patterns like those in the Southern Region. These differences are emphasised when the Ce/Yb ratio is plotted agains Yb, as in Fig. 5.14, where it can be seen that the Northern and Southern Region plutons have much higher Ce/Yb ratios compared to those from the Central Region which have higher Yb.

Similar to the REE variations seen in the Peninsular Ranges Batholith, which also shows flatter patterns in the central section compared to steeper patterns at either edge (Gromet and Silver, 1987), there is an abrupt transition in the Kunlun between the steep

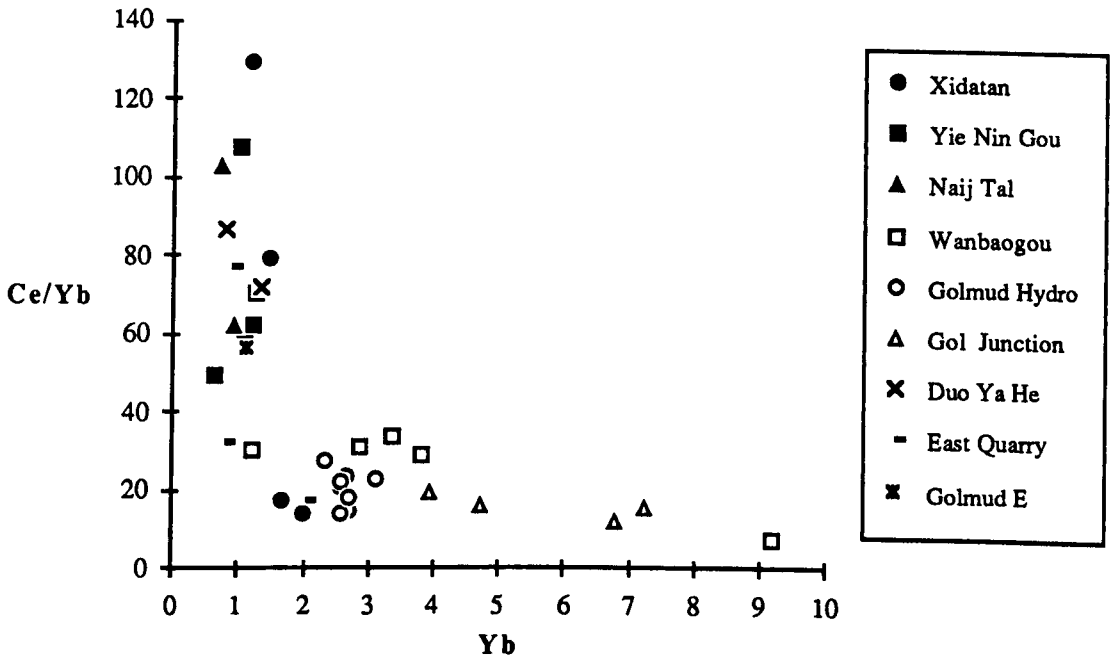

Fig. 5.14 Ce/Yb against Yb for all the Kunlun samples.

patterns of the Northern Region, and the flatter patterns of the Central Region. In the Kunlun this transition is identified as being at the Golmud Fault, already recognised as a major boundary in the region (see Chapter 4). At this stage however, it is unclear whether this pattern difference is due to a fundamental difference in source regions, as inferred by Gromet and Silver for the Peninsular Ranges Batholith, or whether movement on the Golmud Fault has juxtaposed syn-collision type, small degree melts (Central Region) against large degree melts (Northern Region) which have essentially all been derived from a very similar source. If the latter argument is the case, then it must be partial melting rather than fractionation that has caused the LREE to become depleted while the HREE are enriched because, in the Golmud Junction suite (Fig. 5.15b) for example, all samples from the mafic enclave right through to the highly evolved leucogranites of the Golmud Hydro group show the same fundamental pattern shape, and only abundances change with fractionation. The same is seen in the Wanbaogou pluton (Fig.5.15a), although there does seem to have been some reaction of the enclave with the host melt which has resulted in the loss of some LREE.

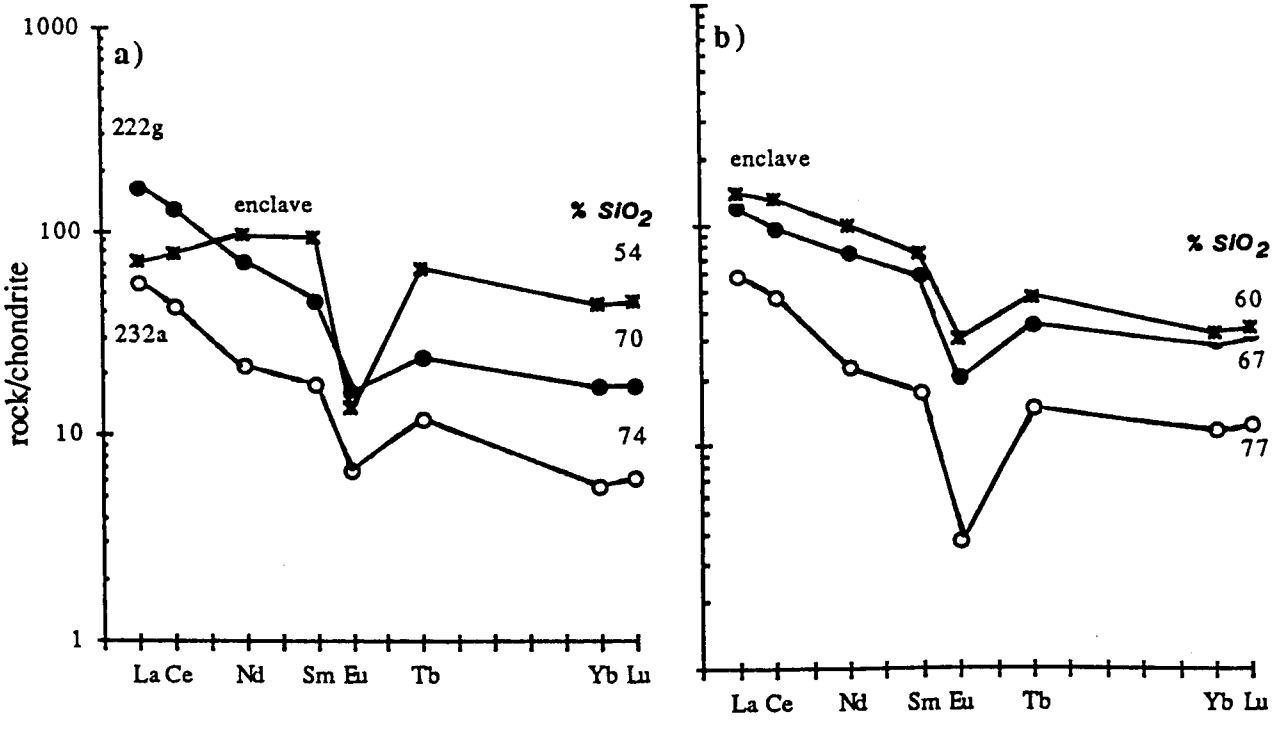

Fig. 5.15 REE diagrams for the Wanbaogou (a) and Central Region (b) plutons.

Similarly, in the Northern Region, the evolved granodiorites of the Duo Ya He pluton (Fig. 5.16a) have almost identical patterns, except for a small negative rather than positive Eu anomaly, to the relatively mafic East Quarry tonalite (Fig.5 16b). In the Southern Region (Figs. 5.17 a-c) fractionation in the Yie Nin Gou pluton (Fig.5 17b) maintains the same steep shape only at lower abundances. Only in the Xidatan pluton (Fig. 5.17a) does there appear to be a change from the steep pattern typical of the Southern Region to the flatter shape of the Central Region in samples considered, respectively, to represent source and melt.

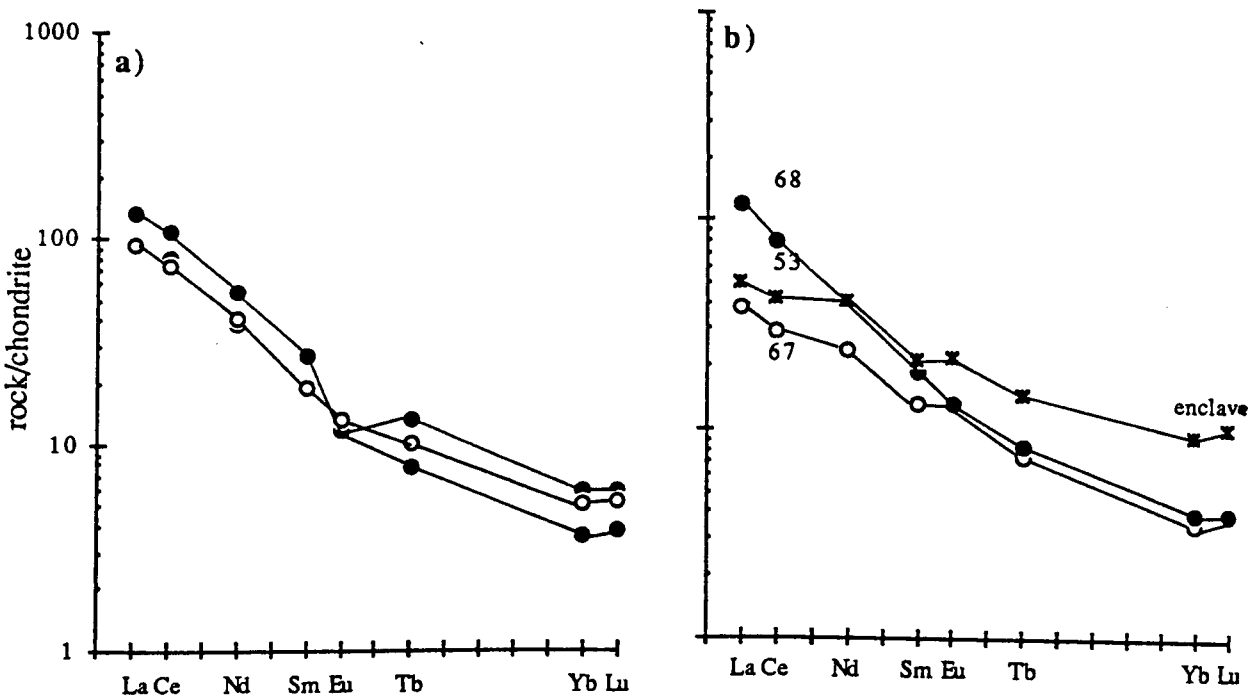

Fig. 5.16 REE diagrams for the Northern Region plutons. a) Duo Ya He (filled circles) and Golmud East (open circles)plutons; b) East Quarry tonalite.

However, that the LREE are held in the residue while the HREE are released into the melt, is somewhat contrary to expectations and suggests that some minor phase such as allanite is in the source holding back the LREE. This is seen in the Xidatan pluton where the 'source' samples are full of allanite resulting in depletion in the 'melt' samples in LREE. This indicates that the source for the Central and Northern Regions is of a granitoid composition and suggests that these granites may have been derived from the old Devonian batholith.

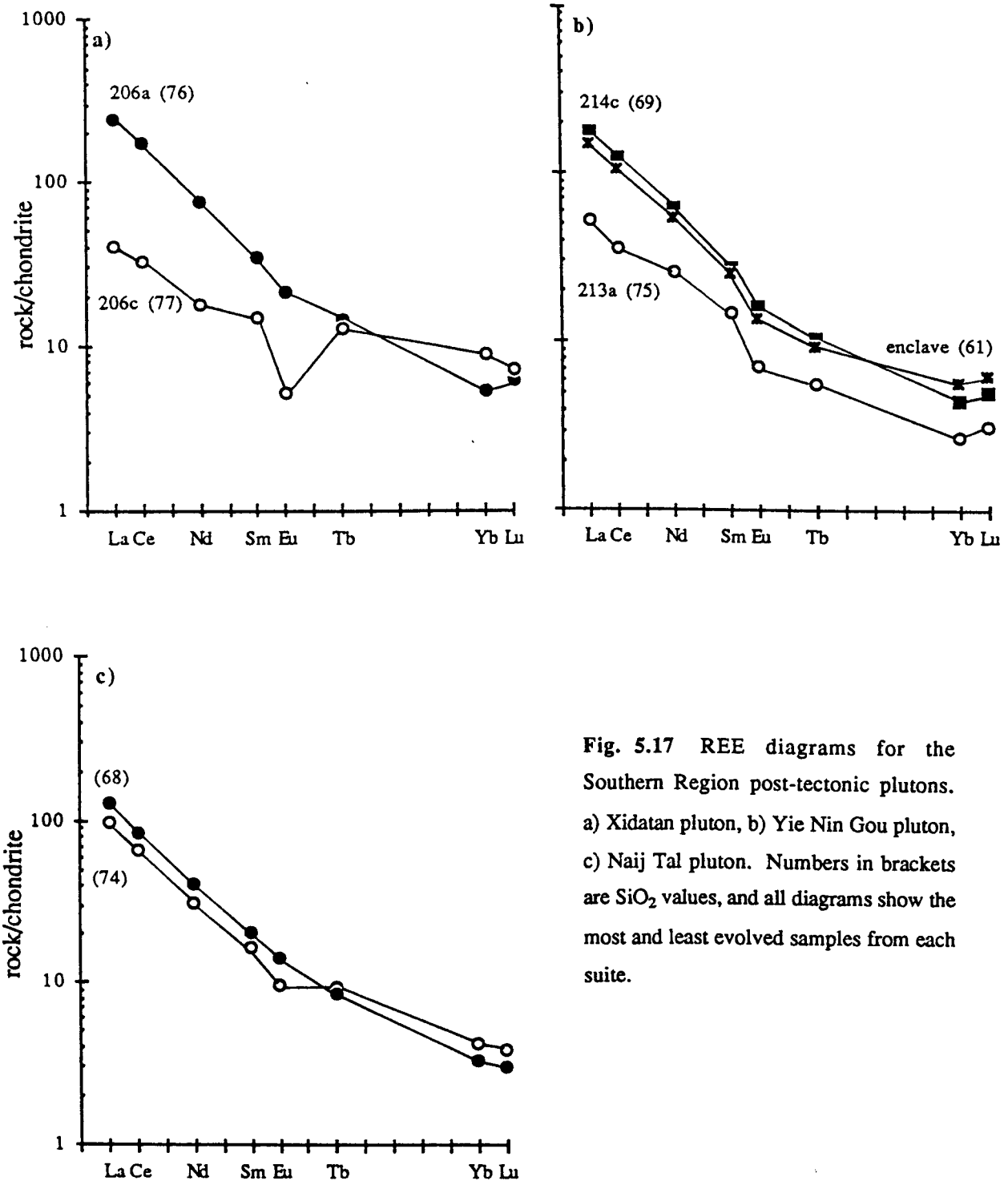

Fig. 5.17 REE diagrams for the Southern Region post-tectonic plutons. a) Xidatan pluton, b) Yie Nin Gou pluton, c) Naij Tal pluton. Numbers in brackets are SiO_2 values, and all diagrams show the most and least evolved samples from each suite.

The least evolved members of all the post-tectonic plutons in the Southern Region show almost identical patterns, further supporting the suggestion that these have all been derived from a similar source but have subsequently experienced different crystallisation histories. The source for the Wanbaogou pluton does however, appear to be somewhat

different, particularly when the high initial Sr ratios are considered (see next section) since these generally tend to reflect derivation from a sedimentary source.

Fig. 5.18 shows a range of chondrite-normalised rare earth element patterns of post-Archaean shale composites, the values for which were taken from Taylor and McLennan (1985). They represent the Post-Archaean average Australian shale (PAAS), the Kuiseb schist average from Namibia (McDermott, 1986) and one example of the Xidatan schist (G209a). These all define an extremely small range in abundance levels around 100x chondrite for the LREE and have identical patterns, demonstrating the remarkable uniformity of shales from around the globe.

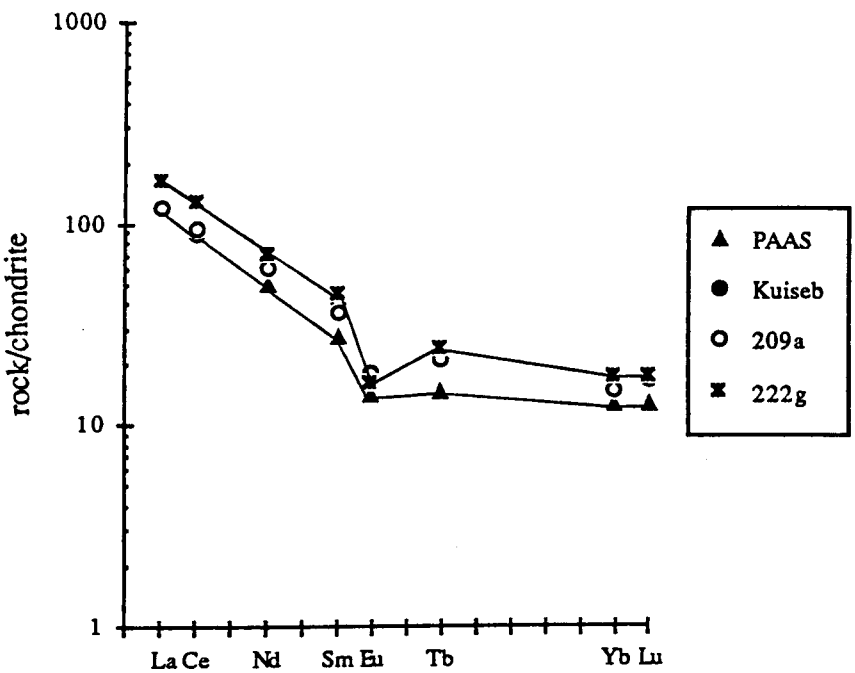

Fig.5.18 REE diagrams for various shale composites, and a schist from the Southern Region compared to the least evolved sample from the Wanbaogou pluton

Sample G222g, the most mafic sample from the Wanbaogou pluton, is also included on Fig. 5.18, and shows a remarkably similar pattern to the shales. This close similarity to the shales and schists illustrated strongly indicates that these granites result from the melting of upper crustal sources, i.e. that these granites "image their sources" (Chappell, 1979). The enclave from the Wanbaogou pluton (G222h) appears to have experienced a degree of melt removal increasing the Eu anomaly and significantly decreasing the LREE

probably as a result of reaction within the host melt. The removal of quartz increases the relative REE abundances, and the melting of feldspar increases the Eu anomaly.

Finally, in this REE section it must be pointed out that the fractionation of Sm and Nd with increased silica content is a significant feature seen in all the plutons and clearly demonstrated in Fig 5.19a. As a result of Sm being marginally less compatible than Nd, particularly in allanite, Nd is markedly more depleted than Sm in the highly evolved samples (see Fig 5.8). This leads to an increase in the Sm/Nd ratio which has important implications for calculating model Nd ages as will be seen in later sections. Another trace element pair generally considered not to fractionate is Hf and Zr, but Fig.5.19b again demonstrates a clear increase of the Hf/Zr ratio with SiO_2 content, very similar to the Sm/Nd trend. However, a rather scattered correlation of Hf/Zr against Sm/Nd suggests that the fractionation is not necessarily being controlled by the same accessory phases. While these highly evolved rock-types may be volumetrically small, they clearly demonstrate that fractionation of these element pairs can occur. This is important since these trace element pairs are often used in trace element modelling precisely because they

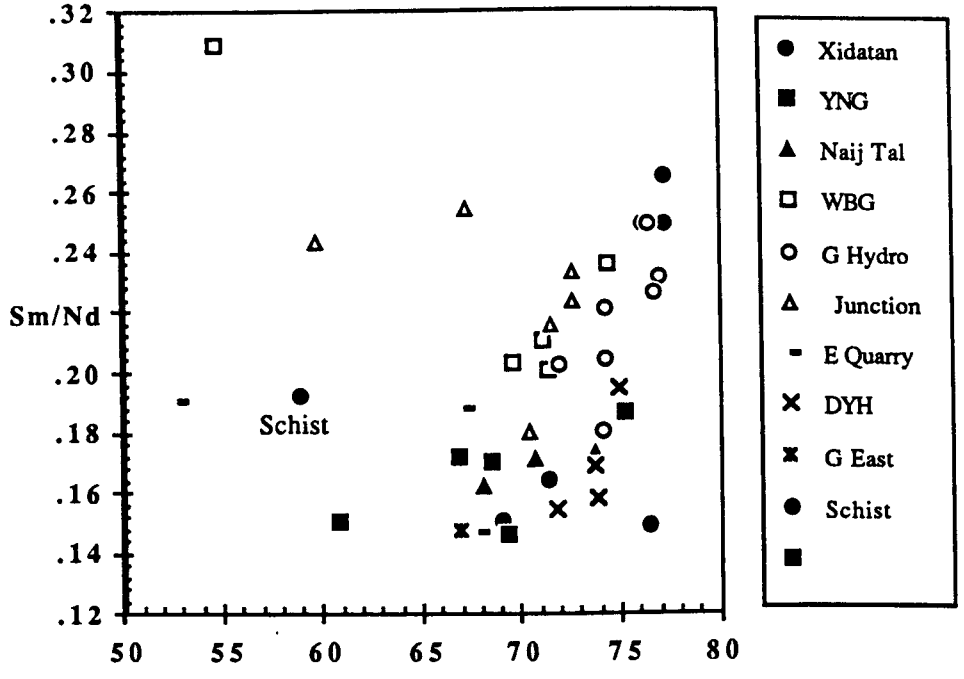

Fig. 5.19a Sm/Nd ratio ratio plotted against silica shows a marked increase with increasing fractionation..

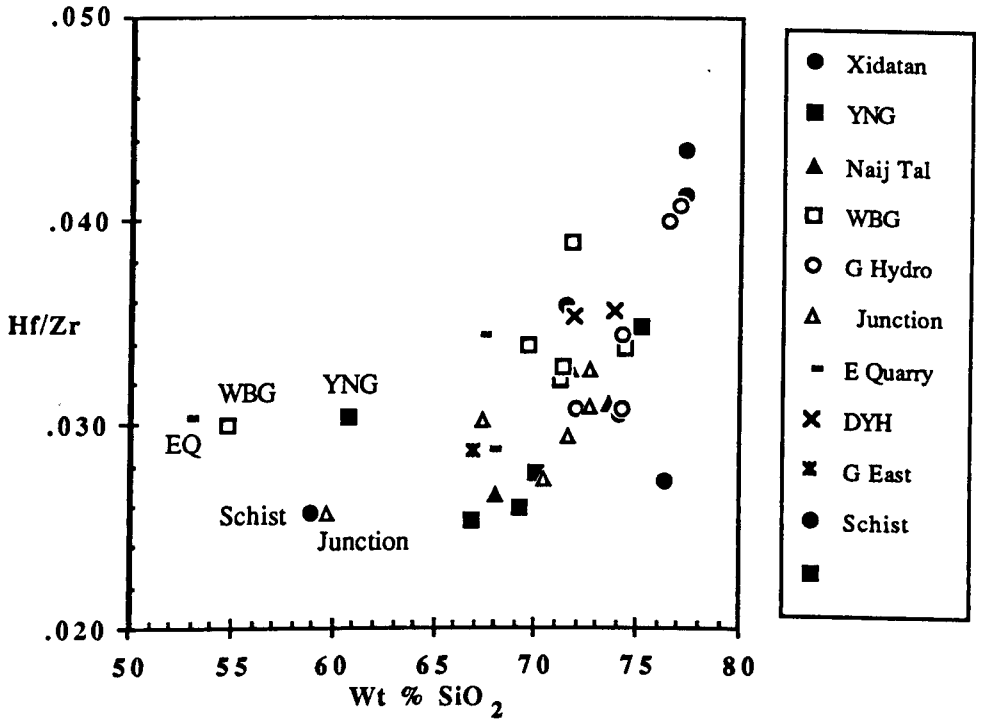

Fig. 5.19b Hf/Zr ratio plotted against silica.also shows considerable fractionation with increased silica content. Data points below 65% SiO_2 represent enclaves.

apparently do not fractionate (McCullock and Wasserberg, 1978) despite the fact that several authors have reported the fractionation of Sm and Nd (Vidal *et al.*, 1984; Bernard-Griffiths *et al.*, 1985, Deniel, *et al.*, 1987).

5.5 ISOTOPE GEOCHEMISTRY

There are three fundamental sources from which granitic magma is believed to be generated.

1 The magma is derived from the mantle, perhaps by the fractional crystallisation of mantle-derived basalts.

2 The magma is derived from the mantle but is contaminated by (mixes with) a crustal component.

3 The magma is derived entirely from melting the crust and does not contain any mantle material.

In the third context 'mantle material' is defined as magma derived from the mantle during this particular episode of melting. Volcanogenic sediments or igneous material formed during a previous melting event are considered to be crustal material and included in category 3, but they will have older enriched isotopic signatures than magmas extracted directly from the mantle during the melting event.

5.5.4 Sr isotope geochemistry

Measured $^{87}Sr/^{86}Sr$ ratios and the calculated initial ratios are presented in Appendix D, and Fig. 5.20 shows the $^{87}Sr/^{86}Sr$ evolution of the Kunlun samples relative to Bulk Earth. For further comparison, samples from the Gangdese batholith in southern Tibet and some High Himalayan leucogranites have also been included. The Gangdese (Transhimalayan) batholith in southern Tibet can be traced for over 2500 km and was intruded into an Andean type continental margin on the southern edge of Tibet as a result of the subduction of India beneath Tibet (Honeggar *et al.*, 1982; Schärer *et al.*, 1983; Debon *et al.*, 1986; Gariepy *et al.*, 1985; Petterson and Windley, 1985). This resulted in granites with low initial ratios between .704 - .707 that fall on the Bulk Earth evolution line indicating that they have been derived largely from mantle sources, although it has been shown that some crustal component was also involved. In complete contrast, the High Himalayan leucogranites have intial ratios that start at about .730 and increase to > .80 (Allègre and Ben Othman, 1980). It has now been convincingly demonstrated that these granites have been derived from the melting of upper crustal sediments (Vidal *et al.*, 1982; Deniel *et al.*, 1987) and contain no mantle-derived magma. These two classic types represent the two end members of granitic magma generation in Tibet.

The Kunlun granites fall between these two granitic end members with $^{87}Sr/^{86}Sr$ ratios in the range of .7073 - .7130. Since these do not fall on the Bulk Earth evolution trend, they could not have been derived from a pure mantle component, so either they are from a mantle source that has been substantially contaminated with sediments, or from an igneous or immature sedimentary crustal source. It is the object of this section to try and establish which is the more probable case.

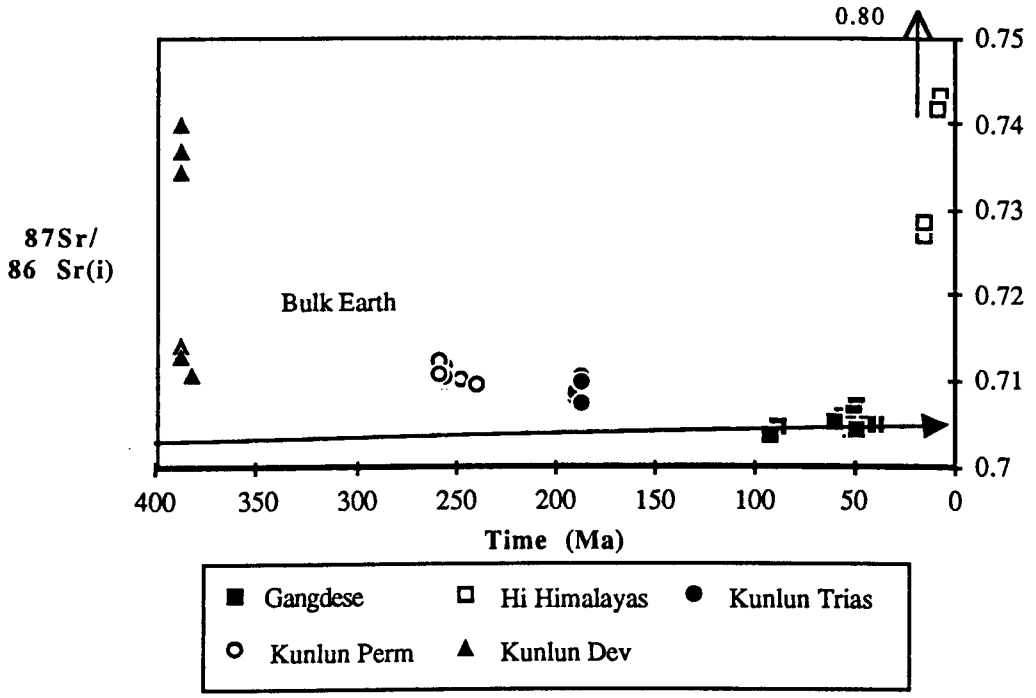

Fig. 5.20 $^{87}Sr/^{86}Sr$ evolution diagram for the Kunlun granites. Samples from the Gangdese belt and the High Himalayas are also included for comparison.

5.5.5 Nd isotope geochemistry

Nd isotopic ratios have been determined for selected granitoids from the Kunlun Terrane and the full data set is presented in Appendix D. Crustal extraction from the mantle significantly fractionates the Sm/Nd ratio, but it is then assumed to be realtively unaffected by intracrustal processes such as weathering, sedimentation, metamorphism, remelting and fractional crystallisation. From the measured $^{143}Nd/^{144}Nd$ and Sm/Nd ratios it is possible to calculate model Nd ages which were originally calculated as an estimate of when a magma, or its crustal precursor, was derived from the upper mantle. In the case of one-stage mantle-derived granites, this should result in the model Nd age being the same as the Sr whole-rock emplacement age, as seen in the Gangdese granites (Allègre and Ben Othman, *op. cit.*). Alternatively, if the source was entirely of a sedimentary composition then the model age will simply be an average model age of all the exposed rocks that contributed to the source material at the time of sedimentation. It then represents an average age at which the crust was extracted from the mantle. However, if the granite comprises part mantle and part old crust then the model age will

be a mixture of the two resulting in an apparent age that is older than the actual time material was derived from the mantle, but younger than the crustal component. In the Kunlun, identification and interpretation of model Nd ages is further complicated by the fact that Sm and Nd clearly have fractionated during the process of fractional crystallisation as demonstrated in Fig 5.19a , which has the effect of greatly increasing the calculated model Nd age as seen in Fig 5.21. In the Golmud Hydro suite, for example, such ages range from 1000 Ma in the least evolved samples to 1900 Ma in the most evolved. And this phenomenon is not just restricted to the highly evolved samples (SiO_2 > 75%) as suggested by Deniel *et al.*, (1987) but is seen even in the East Quarry tonalite. Only the Yie Nin Gou pluton retains the same model age in the highly evolved samples as in the less evolved, despite an increase in the Sm/Nd ratio.

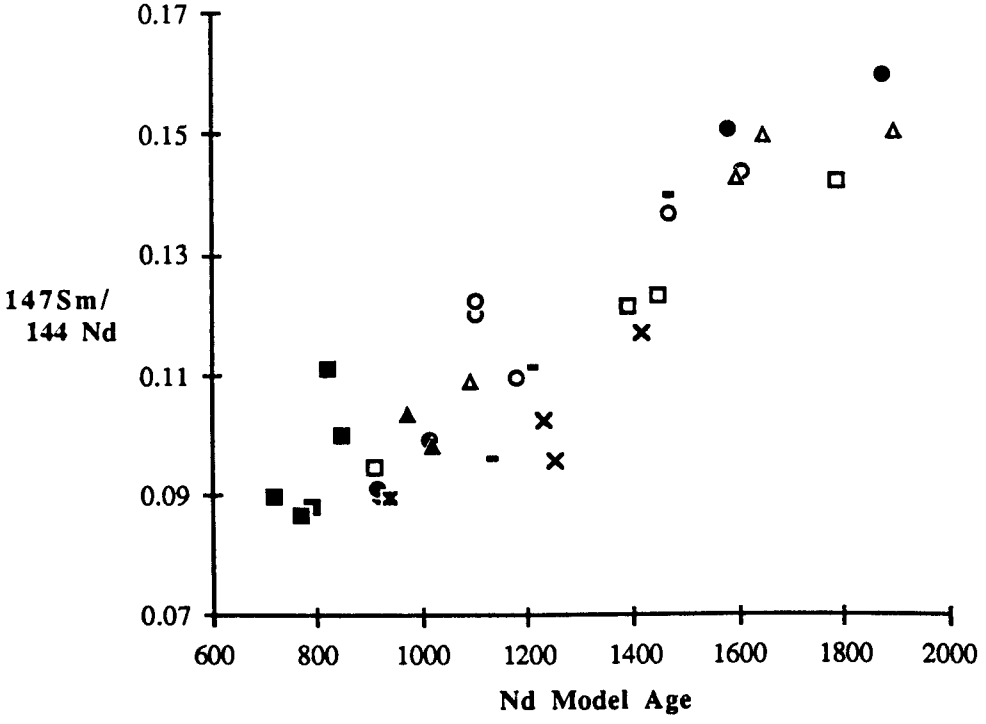

Fig. 5.21 Plot of $^{147}Sm/^{144}Nd$ against model Nd ages. This clearly demonstrates how model Nd age increases with Sm/Nd fractionation.

Of the Southern Region post-tectonic plutons, ages from all the least evolved samples, which are presumably most representative of the true model ages, range from 800 to 1000 Ma. This may simply reflect a sampling bias if the least evolved sample from each pluton was not actually collected, but if the magma is mantle-derived this range in ages

may result from varying amounts of crustal contamination. However, depending on the age of the crust, this requires a high percentage of contaminant to increase the model Nd age in the Yie Nin Gou pluton four fold (i.e. from ~ 200 Ma, the emplacement age and therefore the model age if directly derived from the mantle, to 800 Ma, the measured model Nd age). Assuming the age of the crust to be 1100 Ma, then two thirds of the melt must be from old crustal sources. Although, if the age of the crustal component is ~ 1700 Ma which is the age obtained from the Xidatan schist, then the amount of assimilant required is only 40%. On the other hand, if all the melt has been derived entirely from a crustal source, then the range in model ages reflects a variation of model ages in the source. For future calculations it is assumed that all samples in each suite have a model age represented by the least evolved sample in that suite and Table 5.4 presents these data.

Pluton	Assumed Model Age
Xidatan	900 Ma
Yie Nin Gou	800 Ma
Naij Tal	900 Ma
Wanbaogou	1400 Ma
Golmud Hydro	1100 Ma
East Quarry	1100 Ma
Golmud East	900 Ma
Duo Ya He	1400 Ma

Table 5.4 Model Nd ages for each pluton. The age of the least evolved sample is assumed to be the most representative for each suite, and is used in subsequent calculations

It is significant however, that recalculation of initial Nd ratios for the Devonian plutons at 250 Ma results in $^{143}Nd/^{144}Nd$ ratios around .51220, which is similar to the initial Nd ratios for the Permian plutons . Futhermore, recalulation of Sr initial ratios of the Duo Ya He pluton at 250 Ma also gives initial $^{87}Sr/^{86}Sr$ values identical to those obtained for the East Quarry stock. This is strong evidence to support earlier suggestions that the Permian

batholith has been primarily derived from melting the same source as its Devonian precursor.

5.6 PETROGENETIC MODELLING

5.6.1 Binary mixing model

Rb-Sr and Sm-Nd isotopic data are presented in Fig. 5.22 using the ε notation (De Paolo and Wasserburg, 1976) which enables different rock types of any age to be compared isotopically. Mid-ocean ridge basalts plot in the left-hand top quadrant and oceanic basalts define a 'mantle array' which extends into the lower right-hand quadrant. Lewisian granulites normally fall in the lower left-hand quadrant while granites tend to plot in the lower right-hand quadrant along mixing lines that are conventionally considered to represent a mix between continental crust and depleted magma (Allègre and Ben Othman, 1980; De Paolo, 1981; McCulloch and Chappel, 1982).

The Kunlun data define a narrow range in εNd values falling between -2 for the Yie Nin Gou pluton and -5 in the Golmud Hydro Group. The older Wanbaogou and Duo Ya He plutons have slightly lower values around -5 to -6 εNd. The εSr values show a wider range from +40 in the less evolved Yie Nin Gou intrusion to +140 in the Wanbaogou, suggesting an increasing upper crustal component in these plutons. The hydrothermally affected leucocratic samples from the Wanbaogou stock (G232) however, have values as high as +500 which overlap with the High Himalayan field, shown for comparison in Fig. 5.22.

These high values should imply that this group has been derived from a total crustal melt but $Nd_{(i)}$ values identical to the rest of the pluton indicate either that the whole pluton is derived from a crustal melt or that the crust/mantle mix is the same. Either way, it is further support for the earlier suggestion (section 3.2.3) that this pluton has been affected by late-stage fluids which were either enriched in radiogenic Sr, or that have removed Rb from the system. The same explanation is given for sample X67, which is part of the Xidatan suite but lies directly on the Xidatan fault. This too has been affected by fluids which must account for the high εSr value of +300. The ε values for the Gangdese

samples from diagram 5.22 are also included for further comparison. That they fall near the Bulk Earth value supports the suggestion that they have been derived from a depleted mantle, but they also appear to contain some crustal material.

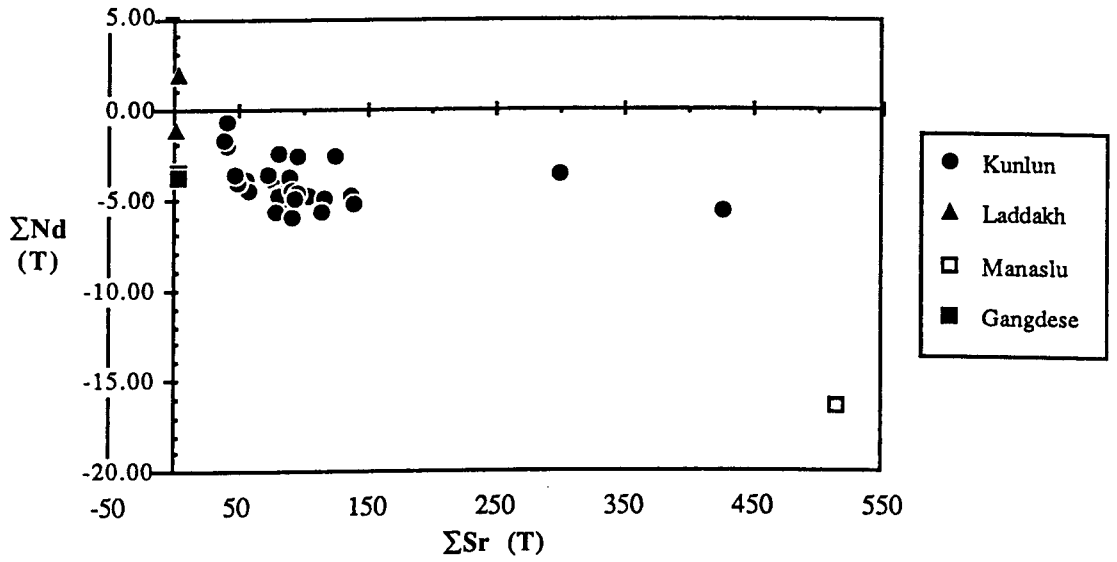

Fig. 5.22 εNd versus εSr diagram compares the Kunlun granites to those from the Gangdese and High Himalayas.

On making the assumption that the Kunlun granitoids are derived from a mix of mantle and crustal material, Harris *et al.*, (1988) deduced that the age of the crustal component was 1100 Ma and that anatexis occurred at 240 Ma. Taking the average Rb/Sr and Sm/Nd ratios of upper and intermediate crust it was possible to determine isotopic ratios for these points which are defined on Fig. 5.23 as UC and IC respectively. Some of the samples lie close to a mixing line between UC and depleted mantle, indicating that up to 80% of crustal material could be involved in the petrogenesis of the Golmud Hydro plutons. However, this simple binary mixing of two end members is considered to be an unlikely process in the petrogenesis of most granites, especially in such highly evolved and fractionated granitoids as those in the Kunlun where simple mixing relations will be destroyed or obscured by partial melting and differentiation (Langmuir *et al.*, 1978; De Paolo, 1981). Furthermore, Taylor (1980) showed that at an initial magma temperature of about 850° C, the assimilation of 1g of country rock (at about 150° C) requires the

crystallisation of 5g of crystals, thereby limiting the amount of assimilated material to a 1:5 ratio. Even allowing for greater assimilation if the crust was at higher temperatures, the magma would need to be super-heated to incorporate 80% of crustal material.

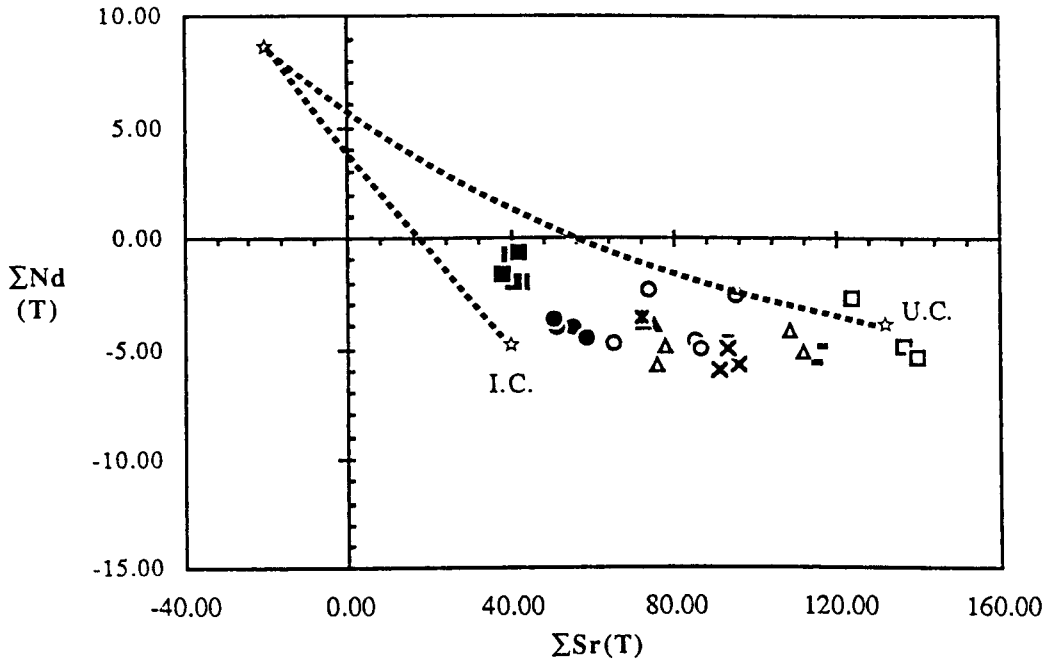

Fig. 5.23 εNd versus εSr diagram for the Kunlun granites. This also shows the mixing curve between upper crust at 1100 Ma and depleted mantle. U.C. = upper crust I.C. = intermediate crust. (Redrawn after Harris et al., 1988a).

5.6.2 AFC modelling

Addressing these problems, De Paolo (1981), investigated the extent to which magmas are modified during ascent and emplacement, with emphasis being placed on the assimilation of wall-rock material and fractional crystallisation (AFC). Using the equations developed by De Paolo and given in Appendix C, it was found that AFC curves could be fitted to the Kunlun data by assuming a hypothetical initial magma similar to a Gangdese diorite, that had assimilated crustal material identical in composition to the Xidatan schist (G209a) in a 1:5 mass assimilated to mass fractionated ratio, i.e. r = 0.2. This is not meant to infer that the Xidatan schist actually represents the crustal component, but as earlier demonstrated it is a good representative of average crust. Further assumptions must also be made about the bulk D values for Nd and Sr in the assimilating

phases, but it was found that if D_{Nd} was held at 2 then a change of D_{Sr} from 2.6 to 2.1 as represented by the upper and lower curves respectively on Fig. 5.24, accounted for most of the data, although the older plutons are not included since the age of the crust is likely to be different for these. However, it is felt that whilst these data may be geologically realistic, the parameters can be so variable and so many assumptions must be made, that it is not possible to be confident about using the model as a definitive explanation for the data set, and so other models should also be explored.

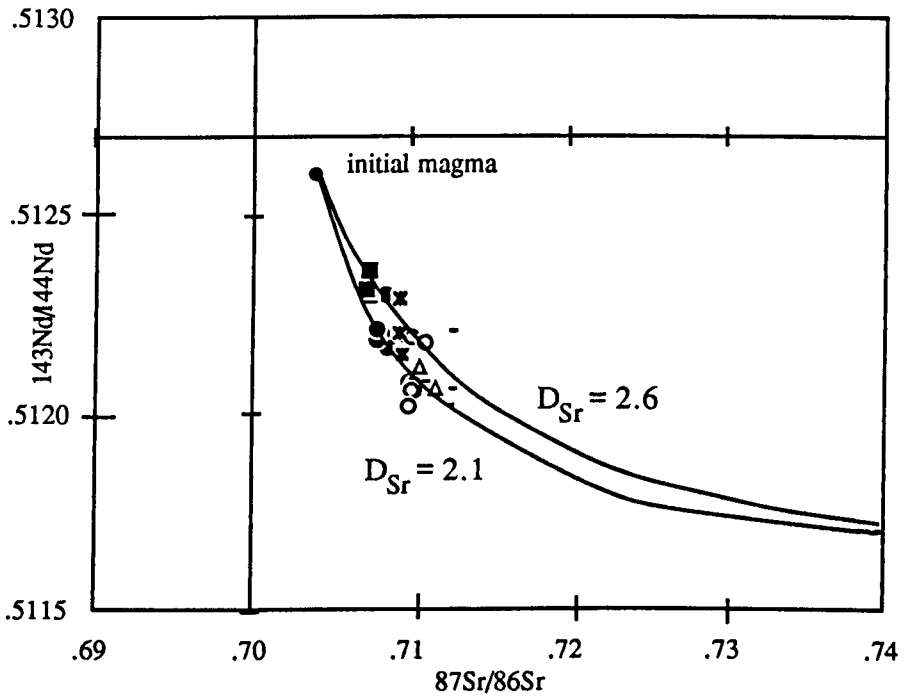

Fig. 5.24 AFC curves for the Kunlun granites.

5.6.3 Batch melting model

Having calculated model Nd ages for the Kunlun granitoids (Table 5.4), it is then possible to estimate the $^{87}Rb/^{86}Sr$ ratio in the source in an attempt to identify the most probable source region. This can be done using the equation:

$$^{87}Rb/^{86}Sr \text{ source} = \frac{R_s t_1 - R_{Dm} t_2}{e^{\lambda (t_1 - t_2)} - 1}$$

where

$R_S{}^{t}{}_1$ = the initial $^{87}Sr/^{86}Sr$ ratio of the sample at the time of emplacement

$R_{Dm}{}^{t}{}_2$ = the initial $^{87}Sr/^{86}Sr$ ratio of the depleted mantle at the time given by the model Nd age

$\lambda\ ^{87}Rb$ = 1.42×10^{-11}

$^{87}Sr/^{86}Sr_{(BE)}$ = .7047

$^{87}Rb/^{86}Sr_{(BE)}$ = .0847

$^{87}Sr/^{86}Sr_{(DM)}$ = .7026 (Jacobsen and Wasserburg, 1979)

$^{87}Rb/^{86}Sr_{(DM)}$ = .0541 (Goldstein and Jacobsen, 1988)

Examination of the data in Fig 5.25 shows that source $^{87}Rb/^{86}Sr$ ratios for all plutons range from 0.5 to 0.9 and fall between average values for bulk continental crust at 0.35 and average upper crustal values of 0.9 (Taylor and McLennan, 1985) further supporting the suggestion that these granites were derived from the melting of a crustal precursor. Even though it is possible to generate a source ratio of 0.5 by mixing an intial magma such as that previously described ($^{87}Rb/^{86}Sr$ = 0.116) with average crust, the 1:1 proportions required are geologically unrealistic when the conditions for assimilation, previously discussed, are considered. As the Wanbaogou monzogranite and East Quarry tonalite in particular have ratios close to average upper crust, a model of partial melting of crustal material, without invoking the presence of any mantle material, will now be examined.

The batch melting equation of Shaw (1970) is used and given below. It assumes that the liquid remains in chemical equilibrim with the solid residue until the liquid is able to escape as a single discrete batch. However, because the viscosity of a granitic melt is so high, the melt phase is not readily extracted. Instead, when the melt proportion gets above the rheological critical melt percentage (Arzi, 1978), or the "critical melt fraction" of Van der Molen and Paterson, (1979) the restite framework breaks up and the whole mass becomes a crystal-rich magma with a relatively lower effective viscosity and density (Chappell *et al.*, 1987), which allows it to move upwards. According to Chappell *et al.*,

the process of differentiation is then an unmixing process in which the melt phase of the magma progressively clears itself of restite, but does not significantly change its composition.

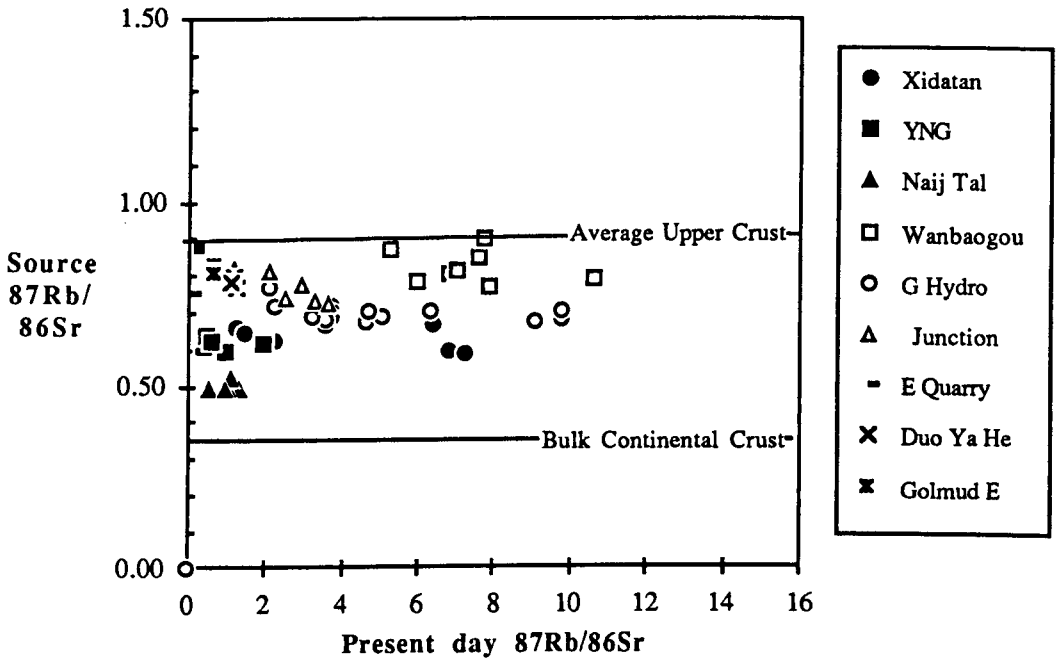

Fig. 5.25 Source Rb/Sr ratios for the Kunlun granites fall between values for average upper crust and bulk continental crust.

In the fractionated granites of the Kunlun batholith, problems immediately arise in identifying the sample that represents the primary melt. However, for the purposes of modelling, the least fractionated sample from each suite is assumed to represent the initial liquid and is therefore used in the calculations.

The batch melting equation states that:

$$C_l^e / C_o^e = \frac{1}{F+D - (F.D)} \qquad (5.4)$$

where

C_l^e = concentration of the element in the initial liquid

C_o^e = concentration of the element in the solid

F = weight fraction of liquid formed

D = element bulk distribution coefficient for the solids when the melt is removed from the system

Since the Wanbaogou pluton has source Rb/Sr ratios similar to upper crust (0.9) it was assumed that sample G222g represented the primary liquid phase (C_l), and that the Xidatan schist (G209a), which typified average upper crustal material although it has a slightly higher Rb/Sr ratio at 1.7, represented the source (C_o). Fig.5.26 shows how D values must change with F, the amount of melt formed, to keep the C_l/C_o ratio constant. It can be seen that Cs is the most incompatible element in the system, and where the curve intersects D = 0 the maximum amount of melting (F) is constrained to about 28%. Except for Eu, all the REE elements are incompatible and go into the melt thereby maintaining a pattern very similar to that seen in the schist, but increasing the negative Eu anomaly. Similar results were obtained using average upper crustal values (Taylor and McLennan, 1985), although the amount of melting required was found to be slightly higher at 30%, as constrained by Th which was the most incompatible element.

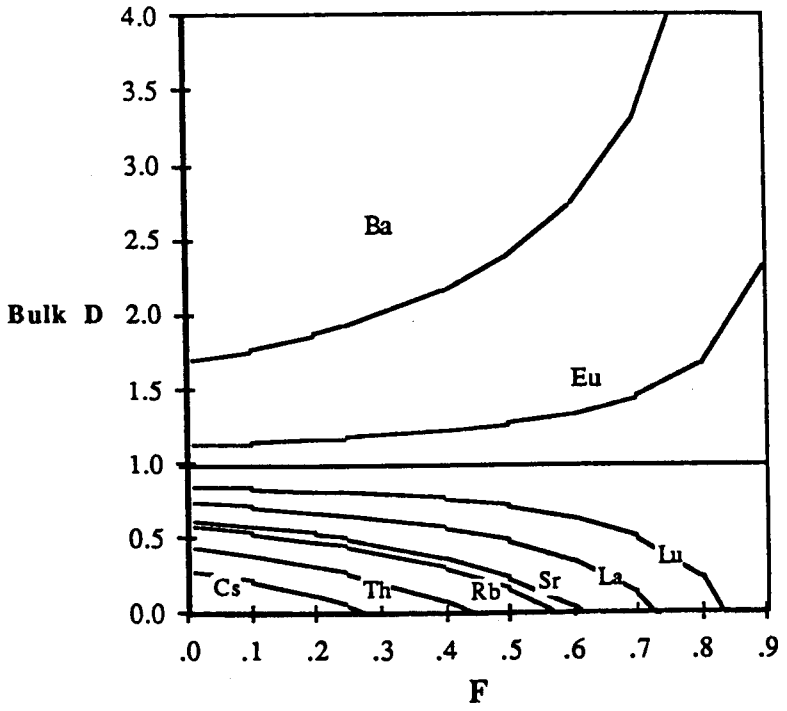

Fig. 5.26 Curves showing how bulk D changes for various elements in the Wanbaogou pluton with increasing degrees of melting.

Taking sample G244a to represent the primary liquid of the Golmud Hydro Group, a similar technique was employed in an attempt to identify a likely source for this pluton. Sr and Nd isotopic evidence has convincingly demonstrated that a likely precursor for this

pluton, and possibly also the Northern Region plutons, was the same source from which the pre-existing Devonian batholith was generated. For this reason then, average continental crustal values (Taylor and Mc Lennan, 1985) were considered to represent the source. These values are given in Table 5.5. Fig. 5.27 shows that the maximum degree of melting required to produce the Golmud Hydro pluton from this type of source is only about 18%, which is consistent with them being small-degree melts formed during the collision.

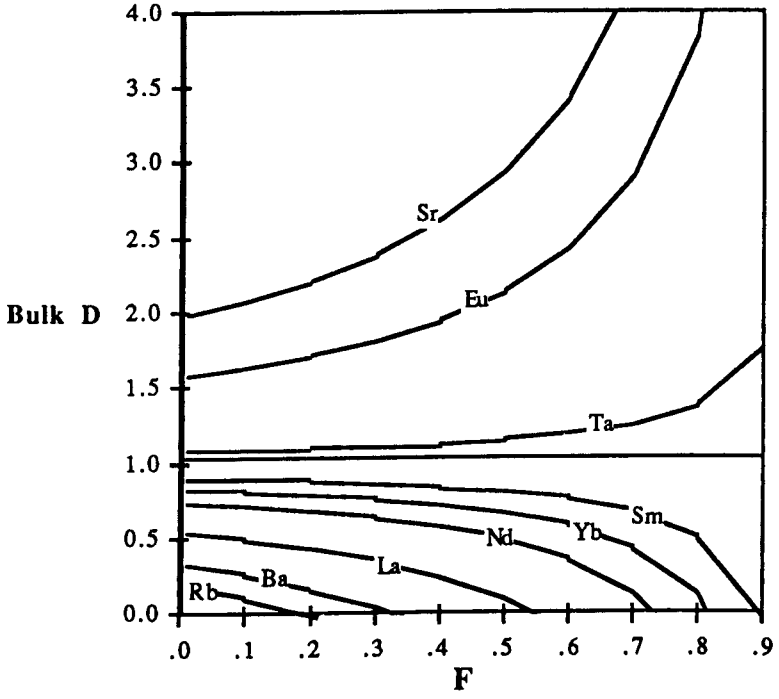

Fig. 5.27 Curves showing how bulk D changes for various elements in the Golmud Hydro pluton with increasing degrees of melting, assuming the source to be represented by average continental crustal values.

Using the same technique, and assuming bulk continental crust again represents the source, both the Golmud East granodiorite and the East Quarry tonalite could be derived by melting increasingly larger amounts of the crust, as demonstrated in Fig. 5.28a and b. In the same way, values of approximately 40% melt were obtained to produce the Xidatan and Yie Nin Gou grandiorites. However, Fig 5.29 shows that it was not possible to generate the small degree melts found in the Xidatan gneiss by melting the

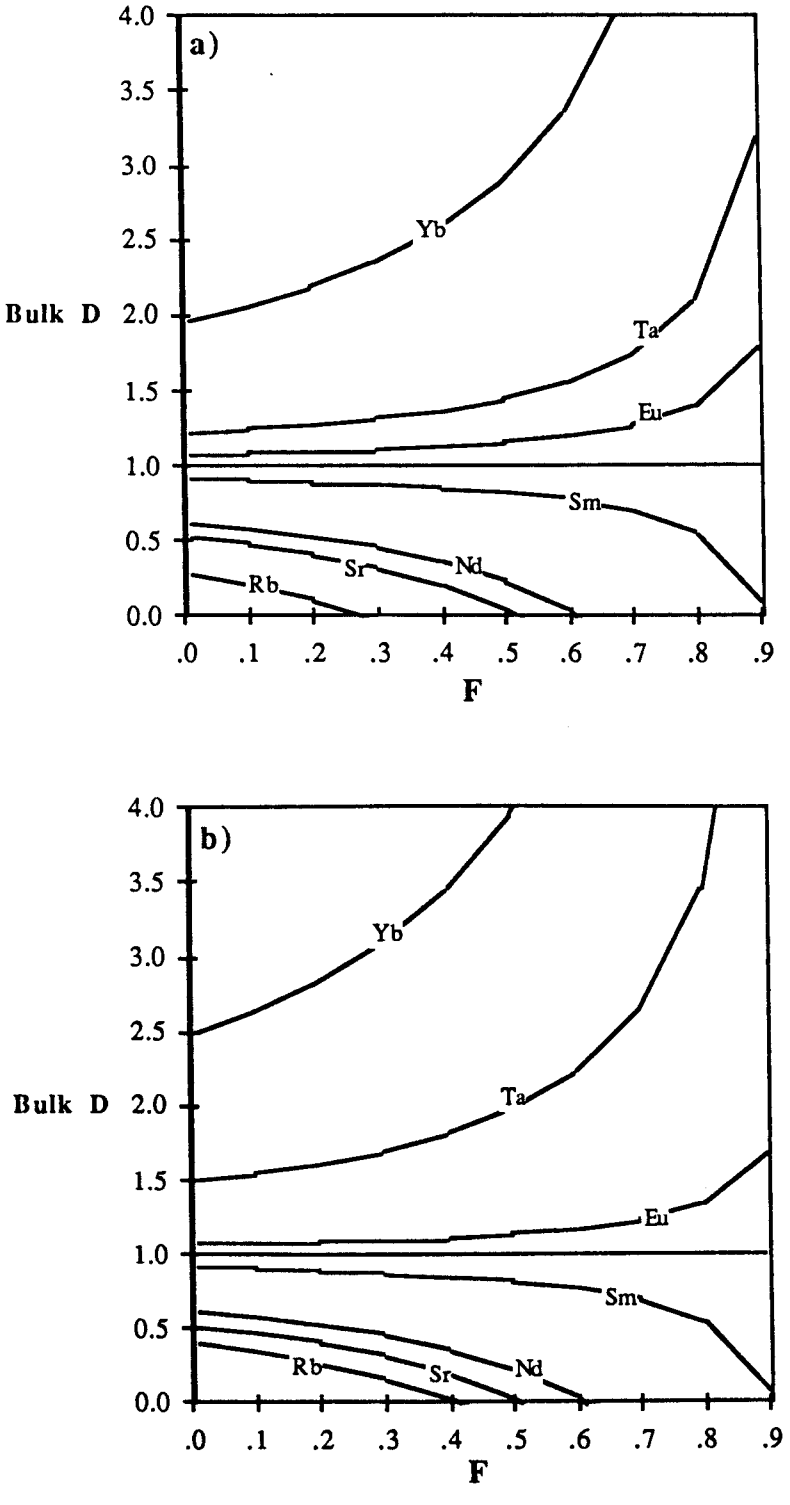

Fig. 5.28 Curves showing how bulk D changes with the degree of melting (F) for a) the Golmud East granodiorite and b) the East Quarry tonalite assuming average continental crust represents the source.

gneiss itself. The results obtained suggested a maximum melt of greater than 60% was required, but clearly this is unrealistic for the small degree, minimum melts seen in this pluton. First it must be emphasised that these values are maximum values, but infact the data imply that at these small degrees of melting all trace elements are predominantly compatible and remain in the source. The REE in particular are probably being held back in minor phases, which confirms the importance of these minerals not only in fractional crystallisation, but also during melting.

Finally, since the Southern Region plutons have different isotopic initial ratios from the main batholith, and have clearly been generated in a different tectonic setting, it is possible that they have been not been generated by the melting of continental crust. The magmagenesis of these granitoids will be investigated in more detail in the following chapter.

5.7 SUMMARY

Major element, trace element and isotope geochemistry indicate that the plutons in the Kunlun batholith have been derived overwhelmingly from pre-existing crustal material of either sedimentary or igneous origin, and that no significant new crust was generated in this part of the batholith either during the Devonian or the Permo-Triassic melting events. At least 4 phases of melting can be identified:

1 Formation of the Devonian Wanbaogou pluton from meta-sedimentary crust, and the peraluminous Duo Ya He pluton, probably from a metaluminous source.
2 Formation of the Permian Golmud Hydro pluton in the Central Region by small degree melting of a source very similar to that for the Devonian plutons.
3 Formation of the Triassic post-tectonic plutons from a source as yet unspecified.
4 Partial melting of the Xidatan granite in the Cretaceous as a result of anatexis during metamorphism.

This demonstrates that multiple episodes of partial melting and fractionation can result in highly evolved rocks that once originated in the mantle, and it becomes apparent that

these processes are essential in the evolution of the crust. Little new material need be generated, while existing material becomes vertically redistributed. Taylor and McLennan (1985) favour a model of crustal evolution in which the upper crust is produced from the total crust by a process of extraction of granitic melts, resulting in an upper crust of predominantly granodioritic composition. The formation of the granites examined in the Kunlun batholith would support this model.

REE patterns demonstrate that both partial melting and fractional crystallisation can fractionate Sm/Nd ratios, and that caution must be used when interpreting model Nd ages. The REE patterns also identify the Golmud Fault as a major boundary in the Kunlun batholith, supporting the fission track data which had already identified this fault as a significant lineament.

CHAPTER SIX

"The ideas about scientific theories assume we are rational beings who are free to observe the universe as we want and to draw logical deductions from what we see. In such a scheme it is reasonable to suppose that we might progress ever closer towards the laws that govern our universe. Yet if there really is a complete unified theory, it would also presumably determine our actions. And so the theory itself would determine the outcome of our search for it! And why should it determine that we come to the right conclusions from the evidence? Might it not equally well determine that we draw the wrong conclusions? Or no conclusions at all?"

Hawking, 1988

6 CONCLUSIONS

6.1 INTRODUCTION

The prime objective of this thesis has been to place time constraints on tectonic events in the Kunlun Terrane, in an attempt to refine (or dispute) models already in existence, and to define the role of the Kunlun in an evolutionary model for Tibet. The first half of this chapter therefore, deals with the geological history of the Kunlun Terrane from the Devonian to the Tertiary. I have tried to extract from the recent literature as much data as I can about the Kunlun Terrane from authors of all geological disciplines. I have then added my own data to this information in an attempt to create an integrated picture of what was going on. At times, building the model proved extremely dificult not only because I have not been to the field (Plate 6.1) and had a chance to evaluate field relations for myself, but because the literature is so controversial, and no-one seems to agree on nomenclature. It is undoubtedly an extremely complicated area tectonically, but the confusion must have been made worse by the multiplicity of names and spelling of names, for sutures, plates, faults, granites, formations, rivers, towns etc. As a novice to

the literature three years ago I clearly remember the problems of trying to find my way through this maze. So perhaps this is an appropriate moment to put in a plea for some uniformity in the literature, and at least an agreement on nomenclature, if not on mechanisms and models.

Plate 6.1 The Kunlun mountains in the Geotraverse region.

The second half of this chapter looks at the various models proposed to explain thickening and uplift in the Tibetan Plateau, and examines whether the fission track data from the Kunlun can support or refute any of these models.

6.2 REGIONAL SUMMARY

The Kunlun Terrane has been subjected to multiple episodes of tectonism that were either a direct result of the Kunlun Terrane colliding with other plates, or an indirect result, in that the effects seen in the Kunlun Terrane are due to plates being progressively accreted to the southern margin of Tibet. Fig 6.1 is a very generalised tectonic map of China which allows the Kunlun Terrane to be located with reference, in particular, to the North and South China blocks which will be discussed in future sections. Table 6.1 summarises all the proposed tectonic events that are believed to have occurred in the Kunlun Terrane. Although many of these events are poorly constrained

geochronlogically, this chapter will propose a tectonic model for the evolution of the Kunlun Terrane that is consistent with the known tectonic, palaeomagnetic, palaeobiogeographical and geochronological data.

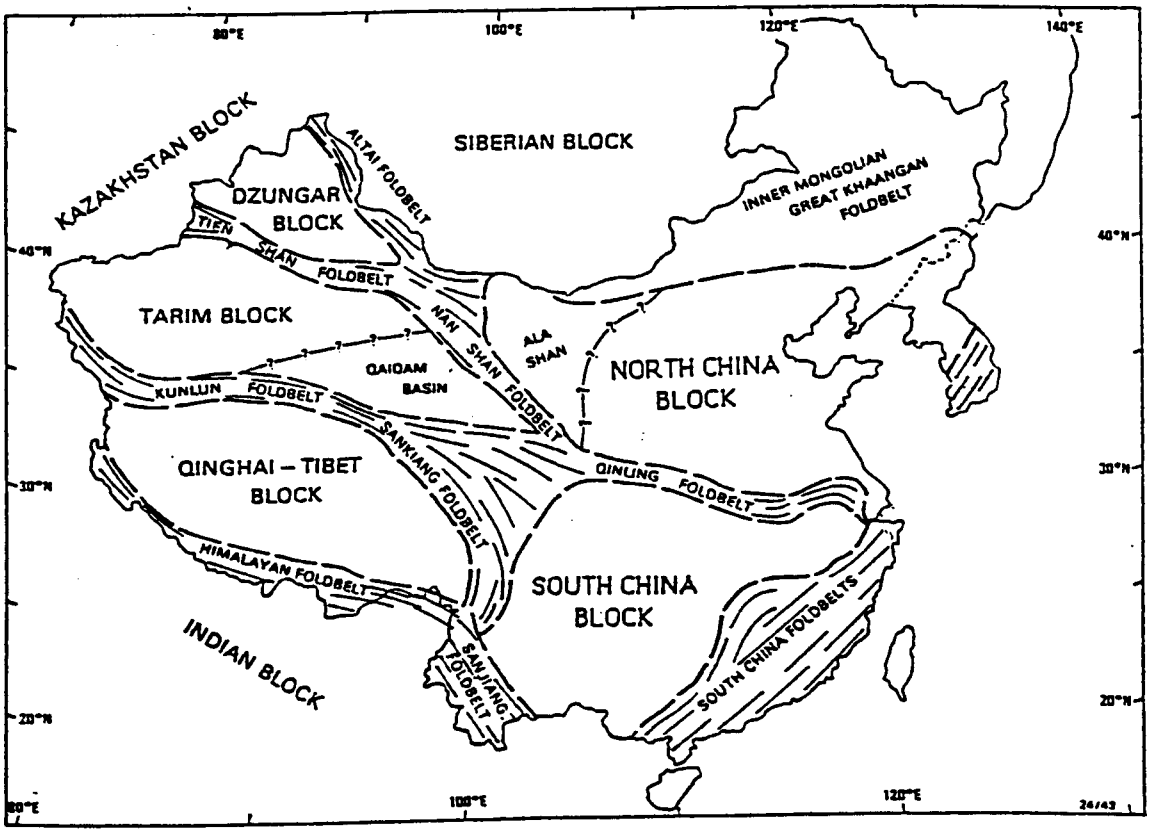

Fig. 6.1 Generalised tectonic map of China. Redrawn after McFadden *et al.* (1988).

AGE	PERIOD	EVENT
- 440?	Late Ordovician	Deposition of Naij Tal Group limestones and turbidites
400 - 380	Early Devonian	Dagangou Volcanics
390 - 380	Early - Mid Devonian	Intrusion of Wanbaogou and Duo Ya He plutons
~ 390	**COLLISION** of Kunlun with Tarim in southern latitudes	
?- 350	Mid-Dev - Early Carb	Uplift. Molasse and red-bed deposition from NE
350 - 330?	Early - Mid Carb	Marine transgression
Early Permian?	**RIFTING** between Qiangtang and Kunlun	
260 - 240	Mid Perm - MidTriassic	Intrusion of the batholith, subduction of the Qiangtang
255 - 230	Permo-Triassic	Rift volcanics in Kunlun and Qiangtang
245 - 225	Mid - Late Triassic	Flysch deposition,formation of Songban-Ganzi 'Terrane'
Early Jurassic	**COLLISION** of Qiangtang with Kunlun	
190	Early Jurassic	Intrusion of Southern Region post-tectonic plutons
125?	**COLLISION** of Lhasa with Qiangtang	
120	Early Cretaceous	Uplift and reactivation of thrusts in the Kunlun
120 - 20	Cretaceous - Tertiary	Period of thermal stability
45	**COLLISION** of India with Tibet	
~10	Miocene	Uplift in the Kunlun

Table. 6.1 Summary of the major tectonic events in the Kunlun Terrane from the Ordovician to the Miocene.

6.2.1 The Devonian Collision

Geochronolocial evidence suggests that the Dagangou volcanics and the Wanboagou and the Dou Ya He plutons are Early-Mid Devonian in age. If, as field evidence indicates, the Wanbaogou pluton (389 ± 10 Ma) is post-tectonic, then this constrains the timing of collision to pre Middle Devonian, which is somewhat older than expected. The previous Late Devonian age for the volcanics was based on palaeontological evidence found in a marine limestone and shale sequence that over-lies the volcanics and gives a Lower Carboniferous age of about 330 Ma. Pearce and Mei (1988), interpret the volcanics as representing an active continental margin environment, followed by post-tectonic volcanism. It seems probable therefore, that the volcanics seen on the northern side of the Dagangou valley (Fig.1.3) are Early Devonian, while those to the south are Middle Devonain. There are then several kilometers of conglomerates and fluviatile sediments between the Devonian volcanics and the Lower Carboniferous fossil-bearing marine beds, which could account for the intervening 50 Ma.

Leeder *et al.* (1988) interpret the thick conglomerate and the massive fluviatile red-bed sequence (the Dagangou Formation, Fig. 1.3) as a molassic phase, derived from an unroofing orogenic belt to the north subsequent to a collision event. Twenty kilometers south of Golmud the basal conglomerate, which contains sheared Ordovician pebbles, rests unconformably on Precambrian rocks which elsewhere are seen to pass up conformably into Ordovician rocks. In the central Kunlun, these Ordovician rocks contain two cleavages at an acute angle to each other. These two cleavages are not seen further south, indicating that either a later event overprinted the Devonian cleavage or, if the Devonian collision was with a plate that lay to the north of the Kunlun, as seems likely, then the older cleavage may have died out in the southern Kunlun. Folding seen in the Devonian volcanics and red-beds occurred before emplacement of the Permian batholith that intrudes them. This is evidenced from dykes related to the batholith that cut the folded volcanics and sediments, but themselves remain unfolded.

To summarise then, it appears that the subduction related volcanics, the post-tectonic granite and volcanics, the folding and cleavage, and the molassic phase of deposition are

strong evidence to support subduction followed by collision in the Kunlun Terrane prior to 390 Ma. This was followed by 50 Ma of uplift, denudation and deposition, before a major marine incursion apparently transgressed the area during the Lower Carboniferous.

Palaeomagnetic data (Lin and Watts, 1988) indicate that during the Lower Carboniferous the Kulun Terrane lay at a palaeolatitude of 20°S. This is in stark contrast to previous ideas which had always assumed that the Kunlun Terrane was already sutured to the Eurasian continent by that time. However, Lin and Watts point out that this Carboniferous southern hemisphere, moderate latitude of the Kunlun Terrane is shared by several other blocks such as the South China block (Lin 1984), Iran (Soffel and Forster, 1980), and Turkey (Lauer, 1984). From the occurrence of semi-arid calcrete nodules, Leeder *et al.* (1988) also favour this savannah-type latitude, and Smith *et al.* (1988) propose that if all the Tibetan microplates represented one continental shelf region, as suggested by their model, then when the 50% shortening seen across the plateau to-day is restored, the whole terrane would have extended some 2900 km to a latitude of 45°S. This is not incompatible with the deposition of glacio-marine sediments found in the Lhasa Terrane at that time.

But the most convincing evidence that the Kunlun Terrane was not sutured to Eurasia in the Devonian is found in recent palaeomagnetic data from the Tarim Terrane, which lies immediately north of the Kunlun Terrane (Fig. 6.1). McFaddon *et al.* (1988), propose that the Tarim Terrane was not sutured to Eurasia even by the Early Triassic, therefore the Kunlun could not possibly have been part of Eurasia in the Devonian. Furthermore, if it is accepted that the Kunlun Terrane collided with a plate lying to the north during the Devonian, then the inference is that this plate must have been the Tarim Terrane, which therefore also lay in southern latitudes at that time. Fig 6.2 shows the palaeogeographic reconstruction for Asia during the Triassic after McFaddon *et al.*, and it must be assumed that the Kunlun Terrane lay to the south of the Tarim Terrane as shown.

Where exactly the suture is located is, of course, another problem. It is variously called the Kunlun-Qinling, Kunlun-Qiling, Kunlun-Qilian, Kuenlun-Qinlin and

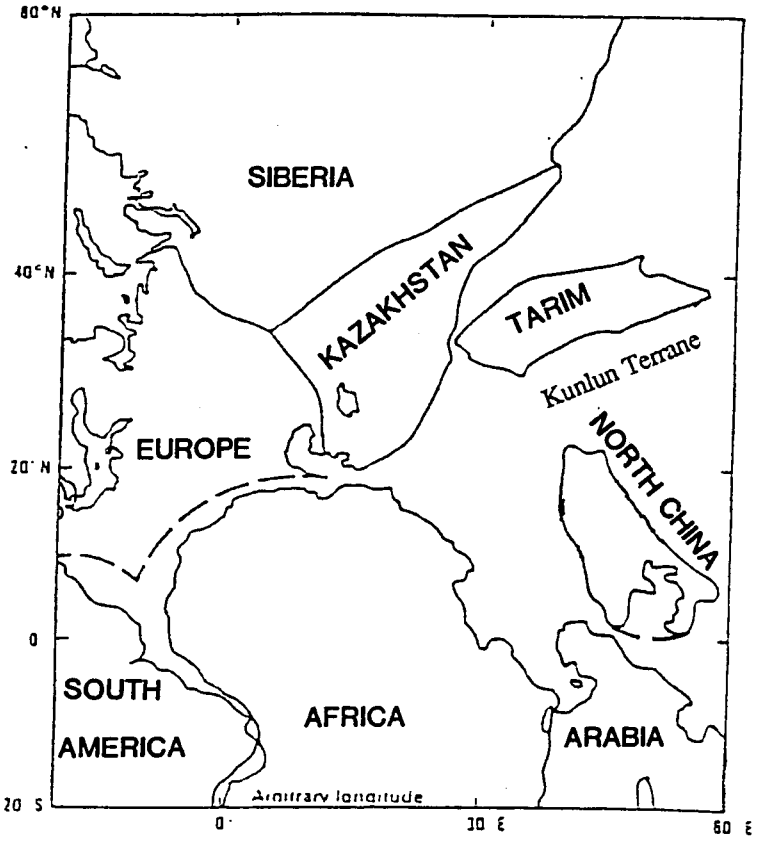

Fig. 6.2 Palaeogeographic reconstruction for the Tarim Terrane during the Early Triassic. Redrawn after McFaddon *et al.* (1988).

Kunlun-Tsinling suture; placed sometimes north and sometimes south of the Kunlun batholith, and it is given either a Devonian, (Mattauer *et al.*, 1985; Laveine *et al.*, 1987; Smith, 1988), a Permian (Zhang *et al.*, 1985; Dewey *et al.*, 1988) or a Triassic age (Sengör, 1985; Klimetz, 1983). Watson *et al.*, (1987) hedge their bets and suggest it closed diachronously - Permian to the east, and Triassic to the west. I shall call it the Kunlun-Qinling suture in line with the majority of authors (Zhang *et al.*, 1984; Watson *et al.*, 1987; Dewey *et al.*, 1988; Smith, 1988). In the light of the evidence stated above I ascribe a Devonian age to it and place it north of the batholith for the same reasons and others that will be discussed below.

The 1:100 000 Geological Map, Qinghai, shows a profusion of ophiolite outcrops along the southern edge of the Tarim Basin and around the Qaidam basin (Fig. 6.3). A linear ophiolite belt also occurs 70km north of the Anyemaqen Shan ophiolite belt (from which it is apparently quite distinct) and extends westwards to within 130 km of Golmud, south

Fig 6.3 Reference map for tectonic features in Tibet and the surrounding regions that are mentioned in the text. Rederawn after Dewey *et al.* (1988).

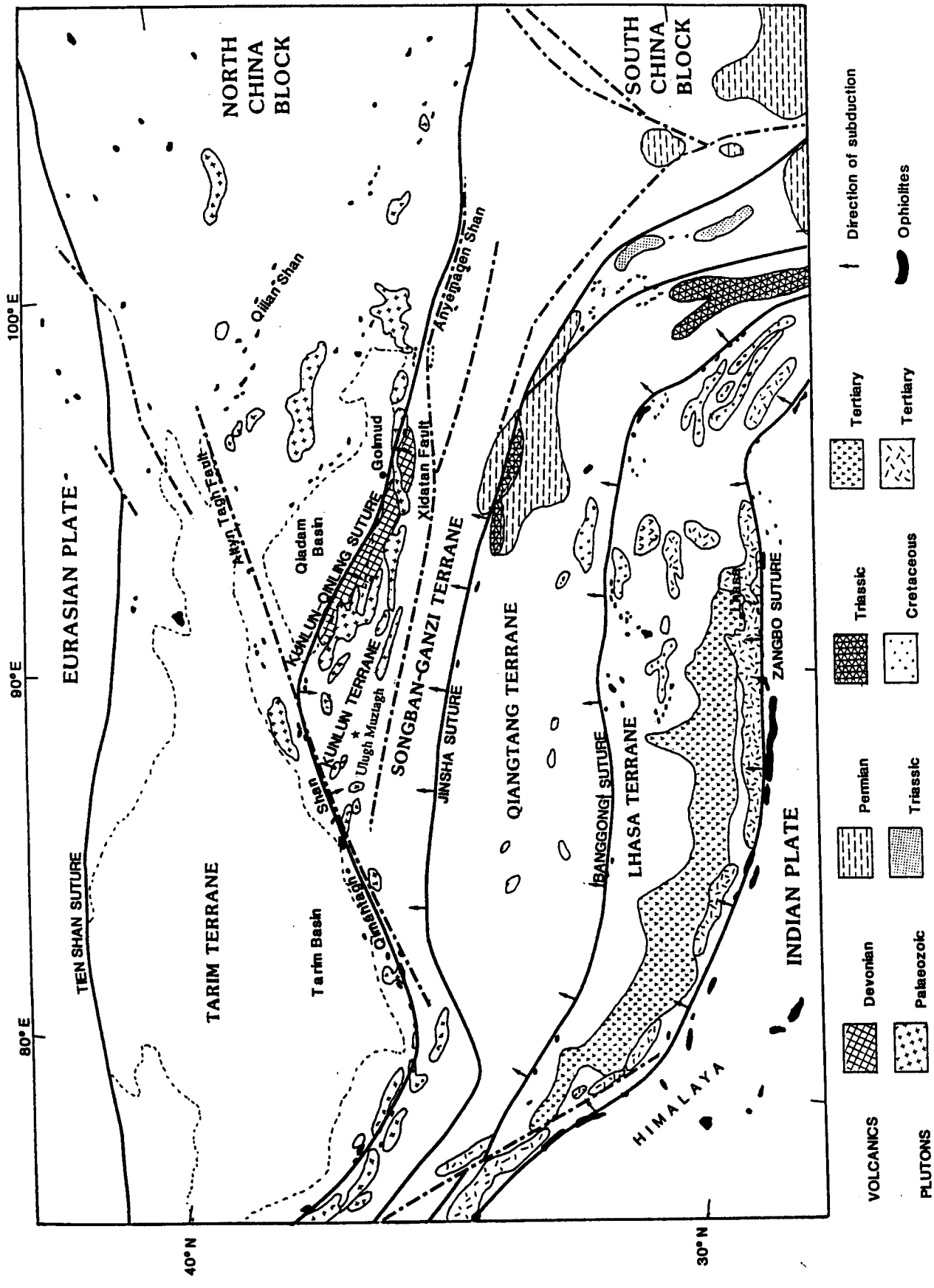

east of the Kunlun batholith (Dewey *et al.*, 1988). The age of these ophiolites is poorly constrained, but Dewey *et al.* suggest a Devonian suture may lie along the Altyn Tagh Fault, where the ophiolite belt is believed to be Lower Palaeozoic. The model they prefer, however, is that the Tarim and Kunlun Terranes represented a single terrane during the Lower Palaeozoic, and they propose that the suture with the Eurasian continent lies at the Tien Shan suture to the north of the Tarim basin. They infer from this, as does Watson *et al.* (1987), that the Kunlun Terrane was part of the North China block at this time.

But, palaeomagnetic, sedimentalogical and palaeobiogeographical data collected by the Tibet Geotraverse team now strongly dispute the possiblity that the Kunlun Terrane was part of the Eurasian continent during the Carboniferous. Independent palaeomagnetic data (McFaddon *et al,* 1988) also show that the Tarim was not sutured to Eurasia until the Triassic which further confirms the Geotraverse team's data. Nevertheless, there is strong evidence for a collision event in the Kunlun Terrane during the Devonian. This means that either the Carboniferous age ascribed to the Tien Shan suture is incorrect (Smith, 1988 and inferred by McFaddon *et al.* 1987), or that this is not the position of the collision that relates to the Devonian deformation and magmatism seen in the Kunlun.

Dewey *et al.* (1988) show that the Himalayan deformation across the plateau is halted at the southern edge of the Tarim and Qaidam basins. These have not been thickened as a result of the India/Tibet collision, and they suggest that this is because they are underlain by stronger Precambrian lithosphere (Molnar and Tapponnier, 1975 and 1978). Fission track data from the Kunlun Terrane show that granites north of the Golmud Fault (Fig. 2.1) have also not been affected by the Himalayan uplift, and retain much older fission track ages. I therefore tentatively suggest, that in the Geotraverse region, the Golmud Fault marks the southern edge of the Tarim Terrane and the region of stronger Precambrian lithosphere that resisted the Himalayan thickening. Consequently this must also mark the suture line between the Kunlun and Tarim Terranes.

Fig. 6.3 shows the ophiolite outcrops in Tibet compiled from Dewey *et al.* (1988) and Kidd *et al.*, (1988b). I have positioned the Devonian Kunlun-Qinling suture line such that

it would follow the Golmud Fault in the Geotraverse region. To the west it follows the ophiolite outcrops along the southern edge of the Qaidam basin, which did not open until the Jurassic, and joins up with the Palaeozoic ophiolite belt that passes through the Qimantagh Shan, south of the Tarim Terrane. It extends eastwards through the area now occupied by the Permian batholith, to join up with the, as yet unnamed, ophiolite belt to the south east of Golmud and the Permian batholith. Examination of the 1:1 Geological Map, Qinghai, shows that these ophiolite outcrops in the south east are scattered along a major fault line which may well be an eastward extension of the Golmud Fault, i.e. the suture line. Positioning the suture line here then includes the Kunlun Terrane as part of the South China block rather than the North China block, which is in accordance with both the palaeomagnetic and the palaeobiogeographical data. That the continental arc volcanics lie to the south of the proposed suture line necessitates that the subduction zone must have dipped southwards, although Mattauer *et al.* (1985) place a Devonian suture between the North and South China blocks as dipping northwards. But this southward direction of subduction is further supported by recent evidence of active southward

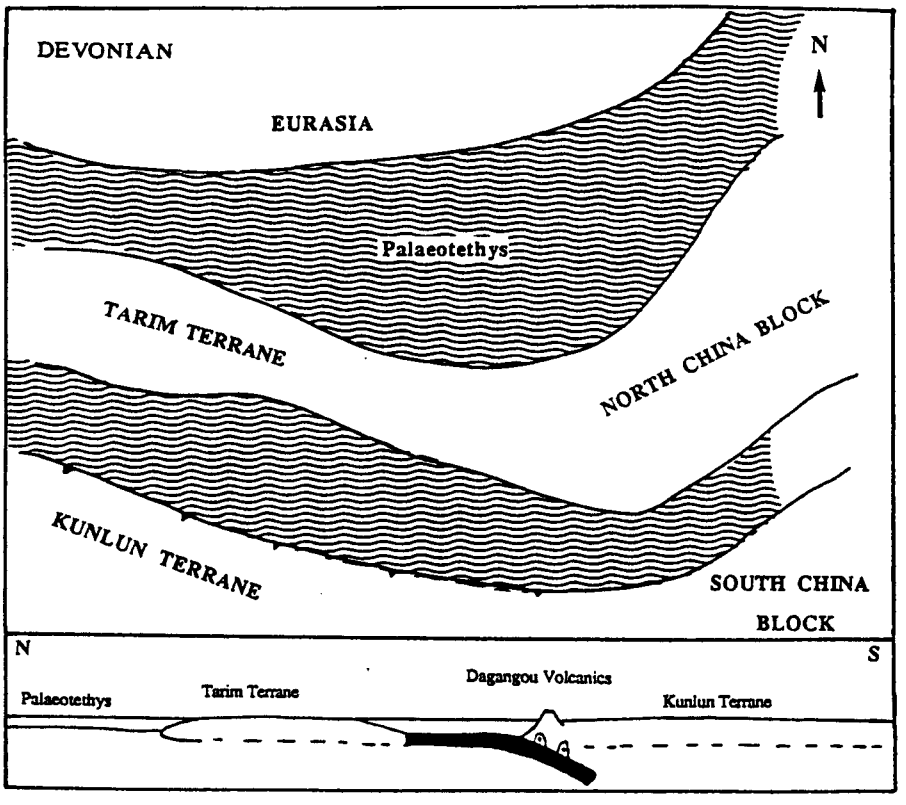

Fig. 6.4 Plate tectonic reconstruction of China during the Devonian.

subduction of the Tarim Terrane beneath the Kunlun Terrane, at the present time (Molnar *et al.*, 1988). Fig. 6.4 shows a plate tectonic reconstruction of the Kunlun and Tarim Terranes, and their positions in relation to Eurasia, during the Devonian. Fig. 6.5 demonstrates the tectonic situation subsequent to closure along the Kunlun-Qinling suture during the Early Carboniferous.

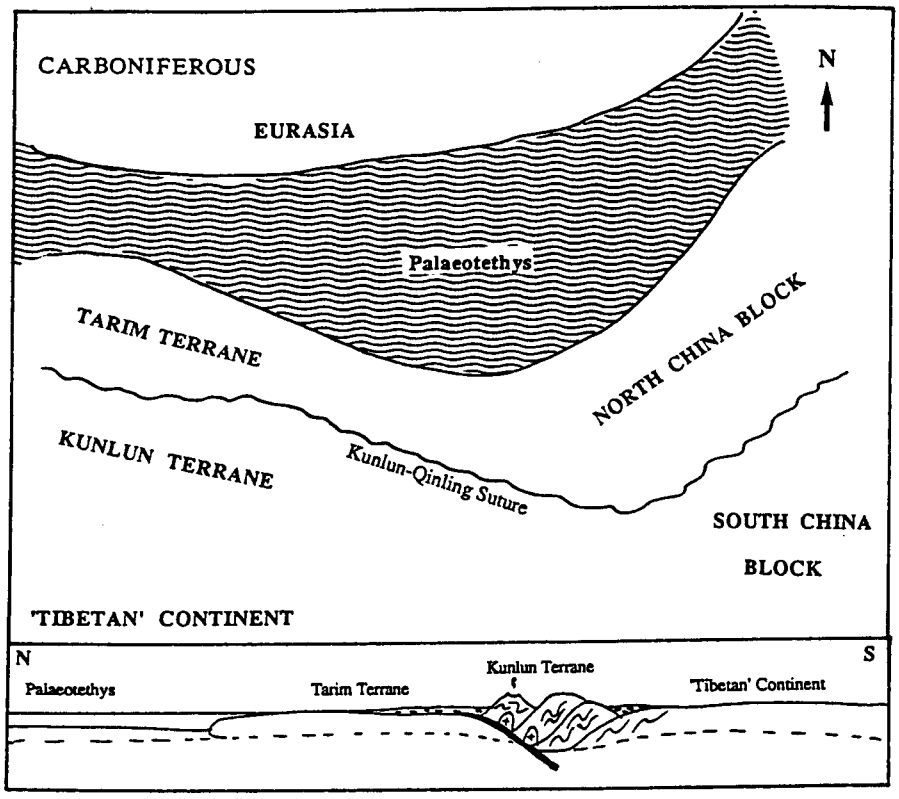

Fig. 6.5 Plate tectonic reconstruction for China during the Early Carboniferous.

6.2.2 The Permo-Triassic Collision

If the model of a continous continent from India to the Tarim proposed by Sengör *et al.* (1984); Li *et al.* (1986); Smith *et al.* (1988) and Smith (1988) is accepted, it is important to identify a period when the terranes broke up and drifted apart. Continental break-up during the Permian is characteristic of many terranes in China and south east Asia (Smith *et al* , 1988) and is considered to represent a period of continental fragmentation by the formation of new spreading centres. Zhang *et al.* (1981) demonstrate how in eastern China particularly, the rifting event was very extensive. Rift volcanics exposed in the Wanbaogou Valley, (Fig.1.4) are consistent with moderate

lithospheric attenuation during continental rifting (Pearce and Mei, 1988). They are conformably overlain by limestones containing Late Permian fauna, which restrict the age of the volcanics to being older than about 250 Ma. Further east in the Kunlun Terrane, incipient spreading is represented by a series of submarine lavas, sill complexes and basic intrusions.

In the Qiangtang Terrane, just south of the Jinsha suture (Figs. 6.3 and 6.6), another outcrop of rift volcanics is well constrained stratigraphically, being underlain by limestones of early Late Permian age, and overlain by coal-bearing clasitics with marine bands dated as Late Permian (Leeder *et al.*, 1988). This confines these volcanics to a period between about 258 and 248 Ma, and correlates them with a similar outcrop to the east. Clearly these volcanics are evidence for continental rifting in the Kunlun and

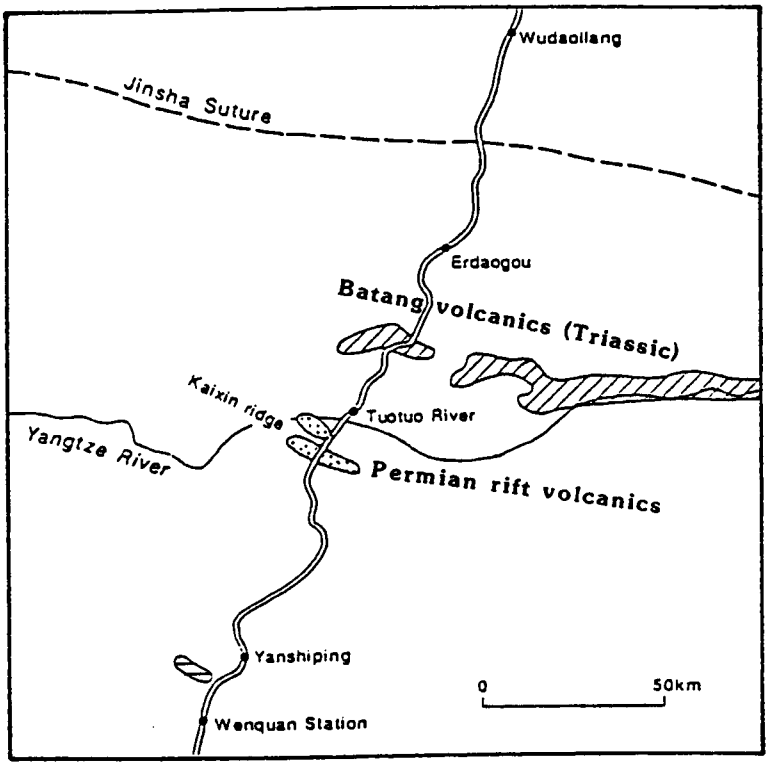

Fig. 6.6 Detail of the region south of the Jinsha suture on the Geotraverse route, showing the exposure and relationship of Permian rift volcanics and Triassic subduction volcanics.

Qiangtang Terranes at various times during the Permian, although it is difficult to reconcile this with the strong evidence for collision and compression occurring in the

Kunlun at apparently the same time (see Chapter 3). Smith (1988) supports a major rifting event of the 'Tibetan' continent during the late Early Permian along lines analogous to the Zangbo and Jinsha sutures. He considers that there may also have been rifting to the north of the batholith along the Kunlun-Qinling suture to account for the separation at that time of the North and South China blocks. He fails however, to acknowledge the presence of the Permian batholith. It is possible of course that rifting in the Kunlun occurred in response to continental collision rather than spreading. This is seen in regions north of the Tarim Basin where the Himalayan collision has generated the massive Baikal rift system in Siberia (Tapponnier and Molnar, 1976). However, this is not consistent with the oceanic sediments found in association with these volcanics. Fig. 6.7 shows the plate tectonic reconstruction for the Kunlun Terrane during the Early Permian.

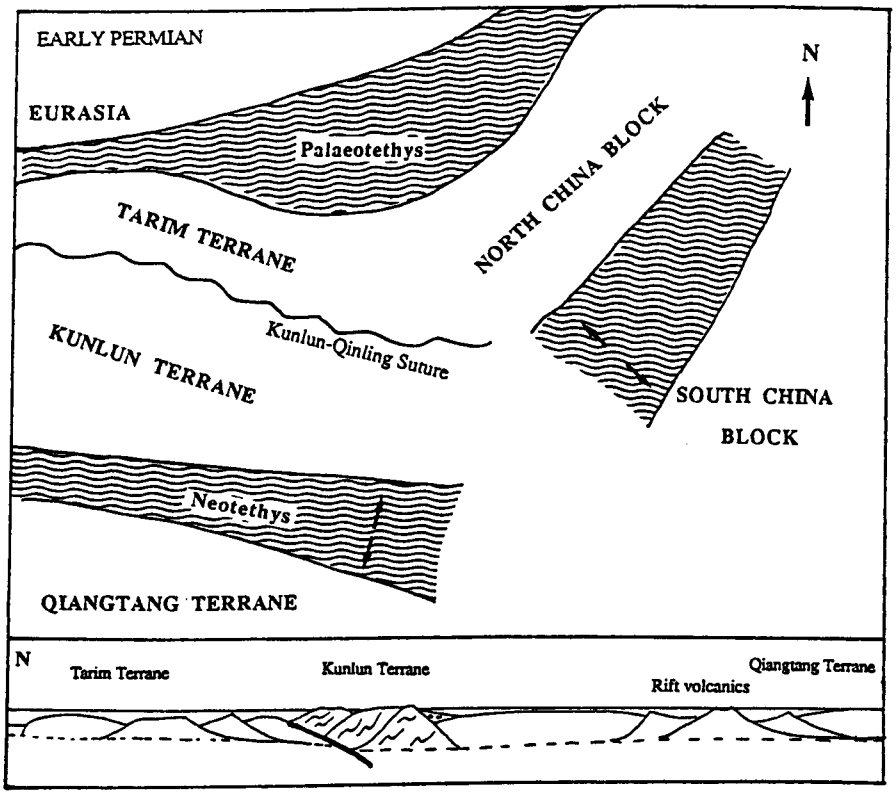

Fig. 6.7 Plate tectonic reconstruction for China during the Early Permian.

Magmatism on a large scale (in the traverse region), was generated to form the plutons of the Kunlun batholith during the period between 260 and 240 Ma, but evidence for subduction is not clear. There are no Permian volcanics in the geotraverse region, although a swarm of basalt-andesite dykes cut the Golmud Hydro pluton and the adjacent

country rocks, while sills of a similar composition cut the Devonian/Carboniferous sediments and volcanics. The nature of the dyke alteration indicates that they were emplaced before the batholith had cooled and are thus of the same age as the batholith. Pearce and Mei (1988), believe these dykes fed the now eroded volcanoes of an active continental margin.

The plutons sampled from the Kunlun batholith however, are not typical of subduction zone magmatism found, for example, in the Gangdese and Andean batholiths where mantle material is clearly involved in granite petrogenesis. In the Kunlun, the plutons have an enriched isotopic signature and have clearly been derived from the melting of intermediate to upper crustal sources. While this may have been as a result of basaltic underplating during subduction, it is more consistent with a melting regime operative during active collision.

Evidence for a suture line in the Geotraverse region associated with the Permian magmatism is yet again, ill-defined. Ophiolites outcrop several hundred kilometers to the west and east where, in particular, a remarkably linear belt extends for about 400 km, through the Anyemaqen Shan. Within 300 km of the geotraverse line it intersects, and is truncated by, the eastward continuation of the Xidatan Fault. Mèlanges associated with the belt contain Permian exotics in a Permo-Triassic flysch matrix (Dewey *et al.* 1988). On the basis of these ophiolites and associated mèlanges, Dewey *et al.* (1988) place the Kunlun-Qinling suture south of the Kunlun batholith and ascribe a Permian age to it.

However, if it is accepted that the Kunlun Terrane was accreted to the Tarim Terrane during the Devonian, then a Permian collision must have been with a plate that lay to the south of the Kunlun Terrane. Consequently, subduction associated with this collision must have dipped northwards to generate magmatism north of the suture. Furthermore, the plutons sampled from both the Devonian and Permian phases of intrusion have isotopic signatures consistent with both episodes of melting having been derived from similar crustal sources. This would therefore support the proposal that the Devonian subduction zone dipped south and the Permian subduction zone dipped north. Any

crustal melting which resulted from basaltic underplating during subduction would consequently tap much the same source during both events, but whether the colliding plate was the Songban-Ganzi Terrane or the Qiangtang Terrane is unclear.

It is not known whether the Songban-Ganzi Terrane is underlain by old continental material since it is covered by several kilometers of Triassic sediments and no basement is exposed. But evidence for uplift, and therefore possibly collision, is seen in the massive conglomerates at the base of the Triassic, which contain volcanic and granitic material, presumably being eroded from the unroofing batholith to the north (Leeder *et al.*, 1988). Unfortunately it was not possible specifically to date these conglomerate boulders which may have placed constraints on the age of the conglomerate, and since both episodes of melting have been derived from very similar sources even the initial ratios did not clarify matters. It is equally possible that the boulders were Devonian rather than Permian, or that the conglomerate contained boulders of both ages.

According to Zhang (1988), metamorphosed Mid-Triassic rocks in the central Kunlun are unconformably overlain by the basal conglomerate which supports a Mid-Triassic uplift of the Kulun Terrane. Furthermore, biotite evidence from the Golmud Hydro plutons (Fig 2.1) suggests a resetting event, and possible reactivation of the Devonian suture along the Golmud Fault line, between 240 and 235 Ma, (mid-Triassic), which may represent the timing of collision along this part of the Songban-Ganzi suture or it may simply be the result of faulting during accretion.

Deposition of the massive Bayan Har group of deep marine turbidites and contourites (Fig. 1.3) is interpreted by Watson *et al.* (1987) as being derived in part from the southern margin of the Kunlun, and deposited in a triangular-shaped deep marine ocean basin that was confined at the eastern extremity by the westward closing North and South China blocks. The age of these deposits remained undated in the Geotraverse region, but further to the east flysch sedimentation appears to have commenced at about 245 Ma and continued until the Late Triassic (~230 Ma). Considering the apparent diachronous nature of events, with closure in the east being earlier in than in the west, it is possible

that these ages do not correlate exactly with those in the Geotraverse region where they may well be somewhat younger. Fig. 6.8 illustrates a plate tectonic reconstruction of the region during the Late Permian.

The sediments became accreted to the Kunlun Terrane, to form a huge accretionary prism as the Qiangtang Terrane moved northwards towards the Kunlun Terrane. Watson *et al.* (1987) use the Cenozoic - Recent accretion of the Bengal submarine fan along the

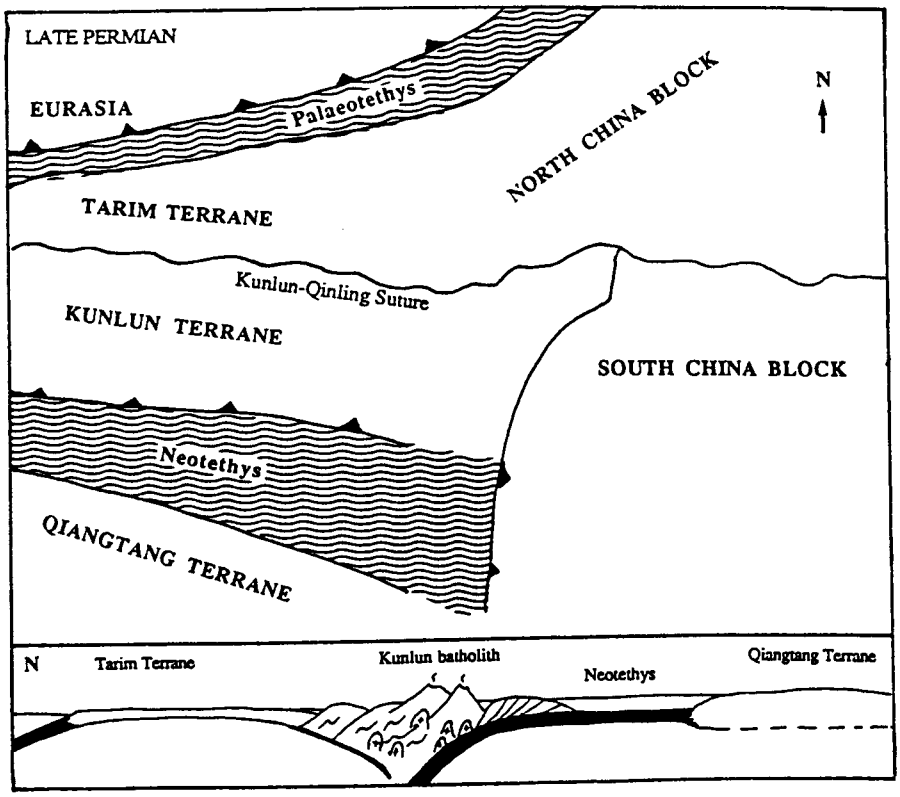

Fig. 6.8 Plate tectonic reconstruction of China during the Late Permian.

Andaman-Nicobar trench as a modern analogy for the Songban-Ganzi accretionary prism. This is interesting because the same analogy was made for the Southern Uplands accretionary prism (Mitchell and McKerrow, 1975), which in turn has many features in common with the Songban-Ganzi Terrane. For some time it was considered that the Southern Uplands Fault, which could be considered to be analogous with the Xidatan Fault, represented the line of closure of the Iapetus Ocean. But a number of geophysical investigations eventually led to the conclusion that final suturing occurred along the Solway Line (Jinsha suture?) and that the Southern Uplands Fault, although the site of a

major structural break, only marks the approximate northern limit of the accretionary prism (Cassidy, 1979 and Tindle, 1982). On balance, it makes more geological sense if the Songban-Ganzi 'Terrane' is considered to represent the suture 'zone' between the Jinsha suture (the line of final ocean closure) and the Xidatan Fault which only marks the northern limit of the accretionary prism. The Anyemaqen Shan ophiolites considered by Dewey *et al.* to represent a major suture line, may well be part of the trench mélange, and their Permian age is quite consistent with the early stages of this very long-lived period of subduction.

The position of the Jinsha suture is poorly defined, since the region is buried under a cover of Neogene and Palaeogene deposits. But there does seem to be general agreement in the literature, that a suture is present in this region, and this is not disputed here. There appears to be little agreement, however, about the direction of dip on the subduction zone. I have already postulated that it must have dipped northwards, and structural evidence (Watson *et al.* 1987; Coward *et al.* 1988) also supports a northward dipping subduction zone based on the recognition of steep, north-side up faults. These are believed to have been initiated as gently dipping thrusts, and been rotated upwards into their present steep position, by the increasing approach of the Qiangtang Terrane. Dewey *et al.* (1988) and Pearce and Mei (1988) favour a southward subduction zone based on magmatic evidence from arc volcanics,the Batang Group, that occur to the south of the Jinsha suture (Figs. 6.3 and 6.5). These are very extensive, continuing some 1000 km to the south east. The Batang volcanics are typical of subduction related lavas errupted on oceanic or thinned continental lithosphere, but their limestone cover in particular supports the former proposal. A third model of double subduction dipping both north and south (Leeder *et al.*, 1988) is a possibilty that would explain both the structural deformation to the north and arc magmatism to the south. Clearly it must have dipped north at some time to generate the accretionary prism and the magmatism seen in the Kunlun batholith. The Batang volcanics are about 225 Ma (Leeder *et al.*, 1988) indicating that the volcanoes became active some 15 - 20 Ma after magmatism had ceased in the Kunlun. Could a fourth scenario be that the subduction zone switched direction in this interval?

Alternatively, the limestones seen above and below the Batang volcanics suggest that they were formed as an oceanic arc rather than at a continental margin, and therefore the associated subduction zone may have lain to the south of the volcanics and become obscured during the collision.

It appears then that during the Late Permian and Early Triassic, active subduction beneath the Kunlun Terrane generated magmatism in a continental arc environment and that true continent-continent collision did not occur until the latest Triassic or earliest Jurassic. Collision with the Qiangtang Terrane is dated from palaeontological evidence as being at about 200 Ma, or Lower Jurassic, and a post tectonic tonalite that intrudes the accretionary prism gives a K-Ar biotite age of 213 ± 6 Ma (Harris *et al.*, 1988). With no other age data for this pluton though, it is difficult to evaluate this age with any degree of confidence, but the strong deformation seen in the Bayan Har Group is considered to have occurred during latest Triassic or earliest Jurassic times. Fig. 6.9 shows a possible plate tectonic reconstruction for the region during the latest Triassic or earliest Jurassic.

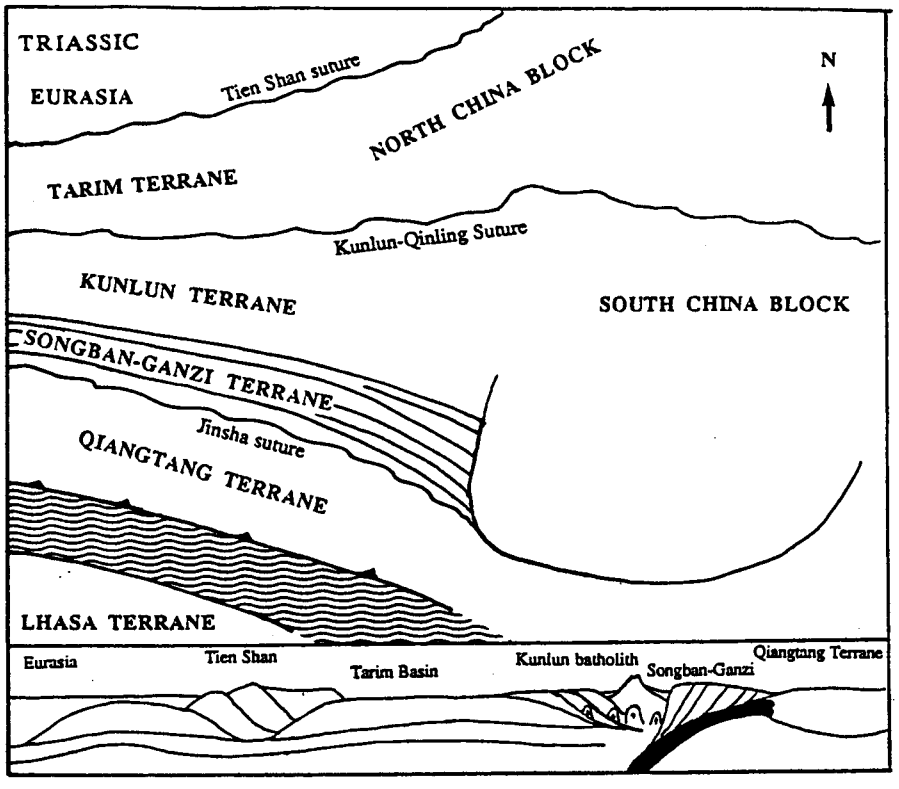

Fig. 6.9 Plate tectonic reconstruction of China during the Late Triassic or Early Jurassic.

In the Kunlun Terrane, the Southern Region post-tectonic plutons that give an age around 190 Ma, may well have been generated in a post-collisional phase of extension. This is a possibility that occurs in regions where the crust has been substantially thickened during collision. When the compressive stresses generated by convergence are released, the extension of these areas occurs due to collapse of the region under its own weight. The classic example being the Basin and Range province (England and Thompson, 1986). England and Thompson consider that the change in crustal thickness, (both during thickening and thinning) is accomplished by distributed strain so that for example, a doubling of crustal thickness results in a doubling in thickness of the entire lithosphere. This homogeneous strain is commonly assumed for extensional deformation during sedimentary basin development (McKenzie, 1978). England and Thompson (1986) demonstrate that melting of the lower crust can be generated without the need for heat generated by basaltic underplating in regions where there has been a long period (>30 Ma) between thickening and the onset of extension. It occurs particularly where recently active continental lithosphere has been involved in the thickening event, as this is considered to generate a greater amount of heat due to radiogenic elements in the crust. However, although there has been at least 30 Ma between thickening of the crust and formation of the Southern Region post-tectonic granites, this model predicts that upper crustal 'S' type magmas would be the dominant granite type and this is clearly not the case.

An alternative model whereby granitic magma is generated by the intrusion of mantle-derived basalt into the continental crust (Huppert and Sparks, 1988) may also account for the generation of the Southern Region plutons. In this model, it is predicted that basaltic sills emplaced into the lower crust, probably also in an extensional regime, form voluminous overlying layers of convecting silicic magma, and that the time-scales for melting and crystallisation are very short (10^2 to 10^3 years), unless the magma ascends to higher levels. It also predicts that because the temperatures of the crustal melt layers are very high (900 - 950°C) the process is closer to total fusion rather than partial melting, and thus the magmas can contain significant proportions of restite crystals. The model indicates that dacitic volcanic rocks fractionated from the melts, and granodiorite/tonalite

plutons would be the dominant rock types generated. The Southern Region plutons are predominantly granodioritic in composition and their isotopic signatures, which are closer to Bulk Earth than the more enriched ones from the main batholith, suggest there may be a mantle-derived component involved in their generation. Some mixing of the mantle-derived basalts and the crustal-derived silicic melts may have occurred at the boundary between the two layers.

6.2.3 The Cretaceous Collision

The Southern Region plutons subsequently played an important role in recording a major tectonic event that must have substantially affected the Kunlun Terrane, but appears to have gone unrecognised by the Tibet Geotraverse team. Watson *et al.* (1987) show how evidence of coarse clastic sedimentary input into the Tarim and Qaidam basins, records reactivation of thrusts (such as the Golmud and Xidatan Faults) along the margins of these basins, and rejuvenation of the mountain front (the Kulun Shan). This occurred as a result of collision of the Lhasa Terrane with the southern edge of Tibet during the Cretaceous. A Rb-Sr whole-rock isochron from a post-tectonic granite related to this collision gives an age of 126 ± 26 Ma, but the timing of the effects of this event in the Kunlun Terrane is more precisely recorded at 120 ± 2 Ma, by both Rb-Sr and Ar-Ar dating of biotites from the Xidatan granite that is cut by the Xidatan Fault. Clearly these data suggest that this impact reactivated the Xidatan Fault, thrusting the Kunlun Terrane southwards over the Songban-Ganzi Terrane, perhaps for some hundreds of kilometers (see Chapter 4) Further evidence for this event is seen in fission track data which record the uplifting of plutons north of the reactivated Golmud Fault, along the southern margin of the Qaidam Basin, to bring the apatites through their closure temperature at about this time.

Very little Jurassic, and no Cretaceous sediments were identified in the geotraverse area of the Kunlun, which further confirms that the region was uplifted during this period. Tertiary basin development occurred across the Jinsha suture zone, but poor time constraints prevents a full explanation of events. It appears that basin developement and source provenance were closely controlled by contemporaneous Palaeogene, Neogene,

and Recent thrust tectonics across the whole geotraverse route (Leeder et al 1988) associated with the Himalayan collision.

But one final question must still be addressed - did a Late Palaeozoic ocean exist between Gondwanaland and Eurasia (Palaeotethys?); and if it did exist, where was it positioned? Helmcke (1985) places it at the Zangbo suture, but this is now considered not to have opened until the Permian, while Allègre *et al.* (1984) and Chang *et al.* (1986) suggest that the Banggong suture is the most likely place. Dewey *et al.* (1988) place it between the the Qiangtang and Kunlun plates at the Jinsha suture on the grounds that it separates two domains where the sedimentary facies and volcanics are very different when they emerge from beneath the Tertiary cover of sediments. Palaeobiogeographical data though do not recognise the major faunal break that is to be expected from opposite sides of a major ocean, either at the Jinsha or Banggong sutures. Furthermore, Nd isotopic data show that all granites from the Kunlun to the Lhasa Terranes have very similar model ages (Harris *et al.*, 1988) consistent with them all being underlain by basement that is of the same age.

Palaeomagnetic data indicates that any major ocean in existence during the Palaeozoic must have lain to the north of the Kunlun Terrane, while geochemical evidence for a Devonian suture between the Kunlun and Tarim Terranes pushes it further north to the Tien Shan suture. This is strongly supported by the palaeontological data which defines a biogeographical barrier in the Late Palaeozoic at the Tien Shan suture. Clearly though, from the extensive period of subduction and the large accretionary prism believed to be associated with closure on the Jinsha suture, an ocean of significant size must have existed there during the Permian. But even at moderate spreading rates of 5 cm/yr, a fairly large ocean could open and close in 50 Ma, the minimum time available for ocean formation according to geochronlogical and palaeontological data. This ocean is considered to be the 'Neo'tethys (Figs. 6.7 and 6.8) of Sengör (1984, 1985). 'Palaeo'tethys lay to the north of the Tarim Terrane (Fig. 6.5), and the 'Tibetan' continent formed an integral part of Gondwanaland.

In summary then, it appears that :

1 The Kunlun Terrane, possibly representing the northern edge of a substantial land-mass of Gondwanaland affinities, collided with the Tarim Terrane during the Early Devonian. This generated subduction related volcanics and post-collision granites. Palaeotethys lay to the north of the Tarim Terrane.

2 The Devonian collision united the 'Tibetan' continent which existed until break-up of the region during the late Early Permian (?) along the Jinsha and Zangbo suture lines. Neotethys developed between the Kunlun and Qiangtang Terranes.

3 Subduction, associated with closure of Neotethys, started in the the Kunlun in the late Early Permian, and continued into the middle of the Triassic, generating the Permian batholith. Subduction must have continued during formation of the accretionary prism in the Middle to Late Triassic, but no associated magmatism has been identified.

4 Collision of the Qiangtang Terrane along the Jinsha suture occurred at about 200 Ma.

5 At 120 Ma, collision of the Lhasa Terrane with the Qiangtang Terrane caused reactivation of the Xidatan and Golmud thrusts and resulted in uplift of the Kunlun Shan. Large quantities of coarse clastic material were deposited in the Tarim and Qaidam basins.

The effects of the Himalayan collision on the Kunlun Terrane will be summarised in the final section.

6.3 THICKENING, UPLIFT AND TIMING

As long ago as 1924, Argand proposed that the Tibetan Plateau was underlain by crust that is double the usual crustal thickness of 35 km. He considered that this was caused by India being underthrust beneath Tibet, as a result of the Himalayan collision. Since then, an abundance of geophysical and structural data have confirmed that in fact the crust does thicken from a normal 33 km beneath the Indian Shield to reach a maximum of 75 km beneath the Himalayas, and averages about 65 km beneath the Tibetan Plateau.

Love and Rayleigh wave velocities are much lower beneath Tibet than India, implying a thinner lithospheric boundary conduction layer beneath Tibet, and consequently higher geothermal gradients (Romanowicz, 1982). Dewey *et al.* (1988), suggest the gradient is about 27°C/km in the upper crust, and 18°C/km in the lower crust, while Min and Wu (1987) argue for it being > 50°C/km near the surface. Widespread recent volcanism across the plateau and particularly in the Qiangtang Terrane (Burke *et al* 1974; Kidd 1975; Deng 1978; Sengor and Kidd, 1979; and Molnar*et al.*,1987), and a low-velocity zone at depths between 17 and 30 km (Min and Wu 1987) supports the idea of a thin boundary conduction layer, high geothermal gradients, and a region of partial melting in the middle crust.

Various rates of uplit and erosion have been calculated for the Himalayas and the plateau, and Dewey *et al*, (1988) suggest that about 20 km have been denuded from the Himalayas, 10km from the Gangdese belt, and an average of 2km from the Tibetan Plateau between the Gangdese Belt and the Kunlun Shan. If this represents the total amount of erosion since the Himalayan collision 45 Ma ago, it implies extremely slow erosion rates of 0.04 mm/yr for the plateau over that period.

Zhao and Morgan (1985) calculated an average uplift rate for the plateau of 0.2 mm/yr over the last 25 Ma, but in a later paper (1987) suggest that the average thickening rate is 1.2 mm/yr. From fission track data Zeitler (1985), indicates a period of rapid acceleration of uplift in the Nanga Parbat in western Pakistan, from about 0.2 mm/yr to 0.9 mm/yr,

during the last 5 Ma, and Copeland *et al.*, (1987) record peak rates of uplift in the Gangdese belt greater than 4 mm/yr during the period 21 to 17 Ma ago.

Since the collision of India with Asia during the Eocene, India has continued to move northward some 1800 - 2500km. (McKenzie and Sclater, 1971; Molnar and Tapponnier, 1975). Although some of this convergence has undoubtedly been taken up by deformation of the northern margin of the Indian plate, most estimates of the deformation leave over 1500 km to be accounted for. So, whereas there does appear to be agreement about the fact of crustal thickening, the mechanisms by which it occurred, and timing of the resultant uplift, are still highly contentious issues.

Broadly, there are three hypotheses which have been suggested to account for crustal thickening and uplift of the Tibetan Plateau. These were outlined in Chapter 4. They will be examined here in more detail in an attempt to constrain, or eliminate models, using data obtained from fission track analysis. While fission track data can only constrain the timing of events, and not the mechanism itself, in some cases the time factor will be a limiting constraint on the mechanism. In this way, it is hoped that a preferred model will emerge.

6.3.1 The Underthrusting Model.

From the interpretation of Pn and Sn waves that traversed the mantle beneath Tibet, Barazangi and Ni (1982), and Ni and Barazangi (1983) suggested that the measured velocities were very similar to those frequently reported from beneath Precambrian shields and stable continental regions. From this they deduced that shield-like material existed in the uppermost mantle beneath Tibet. They explained their observations as being consistent with a model in which the Indian continental lithosphere underthrust the Tibetan Plateau at a very shallow angle. They considered that this would result in the double thickness of crust, and the remarkably uniform elevation of the plateau.

Ni and Barazangi were not specific as to how far they considered underthrusting extended at the present time. The inference was that it lay beneath the whole of Tibet, although diagrams show it extending only to the Qiangtang Terrane where the Sn waves

did not propagate efficiently. This model did not favour the growing opinion that considered thickening occurred as a result of shortening across the plateau. Instead it supported previous models of underthrusting proposed by Powell and Conaghan (1973 and 1975).

Powell (1986) suggested a variation on the underthrusting theme whereby wholesale subduction of continental lithosphere resulted in it becoming detached from the sinking slab, and rising bouyantly beneath the overriding plate. Contact between the underplating Indian continent and the Tibetan crust, was considered to lead first to widespread extention, and then to rapid uplift. They considered that 3-4 km of uplift in the last 2 Ma was a reasonable estimate. This phase of rapid uplift was then used to explain the palaeo faunal and floral assemblages found on the plateau, which suggested elevations of only 1 km as recently as 2 Ma ago (Li *et al* , 1981; Xu 1981).

An alternative to this model was then put forward in 1987 by Zhao and Morgan, and Zhao and Yuen, whereby the stronger Indian crust was injected into the weaker lower crust of Tibet. They calculated that if the critical viscosity of the Tibetan lower crust is 6×10^{18} Pa s, then the advancing Indian crust beneath Tibet, would produce negligible variation in stresses at the bottom of the stronger, brittle Tibetan upper crust. This would allow for uniform and virtually undisturbed uplift of the Tibetan Plateau.

6.3.2 The Horizontal Plane Strain Model

Work by Molnar and Tapponnier (1975, 1976, and 1977) showed that the pattern of faulting in Asia bore a strong resemblance to the slip line field calculated and observed for plane indentation of a plastic medium (Tibet), by a rigid dye (India). The plastic material was considered to be homogeneous, and a state of plane strain was assumed, whereby yielding occurred when the maximum shear stress, $\tau = (\sigma_1, - \sigma_3)/2$, reached a limiting value τ_y, the yield stress. Where σ_1, and σ_3 are, respectively, the maximum and minimum compressive stresses.

Laboratory studies by Tapponnier *et al.*, (1982), then looked at the indentation of a

rigid block into plasticine that was confined at the top and bottom (to maintain plane horizontal strain) and on two lateral sides, but remained unconfined on one edge. This was in an attempt to make simple geometric and kinematic comparisons with the collision between India and Asia, where the convergence rate was about 5 cm/yr and the collision front about 2000 km long.

Their results showed a remarkably close simulation of the Tertiary and active tectonics seen in Tibet and China to-day. In particular, the simulated Altyn Tagh and Red River faults (Fig. 6.10) were dominant features along which the convergence was being taken up in the form of the extrusion of blocks of plasticine (Tibet and China), towards the east, or unconfined edge. They identified two major phases of continental extrusion. In the

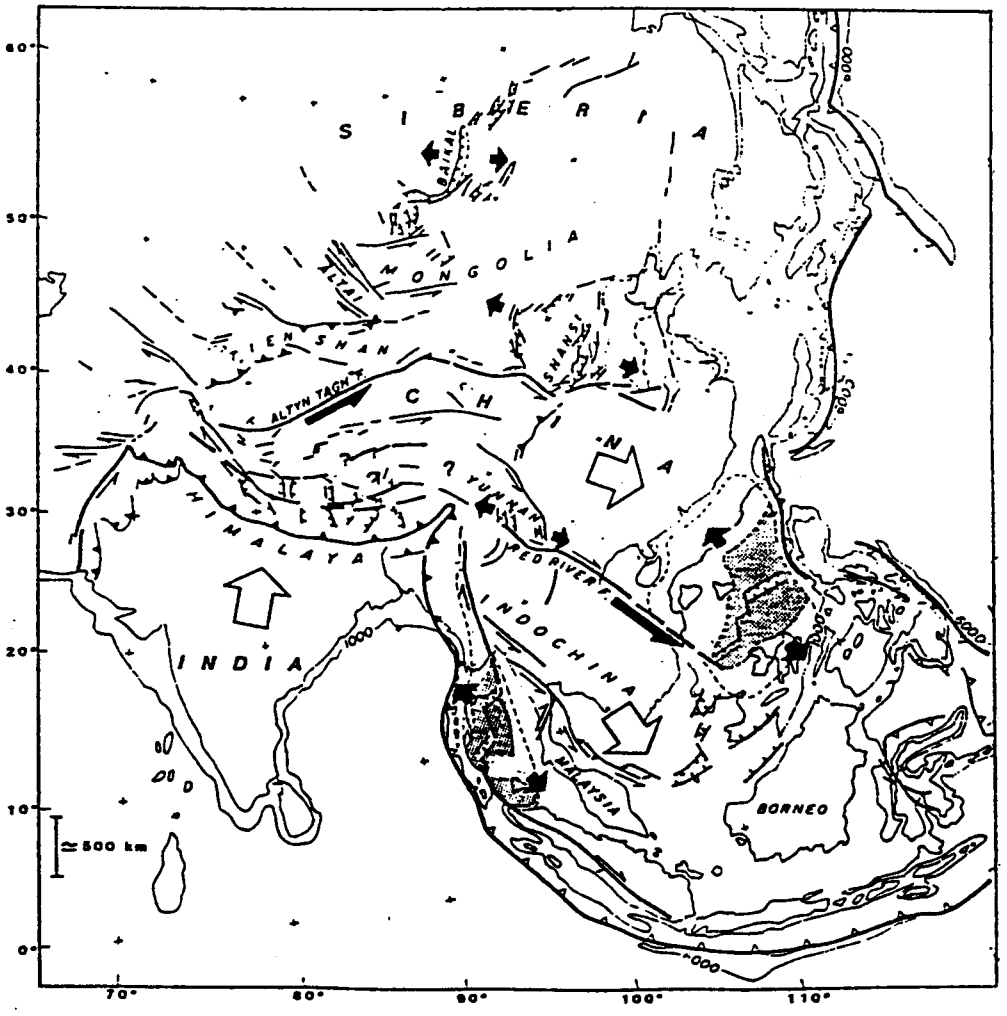

Fig. 6.10 Schematic map of extrusion tectonics and large faults in eastern Asia. Redrawn after Tapponnier *et al.* (1982).

first 20 to 30 Ma after collision, the northward drive of India would have caused extrusion to the southeast on the Red River Fault, and clockwise rotation (~25°) of Indo-China. Then as India moved towards the Red River Fault, the fault became less efficient and left-lateral motion ceased. Extrusion was taken up on the Altyn Tagh Fault, which is one of the world's greatest strike-slip faults, passing between the Altyn Tagh and Kunlun Shan ranges. (Figs. 6.3 and 6.10) It is at least 2500 km long, and the offset may reach between 500 and 700km.

While explaining the mechanism by which the convergence of India upon Tibet is accommodated, the Molnar and Tapponnier models do not provide a specific explanation for why the crust is so thick, or identify when it became uplifted. Molnar *et al* .(1987) simply state that 'the crustal thickening is surely a consequence of the collision and subsequent penetration of India into the rest of Asia in Cenozoic time', and that isostatic compensation of such thick crust causes the plateau to float high above sea level. Molnar (1988) shows how continued convergence manifests itself by a growth in area of the plateau, as thrust faulting leads to crustal thickening at the margins. In fact, the recognition of lateral heterogeneity in the mantle beneath Tibet, suggests that simple Airy-type isostatic compensation does not prevail over all of Tibet.

If variations in surface-wave dispersion imply that the shear wave velocity of the underlying uppermost mantle beneath the Qiangtang, is much lower than elsewhere in the plateau, then the inference from this is that the mantle beneath central Tibet is unusually hot, (which accords with the presence of recent volcanism in the region), and that the crust is relatively thin. If this is the case, then the uniform elevation seen on the plateau, cannot solely result from isostatic compensation. Molnar considers this region of Tibet is the locus of convective up-welling of hot material in the upper mantle, which descends beneath southern, and possibly, also northern Tibet. His conclusion is, that if the crustal thickening has been caused by crustal shortening, then it has not been homogeneously distributed across the plateau.

6.3.3 The Thin-Sheet Approximation Model

In 1985, England and Houseman proposed a model whereby a thin Tibetan crust was thickened and elevated to the level we see to-day, entirely by indentation of the Indian plate. Most investigations into the mechanics of continental deformation have treated the lithosphere as a continuous medium. (Bird and Piper,1980; England and McKenzie, 1982; England and Houseman, 1985). While it is realised that this assumption will not satisfy all the problems, the simple physical arguments that follow from considering the lithosphere as a continuous medium on a large scale, have allowed valuable insights into the mechanics driving the deformation of continents (England and Houseman, 1988).

Paleomagnetic data from Cretaceous and Eocene formations in southern Tibet (north of the Zangbo suture), show that the southern margin of Tibet has moved north by about 2000 km since the collision with India. These data strongly support a model whereby most of the convergence of India with Asia was accommodated by shortening within Asia.

In the England and Houseman model, the continental lithosphere is considered to be an homogeneous viscous layer, the deformation of which can be calculated by considering its rheology and the vertical average of the stresses and strains acting on it. For a given choice of boundary conditions, the calculated deformation depends on 1) the dimensionless Argand number, Ar, which is a measure of the lithospheric strength, and 2) the stress-strain exponent, n, of the rheology. They assumed that before collision, Tibet was at an average elevation between 0 and 500 m, and had an average crustal thickness of 35 km. A simple indenting boundary condition (India), was then applied to these initially laterally homogeneous sheets (Tibet) and produced results that are generally in agreement with what is observed to-day.

In each case considered, the convergence resulted in a plateau-like region forming in front of the indenter. Maximum crustal thicknesses of 74 km were obtained, which is within the range of assumed crustal thickness for the plateau of 65-80 km, when n = 10 and Ar = 1. The model also predicted that the plateau will approximate the same

horizontal dimensions as the indenter. In the calculations, the build-up of the crustal thickness in front of the indenting boundary caused the region of most intense deformation to migrate away from the boundary. After 40 Ma of convergence, this realm of intense deformation is seen in an arcuate region that encircles the plateau. This is in accordance with observed strain rates that are 4 times higher in the regions bordering the plateau (Tien Shan and Ningxia Gansu regions), than within the plateau itself, and suggests that uplift would have migrated northwards and outwards as the deformation front proceeded.

One of the most striking features in the Tibetan Plateau is the extension that occurs on roughly north-south normal faults, (Molnar and Tapponnier, 1978; Tapponnier *et al* , 1981). The thin sheet model however, does not predict this extension, but England and Houseman (1988) suggest that the discrepancy between observation and calculation can be resolved if a change occurs in the balance between the horizontal deviatoric stresses applied on the boundaries of Asia, and the bouyancy stresses in the interior of the continent. This would result in an increase in the potential energy of the plateau causing uplift and extension.

Houseman *et al.* (1981) had previously investigated the stability of the continental lithosphere after thickening, and found that it resulted in gravitational instability of the fluid layer beneath the uppermost mantle, which then rapidly descended into the convecting mantle. England and Houseman (1988) consider that the loss of this layer would have the effect of raising the surface height of the plateau between 1 and 3 km, and that the change in potential energy would be sufficient to effect a change from horizontal shortening to horizontal extension. Armijo *et al.*, (1986) proposed that this extension began fairly recently, and certainly within the past 5 Ma, which concurs with the model of recent rapid extension and uplift proposed by England and Houseman.

6.4 DISCUSSION

In an attempt to identify a preferred model for uplifting the Tibetan Plateau, it is important not to loose sight of the original objective for undertaking the fission track work. This was simply to investigate whether any effects of the Himalayan collision could be identified in the Kunlun Terrane. Undoubtedly, the fission track work has proved extremely worthwhile in this respect, proving as it does, that there has been uplift in the Kunlun Terrane as a result of the Himalayan collision, although the Terrane lies some 1200 km north of the Himalayan collision zone.

In fact, the effects of the Himalayan collision can be seen as far north as the Baikal rift system in Siberia (Fig. 6.10), so even if the missing 2000 km of crust fully underplated Tibet, as proposed by supporters of the underthrusting model, it still would not reach the Baikal rift to cause deformation in that region. Therefore, in the search for a model for uplifting the Tibetan Plateau, this one seems unlikely. Furthermore, palaeomagnetic data from north of the Zangbo suture indicates that, at the time of collision, that region lay 2000 km further south than it does to-day. The inference therefore is, that the missing crust is not Indian, but Tibetan, and that it has been shortened by approximately 50%, while India has stayed much the same size as it was at the time of collision. These two arguments alone are sufficient to rule out any models of extensive underthrusting beneath Tibet. Measurements based on balanced sections for the cover stripped from the basement in the outer Himayalan zones of Parkistan, (Coward and Butler, 1985), do indicate a northward subduction of the Indian crust by about 470 km, but it is considered likely that most of this has been taken up by crustal thickening in the Himalayas.

We have seen that the thin viscous sheet deforms homeogeneously, while plasticine undergoes strain softening that results in narrow shear zones analogous to faults. Clearly these hypothetical models represent the two extremes of how continental deformation is actually being accommodated in the Tibetan Plateau, and it would be presumptuous to suggest that either model could be entirely eliminated by the rather limited fission track data presented here. Nevertheless, fission track data do suggest that the maximum age for

the onset of uplift in the north of the plateau is about 20 Ma. Because this age is a mix between an old slow-cooling event, and a younger period of uplift, it could represent actual uplift at a later date of say 13 Ma, which is the fission track age obtained from the Xidatan granite. If this is the case, comparison with uplift rates in the Gangdese batholith, in the south of Tibet, which are known to have accelerated between 21 and 17 Ma, indicates that a model of northward migration of the uplift front, as proposed by England and Houseman, could explain the data. But the evidence is not very well constrained, and further arguments which support crustal thickening in the Kunlun Terrane at this time, must be examined. These are found in recent data from Molnar *et al.* (1987), who made a reconnaisance expedition across the northern margin of the Tibetan Plateau, to the Ulugh Muztagh mountain in the Kunlun Shan, several hundred kilometers to the west of the Geotraverse line (Fig. 6.3).

Ulugh Muztagh is the highest mountain in the Kulun Shan. It is partly underlain by a tourmaline-bearing, two-mica granite that gives a poorly constrained Rb-Sr bioite-whole rock age of 10.5 Ma (Molnar *et al.*, 1987). A welded rhyolitic tuff rests on a conglomerate that consists of debris from the granite. The Ar-Ar age of the tuff is about 4 Ma. By analogy with the High Himalayan leucogranites, Molnar *et al.* consider that the granite is a crustally derived melt formed in response to crustal thickening in the Kunlun Terrane, at about 10 Ma. The younger cap of volcanic rock sitting on the granite boulders, suggests that uplift and erosion had occurred by 4 Ma. This is in keeping with the fission track data that suggests 8 Ma would be a minimum age for uplift in the Geotraverse part of the Kunlun, although this was based on average erosion rates of 0.5 mm/yr. Even allowing for very shallow depths of intrusion for these crustal melts, 5 km has to be a minimum. This indicates erosion rates, during the 5-6 Ma between intrusion and unroofing of the granite, of twice those used to calculate the minimum age of uplift in the Geotraverse region. Faster rates would result in an even younger minimum age (less than 8 Ma.) for uplift in the Geotraverse region It must be stressed however, that Copeland *et al.* showed that neighbouring blocks did not register uplift of the same intensity, or during the same period. Therefore care must be taken when comparing

regions so widely separated as the Ulugh Muztagh and the Geotraverse areas. Nevertheless, abandoned river terraces and incised rivers are the final evidence for very recent uplift in the Kunlun Terrane (Plate 6.2.)

Plate. 6.2 Abandoned river terraces in the Kunlun Terrane indicate that uplift is still an active force.

On balance then, the fission track data could support a model of northward propagating uplift, generated by indentation of strong Indian continental lithosphere into a hot and weak Tibetan lithosphere. However, while there clearly has been periods of rapid uplift, both in the south and the north of Tibet, these appear to be related to crustal thickening rather than to a period of uniform bouyant uprising of the whole plateau due to delamination of the lower regions of the continental lithosphere. While it should not be expected that fission track data would be able to distinguish between sudden uplift caused by a bouyant rise of the under-plated Indian slab coming into contact with the Tibetan crust (Conaghan and Powell, 1987), or sudden uplift caused by delamination of the unstable roots of the continental lithosphere (England and Houseman, 1988). Any uplift of these dimensions (say 3km in the last 5Ma) by either mechanism, would result in a predominance of long fission tracks that had clearly entered the zone of full track stability. These would therefore record true uplift ages, unless erosion had been sufficiently fast so

as to penetrate the new zone of partial annealing. If this catastrophic uplift has occurred within the last 5 - 2 Ma, it has not been registered in the fission tracks at either the northern or the southern edges of the plateau.

6.5 CONCLUDING REMARKS

This has been an exciting project to work on, drawing on many aspects of geology in an attempt to fit together a huge jig-saw puzzle, for which the picture was lost in the move, and half the pieces are missing! The very diversity of the project has highlighted innumerable gaps in the data, which should be able to point us in the direction of new research.

Paramount amongst these should be an examination of the centre of the plateau for evidence of rapid uplift around 15 Ma. This would be the approximate time of uplift predicted by the England and Houseman model, if uplift has propagated northwards from approximately 20 Ma in the south to about 10 Ma in the north. Confirmation of this would constrain the model more precisely. At the moment, the Molnar and Tapponnier model could also fit the fission track data if crustal thickening occurred at the margins of the confined region, as suggested by Molnar (1988). However, this model does not explain the crustal thickening seen north of the Altyn Tagh Fault. The Tarim Basin, underlain by strong Precambrian lithosphere, presumably represents one of the confining edges to the plateau where thickening occurs with increasing convergence. If extrusion to the east by strike-slip movement occurs south of the fault, it is difficult to see how thickening is explained north of both the Altyn Tagh Fault and the Tarim Basin. A full Ar-Ar and fission track analysis of samples collected specifically for an uplift project, from as large a vertical height distribution as possible, would undoubtedly help constrain the preliminary fission track data presented here.

Fianlly, it cannot be more strongly emphasised how small a region of the Kunlun Terrane has been examined and how in turn the Kunlun Terrane is but a small part of the Tibetan Plateau. Eleven plutons in the massive 2000 km granitoid belt can reveal only the smallest glimpse of what has happened in the Kunlun since the Devonian. Further data

from all geological disciplines, from sites both east and west of the Geotraverse line, would help constrain the timing and positioning of suture closure and, importantly, enable us to be more specific about the rifting event during the Permian.

Clearly there is a huge amount of work still to be done if we are ever to fully understand the formation of the Tibetan Plateau and the mechanisms by which it has been thickened and uplifted.

REFERENCES

Achache J., Courtillot V. and Zhou Y.X. (1984) Palaeogeographic and tectonic evolution of southern Tibet since Middle Cretaceous time: new palaeomagnetic data and synthesis. *J. Geophys. Res.* **89** 10311-10339

Allègre C.J. and Ben Othman D. (1980) Nd-Sr isotopic relationship in granitoid rocks and continental crust development: a chemical approach to orogensis. *Nature.* **286** 335-340

Allègre C.J. and 34 others (1984) Structure and evolution of the Himalaya-Tibet orogenic belt. *Nature.* **307** 17-22

Allègre C.J., Treuil M., Minster J.F., Minster B. and Albarède F. (1977) Systematic use of trace element in igneous process. Part 1: Fractional crystallisation processes in volcanic suites. *Contrib. Mineral. and Petrol.* **60** 57-75

Argand E. (1924) La techtonique de l'Asie. *Proc. 13th Int. Geol. Congr.* **1** 171-372

Armijo R., Tapponnier P., Mercier J.L. and Han T. (1986) Quaternary extension in Southern Tibet: field observations and tectonic implications. *J. Geophys. Res.* **91** 13803-13872

Armstrong R.L. and Jäger E. (1966) A comparison of K-Ar and Rb-Sr ages on Alpine biotites. *Earth Planet. Sci. Lett.* **1** 13-19

Arth J.G. and Hanson G.M. (1975) Geochemistry and origin of the early Pre-cambrian crust of northeastern Minnesota. *Geochem. Cosmochim. Acta.* **39** 325-362

Arzi A.A. (1978) Critical phenomena in the rheology of partially melted rocks. *Tectonophysics.* **44** 173-184

Barazangi M. and Ni J. (1982) Velocities and propagation characteristics of Pn and Sn beneath the Himalayan arc and Tibetan plates: Possible evidence for the underthrusting of Indian continental lithosphere beneath Tibet. *Geology.* **April** 179-185

Bernard-Griffiths J., Peucat J.J., Sheppard S.M., and Vidal P. (1985) Petrogenesis of Hercynian leucogranites from the Southern Armorican massif: contribution of REE and isotopic (Sr, Nd, Pb and O) geochemical data to the study of source rock characteristics and ages. *Earth Planet. Sci. Lett.* **74** 235-251

Bird P. and Piper K. (1980) Plane stress finite element models of tectonic flow in southern California. *Phys. Earth. Planet. Inter.* **21** 158-175

Bird P. (1978) Initiation of intracontinental subduction in the Himalaya, *J. Geophys. Res.* **83** 4975-4987

Brace W.F. (1980) Permeability of crystalline and argillaceous rocks. *Int. J. Rock. Mech. Min. Sci. and Geomech. Abstr.* **17** 241-251

Brewer M.S. (1969) Excess radiogenic argon in metamorphic micas from the Eastern Alps, Austria. *Earth Planet. Sci. Lett.* **6** 321

Brewer M.S. (1981) Thermal effects of thrust faulting *Earth Planet. Sci. Lett.* **56** 233-244

Brodie K.H., Rex D. and Rutter E.H. (1988) On the age of deep crustal extentional faulting in the Ivrea zone, northern Italy, *In press.*

Brown G.C. (1982) Calc-alkaline intrusive rocks: their diversity, evolution, and relation to volcanic arcs. In: *Andesites. R.S. Thorpe (Ed) John Wiley and Sons*

Burke K. and Sengor C. (1986) Tectonic escape in the evolution of the continental crust. *In: Reflection Seismology: The Continental Crust, Am Geophys. Union, Goedyn Ser.* **14** 41-53

Burke K.C.A., Dewey J.F., and Kidd W.S.F. (1974) The Tibetan Plateau, its significance for tectonics and petrology. *Geol Soc. Am.Abstr. Programs.* **6** 1-18

Cassidy J. (1979) Gamma-ray spectrometric surveys of Caledonian granites: method and interpretation. *Unpub. Ph.D. thesis, Liverpool Univ.*

Cawthorn R.G. and Brown P.A. (1976) A model for the formation and crystallisation of corundum-normative calc-alkaline magmas through amphibole fractionation. *Jour. of Geol.* **84** 467-476

Chang C. and 26 others. (1986) Preliminary conclusions of the Royal Society and Academia Sinica 1985 geotraverse of Tibet. *Nature.* **323** 501-507

Chang C. and Pan Y. (1981) A brief discusstion on the tectonic evolution of the Qinghai-Xizang (Tibet) Plateau. *Geological and ecological studies of Qinghai-Xiang Plateau.* **1** 1-18

Chang C. and Zheng X. (1973) Some tectonic features of the Mt. Jomo area, southern Tibet, China.*Sci. Sinica.* **16** 257-265

Chappell B.W. and Stephens W.E. (1988) Origin of infracrustal (I-type) granite magmas. *Trans. R. Soc. Edinburgh: Earth Sciences.* **79** 71-86

Chappell B.W. and White A.J.R. (1974) Two contrasting granite types. *Pacific Geology.* **8** 173-174

Chappell B.W. (1978) Granitoids from the Moonbi district, New England Batholith, eastern Australia. *J. Geol. Soc. Aust.* **25** 267-283

Chappell B.W., White A.J.R. and Wyborn D. (1987) The importance of residual source material (restite) in granite petrogenesis. *J. Petrology.* **28** 1111-1138

Chopin C. and Maluski H. (1980) 40Ar-39Ar dating of high pressure metamorpic micas from the Gran Paradiso Area (Western Alps): evidence against the blocking temperature concept *Contrib. Mineral. and Petrol.* **74** 109-122

Chopin C. and Maluski H. (1982) Unconvincing evidence against the blocking temperature concept? A reply *Contrib. Mineral. and Petrol.* **80** 391-394

Clemens J.D. and Wall V.J. (1981) Origin and crystallization of some peraluminous (S-type) granitic magmas. *Can. Mineral.* **19** 111-131

Condie K.C. and Hunter D.C. (1978) Geochemistry of Proterozoic granitic plutons from New Mexico, U.S.A., *Chemical Geology.* **21** 131-149

Copeland P., Harrison T.M., Kidd W.S.F., Xu R. and Zhang Y. (1987) Rapid early Miocene acceleration of uplift in the Gangdese Belt Xizang (southern Tibet), and its bearing on accommodation mechanisms of the India-Asia collision, *Earth Planet. Sci. Lett.* **86** 240-252

Coward M.P. and Butler R.W.H. (1985) Thrust tectonics and the deep structure of the Pakistan Himalayas. *Geology.* **13** 417-420

Coward M.P., Kidd W.S.F., Yun P., Shackleton R.M. and Zhang H. (1988) The structure of the 1985 Tibet Geotraverse, Lhasa to Golmud. *Philos. Trans. R. Soc. Lond.* **A 327**

Crowley K.D. and Cameron M. (1988) Effects of composition on annealing of fission tracks in apatite: 1. Systematics and preliminary interpretations. *Preprint of paper presented at 6th International Fission Track Dating Workshop, 5th-9th Sept., 1988.*

Dallmeyer R.D. (1979) 40Ar/39Ar dating: principles, techniques and applications in orogenic terranes, *Lectures in Isosopte Geology, E. Jäger and J.C. Hunziker eds, Springer Verlag, Berlin.* 77-104

Debon F., Le Fort P., Sheppard S.M.F., Sonet J. (1986) The Four Plutonic Belts of the Transhimalaya-Himalaya: a Chemical, Mineralogical, Isotopic and Chronological Synthesis along a Tibet-Nepal section. *J. Petrology.* **27** 219-250

Dempster T.J. (1986) Isotope systematics in minerals: biotite rejuvenation and exchange during Alpine metamorphism, *Earth Planet. Sci. Lett.* **78** 355-367

Deng W. (1978) A preliminary study on the petrology and petrochemistry of the Quaternary volcanic rocks of Northern Tibet Autonomous region. *Acta. Geol. Sin. Eng. Ed.* **52** 148-152

Deniel C., Vidal P., Fernandez A., Le Fort P and Peucat P.P. (1987) Isotopic study of the Manaslu granite (Himalaya, Nepal): inferences on the age and source of Himalayan leucogranites. *Contrib. Mineral. and Petrol.* **96** 78 - 92

DePaolo D.J. and Wasserburg G.J. (1976) Inferences about magma sources and mantle structure from variations of 143/144 Nd. *Geophys. Res. Lett.* **3** 743-746

DePaolo D.J. (1980) Sources of continental crust: Neodymium isotope evidence from the Sierra Nevada and Peninsular Ranges. *Science.* **209** 684-687

DePaolo D.J. (1981) Trace element and isotopic effects of combined wallrock assimilation and fractional crystallisation. *Earth Planet. Sci. Lett.* **53** 189-202

Desmons J., Hunziker J.C and Delaloye M (1982) Unconvincing evidence against the blocking temperature concept. Comments on: "40Ar-39Ar dating of high

pressure metamorpic micas from the Gran Paradiso Area (Western Alps): evidence against the blocking temperature concept" by C.Chopin and H. Maluski., *Contrib. Mineral. and Petrol.* **80** 386-390

Deutsch A. and Steiger R.H. (1985) Hornblende K-Ar ages and the climax of Tertiary metamorphism in the Lepontine Alps (south-central Switzerland): and old problem reassessed. *Earth Planet. Sci. Lett.* **72** 175-189

Dewey J.F. and Burke K.C.A. (1973) Tibetan, Variscan and Precambrian basement reactivation: products of continental collision. *J. Geol.* **81** 683-692

Dewey J.F., Shackleton R.M., Chengfa C. and Yin S. (1988) The tectonic evolution of the Tibetan Plateau *Philos. Trans. R. Soc. Lond.*. A **327** 379-413

Dietrich V. and Gansser A. (1981) The leucogranites of the Bhutan Himalayas. (Crustal anatexis versus mantle melting). *Schweiz. Mineral. Petrogr. Mitt.* **61** 177-202

Dodson M.H. (1973) Closure temperature in cooling geochronological and petrological systems, *Contrib. Mineral. and Petrol.* **40** 259-274

Dodson M.H. (1979) Theory of cooling ages. In: *Lectures in Isosopte Geology, E. Jäger and J.C. Hunziker eds, Springer Verlag, Berlin.* 194-206

Dodson M.H. (1981) Thermochronometry *Nature.* **293** 606-607

England P.C. and Houseman G.A. (1986) Finite strain calulations of continental deformation: II. Comparison with the Indian-Asia collision zone. *Jour. Geophys. Res.* **91** 3664-3674

England P.C. and Houseman G.A. (1988) The mechanics of the Tibetan Plateau. *Philos. Trans. R. Soc. Lond.* **A 326** 301-320

England P.C. and McKenzie D.P. (1982) A thin viscous sheet model for continental deformation. *Geophys. J. R. astr. Soc.* **70** 295-321

England P.C. and Thompson A. (1986) Some thermal and tectonic models for crustal melting in continental collision zones. *Collision Tectonics, M.P. Coward and A.C. Reis, eds., Geol. Soc. London, Spec. Publ.* **19** 83-94

England P.C. and Thompson A.B. (1984) Pressure - temperature - time paths of regional metamorphism I. Heat transfer during the evolution of regions of thickened continental crust, *J. Petrology.* **25** 894-928

Ferry J.M. (1979) Reaction mechanisms, physical conditions, and mass transfer during hydrothermal alteration of mica and feldspar in granitic rocks from south-central Maine, USA. *Contrib. Mineral. and Petrol.* **68** 125-139

Ferry J.M. (1979) Reaction mechanisms, physical conditions and mass transfer during hydrothermal alteration of mica and feldspar in granitic rocks from south-central Maine, U.S.A. *Contrib. Mineral. and Petrol.* **68** 125-139

Fitzgerald P.G. and Gleadow A.J. (1988) New approaches in fission track geochronology as a tectonic tool: examples from the Transantarctic mountains.

Preprint of paper presented at 6th International Fission Track Dating Workshop, 5th-9th Sept., 1988.

Fitzgerald P.G., Sandiford M., Barrett P.J., Gleadow A.J. (1986/87) Asymmetric extension associated with uplift and subsidence in the Transantarctic Mountains and Ross Embayment. *Earth Planet. Sci. Lett.* **81** 67-78

Fleischer R.L. and Hart H.R. (1972) Fission track dating: techniques and problems. In: *Calibration of Hominoid Evolution. (W.W. Bishop, J.A. Miller and S. Cole eds.) Scottish Academic Press, Edinburgh.* 135-170

Fleischer R.L. and Price P.B. (1964) Decay constant for the spontaneous fission of ^{238}U, *Phys. Rev.* **133** B63 - B64

Fleischer R.L. et al (1965) The Ion Explosion Spike Mechanism. *J. App. Phys.* **36** 3645

Foland K.A. (1979) Limited mobility of argon in a metamorphic terrain. *Geochem. Cosmochim. Acta.* **43** 793

Fourcadre S. and Allègre C.J. (1981) Trace element behaviour in granite genesis - a study of a calc-alkaline association from the Queriquot complex (Pyrenees, France). *Contrib. Mineral. and Petrol.* **76** 177-195

France-Lanord C., Sheppard M.F. and Le Fort P. (1988) Hydrogen and oxygen isotope variations in the High Himalaya peraluminous Manaslu leucogranite: Evidence for heterogeneous sedimentary source. *Geochem. Cosmochim. Acta.* **52** 513-526

Frost T.P. and Mahood G.A. (1987) Field, chemical, and physical constraints on mafic-felsic magma interaction in the Lamarck Granodiorite, Sierra Nevada, California. *Geol. Soc. Am. Bull.* **99** 272-291

Galbraith R.F. (1981) On statistical models for fission track counts *Mathematical Geology.* **13** 471-488

Gariepy C., Allègre and Xu R.H. (1985) The Pb-isotope geochemistry of granitoids from the Himalaya-Tibet collision zone: implications for crustal evolution. *Earth Planet. Sci. Lett.* **74** 220-234

Girardeau J., Marcoux J., Allègre C.J., Bassoullet J.P., Tang Y., Xiao X., Zao Y. and Wang X. (1984) Tectonic environment and geodynamic significance of the Neo-Cimmerian Donqiao ophiolite, Bangong-Nujiang suture zone, Tibet. *Nature.* **307** 27-31

Gleadow A.J.W. (1978) Anisotropic and variable etching characteristics in natural sphenes. *Nuclear Track Detection.* **2** 107-117

Gleadow A.J.W. and Duddy I.R. (1981) A natural long term annealing experiment for apatite. *Nucl. Tracks.* **5** 169-174

Gleadow A.J.W., Duddy I.R., Lovering J.F. (1983) Fission track analysis: a new tool for the evaluation of thermal histories and hydrocarbon potential. *APEA Journal.* **23** 93-102

Gleadow A.J.W., Duddy I.R., Green P.F., Hegarty K.A. (1986) Fission track lengths in the apatite annealing zone and interpretation of mixed ages. *Earth Planet. Sci. Lett.* **78** 245-254

Gleadow A.J.W., Duddy I.R., Green P.F., Lovering J.F. (1986) Confined fission track lengths in apatite: a diagnostic tool for thermal history analysis. *Contrib. Mineral. and Petrol.* **94** 405-415

Graham C.M. and England P.C. (1976) Thermal regimes and regional metamorphism in the vicinity of overthrust faults: an example of shear heating and inverted metamorphic zonation from southern California. *Earth Planet. Sci. Lett.*. **31** 142-152

Green P.F. (1985) Comparison of zeta calibration baselines for fission-track dating of apatite, zircon and sphene. *Chemical Geol (Isotope Geoscience Section).* **58** 1-22

Green P.F. (1988) The relationship between track shortening and fission track age reduction in apatite: Combined influences of inherent instability, annealing anisotropy, length bias and system calibration. *Earth Planet. Sci. Lett.*. **In press**

Green P.F., Duddy I.R. and Laslett G.M., (1988) Can fission track annealing in apatite be described by first-order kinetics? *Earth Planet. Sci. Lett.* **87** 216-228

Green P.F., Duddy I.R., Gleadow A.J.W. and Tingate P.R. (1985) Fission track annealing in apatite: track length measurements and the form of the Arrhenius plot.*Nucl. Tracks.* **10** 323-328

Green P.F., Duddy I.R., Gleadow A.J.W., Tingate P.R. and Laslett G.M. (1986) Thermal annealing of fission tracks in apatite. 1. A qualitative description. *Chemical Geol (Isotope Geoscience Section).* **59** 237-253

Gromet P. and Silver L.T. (1987) REE variations across the Peninsular Ranges Batholith: implications for batholithic petrogenesis and crustal growth in magmatic arcs. *J. Petrology.* **28** 75-125

Haack U. (1977) The closing temperature for fission track retention in minerals. *American Journal of Science.* **277** 439-464

Hammerschmidt K., Wagner G.A. and Wagner M. (1984) Radiometric dating on research drill core Urach III - A contribution to its geothermal history. *J. Geophys. Res.* **54** 97-105

Hanson G.N. (1978) The application of tracel elements to the petrogenesis of igneous composition. *Earth Planet. Sci. Lett.* **38** 26-43

Harris N.B.W. (1981) The role of fluorine and chlorine in the petrogenesis of a peralkaline complex from Saudi Arabia. *Chem. Geol.* **31** 303-310

Harris N.B.W., Xu R., Lewis C.L., Hawkesworth C.J. and Zhang Y. (1988a) Isotope geochemistry of the 1985 Tibet Geotraverse, Lhasa to Golmud *Philos. Trans. R. Soc. London.* **A 327** 263-285

Harris N.B.W., Holland T.J.B. and Tindle A.G. (1988b) Metamorphic rocks of the 1985 Tibet Geotraverse, Lhasa to Golmud *Philos. Trans. R. Soc. Lond.* A **327** 203-213

Harris N.B.W., Xu R., Lewis C.L.E. and Jin C (1988c) Plutonic rocks of the 1985 Tibet Geotraverse, Lhasa to Golmud *Philos. Trans. R. Soc. Lond.* A **327** 145-168

Harrison T.M. (1981) Diffusion of 40Ar in Hornblende *Contrib. Mineral. and Petrol.* **78** 324-331

Harrison T.M. Aleinikoff J.N. and Compston W. (1987) Observations and controls on the occurrence of inherited zircon in Concord-type granitoids, New Hampshire. *Geochem. Cosmochim. Acta.* **51** 2549-2558

Harrison T.M., Armstrong R.L., Naeser C.W. and Harakal J.E. (1979) Geochronology and thermal history of the Coast Plutonic Complex, near Prince Rupert, British Columbia, *Can. J. Earth Sci.* **16** 400-410

Hawking S.W. (1988) A brief history of time. From the big bang to black holes. *Bantam Press, London.*

Hayatsu A. and Carmichael C.M. (1970) K-Ar isochron method and initial argon ratios. *Earth Planet. Sci. Lett.* **8** 71

Hebeda E.H., Boelrijk N.A.I.M., Priem H.N.A., Verdurmen E.A. Th, Verschure R.H. and Simon O.J. (1980) Excess radiogenic Ar and undisturbed Rb-Sr systems in basic intrusives subjected to Alpine metamorphism in south eastern Spain, *Earth Planet. Sci. Lett.* **47** 81-91

Hirn A. and 11 others. (1984a) Crustal structure and variability of the Himalayan border of Tibet. *Nature.* **307** 23-25

Hirn A. and 7 others. (1984b) Lhasa block and bordering suture - a continuation of a 500 km Moho traverse through Tibet. *Nature.* **307** 25-27

Hofmann A.W. and Giletti B.J. (1970) Diffusion of geochemically important nuclides under hydrothermal conditions. *Eclogae. Geol. Helv.* **63** 141-150

Hofmann A.W. (1979) Diffusion Experiments in Isotope Geology. *Lectures in Isosopte Geology, E. Jäger and J.C. Hunziker eds, Springer Verlag, Berlin.* 189-193

Holdaway M.J. (1972) Thermal stability of Al-Fe epidote as a function of fO_2 and Fe content. *Contrib. Mineral. and Petrol.* **37** 307-340

Holden P., Halliday A.N. and Stephens W.E. (1987) Neodymium and strontium isotope content of microdiorite enclaves points to mantle input to granitoid production. *Nature.* **330** 53-56

Holmes A. (1915) Radioactivity and the measurement of geological time. *Proc. Geol. Ass.* **26** 289-309

Honegger K., Dietrich V., Frank W., Gansser A., Thöni M. and Trommsdorff V. (1982) Magmatism and metamorphism in the Ladakh Himalayas (the Indus-Tsangpo suture zone) *Earth Planet. Sci. Lett.* **60** 253-292

Houseman G.A. and England P.C. (1986) Finite strain calculations of continental deformation. 1: Method and general results for convergent zones. *Jour. Geophys. Res.* **91** 3651-3663

Houseman G.A., McKenzie D.P. and Molnar P. (1981) Convective instability of a thickened boundary layer and its relevance for the thermal evolution of continental convergent belts. *J. Geophys. Res.* **86** 6115-6132

Hunziker J.C. (1979) Potassium argon dating, In: *Lectures in Isosopte Geology, E. Jäger and J.C. Hunziker eds, Springer Verlag, Berlin.* 52-76

Huppert H.E. and Sparks R.S.J. (1988) The generation of granitic magmas by intrusion of basalt into continental crust. *Jour. Pet.* **29** 599-624

Hurford A.J. (1986) Cooling and uplift patterns in the Lepontine Alps, South Central Switzerland and an age of vertical movement on the Insubric fault line. *Contrib. Mineral. and Petrol.* **92** 413-427

Hurford A.J. (1977) A preliminary fission track dating survey of Caledonian "newer and last granites" from the Highlands of Scotland. *Scottish Journal of Geology.* **13** 271-274

Hurford A.J., Fitch F.J., Clarke A. (1984) Resolution of the age structure of the detrital ziron populations of two Lower Cretaceous Sandstones from the Weald of England by fission track dating. *Geolgical Magazine.* **121** 269-277

Hurford A.J., Green P.F. (1982) A user's guide to fission track dating calibration. *Earth Planet. Sci. Lett.* **59** 343-354

Hurford A.J., Green P.F. (1983) The zeta age calibration of fission track dating *Isotope Geoscience.* **1** 285-317

Ijlst L. (1973) A laboratory overflow-centrifuge for heavy liquid mineral separation. *Am. Mineral.* **58** 1088-1093

Irving. E. (1977) Drift of the major continental blocks since the Devonian *Nature.* **270** 304-309

Jacobsen S.B. and Wasserburg G.H. (1979) The mean age of mantle and crustal resevoirs. *Jour. Geophys. Res.* **84** 7411-7426

Jäger E. (1979) Introduction to geochronology. In: *Lectures in Isosopte Geology, E. Jäger and J.C. Hunziker eds, Springer Verlag, Berlin.* 1-12

Jäger E. (1979) The Rb-Sr method. In: *Lectures in Isosopte Geology, E. Jäger and J.C. Hunziker eds, Springer Verlag, Berlin.* 13-26

Jowett E.C., Pearce G.W. and Rydzewski A. (1987) A mid-Triassic paleaomagnetic age of the Kupferschiefer mineralization in Poland based on a revised apparent polar wander path for Europe and Russia. *J. Geophys. Res.* **92** 581-598

Kidd W.S.F. (1975) Widespread late Neogene and Quaternary alkaline vulcanism on the Tibetan Plateau (abstract). *Eos, Wash.* **56** 453

Kidd W.S.F. and Molnar P. (1988a) Quaternary and active faulting observed on the 1985 Academia Sinica - Royal Society Geotraverse of Tibet. *Philos. Trans. R. Soc. Lond.* **A 327** 337-363

Kidd W.S.F., Pan Y., Chang C., Coward M.P., Dewey J.F., Gansser A., Molnar P., Shackleton R.M. and Sun Y. (1988b) Geological mapping of the 1985 Chinese - British (Xizang-Qinghai) Plateau Geotraverse route. *Philos. Trans. R. Soc. Lond.* **A 327** 287-306

Klimetz M.P. (1983) Speculations on the Mesozoic plate tectonic evolution of Eastern China. *Tectonics.* **2** 129-166

Kulp J.L. and Engles J. (1962) Discordances in K-Ar and Rb-Sr isotopic ages. *Radioactive Dating Symposiun Athens.* 219

Langmuir C.H., Vocke, Jr. D.R. and Hanson G.N. (1978) A general mixing equation with applications to Icelandic basalts. *Earth Planet. Sci. Lett.* **37** 380-392

Laslett G.M., Gleadow A.J.W. and Duddy I.R.,(1984) The relationship between fission track length and density in apatite *Nucl. Tracks.* **9** 29-38

Laslett G.M., Green P.F., Duddy I.R., and Gleadow A.J.W. (1987) Thermal annealing of fission tracks in apatite. 2. A quantative analysis. *Chemical Geol (Isotope Geoscience Section).* **65** 1-13

Lauer J.P. (1984) The geodynamic evolution of Turkey and Cyprus in the light of recent palaeomagnetic data. In: *The Geological Evolution of the Eastern Mediterranean. Spec. Publ. Geol. Soc. London.* **17** 483-491

Leeder M.R., Smith A.B., Yin J., Xu J. and Chen N. (1988) Sedimentology, palaeoecolgy and palaeoenvironmental evolution of the 1985 Tibet Geotraverse, Lhasa to Golmud. *Philos. Trans. R. Soc. Lond..* **A 327** 107-144

Li J., Li B., Wang F., Zhang Q., Wen S., Zhang B. (1981) The process of the uplift of the Qingai-Xizang plateau. In: *Proceedings of the Symposium on Qinghai-Xizhang (Tibet) Plateau, Geology, Geological History and Origin of the Qinghai-Xizhang Plateau.* **1** 111-118

Li T., Xiao X., Li G., Gao Y. and Zhou W. (1986) The crustal evolution and uplift mechamism of the Qinghai-Tibet plateau. *Tectonophysics.* **127** 279-289

Lin J. and Watts D.R. (1988) Palaeomagnetic results from the 1985 Tibetan Plateau. *Philos. Trans. R. Soc. Lond..* **A 327**

Lin J.L. (1984) The apparent polar wander paths for the North and South China blocks. *Unpub. Ph.D. thesis, University of California, Santa Barbara..*

Mahood G. and Hildreth W. (1983) Large partition coefficients for trace elements in high silica rhyolites. *Geochem. Cosmochim. Acta.* **47** 1-30

Mattauer M. (1986) Intracontinental subduction, crust-mantle décollement and crustal stacking wedge in the Himalayas and other collision belts. In: *Collision Tectonics, M.P. Coward and A.C. Reis, eds., Geol. Soc. London, Spec. Publ.* **19** 37-50

Mattauer M., Mathe P., Malaveille J., Tapponier P., Maluski H., Xu Z., Lu Y., and Tang Y. (1985) Tectonics of the Qinling Belt: build-up and evolution of eastern Asia. *Nature.* **317** 496-500

Mc Carthy T.S. and Groves D.I. (1979) The Blue Tier Batholith, northern Tasmania. *Contrib. Mineral. and Petrol.* **71** 193-209

Mc Carthy T.S. and Hasty R.A. (1976) Trace element distribution patterns and their relationship to the crystallisation of granitic melts. *Geochem. Cosmochim. Acta.* **4** 1351-1358

Mc Culloch M.T. and Wasserburg G.J. (1978) Sm-Nd and Rb-Sr geochronology of continental crust formation. Times of addition to continents of chemically-fractionated mantle derived materials are determined. *Science.* **200** 1003-1011

Mc Dermott F. (1986) Granite petrogenesis and crustal evolution studies in the Damara Pan-African orogenic belt, Namibia. *Unpubl. Ph.D. Thesis. Open University*

McCulloch M.T. and Chappell B.W. (1982) Nd isotopic characteristics of S- and I-type granites. *Earth Planet. Sci. Lett.* **58** 51-64

McCulloch M.T. and Wasserburg G. J. (1978) Sm-Nd and Rb-Sr geochronology of continental crust formation. Times of addition to continents of chemically-fractionated mantle derived materials are determined. *Science.* **200** 1003-1011

McFadden P.L., Ma X.H., Mc Elhinny M.W. and Zhang Z.K. (1988) Permo-Triassic magnetostratigraphy in China: northern Tarim. *Earth Planet. Sci. Lett.* **87** 152-160

McKenzie D.P. (1978) Some remarks on the development of sedimentary basins. *Earth Planet. Sci. Lett.* **40** 25-32

McKenzie D.P., and Sclater J.G. (1971) The evolution of the Indian Ocean since the late Cretaceous. *Geophys. J. R. astr. Soc.* **24** 437-528

Miller C.F. and Mittlefehldt B.W. (1982) Depletion of the light rare earth elements in felsic magmas. *Geology.* **10** 129-133

Miller C.F. (1985) Are strongly peraluminous magmas derived from pelitic sedimentary sources? *Jour. of Geol.* **93** 673-689

Miller J. (1988) Granite petrogenesis in the Cordillera Real, Bolivia and crustal evolution in the Central Andes. *Unpubl. Ph.D thesis. Opin University.*

Min Z. and Wu F.T. (1987) Nature of the upper crust beneath central Tibet. *Earth Planet. Sci. Lett.* **84** 204-210

Mitchell A.H.G. and McKerrow W.S. (1975) Analogous evolution of the Burma orogen and the Scottish Caledonides. *Geol Soc. Am. Bull.* **86** 305-315

Molnar P. and Tapponier P. (1981) A possible dependence of tectonic strength on the age of the crust in Asia. *Earth Planet. Sci. Lett.* **52** 107-114

Molnar P. and Tapponnier P. (1978) Active tectonics of Tibet *J. Geophys. Res.* **83** 5631-5375

Molnar P. and Tapponnier P. (1975) Cenozoic tectonics of Asia: effects of a continental collision. *Science.* **189** 419-426

Molnar P. (1988) A review of geophyisical constraints on the deep structure of the Tibetan Plateau, the Himalaya and the Karakoram, and their tectonic implications. *Philos. Trans. R. Soc. Lond.* **A 326** 33-88

Molnar P., Burchfield B.C., Liang K. and Zhao A., (1987a) Geomorphic evidence for active faulting in the Altyn Tagh and northern Tibet and qualitative estimates of its contribution to the convergence of India and Eurasia, *Geology.* **15** 249-253

Molnar P., Burchfield B.C., Zhao A., Liang K., Wang S. and Huang M. (1987b) Geologic evolution of Northern Tibet: results of an expedition to Ulugh Muztagh. *Science.* **235** 299-305

Moore M.E., Gleadow A.J.W., Lovering J.F. (1986) Thermal evolution of rifted continental margins: new evidence from fission tracks in basement apatites from southeastern Australia. *Earth Planet. Sci. Lett.* **78** 255-270

Naeser C.W. and Faul. H. (1969) Fission track annealing in apatite and sphene, *J. Geophys. Res.* **74** 705-710

Naeser C.W.,(1981) The fading of fission tracks in the geological environment - data from deep drill holes. *Nucl. Tracks.* **5** 248-250

Naeser C.W., Izett G.A. and Obradovich J.D. (1980) Fission track and K/Ar ages of natural glasses. *U.S.G.S.Bull.* **1489** 31pp

Ni J. and Barazangi M. (1983) High frequency seismic wave propagation beneath the Indian Shield, Himalayan arc, Tibetan Plateau, and surrounding regions: high uppermost mantle velocities and efficient Sn propagation beneath Tibet. *Geophys. J. R. astr. Soc.* **72** 665-689

Onstott T.C and Peacock M.W. (1987) Argon retentivity of hornblendes: a field experiment in a slowly cooled metamorphic terrane, *Geochem. Cosmochim. Acta.* **51** 2891-2903

Parrish R.R. (1983) Cenozoic thermal evolution and tectonics of the Coast Mountains of British Columbia. 1. Fission track dating, apparent uplift rates, and patterns of uplift. *Tectonics.* **2** 601-631

Peacock M.A. (1931) Classification of igneous rock series. *Jour. of Geol.* **39** 65-67

Pearce A.J., Harris N.B.W. and Tindle A.G., (1984) Trace element discrimination diagrams for the tectonic interpretation of igneous rocks. *J. Petrol.* **25** 956-983

Pearce J.A. and Mei H.J. (1988) Volcanic rocks of the 1985 Tibet Geotraverse: Lhasa to Golmud *Philos. Trans. R. Soc. Lond.* **A 327**

Petterson M.G. and Windley B.F. (1985) Rb-Sr dating of the Kohistan arc-batholith in the Trans-Himalaya of north Pakistan, and tectonic implications. *Earth Planet. Sci. Lett.* **74** 45-57

Powell C. McA. (1986) Continental underplating model for the rise of the Tibetan Plateau, *Earth Planet. Sci. Lett.* **81** 79-94

Powell C.M. and Conaghan P.J. (1975) Tectonic models of the Tibetan Plateau. *Geology.* **3** 727-731

Powell C.M. and Conaghan P.J. (1973) Plate tectonics and the Himalayas. *Earth Planet. Sci. Lett.* **20** 1-12

Roberts J.H., Gold R. and Armani R.J. (1968) Spontaneous fission decay constant of ^{238}U, *Phys. Rev.* **174** 1482-1484

Roddick J.C. and Farrar E. (1971) High initial argon ratios in hornblendes. *Earth Planet. Sci. Lett.* **12** 208

Roddick J.C., Cliff R.A. and Rex D.C. (1980) The evolution of excess argon in alpine biotites - a $^{40}Ar/^{39}Ar$ analysis. *Earth Planet. Sci. Lett.* **48** 185-208

Romanowicz B.A. (1982) Constraints on the structure of the Tibet Plateau from pure path phase velocities of Love and Rayleigh waves. *J. Geophys. Res.* **87** 6865-6883

Schärer U., Allègre C.J. (1983) The Palung granite (Himalaya); high resolution U-Pb systematics in zircon and monazite. *Earth Planet. Sci. Lett.* **63** 423-432

Schärer U., Hamet J., Allègre C.J. (1984) The Transhimalaya (Gangdese) plutonism in the Ladakh region: a U-Pb and Rb-Sr study. *Earth Planet. Sci. Lett..* **67** 327-339

Searle M.P., Windley B.F., Coward M.P., Cooper D.J.W., Rex A.J., Rex D., Tingdong L., Xuchang X., Jan M.Q., Thakur V.X., Kumar S. (1987) The closing of Tethys and the tectonics of the Himalaya *Geol. Soc. Am. Bull.* **98** 678-701

Sengör A.M.C. (1985) East Asian tectonic collage. *Nature.* **318** 16-17

Shand S.J. (1927) Eruptive rocks. *J. Wiley (publisher) N. York.*

Shaw D.M. (1970) Trace element variations during anatexis *Geochem. Cosmochim. Acta.* **34** 239-243

Smith. A.B. and Xu J. (1988) Palaeontology of the 1985 Tibet Geotraverse, Lhasa to Golmud. *Philos. Trans. R. Soc. Lond.* A **327** 53-106

Smith A.B. (1988) Palaeobiogeography of East Asia. *Philos. Trans. R. Soc. Lond.* A **326** 189-227

Soffel H.C. and Forster H.G. (1980) Apparent polar wander path of central Iran and its geotectonic interpretation. *J. Geomag. Geoelect.* **32** 117-135

Sollas W.J. (1900) In: Geology and time, L. Hawkes (1952). *Abbott Memorial Lecture.*

Spadaveccia A. and Hahn B. (1967) Die Rotationskammer und einige Anwendungen, *Phys. Acta.* **40** 1063-1079

Sparks R.S.J. and Marshall L. (1986) Thermal and chemical constraints on mixing between mafic and silicic magmas. *J. Vol. Geothermal Res.* **29** 99-124

St. George Littledale R. (1896) A journey across Tibet, from north to south, and west to Ladak. *The Geographical Journal.* **7** 463-483

Streckeisen A. (1975) To each plutonic rock its proper name. *Earth-Sci. Rev.* **12** 1-33

Tapponnier P. and 28 others. (1981) The Tibetan side of the India-Eurasia collision. *Nature.* **294** 405

Tapponnier P. and Molnar P. (1976) Slip-line field theory and large-scale continental tectonics. *Nature.* **264** 319-324

Tapponnier P., Peltzer G. and Armijo R. (1986) On the mechanics of the collision between India and Asia. In: *Collision Tectonics, M.P. Coward and A.C. Reis, eds., Geol. Soc. London, Spec. Publ.* **19** 115-157

Tapponnier P., Peltzer G. Le Dain A.Y., Armijo R. and Cobbold D. (1982) Propagating extrusion tectonics in Asia; new insights from simple experiments with plasticine *Geology.* **10** 611-616

Taylor R.P., Strong D.F. and Fryer B.J. (1981) Volatile control of contrasting trace element distributions in peralkaline granitic and volcanic rocks. *Contrib. Mineral. and Petrol.* **78** 267-271

Taylor H.P. (1980) The effects on assimilation of country rocks by magmas on $^{18}O/^{16}O$ and $^{87}Sr/^{86}Sr$ systematics of igneous rocks. *Earth Planet. Sci. Lett.* **47** 243-254

Taylor R.P. and Mc Clennan S.M. (1985) The continental crust: it's composition and evolution. *Geoscience Texts, Blackwell Scientific Publications.*

Tindle A.G. and Pearce J.A. (1981) Petrogenetic modelling of in-situ fractional crystallisation in the zoned Loch Doon pluton, Scotland. *Contrib. Mineral. and Petrol.* **78** 198-207

Tindle A.G. (1982) Petrogenesis of the Loch Doon granitic intrusion, Southern Uplands of Scotland. *Unpub. Ph.D. thesis, Open University*

Treuil M and Varet J., (1973) Critieres volcanologiques, petrologiques et geochemiques de la geneses et de la differentation des magmas basaltiques: exemples de l'Afar. *Bull. Soc. Geol. France* . **15** 401-444

Tuttle O.F. (1955) The origin of granite. *Reprint from Scientific American.*

Van Den Haute P. (1986) Apatite fission track dating applied to Precambrian terranes. *Chemical Geology.* **57** 155-165

van der Molen I. and Paterson M.S. (1979) Experimental deformation of partially melted granite. *Contrib. Mineral. and Petrol.* **70** 299-318

Verschure R.H., Andriessen P.A.M., Boelrijk N.A.I.M., Hebeda E.H., Maijer C., Priem H.N.A. and Verdurmen E.A.Th (1980) On the thermal stability of Rb-Sr and K-Ar biotite systems: evidence from coexisting Sveconorwegian (ca 870 Ma) and Caledonian (ca 400 Ma) biotites in SW Norway, *Contrib. Mineral. and Petrol.* **74** 245-252

Vidal P., Bernard-Griffiths J., Cocherie A., Le Fort P., Peucat J.J. and Sheppard S.M. (1984) Geochemical comparison between Himalayan and Hercynian leucogranites. *Phys. Earth Planet. Int.* **35** 179-190

Vidal Ph., Cocherie A., Le Fort P. (1982) Geochemical investigations of the origin of the Manaslu leucogranite (Himalaya, Nepal). *Geochem. Cosmochim. Acta.* **46** 2279-2292

Wagner G.A. (1968) Fission track dating of apatites. *Earth Planet. Sci. Lett.* **4** 411-415

Wagner G.A. and Storzer D. (1972) Fission track length reduction minerals and the thermal history of rocks. *Trans. Am. Nucl. Soc* . **15** 127-128

Wagner G.A., and Reimer G.M. (1972) Fission track tectonics: the tectonic interpretation of fission track apatite ages. *Earth Planet. Sci. Lett.* **14** 263-268

Wagner G.A., Reimer G.M. and Jäger E (1977) Cooling ages derived by apatite fission-track, mica Rb-Sr and K-Ar dating: the uplift and cooling history of the Central Alps, *Mem. Inst. Geol. Miner. Univ. Padova.* **30** 1-27

Wagner G.A., Reimer G.M., Carpenter B.S., Faul H., Van der Linden R and Gijbels R. (1975) The spontaneous fission rate of ^{238}U and fission track dating *Geochem. Cosmochim. Acta.* **39** 1279-1286

Walther J.V. and Orville P.M. (1982) Volatile production and transport in regional metamorphism *Contrib. Mineral. and Petrol.* **79** 252-257

Watson E.B. Harrison T.M. (1983) Zircon saturation revisited: temperature and compopsition effects in a variety of crustal magma types *Earth Planet. Sci. Lett.* **64** 295-304

Watson M.P., Hayward A.B., Parkinson D.N. and Zhang Z. (1987) Plate tectonic history, basin development and petroleum source rock deposition of onshore China.*J. Marine Petrol. Geol.* **4** 205-225

Watt S., Green P.F. and Duranni S.,(1984) Studies of annealing anisotropy of fission tracks in mineral apatite using track-in-track (TINT) measurements. *Nucl. Tracks.* **8** 371-375

Westphal M., Bazhenov M.L., Lauer J.P., Pechersky D.M. and Sibuet J.C. (1986) Paleaomagnetic implications on the evolution of the Tethys Belt from the Atlantic Ocean to the Pamirs since the Triassic. *Tectonophysics.* **123** 37-82

White A.J.R., Clemens J.D., Holloway J.R., Silver L.T., Chappell B.W. and Wall V.J. (1986) S-type granites and their probable absence in southwestern North America *Geology.* **14** 115-118

Wyllie P.J. and Cox K.G. (1962) The habit of apatite in synthetic systems and igneous rocks. *Jour. Pet.* **3** 238-243

Xu R. (1981) Vegetational changes in the past and the uplift of Qinghai-Xizhang plateau. In: *Proceedings of the Symposium on Qinghai-Xizhang (Tibet) Plateau, Geology, Geological History and Origin of the Qinghai-Xizhang Plateau.* **1** 139-141

York D. (1969) Least squares fitting of a straight line with correlated errors. *Earth Planet. Sci. Lett.* **5** 320-324

Zeitler P.K. (1985) Cooling history of the NW Himalaya, Pakistan. *Tectonics.* **4** 127-151

Zeitler P.K., Tahirkeli R.A.K., Naeser C.W., Johnson N.M. (1982) Unroofing history of a suture zone in the Himalaya of Pakistan by means of fission track annealing ages. *Earth Planet. Sci. Lett.* **57** 227-240

Zen E-an and Hammerstrom J.M. (1984) Magmatic epidote and its petrologic significance. *Geology.* **12** 515-518

Zhang H. (1988) Appendix to: The structure of the 1985 Tibet Geotraverse, Lhasa to Golmud. *Philos. Trans. R. Soc. Lond.* **A327**

Zhang Z. M., Liou J.G., and Coleman R.G. (1984) An outline of the plate tectonics of China. *Geol. Soc. Am. Bull.* **95** 295-312

Zhao W. and Morgan W.J. (1985) Uplift of the Tibetan Plateau. *Tectonics.* **4** 359-369

Zhao W. and Morgan W.J. (1987) Injection of Indian crust into Tibetan lower crust: a two-dimensional finite element model study. *Tectonics.* **6** 489-504

Zhao W. and Yuen D.A. (1987) Injection of Indian crust into Tibetan lower crust; a temperature-dependent viscous model. *Tectonics.* **6** 505-514

APPENDIX

A ANALYTICAL TECHNIQUES FOR GEOCHEMISTRY

A.1 SAMPLING AND CRUSHING

Granite samples were typically 1-2 kg in weight when collected. All samples were cleared of weathered surfaces and markings using a hydraulic splitter. Each sample was split into small cubes which were washed in distilled H_2O and allowed to dry in order to remove any dust contaminant. The cubes were then crushed in a hardened steel jaw and crushed to less than 0.5 cm fragments. A representative sample of about 100 g of this crushite material was sampled by cone and quartering techniques to obtain a representative sub-sample. The sub-sample was then placed in an agate lined tema barrell and ground for 15-20 minutes until the powder was less than 200 mesh size.

A.2 XRF DETERMINATION

A.2.1 Sample preparation

Trace elements were determined on pressed powder pellets while major elements were analysed on glass beads. For pressed pellets about 8 g of rock powder was mixed with Movil binder and pressed into a 3 cm diameter pellet using a hydraulic press. Pellets were dried and hardened overhight in an oven at 110°C.

Glass beads were prepared by mixing a 4:1 lithium metaborate:tetraborate mixture (Spectraflux 100B), with pre-dried rock powder in the ratio 6:1 and fusing the mixture in a platinum-gold alloy crucible in a muffle furnace at 1100°C for twenty minutes. A flux loss correction was applied to each batch of eight samples. Loss on ignition data were obtained by heating about 2.5 g of rock powder in a silica crucible at 1000°C for twenty minutes and calculating the percentage weight loss.

A.2.2 Sample analysis

All samples were analysed for major and trace elements using the energy dispersive (EDXRF) system at the Open University. This is a Link Systems Meca 10-44 EDXRF spectrometer. It incorporates a low power (49W) silver anode side window X-ray tube operated in pulsed mode with maximum setting of 49 Kv or 1 Ma, and a Si(Li) detector with a resolution of 125 eV at 5.9 KeV. Instrument drift within single batches (16 samples and 4 standards per batch) was monitored by analysing international and internal standards several times during each run, and representative analyses of standards obtained over the period of this study are given in Appendix D.

For major elements, the glass beads were counted in duplicate for 500 seconds at 10 Kv, 0.2 mA with no primary beam filter. Powder pellets for trace element analyses were counted twice for 800 seconds at 45 Kv, 0.3 mA with a 127 micron silver primary beam filter in position. Detection limits for the major elements are generally 0.05 wt %, except for the light elements Na, Mg, Al and Si, where detection limits are between 0.2 and 0.96 wt % for Si and Na respectively. Precision is better than 1% relative at the 2 sigma level, except for Al (2%), Mg (3%) and Na (10%). For trace elements detection limits are 6 ppm for Rb, Sr, Y, Nb and Ni and 15 ppm for Zr. Precision for all trace elements is about 2% at the 100 ppm level. . All XRF data are tabulated in Appendix D.

A.3 INSTRUMENTAL NEUTRON ACTIVATION ANALYSIS (INAA)

A.3.1 Sample preparation

INAA was carried out to determine the concentrations of REE as well as the abundances of Cs, Th, Ta, Hf, U, Co and Sc. Rock powders were dried overnight at 110°C. Approximately 0.3 g of each powder was accurately weighed into polythene capsules. The capsule lids were sealed to prevent leakage of radioactive powder. The irradiation capsules were then stacked in a polythene tube, and a pre-weighed lacquered iron foil was placed between each irradiation capsule to monitor neutron flux variations along the length of the tube. Each irradiation package contained nine samples and two

standards which were the irradiation standard AC (OURS), and a sample of the Whin Sill which is used as an internal standard.

A.3.2 Sample analysis

Samples were irradiated in a core tube at the Imperial College reactor centre, Silwood Park, Ascot in a thermal flux of 5 x 10^{12} n cm^2 S^{-1} for 24-30 hours. Following irradiation the samples were "counted" at the Open University using two detectors on either side of the sample capsule - a planar low energy photon spectrometer (LEPS) and a coaxial Ge(Li) detector. Each sample was counted for 800 seconds on the LEPS detector for Sm, and on the coaxial detector for La, Co and Sc. The other elements were determined by counting each sample for 2.5 x 10^4 to 5 x 10^4 seconds using the LEPS detector. The iron foils were "counted" using the coaxial detector for 300 seconds each, to assess variations in the neutron flux. Data were processed using spectroscopy amplifiers and a multichannel analyser. Photopeak data were corrected for neutron flux variations calculated using the iron foil data. Details of counting conditions, peak fitting, calibration and corrections are given in Potts *et al.*, (1980 and 1985)

A.4 RADIOGENIC ISOTOPE ANALYSIS

All isotopic analysis and sample preparations were carried out in a clean-air laboratory in which a positive air pressure is maintained. Sample dissolutions and beaker handling are carried out in laminar flow units. All dissolutions were carried out in PTFE bombs to ensure complete dissolution of all accessory phases, and aliquots were collected off the ion exchange columns in teflon beakers. Bombs and beakers are thoroughly cleaned between sample batches to prevent cross contamination. The teflon beakers are cleaned by rinsing in quartz distilled (QD) H_2O; soaking for at least 24 hours in conc. HNO_3 at 80° C and finally soaking in QD H_2O for a further 24 hours. They are then rinsed and allowed to dry under the evaporation lamps. The PTFE bombs are cleaned by fillling them with 6M HCl and placing them in the monel jackets in the oven at 180°C for 24 hours, before soaking them in QD H_2O for a further 24 hours

All H_2O is distilled by a two-stage quartz still, or produced by a Milli-Q reverse osmosis water purification system. HCl and HNO_3 are doubly distilled in quatrz still and finally purified in sub-boiling teflon still. HF is also purified in sub-boiling stills. Total procedural blanks for Sm and Nd are > 1 ng, and 8 ng for Sr.

A.4.1 Sr whole rock chemistry

About 100 - 150 Mg of rock posder is weighed into a teflon bomb to which a couple of drops of QD H_2O are added to avoid spattering when the acid is added. About 5 ml of 40% HF and 2 ml of concentrated HNO_3 is then added to the water/powder mixture. The PTFE bomb is then placed in a polythene sleeve which holds the top of the bomb in position. This assembly is then placed in a monel jacket and allowed to stand overnight in an oven at 180°C. When the bomb is removed from the oven, the solution is evaporated down under the evaporating lamps to near dryness. 6 ml of 6M QD HCl are then added, and when complete dissolution has been achieved the solution is evaporated to near-dryness and the residue is redissolved in 1 ml of QD 2.5M HCl for loading on to the cation exchange columns. Any residue is centrifuged off, and the clear solution is carefully pipetted on to pre-conditioned cation exchange columns. The sample is slowly washed into the column using two 1 ml aliquots of 2.5M HCl. A further 40 ml of 2.3M HCl is then allowed to percolated through the columns and the Sr fraction is collected with 10 ml of QD 2.5M HCl. The solution containing the Sr fraction is evaporated to dryness and the beakers are sealed with Parafilm and stored for isotopic analysis.

A.4.2 Rb and Sr biotite chemistry

100 mg of biotite flakes were separated from a crushed whole rock size fraction of 20-40 mesh. Hand-picking was found to be the fastest method of separation and enabled a high degree of purity to be obtained. Samples were accurately weighed and spiked with an accurately known quantity of ^{87}Rb and ^{84}Sr spike in a weight ratio of about 1:1 sample to spike mixture. They were then dissolved and prepared in the same way as for whole rock samples before being passed through the ion exchange columns.

The base of the exchange column was then washed with QD H_2O to remove any excess Rb remaining on the outside. The collected Sr aliquot was then evaporated down, re-dissolved and passed through the ion exchange column a second time in order to remove excess Rb. This was found to greatly improve the problem of Rb interference. The aliquots were then evaporated to dryness.

A.4.3 Nd whole rock chemistry

The procedure for dissolving samples for Nd chemistry is identical to that for Sr and usually done on the same aliquot. After the Sr fraction has been collected, the columns are washed with 1 ml of QD H_2O and eluted with 6 ml of 3M HNO_3, after which 4 ml of 3M HNO_3 are collected. This fraction is then evaporated to dryness.

A.5 MASS-SPECTROMETRY

Sr and Nd are analysed on, respectively, outgassed single Ta and triple Re/Ta filaments (with Re in the centre). The Sr fraction is redissolved in about 0.5 ml QD H_2O and loaded into a drop of H_3PO_4 on the centre of a single Ta filament using a micro-pipette. A current is passed through the filament and gradually increased until the phosphoric acid fumes off, then it is further increased until a dull red glow is observed and the sample has dried.

Rb fractions are redissolved in a small drop of QD H_2O and carefully loaded on to the side filaments (Ta) of a triple filament. The current is slowly increased until the sample has dried. The same procedure is used for loading Nd.

Loaded filaments are carefully positioned in a clean sample turret. Electrical connectors are checked and the turret is allowed to stand in a vacuum oven until ready for loading into the mass-spectrometer. All radiogenic isotope mass-spectrometry was carried out an a V.G. 54E mass spectrometer interfaced with a HP 9845T computer which runs the analyses automatically using software developed by D.W. Wright and P.W.C. Van Calsteren.

A.5.1 Sr isotopic measurement

The computer adjusts the filament current until a beam intensity of 15 pA is obtained. The measuring cycle is mass 88, 87, 86.5, 85 and 84. When the Rb contribution to the 87 peak is > 0.01% the 85 peak is no longer counted. The intensities are calculated using a double interpolation algorithm (Dodson, 1978). Corrections are applied for zero, dynamic memory and Rb interference. The $^{87}Sr/^{86}Rb$ ratio is corrected for mass fractionation assuming that the fractionation is linearly dependent on mass difference, and that $^{87}Sr/^{88}Sr = 0.1194$. As an anlysis proceeds ratios are stored by the computer in sets of 10. Means and errors are calculated, and the ratios are rejected if Chauvenets criterion is not satisfied. If the total error for the set is greater or equal to 100 then the whole set is rejected. If the total error is greater than 500 the whole set is ignored. The run for an individual sample is terminated when at least 100 ratios have been accumulated and the $^{87}Sr/^{86}Sr$ ratio error is better than 0.00002 at the one sigma level.

A.5.2 Nd isotopic measurement

Nd beams are run at an intensity of about 7 pA. The measuring cycle is mass 146, 144, 142.5 142, 147. The 147 peak is eliminated when the Sm contribution to the 144 peak is < 0.01%. The $^{143}Nd/^{144}Nd$ ratio is corrected for mass-fractionation assuming $^{146}Nd/^{144}Nd = 0.7219$. A run is terminated when at least 200 ratios are accumulated and the error is better than 0.00001 at the one sigma level.

B ANALYTICAL TECHNIQUES FOR FISSION TRACK DATING

Rock crushing and mineral separation for fission track dating is primarily aimed at the recovery of three minerals: apatite, zircon and sphene. In this study the external detector method of analysis was used therefore only this method will be described here, although there are several other techniques in common use.

B.1 MINERAL SEPARATION

B.1.1 Sieving

Crushite material recovered during the jaw crushing stage of sample crushing for the geochemistry was sieved through a selection of sieves ranging from 60 to 250 μ. From this, the most suitable fraction for each particular granite was selected - usually 150 - 200 μ. The selection was then washed to remove the fines and dried in a clean dustless area.

B.1.2 TBE heavy liquid separation

Separation of the required minerals is acheived by exploiting differences in mineral density with heavy liquids, and differences in magnetic susceptability with a Frantz isodynamic magnetic separator. Heavy liquids are dangerous and any amount should be washed from gloves, skin etc. Separations must always be carried out in a fume cupboard.

The first step uses tetrabromoethane (TBE) of specific gravity equal to approximately 2.95 g/cc. A 500 ml glass beaker was half filled with TBE to which the sample was added in an approximate 3:1, TBE:sample ratio. This was vigourously stirred and quickly poured into a spinning Overflow-Centrifuge (Ijlst, 1973) before the heavy minerals had time to settle. The 'light' minerals (predominantly biotite, quartz and feldspar) become caught in the centrifuge while the 'heavy' minerals remain in the liquid which is recovered. The heavy fraction is then filtered in a vacuum filter flask to remove the TBE, which can be reused, then both the lights and heavies are washed with

trichloroethylene until all traces of TBE are removed. They are then dried under an evaporation lamp. The heavy fraction should by now consist of the required minerals plus, inevitably, some contamination from the lights. If the proportion of contaminant was high, the TBE separation was repeated.

B.1.3 Magnetic separation

Using the mechanical vibrator and a moderate feed rate, the heavy mineral fraction was processed through the Frantz in a number of steps increasing the current at each stage. This typically left apatite and zircon on the non-magnetic side which can then be separated with diodomethane.

B.1.4 DIM heavy liquid separation

This is usually the final step and results in individual, relatively pure apatite and zircon separates. The separation is carried out in a small (100 ml) separating funnel in which a small amount of the diodomethane (DIM) is placed. The sample is added, then stirred to make sure all the zircons are wet, otherwise surface tension will cause them to float with the apatites. After a few minutes settling time, the heavier zircon fraction is drawn off and both apatites and zircons are filtered and washed. A final run through the Frantz separator will clean up the samples so that almost 100% purity is achieved. However, at a later stage during track counting it was found useful to have a few zircon grains in the apatite fraction to help locate grain positions on the mica detector.

B.2 MOUNTING, POLISHING AND ETCHING TECHNIQUES

B.2.1 Apatite

Araldite MY753 resin and HY956 hardener are mixed in a 5:1 ratio by volume, and a small amount is placed on a glass slide heated on a hotplate to 120°C. The sample number is inscribed with a diamond pencil on the back of the glass. Apatite grains are distributed over an area of the resin, less than 1 x 1 cm, in a distinct pattern (usually star-shaped). This is allowed to cure on the hotplate for about 10 minutes.

When cold, the excess epoxy resin is ground away using 400 waterproof SiC abrasive paper on a wet rotating lap, until it is approximately 0.4-0.5 mm thick. The mount is then ground with 600 paper until the grains are fully exposed but still firmly held in the resin. Finally the mount is polished using 0.3 μm Al_2O_3 slurry in H_2O (A) on a rotating nylon cloth lap.

The etching medium is 5N HNO_3 at a temperature of 20 - 22°C which must be constantly monitored and maintained throughout the procedure. The apatite mount is held with forceps and dipped into the acid for exactly 20 seconds. It is then instantly washed in water to stop the etching. When dry, the sample is inspected for sharp polishing scratches which are an indication that the sample has been sufficiently etched. If necessary, the mount can be returned to the acid and re-etched for a few extra seconds. The glass mount is then trimmed to 1 x 1.5 cm so that it will fit into the aluminium irradiation package.

B.2.2 Zircon

The mounting medium for zircons is FEP teflon sheet cut into 2 x 2 cm squares. Zircons are sprinkled onto a glass slide and spread over an area about 1 cm^2. This is placed on a hotplate pre-heated to 330°C, along with a blank glass slide. A teflon square is then placed very carefully over the zircons and pressed down with the blank glass slide. The teflon will melt and the zircons become embedded in it. When cool the teflon will peel away from the glass.

Very little grinding is required since the zircons are already exposed at the surface, and over-grinding results in the zircons falling out of the mount. However, it is necessary to expose an internal surface of the zircon. The mounts are then polished in the same way as for apatite.

Etching can be a long procedure, between 4 and 100 hours, commonly around 24. The etching meduim is a 50 mole %: 50 mole % KOH:NaOH eutectic which is heated in a ceramic beaker on a hotplate to 215°C. The zircon mounts are placed face down in the etchant and initially left for 4 hours. Before viewing under the microscope it is essential

to thoroughly wash the mounts as many of the etchants can corrode the microscope lens. The zircons are inspected for the degree of etching and returned to the etchant if necessary. The tracks were inspected every few hours until results were satisfactory.

B.2.3 External detector method

For the external detector method a mica detector is clamped against each mineral mount and this 'sandwich' is irradiated with thermal neutrons. An image of each crystal is formed in the mica by neutron induced ^{235}U fission tracks, permitting a calculation of the uranium content of each crystal. Uranium dosimeter glasses and age standards that have been polished and etched are also placed in contact with a mica detector and included in each irradiation package at various intervals along the length. The micas are cut to the same size as the samples and the sample number is inscribed on the back. Two holes are then pierced through the mica into the sample at opposite corners, to aid in the location of grains during counting. The sandwich is then wrapped in heat-shrink plastic to ensure close contact between sample and detector. These are placed in an aluminuim irradiation tube and sent to the reactor.

B.2.4 Thermal neutron irradiation

Samples were sent to the Harwell reactor in Didcot, Oxforshire and placed in the reactor so that the apatites received the requested fluence of 6 - 7 x 10^{15} n cm^2, and zircons received the requested fluence of 8 x 10^{14} n cm^2. After removal of the samples from the irradiation package, the mica detectors are etched to reveal the induced tracks by placing them for 45 minutes in 40% HF at 20°C. They must then be very carefully washed in distilled H_2O and then left to soak overnight. After further washing they are dried under an infra-red lamp for 5 hours to drive off any remaining HF. Samples and matching micas were then mounted on a glass slide ready for counting.

B.3 FISSION TRACK COUNTING CONDITIONS

All fission tracks were counted with a Leitz Orthoplan microscope using a stage micrometer to calibrate the counting graticule. Dosimeter glasses were counted using the 25 x eyepiece with the 63 x objective. This combination gave the area of a graticule

square to be 1.21 x 10^6 cm^2. Apatites were counted in dry conditions using 12.5 x eyepiece with 100 x objective resulting in an area square of 1.266 x 10^6 cm^2. Zircons were counted under oil using the 12.5 x eyepiece with the 100 x oil objective resulting in an area square of 1.277 x 10^6 cm^2. Age standard data are given in Table B.1 and sample data in Table B.2.

Track lengths were measured by Dr. Hurford using the semi-automatic Morphomat image analysis unit, and a drawing tube attachment on the microscope.

AGE STANDARDS IRRADIATION DATA

Standard	Mineral	No. crystals	ps/pi	Ns/Ni	Chi square %	Irradiation	Glass	pd/cm2	Zeta
Buluk Member *	Zircon	10		0.487 ± .022	100.0	Bern-H2	CN1	534059	125
Buluk Member	Zircon	10		0.494 ± .025	5.0	Bern-H2	CN1	544691	121
Fish Canyon Tuff*	Zircon	6	0.771 ± .050		< 2.0	Bern-H2	CN1	545678	135
Fish Canyon Tuff	Zircon	8		0.680 ± .023	76.0	Bern-H2	CN1	535312	148
Tardree rhyolite	Zircon	9	1.641 ± .103		< 2.0	Bern-H2	CN1	543704	133
Tardree rhyolite*	Zircon	10	1.588 ± .087		< 2.0	Bern-H2	CN1	532806	140
Fish Canyon Tuff	Apatite	18		0.129 ± .011	30.0	Bern-H1	SRM	116533	370 ± 30
Mount Dromedary*	Apatite	9		0.473 ± .034	87.0	Bern-H1	SRM	116579	358 ± 26
Fish Canyon Tuff	Apatite	10		0.118 ± .013	94.0	Bern-H1	SRM	116533	405 ± 46
Fish Canyon Tuff	Apatite	10		0.114 ± .015	32.0	Bern-33	SRM	124625	392 ± 51
Fish Canyon Tuff	Apatite	19		0.066 ± .006	100.0	Bern-19	SRM	212430	397 ± 34
RECOUNTS									
Fish Canyon Tuff	Apatite	10		0.137 ± .014	100.0	Bern-H1	SRM	116533	349 ± 47
Mount Dromedary	Apatite	9		0.443 ± .029	77.0	Bern-H1	SRM	116579	382 ± 25
Fish Canyon Tuff	Apatite	9		0.120 ± .015	96.0	Bern-33	SRM	124625	372 ± 47
Fish Canyon Tuff	Apatite	11		0.073 ± .008	98.0	Bern-19	SRM	212430	359 ± 39

*Standard	Ages
Buluk Member	16.2
Fish Canyon Tuff	27.4
Mount Dromedary	98.7
Tardree Rhyolite	59.0

Average Zeta
376 ± 19

Table B.1 Irradiation data for age standards used in calculating zeta values.

KUNLUN FISSION TRACK DATA

Location	Sample	Mineral	No. crystals	ps/pi	Ns/Ni	Chi square %	Dos. pd/cm2	Age ± 1 sigma
S. Xidatan Fault	G215b	Zircon	9		3.40	51	542829	120.6 ± 11.3
Xidatan	G206d	Zircon	15		2.24	32	549620	81.3 ± 2.8
Xidatan	X67	Zircon	12	2.12		< 5	546588	73.5 ± 6.5
Wanbaogou	G222c	Zircon	12		2.31	96	545335	83.1 ± 3.2
Golmud Hydro	G263	Zircon	7	2.89		< 5	540324	103.1 ± 10
Golmud East	G273a	Zircon	11		3.77	11	549094	136.1 ± 13
Duo Ya He	G266a	Zircon	15		4.51	30	547640	162.0 ± 7
Xidatan	G208	Apatite	9		0.06	100	1169880	12.8 ± 1.9
Yie Nin Gou X	G214c	Apatite	11		0.08	100	1170790	17.4 ± 2.5
Yie Nin Gou	G221b	Apatite	18		0.10	58	1167150	20.8 ± 1.8
Wanbaogou	G222c	Apatite	10		0.09	99	1172610	20.1 ± 2.5
Golmud Hydro	G244a	Apatite	10		0.09	100	1168970	19.4 ± 2.9
Golmud East	G273a	Apatite	14		0.49	100	1168060	106.0 ± 7.6
Duo Ya He	G266a	Apatite	8		0.55	12	1171240	118.9 ± 8.9

Table B.2 Fission track age data for the Kunlun samples.

C CALCULATIONS

C.1 THE Rb-Sr AGE EQUATION

The Rb-Sr method of dating minerals is based on the β-decay of ^{87}Rb to ^{87}Sr with a half-life of 48.8 x 10^9 yrs (Jäger, 1979). This half-life corresponds to the recommended decay constant of 1.42 x 10^{11}. The equation for determining the age of a sample from the decay of ^{87}Rb to ^{86}Sr is expressed as:

$$\left(\frac{^{87}Sr}{^{86}Sr}\right)_p = \left(\frac{^{87}Sr}{^{86}Sr}\right)_o + \frac{^{87}Rb}{^{86}Sr}\, e^{\lambda t} - 1 \qquad (1)$$

where t = age of biotite

λ = decay constant

$^{87}Sr/^{86}Sr_p$ = measured ratio

$^{87}S/^{86}Sr_o$ = initial ratio

This can then be solved simlutaneously for the age t, of the biotite, using the $^{87}Sr/^{86}Sr_p$ and $^{87}Rb/^{86}Sr$ of the whole rock sample from which the biotite has been extracted, and the $^{87}Sr/^{86}Sr_p$ and $^{87}Rb/^{86}Sr$ of the biotite. The age equation used is given below:

$$t = \frac{1}{\lambda} \ln\left(1 + \frac{^{87}Sr}{^{87}Rb}\right) \qquad (2)$$

C.2 THE K-Ar AGE EQUATION

The decay scheme of ^{40}K is more complicated than that of ^{87}Rb due to the double decay of ^{40}K to ^{40}Ar and ^{40}Ca. As a result, the age equation is also more complicated, and although the decay of ^{40}K to ^{40}Ar is the system used for dating minerals, the decay of ^{40}K to ^{40}Ca must be taken into account in the age equation. Therefore, for the ^{40}Ca branch:

$$T_1 = \frac{\lambda \beta^-}{\lambda} N_0 (e^{\lambda \tau} - 1) \qquad (3)$$

and for the ^{40}Ar branch:

$$T_2 = \frac{\lambda e}{\lambda} N_0 (e^{\lambda \tau} - 1) \qquad (4)$$

where

λ = decay constant of ^{40}K total = $5.543 \times 10^{-10} yr^{-1}$

$\lambda\beta^-$ = decay constant of ^{40}K by β^- emission = $4.962 \times 10^{-10} yr^{-1}$

λ_e = decay constant of ^{40}K by electron capture = $0.581 \times 10^{-10} yr^{-1}$

t = age of sample

$T_{1 \text{ and } 2}$ = daughter isotopes of ^{40}Ca and ^{40}Ar respectively

N_0 = parent isotope at time zero

N_t = parent isotope at time t

dividing (3) by (4) we obtain

$$\frac{T_1}{T_2} = \frac{\lambda \beta -}{\lambda_e} \qquad (5)$$

and can rewrite the final equation as:

$$t = \frac{1}{\lambda} \ln \left(\frac{N_0 \lambda_e}{N_0 \lambda_e - T_2 \lambda} \right) \qquad (6)$$

C.3 THE Ar-Ar AGE EQUATION

To evaluate the $^{40}Ar/^{39}Ar$ ratio it is necessary to include the irradiation parameters in the equation which is expressed so:

$$\frac{^{40}Ar^*}{^{39}Ar} = \frac{^{40}K}{^{39}K} \quad \frac{\lambda}{\lambda_e + \lambda_\beta} \quad \frac{1}{\Delta} \quad \frac{(e^{\lambda t} - 1)}{\int \phi(\varepsilon)\sigma(\varepsilon)d\varepsilon} \qquad (7)$$

where

$^{40}Ar^*$	=	No. of radiogenic ^{40}Ar atoms present in sample
$^{39}Ar_K$	=	No. of ^{39}Ar atoms produced during irradiation of ^{39}K
^{39}K	=	No. of ^{39}K atoms present in sample
^{40}K	=	No. of ^{40}K atoms present in sample
$\phi(\varepsilon)$	=	Fast neutron flux at energy ε
$\sigma(\varepsilon)$	=	Neutron capture cross section of $^{39}K(n,p)^{39}Ar$ at energy ε
ΔT	=	Duration of the irradiation
λ	=	Decay constant of ^{40}K total
λ_e	=	Decay constant of ^{40}K by electron capture
λ_β	=	Decay constant of ^{40}K by β-emission
		(The integration is performed over all incident neutron energies)

However, this results in a rather cumbersome age equation and since standards of a precisely known K/Ar age are included in the irradiation package, equation (5) can be greatly simplified by substituting a value, J, (Dallmeyer, 1979) which is defined as:

$$J = \frac{^{39}K}{^{40}K} \quad \frac{\lambda_e + \lambda_\beta}{\lambda_e} \quad \Delta T \int \phi(\varepsilon)\sigma(\varepsilon)d\varepsilon \qquad (8)$$

so the age equation can then be written as:

$$t = \frac{1}{\lambda} \ln\left(1 + J \frac{^{40}Ar^*}{^{39}Ar_k}\right) \quad (9)$$

By substituting the known K-Ar age of the standard for t in equation (9), the value of J can be directly calculated from measurement of the $^{40}Ar/^{39}Ar_K$ ratio of the irradiated standard. However, because the fast neutron flux is inhomogeneous over short distances within the reactor core it is necessary to include several standards and so calculate the value of J for specific intervals within the package. Once this has been determined, ages of unknown samples may be directly calculated from the measurement of their $^{40}Ar/^{39}Ar_K$ ratios using the appropriate value for J in equation (9).

C.4 ND MODEL AGE CALCULATIONS

Model ages are reported relative to CHUR and the equation used is given below;

$$T_{Nd}^{CHUR} = \frac{1}{\lambda} \ln\left(\frac{^{143}Nd/^{144}Nd \text{ of sample} - ^{143}Nd/^{144}Nd_{CHUR}}{^{147}Sm/^{144}Nd \text{ of sample} - ^{147}Sm/^{144}Nd_{CHUR}}\right) + 1$$

and ε values are calculated according to De Paolo and Wasserburg (1976):

$$\varepsilon Nd = \frac{^{143}Nd/^{144}Nd \text{ sample at time t}}{^{143}Nd/^{144}Nd_{CHUR} \text{ at time t}}$$

$$\varepsilon Sr = \frac{^{87}Sr/^{86}Sr \text{ sample at time t}}{^{87}Sr/^{86}Sr \text{ of bulk earth at time t}}$$

where

$\lambda^{147}Sm$	=	6.54×10^{-12} a^{-1}
$(^{143}Nd/^{144}Nd)_{CHUR}$	=	0.51264
$(^{147}Sm/^{144}Nd)_{CHUR}$	=	0.1967
$\lambda^{87}Rb$	=	1.42×10^{-11} a^{-1}
$(^{87}Sr/^{86}Sr)_{BE}$	=	0.7047
$(^{87}Rb/^{86}Sr)_{BE}$	=	0.0847

C.5 A.F.C. EQUATIONS

$$m = \frac{\frac{r}{r-1}\ \frac{C_a}{Z}\ (1-F^{-Z})\ \varepsilon_a + C_m^o\ F^{-Z}\ \varepsilon_m^o}{\frac{r}{r-1}\ \frac{C_a}{Z}\ (1-F^{-Z}) + C_m^o\ F^{-Z}}$$

where

m	=	the isopote ratio of the final magma
m^o	=	the isotope ratio of the original magma
ε_a	=	the isotope ratio of the assimilated material
C_m^o	=	the concentration of the element in the original magma
C_a	=	the concentration of the element in the assimilated material
r	=	the ratio of mass assimilated (M_a) to mass of crystals fractionated (M_c)
Z	=	$\frac{r+D-1}{r-1}$ where D is the bulk distribution coefficient

SOUTHERN REGION MAJOR ELEMENTS

Xidatan	SiO2 Xidatan	TiO2 Xidatan	Al2O3 Xidatan	Fe2O3 Xidatan	MnO Xidatan	MgO Xidatan	CaO Xidatan	Na2O Xidatan	K2O Xidatan	P2O5 Xidatan	LOI Xidatan	Total Xidatan
206a	66.40	0.68	17.68	4.03	0.06	1.60	3.84	4.56	1.75	0.29	0.53	101.42
206b	71.40	0.39	15.30	2.61	0.06	0.88	2.57	3.83	3.67	0.14	0.47	101.32
207	74.54	0.16	14.44	1.14	0.03	0.28	1.43	3.48	5.18	0.07	0.41	101.16
208	72.34	0.33	14.95	2.34	0.06	0.70	2.02	3.82	4.01	0.17	0.56	101.30
x67	69.09	0.40	16.90	2.63	0.06	1.34	3.48	4.26	3.50	0.23	0.90	102.79
206c	77.29	0.08	13.80	0.84	0.03	0.15	0.93	3.61	5.04	0.08	0.26	102.11
206d	77.30	0.10	13.37	0.84	0.03	0.15	0.88	3.64	4.93	0.07	0.42	101.73
206e	76.11	0.90	13.32	0.65	0.02	0.25	0.87	3.86	4.86	0.04	0.47	101.35
YNG	YNG	YNG	YNG	YNG	YNG	YNG	YNG	YNG	YNG	YNG	YNG	YNG
213a	75.19	0.11	13.96	1.01	0.03	0.13	1.22	4.21	4.26	0.03	0.50	100.65
213b	75.61	0.11	13.92	1.02	0.02	0.13	1.18	4.01	4.50	0.03	0.57	113.97
214a	70.03	0.41	15.01	2.43	0.04	0.69	2.60	3.98	3.23	0.10	0.71	99.23
214b	68.59	0.42	15.73	2.50	0.05	0.85	2.75	4.97	3.30	0.13	0.72	100.01
214c	69.25	0.44	16.04	2.65	0.05	0.89	2.66	4.48	3.22	0.17	0.54	100.39
221a	68.54	0.48	16.38	2.92	0.05	1.12	3.27	4.57	2.92	0.20	0.67	101.12
221b	66.81	0.62	16.69	3.67	0.06	1.40	3.88	4.58	2.19	0.24	0.57	100.71
221c	68.92	0.46	16.34	2.76	0.05	1.03	3.33	4.57	2.57	0.17	0.61	100.81
221d	69.66	0.45	16.18	2.64	0.05	0.92	2.89	4.74	3.00	0.19	0.60	101.32
221e	68.53	0.51	15.98	2.94	0.06	1.06	3.14	4.49	2.88	0.20	0.81	100.60
221f	68.26	0.44	16.41	2.68	0.05	0.96	3.12	4.62	3.02	0.16	0.53	100.25
221h (en)	61.92	0.74	16.92	6.57	0.14	2.82	3.86	4.23	3.33	0.53	0.83	101.90
221i (en)	68.82	0.47	16.10	2.88	0.05	1.11	3.19	4.54	2.70	0.19	0.69	100.74
Naij Tal	Naij Tal	Naij Tal	Naij Tal	Naij Tal	Naij Tal	Naij Tal	Naij Tal	Naij Tal	Naij Tal	Naij Tal	Naij Tal	Naij Tal
236a	73.63	0.27	14.64	1.75	0.04	0.75	2.35	3.96	3.41	0.08	0.57	101.45
236d	68.07	0.44	15.73	2.68	0.04	1.30	3.63	4.27	2.62	0.21	0.51	99.50
236e	70.66	0.30	14.66	1.85	0.04	0.87	2.49	3.99	3.60	0.12	0.32	98.90
236f	71.78	0.32	15.70	1.97	0.04	0.74	2.55	4.40	3.71	0.13	0.40	101.74
236g	71.60	0.33	16.15	2.08	0.04	0.92	2.78	4.57	3.46	0.12	0.48	102.53
237	71.15	0.38	15.43	2.60	0.06	1.01	2.55	3.79	3.58	0.14	0.51	101.20
WBG	WBG	WBG	WBG	WBG	WBG	WBG	WBG	WBG	WBG	WBG	WBG	WBG
222a	71.13	0.39	13.91	3.14	0.06	0.48	1.92	3.71	4.23	0.06	0.82	99.85
222b	70.06	0.44	13.83	3.15	0.05	0.46	1.62	3.23	4.54	0.12	0.88	98.38
222c	71.75	0.35	14.59	2.90	0.04	0.46	2.03	3.68	4.29	0.12	0.88	101.09
222d	71.31	0.32	14.99	2.59	0.04	0.40	1.82	3.73	4.73	0.06	0.88	100.87
222e	71.63	0.35	14.40	2.88	0.05	0.49	1.69	3.37	4.72	0.07	1.05	100.70
222f	72.30	0.36	13.56	2.88	0.05	0.36	2.06	3.39	3.52	0.03	0.80	99.31
222g	69.63	0.41	14.88	3.32	0.05	0.52	2.05	3.76	4.65	0.10	0.71	100.08
222h (en)	55.53	1.23	17.24	11.12	0.18	2.15	4.75	5.06	2.58	0.76	0.85	101.46
232a	74.42	0.12	14.63	1.21	0.02	0.15	0.80	3.75	4.95	0.16	1.24	101.45
232b	74.12	0.11	14.48	1.19	0.03	0.14	0.77	3.76	5.01	0.15	1.14	100.90
232c	73.91	0.14	14.63	1.32	0.02	0.14	0.84	3.62	4.95	0.14	0.97	100.68

CENTRAL REGION MAJOR ELEMENTS

G HYDRO	SiO2 G HYDRO	TiO2 G HYDRO	Al2O3 G HYDRO	Fe2O3 G HYDRO	MnO G HYDRO	MgO G HYDRO	CaO G HYDRO	Na2O G HYDRO	K2O G HYDRO	P2O5 G HYDRO	LOI G HYDRO	Total G HYDRO
Central	**Central**	**Central**	**Central**	**Central**	**Central**	**Central**	**Central**	**Central**	**Central**	**Central**	**Central**	**Central**
245a	76.42	0.04	13.26	1.13	0.04	0.18	0.83	3.86	4.62	0.04	0.38	100.80
245b	77.01	0.05	13.67	1.13	0.05	0.22	0.86	3.60	4.77	0.09	0.40	101.85
245e	75.33	0.10	13.35	1.63	0.06	0.15	1.21	3.91	4.19	0.03	0.38	100.34
245f	74.25	0.90	13.53	1.64	0.06	0.26	1.20	4.16	4.25	0.03	0.40	100.68
Pink	**Pink**	**Pink**	**Pink**	**Pink**	**Pink**	**Pink**	**Pink**	**Pink**	**Pink**	**Pink**	**Pink**	**Pink**
245c	76.67	0.04	13.35	1.17	0.04	0.15	0.83	3.87	4.52	0.05	0.36	101.05
244a	74.06	0.22	13.93	2.42	0.06	0.44	1.78	3.92	3.95	0.07	0.35	101.20
244b	73.75	0.20	14.03	2.40	0.04	0.50	1.76	3.82	3.92	0.05	0.51	100.98
260	72.08	0.31	14.37	3.54	0.07	0.75	2.46	3.65	3.37	0.08	0.47	101.15
261	71.93	0.33	14.33	3.52	0.08	0.77	2.41	4.14	3.08	0.08	0.55	101.22
263	74.21	0.16	13.95	2.03	0.05	0.21	1.40	3.75	4.67	0.06	0.49	100.98
264	72.70	0.20	13.94	2.50	0.07	0.31	1.63	3.87	4.10	0.04	0.63	99.99
Little	**Little**	**Little**	**Little**	**Little**	**Little**	**Little**	**Little**	**Little**	**Little**	**Little**	**Little**	**Little**
248a	74.20	0.17	14.55	2.31	0.06	0.42	1.55	3.73	4.31	0.14	0.38	101.82
248b	73.88	0.17	14.73	2.43	0.06	0.47	1.68	3.65	4.15	0.10	0.41	101.74
248c	73.09	0.15	14.41	2.28	0.05	0.43	1.58	3.61	4.38	0.07	0.53	100.59
248d	74.03	0.16	14.74	2.36	0.04	0.57	1.63	3.78	4.28	0.16	0.40	102.17
Junction	**Junction**	**Junction**	**Junction**	**Junction**	**Junction**	**Junction**	**Junction**	**Junction**	**Junction**	**Junction**	**Junction**	**Junction**
249a	71.69	0.26	15.26	3.14	0.07	0.53	2.06	4.12	3.95	0.10	0.34	101.52
249b	68.65	0.38	16.32	4.09	0.10	0.91	3.19	4.24	3.40	0.16	0.58	102.05
249c	70.42	0.29	15.08	3.32	0.07	0.28	2.07	4.30	3.99	0.03	0.36	100.21
249d	74.27	0.16	14.01	1.58	0.03	0.16	1.72	3.93	4.06	0.03	0.22	100.17
249e	59.67	0.97	15.80	8.29	0.21	2.16	5.52	4.46	2.40	0.21	0.48	100.17
238	71.55	0.27	15.17	3.19	0.08	0.36	1.96	4.32	4.05	0.04	0.35	101.34

NORTHERN REGION MAJOR ELEMENTS

E Quarry	SiO2 E Quarry	TiO2 E Quarry	Al2O3 E Quarry	Fe2O3 E Quarry	MnO E Quarry	MgO E Quarry	CaO E Quarry	Na2O E Quarry	K2O E Quarry	P2O5 E Quarry	LOI E Quarry	Total E Quarry
246a	68.44	0.51	16.69	4.07	0.08	1.55	4.39	3.55	1.84	0.25	0.54	101.94
246b	69.09	0.48	16.50	3.80	0.09	1.50	4.11	4.12	1.92	0.23	0.45	102.31
246c	66.89	0.57	16.85	4.58	0.09	1.77	4.74	3.75	1.69	0.25	0.54	101.74
246d	68.02	0.51	17.27	3.90	0.11	1.56	4.31	4.24	1.70	0.22	0.46	102.33
246e	67.75	0.46	16.58	3.46	0.09	1.36	3.61	4.05	2.31	0.30	0.03	100.00
246f (en)	53.46	1.24	18.28	9.63	0.18	4.84	8.64	3.66	0.77	0.30	0.29	101.31
246g (peg)	75.78	0.06	14.99	0.57	0.02	0.29	1.76	5.15	2.76	0.03	0.26	101.65
DYH	**DYH**	**DYH**	**DYH**	**DYH**	**DYH**	**DYH**	**DYH**	**DYH**	**DYH**	**DYH**	**DYH**	**DYH**
266a	73.81	0.37	14.97	2.49	0.03	0.83	2.91	3.81	2.54	0.12	0.57	102.45
266b	71.82	0.21	13.26	1.60	0.02	0.51	2.44	3.94	2.51	0.05	0.51	96.87
266c	74.94	0.25	14.23	1.71	0.03	0.65	2.52	3.66	2.75	0.08	0.52	101.34
266d	75.23	0.21	14.58	1.59	0.03	0.53	2.62	4.14	2.33	0.06	0.49	101.81
266e	73.67	0.31	14.62	2.11	0.03	0.80	2.70	3.88	2.71	0.08	0.50	101.41
G East	**G East**	**G East**	**G East**	**G East**	**G East**	**G East**	**G East**	**G East**	**G East**	**G East**	**G East**	**G East**
273a	66.96	0.58	16.41	3.95	0.06	1.58	4.24	3.71	2.85	0.20	0.65	101.19
273b	67.34	0.52	16.22	3.70	0.06	1.49	3.98	3.76	3.18	0.20	0.65	101.10
273c	66.97	0.57	16.31	3.97	0.06	1.44	4.10	3.81	3.14	0..2	0.70	101.07
273d	67.73	0.54	15.97	3.62	0.06	1.42	3.87	3.73	3.45	0.17	0.69	101.25
273e	66.80	0.58	16.34	4.25	0.07	1.68	4.23	3.86	2.96	0.20	0.65	101.62

OTHER MAJOR ELEMENTS

Boulders	SiO2 Boulders	TiO2 Boulders	Al2O3 Boulders	Fe2O3 Boulders	MnO Boulders	MgO Boulders	CaO Boulders	Na2O Boulders	K2O Boulders	P2O5 Boulders	LOI Boulders	Total Boulders
225a	75.44	0.20	13.41	1.85	0.05	0.15	1.49	4.45	3.15	0.03	0.48	100.70
225b	72.96	0.29	14.45	2.49	0.06	0.68	2.32	4.18	2.95	0.06	0.84	101.28
225c	74.28	0.21	13.61	1.94	0.05	0.44	1.29	4.09	3.79	0.03	0.59	100.32
Clasts	**Clasts**	**Clasts**	**Clasts**	**Clasts**	**Clasts**	**Clasts**	**Clasts**	**Clasts**	**Clasts**	**Clasts**	**Clasts**	**Clasts**
242b	74.95	0.18	13.04	1.13	0.02	0.55	1.46	4.01	4.00	0.03	1.51	100.88
242c	73.66	0.17	12.66	0.39	0.02	0.28	2.51	3.92	4.26	0.03	2.32	100.22
242d	73.40	0.19	12.67	1.39	0.02	0.64	2.32	3.84	4.10	0.07	2.31	100.95
242f	73.68	0.16	13.13	1.35	0.03	0.77	2.45	6.61	0.36	0.04	2.42	101.00
242g	53.84	0.55	14.25	9.80	0.18	6.00	6.02	0.98	4.25	0.08	2.83	98.78
262a	76.55	0.08	13.29	1.42	0.02	0.31	0.67	6.95	0.43	0.03	1.06	100.81
262b	77.31	0.07	13.29	1.28	0.02	0.64	0.77	6.53	0.50	0.03	1.32	101.76
262c	74.79	0.17	13.74	1.70	0.04	0.75	1.08	5.80	1.33	0.06	2.12	101.58
x69a	77.76	0.05	13.25	1.16	0.02	0.49	0.51	6.52	0.58	0.03	1.12	101.49
x69b	77.43	0.06	13.30	1.29	0.02	0.36	0.54	6.84	0.48	0.03	1.06	101.41
Schist	**Schist**	**Schist**	**Schist**	**Schist**	**Schist**	**Schist**	**Schist**	**Schist**	**Schist**	**Schist**	**Schist**	**Schist**
209a	58.93	0.84	17.91	8.30	0.10	4.45	0.89	1.33	3.51	0.11	3.33	99.70

STANDARDS MAJOR ELEMENTS

18.3.86	SiO2	TiO2	Al2O3	Fe2O3	MnO	MgO	CaO	Na2O	K2O	P2O5	LOI	Total
MONAGV-1	59.38	1.08	17.16	6.97	0.10	1.57	5.06	4.33	2.96	0.54	0.57	99.74
QAB1	47.16	1.54	15.71	12.72	0.19	7.02	10.26	2.43	0.42	0.29	1.99	99.74
20.3.87												
MONAGV-1	59.42	1.08	17.13	6.80	0.10	1.56	4.95	4.29	2.89	0.49	0.57	99.30
QAB1	46.93	1.54	15.38	12.99	0.19	6.62	10.28	2.27	0.43	0.24	1.99	98.87
9.5.88												
MONAGV-1	59.54	1.06	17.37	6.82	0.10	1.76	4.97	4.35	2.97	0.57	0.57	100.08
QAB1	46.87	1.55	15.52	13.03	0.19	6.87	10.32	2.42	0.46	0.24	1.99	99.48

VOLCANICS MAJOR ELEMENTS

	SiO2	TiO2	Al2O3	Fe2O3	MnO	MgO	CaO	Na2O	K2O	P2O5	LOI	Total
Carb lavas	**Carb lavas**	**Carb lavas**	**Carb lavas**	**Carb lavas**	**Carb lavas**	**Carb lavas**	**Carb lavas**	**Carb lavas**	**Carb lavas**	**Carb lavas**	**Carb lavas**	**Carb lavas**
G250A	66.40	0.49	15.80	5.59	0.10	2.08	2.16	2.80	2.70	0.13	2.05	100.30
G250B	70.60	0.38	14.80	3.16	0.09	0.74	2.60	3.68	2.70	0.10	1.94	100.79
G250C	53.60	1.03	18.60	9.34	0.17	3.64	7.68	2.60	1.14	0.13	2.62	100.55
G250D	59.20	1.07	17.90	7.66	0.13	2.35	6.97	2.41	1.49	0.24	1.33	100.75
G250E	71.70	0.38	15.10	3.13	0.07	0.66	2.65	3.82	2.81	0.10	0.78	101.20
G250F	58.30	0.77	17.80	8.83	0.15	3.01	6.01	2.78	0.87	0.16	1.12	99.80
G250G	60.00	0.81	16.70	7.24	0.12	3.04	6.46	2.98	1.80	0.13	1.00	100.28
G254C	45.90	1.10	22.40	10.40	0.23	4.20	8.93	2.93	0.60	0.18	2.71	99.58
G254F	54.00	0.77	15.50	6.74	0.14	3.24	7.40	2.58	2.33	0.07	7.78	100.55
G258A	78.00	0.12	12.00	1.90	0.01	0.26	0.38	1.36	6.04	0.03	0.92	101.02
Dev lavas	**Dev lavas**	**Dev lavas**	**Dev lavas**	**Dev lavas**	**Dev lavas**	**Dev lavas**	**Dev lavas**	**Dev lavas**	**Dev lavas**	**Dev lavas**	**Dev lavas**	**Dev lavas**
G253E	47.80	1.22	18.40	10.30	0.20	6.66	10.80	2.12	1.54	0.19	0.80	100.03
G253H	69.10	0.49	15.90	3.18	0.05	2.14	2.10	6.40	0.96	0.10	0.51	100.93
G253I	51.60	1.50	17.70	9.74	0.15	7.66	5.16	4.16	2.10	0.27	0.72	100.76
G253L	50.40	0.98	15.30	9.50	0.19	10.10	10.60	1.48	1.28	0.10	1.06	100.99
G253M	50.20	2.03	16.10	10.30	0.16	6.59	9.29	3.50	1.25	0.32	1.23	100.97
G253S	56.00	0.97	16.90	9.33	0.17	4.29	8.10	2.50	1.35	0.15	0.64	100.40
G253W	65.90	0.93	15.10	6.23	0.08	1.54	3.79	3.69	2.77	0.27	0.52	100.82
G255B	68.80	0.34	15.70	3.51	0.08	0.38	2.51	4.53	2.93	0.13	1.19	100.10
Dykes	**Dykes**	**Dykes**	**Dykes**	**Dykes**	**Dykes**	**Dykes**	**Dykes**	**Dykes**	**Dykes**	**Dykes**	**Dykes**	**Dykes**
G272C	44.63	1.41	17.90	12.19	0.17	8.23	12.61	1.53	0.16	0.03	0.56	99.42
G239B	62.60	0.63	16.80	6.67	0.14	1.53	4.76	4.02	1.63	0.30	1.95	101.03
G248E	60.50	1.35	16.20	7.65	0.16	2.36	5.64	3.67	1.73	0.39	0.60	100.25
G253Y	54.20	2.45	15.20	12.50	0.17	3.62	2.45	2.47	6.08	0.77	0.49	100.40
G252A	59.70	0.87	16.10	8.36	0.18	1.35	4.99	2.74	3.16	0.27	2.63	100.35
G258C	56.40	0.93	19.60	7.38	0.12	1.93	6.25	4.42	1.15	0.14	1.99	100.31
G259C	47.30	1.23	17.50	9.33	0.19	5.59	9.07	1.92	1.26	0.27	6.10	99.76

SOUTHERN REGION TRACE ELEMENTS

Xidatan	Cs Xidatan	Rb Xidatan	Sr Xidatan	Ba Xidatan	Zr Xidatan	Hf Xidatan	Nb Xidatan	Ta Xidatan	Y Xidatan	Th Xidatan	U Xidatan
206a	4.23	99.00	495.00	1023.00	253.00	6.89	18.40	0.96	14.00	19.00	4.00
206b	2.90	125.00	300.00	663.00	143.00	5.12	15.80	1.57	18.00	22.80	1.60
207		115.00	150.00	283.00	76.00		9.40		5.00	6.00	3.00
208		136.00	271.00	628.00	153.00		19.00		18.00	18.00	1.98
x67		115.00	402.00	901.00	132.00		15.50		11.00	12.00	3.00
206c	3.23	152.00	65.00	171.00	63.00	2.60	15.80	1.63	23.00	16.10	3.15
206d	2.32	155.00	62.00	193.00	65.00	2.83	14.10	1.48	17.00	15.40	2.61
206e		156.00	71.00	228.00	64.00		11.30	1.43	11.00	15.00	3.00
YNG	YNG	YNG	YNG	YNG	YNG	YNG	YNG	YNG	YNG	YNG	YNG
213a	1.84	132.00	198.00	562.00	77.00	2.68	10.90	0.99	8.00	13.00	2.33
213b		120.00	203.00	762.00	86.00		14.80		9.00	12.00	2.00
214a		114.00	511.00	744.00	201.00	5.56	14.10		10.00	12.00	1.58
214b		116.00	539.00	781.00	215.00		15.90		11.00	14.00	3.00
214c	2.00	113.00	547.00	756.00	218.00	5.67	15.50	1.24	12.00	15.00	2.01
221a		99.00	529.00	739.00	187.00		17.90		12.00	7.00	3.00
221b	2.36	82.00	649.00	904.00	233.00	5.88	21.30	1.80	17.00	10.00	1.30
221c		92.00	536.00	713.00	184.00		18.40		12.00	11.00	3.00
221d		106.00	546.00	829.00	201.00		17.00		10.00	8.00	3.00
221e		98.00	525.00	785.00	197.00		19.40		14.00	10.00	3.00
221f		93.00	577.00	930.00	194.00		14.10		10.00	7.00	3.00
221h	3.81	153.00	464.00	1285.00	311.00	9.44	21.10	0.62	15.00	14.80	1.65
221i	2.85	101.00	492.00	431.00	177.00	4.80	17.10	1.18	12.00	9.00	2.12
Naij Tal	Naij Tal	Naij Tal	Naij Tal	Naij Tal	Naij Tal	Naij Tal	Naij Tal	Naij Tal	Naij Tal	Naij Tal	Naij Tal
236a	3.04	135.00	291.00	711.00	132.00	4.09	10.90	1.14	11.00	12.00	3.00
236d	3.21	93.00	492.00	719.00	177.00	4.70	10.70	0.79	9.00	11.00	3.00
236e		119.00	327.00	842.00	140.00		9.60		9.00	12.00	3.00
236f		135.00	342.00	687.00	141.00	4.61	10.60		10.00	12.00	3.00
236g		123.00	381.00	891.00	158.00		10.90		10.00	11.00	3.00
237		103.00	535.00	817.00	222.00		10.40		12.00	13.00	3.00
WBG	WBG	WBG	WBG	WBG	WBG	WBG	WBG	WBG	WBG	WBG	WBG
222a	14.32	262.00	112.00	358.00	210.00	6.76	12.60	1.35	40.00	41.00	3.72
222b		290.00	107.00	238.00	231.00		13.80		54.00	44.00	5.00
222c		276.00	114.00	263.00	196.00	7.64	13.20		42.00	40.00	2.86
222d	18.66	301.00	114.00	340.00	180.00	5.90	11.50	1.37	35.00	34.00	3.94
222e		295.00	111.00	456.00	199.00		12.20		42.00	36.00	3.00
222f		226.00	111.00	231.00	198.00		11.30		37.00	36.00	3.00
222g	19.71	254.00	135.00	291.00	211.00	7.15	13.30	1.48	45.00	36.00	3.80
222h	19.90	329.00	90.00	364.00	376.00	11.28	34.20	2.48	121.00	10.50	3.01
232a	33.14	351.00	66.00	196.00	69.00	2.33	15.40	2.71	22.00	14.00	2.79
232b		349.00	66.00	192.00	64.00		13.70		24.00	13.00	2.40
232c		347.00	72.00	195.00	75.00		14.90		25.00	15.00	3.00

CENTRAL REGION TRACE ELEMENTS

G HYDRO Central	Cs G HYDRO Central	Rb G HYDRO Central	Sr G HYDRO Central	Ba G HYDRO Central	Zr G HYDRO Central	Hf G HYDRO Central	Nb G HYDRO Central	Ta G HYDRO Central	Y G HYDRO Central	Th G HYDRO Central	U G HYDRO Central
245a	6.19	178.00	53.00	219.00	74.00	2.96	9.00	1.47	27.00	21.00	3.00
245b	5.94	181.00	58.00	294.00	63.00	2.57	9.00	1.60	23.00	18.00	2.68
245e		177.00	111.00	665.00	95.00		8.50		21.00	19.00	6.00
245f	7.41	183.00	105.00	624.00	92.00	3.16	9.50	1.15	25.00	21.00	5.00
Pink	**Pink**	**Pink**	**Pink**	**Pink**	**Pink**	**Pink**	**Pink**	**Pink**	**Pink**	**Pink**	**Pink**
245c		175.00	52.00	228.00	72.00		8.60		28.00	21.00	3.00
244a	6.03	170.00	132.00	767.00	129.00	3.94	8.70	0.93	29.00	22.00	3.00
244b		174.00	139.00	754.00	132.00		7.90		26.00	18.00	3.00
260		137.00	180.00	700.00	167.00		11.80		26.00	23.00	3.00
261	3.10	132.00	182.00	744.00	162.00	4.99	11.00	1.12	30.00	23.00	3.00
263	6.63	200.00	92.00	555.00	117.00	3.60	7.90	0.69	24.00	28.10	3.70
264		187.00	116.00	653.00	145.00		9.70		34.00	25.00	3.00
Little	**Little**	**Little**	**Little**	**Little**	**Little**	**Little**	**Little**	**Little**	**Little**	**Little**	**Little**
248a		172.00	140.00	562.00	143.00		12.30		31.00	23.00	5.00
248b	2.45	167.00	130.00	331.00	137.00	4.23	11.40	1.10	29.00	22.00	3.13
248c	2.17	166.00	134.00	447.00	133.00	4.35	11.50	1.34	28.00	2.99	3.00
248d		158.00	141.00	295.00	137.00		10.80		28.00	21.00	3.00
Junction	**Junction**	**Junction**	**Junction**	**Junction**	**Junction**	**Junction**	**Junction**	**Junction**	**Junction**	**Junction**	**Junction**
249a		166.00	165.00	1148.00	291.00		8.60		38.00	21.00	3.00
249b	9.36	155.00	217.00	783.00	323.00	9.75	15.10	1.54	62.00	20.00	7.07
249c	3.54	137.00	159.00	542.00	309.00	8.44	12.80	0.59	45.00	14.00	2.03
249d		164.00	144.00	424.00	171.00		6.80		26.00	24.00	5.00
249e	2.84	105.00	254.00	1150.00	245.00	6.28	30.60	1.78	85.00	7.00	3.00
238	10.35	191.00	152.00	651.00	298.00	8.77	15.20	1.47	50.00	21.00	3.32

NORTHERN REGION TRACE ELEMENTS

	Cs	Rb	Sr	Ba	Zr	Hf	Nb	Ta	Y	Th	U
E Quarry	**E Quarry**	**E Quarry**	**E Quarry**	**E Quarry**	**E Quarry**	**E Quarry**	**E Quarry**	**E Quarry**	**E Quarry**	**E Quarry**	**E Quarry**
246a	1.48	61.00	519.00	695.00	119.00	4.10	10.90	0.62	12.00	3.97	0.90
246b		57.00	507.00	820.00	128.00		8.20		11.00	3.00	3.00
246c		52.00	509.00	630.00	139.00		10.40		14.00	7.00	3.00
246d		58.00	563.00	551.00	133.00		11.30		10.00	5.00	3.00
246e	1.24	78.00	504.00	1135.00	123.00	3.54	11.20	0.67	11.00	7.00	1.15
246f	1.27	23.00	463.00	392.00	78.00	2.37	8.60	0.55	23.00	3.00	3.00
246g		51.00	154.00	202.00	36.00		5.10		3.00	10.00	2.00
DYH	**DYH**	**DYH**	**DYH**	**DYH**	**DYH**	**DYH**	**DYH**	**DYH**	**DYH**	**DYH**	**DYH**
266a	3.10	102.00	245.00	575.00	136.00	4.84	7.90	0.58	15.00	20.00	4.00
266b	2.28	85.00	227.00	584.00	116.00	4.10	6.40	0.39	9.00	10.00	3.00
266c		94.00	228.00	539.00	128.00		5.30		13.00	20.00	3.00
266d		99.00	233.00	600.00	115.00		6.60		12.00	13.00	3.00
266e		82.00	218.00	505.00	97.00		6.10		13.00	11.00	3.00
G East	**G East**	**G East**	**G East**	**G East**	**G East**	**G East**	**G East**	**G East**	**G East**	**G East**	**G East**
273a		104.00	504.00	826.00	163.00		10.30		15.00	11.00	3.00
273b		112.00	491.00	911.00	160.00		7.60		9.00	10.00	3.00
273c	1.81	114.00	500.00	895.00	162.00	4.64	9.80	0.82	12.00	12.00	4.00
273d		115.00	487.00	1005.00	155.00		10.00		13.00	12.00	4.00
273e		108.00	484.00	813.00	173.00		8.70		11.00	9.00	3.00

OTHER TRACE ELEMENTS

Boulders	Cs Boulders	Rb Boulders	Sr Boulders	Ba Boulders	Zr Boulders	Hf Boulders	Nb Boulders	Ta Boulders	Y Boulders	Th Boulders	U Boulders
225a		128.00	106.00	504.00	128.00		9.20		30.00	16.00	2.00
225b	2.56	123.00	192.00	421.00	123.00	3.87	10.20	0.99	17.00	16.00	1.52
225c		164.00	111.00	775.00	121.00		11.40		30.00	17.00	3.00
Clasts	**Clasts**	**Clasts**	**Clasts**	**Clasts**	**Clasts**	**Clasts**	**Clasts**	**Clasts**	**Clasts**	**Clasts**	**Clasts**
242b		70.00	193.00	1035.00	106.00		5.70		13.00	27.00	3.00
242c	0.98	84.00	250.00	2372.00	96.00	2.31	5.10	0.36	13.00	25.00	2.47
242d		70.00	191.00	1057.00	89.00		4.20		13.00	14.00	2.00
242f		13.00	134.00	235.00	97.00		7.20		18.00	28.00	2.00
242g	3.12	148.00	275.00	2614.00	42.00	1.37	2.50		17.00	3.00	0.72
262a	4.00	40.00	59.00	473.00	122.00	6.64	27.60	2.12	54.00	37.00	5.29
262b		44.00	83.00	788.00	110.00		28.50		89.00	32.00	3.00
262c	9.65	109.00	131.00	423.00	143.00	5.42	22.00	4.32	31.00	26.00	3.19
x69a		39.00	91.00	315.00	104.00		25.90		87.00	30.00	3.00
x69b	3.53	35.00	93.00	435.00	97.00	5.71	25.80	3.00	76.00	27.00	3.60
Schist		**Schist**	**Schist**	**Schist**	**Schist**	**Schist**	**Schist**	**Schist**	**Schist**	**Schist**	**Schist**
209a	5.70	147.00	83.00	493.00	162.00	4.17	15.80	1.28	36.00	16.00	3.37

STANDARDS TRACE ELEMENTS

5.2.86	Cs	Rb	Sr	Ba	Zr	Hf	Nb	Ta	Y	Th	U
MONGSP-1	2.90*	253.00	234.00	1328.00	498.00	26.60*	24.20	7.30*	26.00	107.00	4.81*
G-2	2.86*	169.00	480.00	1896.00	303.00	26.61*	11.30	7.01*	10.00	27.00	4.70*
17.2.87											
MONGSP-1	2.90*	254.00	232.00	1254.00	492.00	26.60*	24.00	7.30*	29.00	102.00	4.81*
G-2	1.21^	171.00	476.00	1725.00	301.00	4.73^	12.20	1.42^	13.00	27.00	0.79^
15.2.88											
MONGSP-1	2.86*	255.00	233.00	1204.00	487.00	26.34*	23.70	6.70*	28.00	103.00	4.62*
G-2	0.95^	170.00	482.00	1801.00	297.00	4.74^	11.80	1.30^	12.00	26.00	

* = INAA analysis - Ailsa Craig

^ = INAA analysis - Whin Sill

VOLCANICS TRACE ELEMENTS

	Cs	Rb	Sr	Ba	Zr	Hf	Nb	Ta	Y	Th	U
Carb lavas	**Carb lavas**	**Carb lavas**	**Carb lavas**	**Carb lavas**	**Carb lavas**	**Carb lavas**	**Carb lavas**	**Carb lavas**	**Carb lavas**	**Carb lavas**	**Carb lavas**
G250A		122.00	232.00	846.00	250.00	6.77	12.70	1.07	35.00	15.65	3.45
G250B		108.00	262.00	588.00	146.00		8.90		18.00	15.00	3.00
G250C		68.60	262.00	441.00	197.00	4.93	9.80	0.82	36.00	8.32	2.33
G250D		70.00	291.00	547.00	143.00		8.50		26.00	5.00	3.00
G250E		110.00	218.00	508.00	156.00		8.60		18.00	16.00	3.00
G250F		38.44	215.00	664.00	147.00	3.86	7.20	0.62	36.00	10.05	3.25
G250G		76.00	238.00	622.00	162.00		7.70		30.00	11.00	3.00
G254C		26.00	341.00	359.00	172.00		8.20		41.00	5.00	3.00
G254F		114.00	205.00	687.00	218.00		12.10		46.00	13.00	5.00
G258A		218.00	84.00	388.00	128.00		8.60		28.00	26.00	4.00
Dev lavas	**Dev lavas**	**Dev lavas**	**Dev lavas**	**Dev lavas**	**Dev lavas**	**Dev lavas**	**Dev lavas**	**Dev lavas**	**Dev lavas**	**Dev lavas**	**Dev lavas**
G253E		126.00	359.00	387.00	103.00		6.80		25.00	3.00	4.00
G253H		37.36	314.00	280.00	155.00	3.93	3.30	0.29	12.00	3.15	0.94
G253I		163.80	279.00	363.00	217.00	4.92	5.70	0.46	36.00	1.98	4.00
G253L		72.00	211.00	356.00	88.00		6.60		22.00	2.00	3.00
G253M		59.00	349.00	609.00	213.00		9.20		43.00	3.00	3.00
G253S		66.00	208.00	382.00	138.00		7.70		31.00	6.00	3.00
G253W		145.00	141.00	314.00	327.00		10.80		41.00	7.00	3.00
G255B		136.30	225.00	727.00	329.00	8.93	10.80	1.03	33.00	16.60	4.18
Dykes	**Dykes**	**Dykes**	**Dykes**	**Dykes**	**Dykes**	**Dykes**	**Dykes**	**Dykes**	**Dykes**	**Dykes**	**Dykes**
G272C		3.00	295.00	356.00	33.00		3.80		17.00	2.00	3.00
G239B		100.00	413.00	302.00	179.00		9.50		25.00	2.00	4.00
G248E		67.00	353.00	365.00	209.00		9.40		35.00	5.00	3.00
G253Y		243.70	182.00	898.00	1564.00	26.67	15.10	1.27	76.00	11.78	3.15
G252A		180.00	284.00	571.00	237.00		13.30		46.00	13.00	4.00
G258C		34.00	394.00	638.00	150.00		7.60		29.00	4.00	3.00
G259C		88.00	443.00	391.00	123.00		6.60		22.00	3.00	4.00

SOUTHERN REGION REE ELEMENTS

Xidatan	La Xidatan	Ce Xidatan	Nd Xidatan	Sm Xidatan	Eu Xidatan	Tb Xidatan	Tm Xidatan	Yb Xidatan	Lu Xidatan
206a	79.30	154.00	47.58	7.08	1.67	0.75	0.26	1.19	0.21
206b	59.70	114.00	40.30	6.60	1.14	0.81		1.44	0.25
207									
208	46.70	79.80	35.75	4.77	1.02	0.50		1.55	0.22
x67			19.60	2.95					
206c	13.10	28.20	11.41	3.02	0.40	0.68		1.98	0.25
206d	13.50	29.00	11.23	2.80	0.40	0.56		1.65	0.25
206e	16.60	28.90	13.50	3.36	0.41	0.65		2.27	0.34
YNG	YNG	YNG	YNG	YNG	YNG	YNG	YNG	YNG	YNG
213a	17.10	30.41	16.14	3.01	0.56	0.30		0.61	0.11
213b									
214a	70.20	88.40	39.00	5.27	1.26	0.51		0.83	0.10
214b									
214c	58.40	107.90	38.60	5.66	1.26	0.54		1.00	0.17
221a	57.30	78.00	31.40	5.34	1.01	0.36		0.90	0.13
221b	36.90	74.50	33.70	5.80	1.60	0.70		1.20	0.18
221c									
221d									
221e									
221f									
221h	49.10	89.96	33.81	5.10	1.08	0.49	0.15	1.27	0.21
221i	34.50	61.65	26.55	4.11	1.06	0.40	0.33	1.07	0.15
Naij Tal	Naij Tal	Naij Tal	Naij Tal	Naij Tal	Naij Tal	Naij Tal	Naij Tal	Naij Tal	Naij Tal
236a	32.40	56.70	19.70	3.40	0.74	0.49		0.91	0.13
236d	42.10	73.30	26.00	4.22	1.10	0.44		0.71	0.10
236e			20.04	3.44					
236f	36.00	46.40	25.40	3.28	0.86	0.30		1.01	0.10
236g									
237									
WBG	WBG	WBG	WBG	WBG	WBG	WBG	WBG	WBG	WBG
222a	55.45	114.50	44.46	9.33	1.05	1.37	0.46	3.36	0.56
222b									
222c	59.60	104.00	52.90	8.84	1.09	1.07		4.73	0.70
222d	46.22	90.34	31.06	6.23	1.04	1.08	0.35	2.88	0.50
222e									
222f									
222g	53.98	109.50	44.48	9.04	1.24	1.24	0.57	3.81	0.68
222h	23.08	66.88	60.50	18.70	1.05	3.42	1.36	9.31	1.46
232a	17.91	36.93	18.21	4.29	0.52	0.63		1.23	0.21
232b									
232c									

CENTRAL REGION REE ELEMENTS

G HYDRO Central	La G HYDRO Central	Ce G HYDRO Central	Nd G HYDRO Central	Sm G HYDRO Central	Eu G HYDRO Central	Tb G HYDRO Central	Tm G HYDRO Central	Yb G HYDRO Central	Lu G HYDRO Central
245a	19.07	39.86	14.11	3.52	0.29	0.79		2.68	0.43
245b	19.40	36.30	13.40	3.10	0.32	0.66		2.58	0.36
245e									
245f	27.38	53.74	18.09	3.99	0.47	0.79	0.40	2.58	0.43
Pink	**Pink**	**Pink**	**Pink**	**Pink**	**Pink**	**Pink**	**Pink**	**Pink**	**Pink**
245c			12.02	2.72					
244a	29.40	62.11	21.60	3.90	0.70	0.84	0.45	2.66	0.43
244b									
260									
261	34.60	72.00	25.70	5.20	0.84	0.96	0.46	3.09	0.48
263	31.90	63.30	21.40	4.37	0.54	0.75		2.31	0.38
264	36.30	48.70	31.50	4.46	0.62	0.64		3.14	0.46
Little	**Little**	**Little**	**Little**	**Little**	**Little**	**Little**	**Little**	**Little**	**Little**
248a									
248b	34.50	57.52	23.43	5.24	0.62	0.75	0.42	2.57	0.44
248c	29.50	49.39	21.37	4.98	0.63	0.74	0.43	2.68	0.47
248d									
Junction	**Junction**	**Junction**	**Junction**	**Junction**	**Junction**	**Junction**	**Junction**	**Junction**	**Junction**
249a									
249b	39.38	83.27	47.35	12.03	1.60	1.85	0.84	6.80	1.14
249c	38.16	75.85	37.99	6.85	1.28	1.18	0.39	3.93	0.73
249d	103.00	146.00	62.50	9.00	1.65	1.00		3.90	0.61
249e	44.49	112.80	61.78	15.05	2.38	2.46	0.97	7.26	1.18
238	38.30	77.49	33.15	7.15	1.24	1.23	0.59	4.71	0.83

NORTHERN REGION REE ELEMENTS

	La	Ce	Nd	Sm	Eu	Tb	Tm	Yb	Lu
E Quarry	**E Quarry**	**E Quarry**	**E Quarry**	**E Quarry**	**E Quarry**	**E Quarry**	**E Quarry**	**E Quarry**	**E Quarry**
246a	12.46	25.90	14.44	2.72	1.01	0.39		0.79	0.13
246b									
246c									
246d									
246e	38.92	68.26	26.13	3.86	1.03	0.43	0.21	0.89	0.13
246f	16.41	35.84	22.60	4.32	1.67	0.75	0.26	2.05	0.34
246g									
DYH	**DYH**	**DYH**	**DYH**	**DYH**	**DYH**	**DYH**	**DYH**	**DYH**	**DYH**
266a	43.51	94.60	34.84	5.52	0.90	0.68	0.20	1.32	0.20
266b	31.52	69.13	24.28	3.76	0.91	0.40	0.12	0.80	0.13
266c			25.76	5.00					
266d									
266e			29.00	4.90					
G East	**G East**	**G East**	**G East**	**G East**	**G East**	**G East**	**G East**	**G East**	**G East**
273a									
273b									
273c	30.46	63.66	26.07	3.85	1.02	0.52		1.13	0.18
273d				4.26					
273e				3.79					

OTHER REE ELEMENTS

Boulders	La Boulders	Ce Boulders	Nd Boulders	Sm Boulders	Eu Boulders	Tb Boulders	Tm Boulders	Yb Boulders	Lu Boulders
225a									
225b	27.20	46.59	18.90	2.96	0.61	0.51	0.29	1.78	0.35
225c									
Clasts	Clasts	Clasts	Clasts	Clasts	Clasts	Clasts	Clasts	Clasts	Clasts
242b									
242c	43.56	67.58	18.34	2.69	0.51	0.42		1.73	0.30
242d									
242f									
242g	6.10	11.46	4.54	1.45	0.62	0.43		1.65	0.30
262a	14.94	37.37	21.37	7.55	0.22	1.42	0.75	5.46	1.07
262b									
262c	28.68	61.87	26.67	6.13	0.53	1.10	0.26	2.72	0.46
x69a			12.95	4.63					
x69b	11.54	29.01	16.99	6.21	0.47	1.85	1.04	6.30	0.99
Schist	Schist	Schist	Schist	Schist	Schist	Schist	Schist	Schist	Schist
209a	39.69	81.86	38.10	7.33	1.40	1.09	0.56	3.23	0.56

STANDARDS REE ELEMENTS

16.6.86	La	Ce	Nd	Sm	Eu	Tb	Tm	Yb	Lu
Ailsa Craig	60.00	161.00	95.10	25.40	2.02	4.90	2.80	17.50	2.67
Ailsa Craig	59.18	160.80	95.20	25.12	1.97	4.93	2.78	17.39	2.67
14.1.87									
Ailsa Craig	60.00	161.00	95.10	25.40	2.02	4.90	2.80	17.50	2.67
Whin Sill	25.13	57.79	33.52	7.51	2.27	1.15	0.25	2.63	0.41
15.4.88									
Ailsa Craig	60.08	152.60	93.90	25.40	2.00	4.91	2.52	16.33	2.50
Whin Sill	25.24	58.67	33.89	7.24	2.30	1.21	0.46	2.42	0.37

VOLCANICS REE ELEMENTS

	La	Ce	Nd	Sm	Eu	Tb	Tm	Yb	Lu
Carb lavas	**Carb lavas**	**Carb lavas**	**Carb lavas**	**Carb lavas**	**Carb lavas**	**Carb lavas**	**Carb lavas**	**Carb lavas**	**Carb lavas**
G250A	38.40	78.60	35.80	7.90	1.50	1.02	0.50	3.65	0.56
G250B									
G250C	23.03	50.53	26.45	6.44	1.56	1.06	0.33	3.60	0.55
G250D									
G250E									
G250F	20.83	43.03	25.06	6.09	1.26	0.96	0.29	3.55	0.54
G250G									
G254C									
G254F									
G258A									
Dev lavas	**Dev lavas**	**Dev lavas**	**Dev lavas**	**Dev lavas**	**Dev lavas**	**Dev lavas**	**Dev lavas**	**Dev lavas**	**Dev lavas**
G253E									
G253H	12.77	28.54	15.33	3.20	0.88	2.46	0.46	1.09	0.16
G253I	12.16	30.58	19.88	5.16	1.59	3.83	0.99	3.45	0.53
G253L									
G253M									
G253S									
G253W									
G255B	32.66	63.57	26.95	5.40	1.57	8.18	0.88	3.34	0.54
Dykes	**Dykes**	**Dykes**	**Dykes**	**Dykes**	**Dykes**	**Dykes**	**Dykes**	**Dykes**	**Dykes**
272c									
G239B									
G248E									
G253Y	38.33	86.67	51.16	12.04	4.75	2.14	0.62	7.48	1.22
G252A									
G258C									
G259C									

SOUTHERN REGION ISOTOPE DATA

Sample	Age	87Sr/86Sr	+/-	87Rb/86Sr	ΣSr	143/144Nd	+/-	Sm	Nd	147Sm/144Nd	Σ Nd	TDM (Ma)
Xidatan	(2 sigma errors)											
206a		.709893	3	0.58	54.82	.512305	1	7.10	47.58	.090	-3.96	921
206b	190 ± 7	.711853	4	1.22	58.19	.512286	1	6.60	40.30	.099	-4.55	1016
207	(w.r. 7 pts)	.714235	3	2.23	53.44							
208	MSWD 3	.712335	3	1.45	56.22	.512301	1					
x67	Sr(i) .70837 ± 7	.727762	5	0.81	299.67	.512320	4	2.95	19.60	.091	-3.69	914
206c		.726254	2	6.78	50.49	.512386	2	3.00	11.41	.160	-4.08	1880
206d		.727472	4	7.25	49.88	.512399	2	2.80	11.23	.151	-3.60	1586
206e		.725920	3	6.38	61.07			3.36	13.50			
Yie Nin Gou												
213a		.712518	5	1.93	39.09	.512496	2	*2.77	15.00	.111	-0.71	820
214c	187 ± 21	.709060	4	0.60	41.82	.512402	2	*5.67	38.58	.088	-1.97	790
221b	(w.r. 6 pts)	.708290	3	0.37	39.85	.512420	2	*5.8	33.70	.100	-1.91	847
221f	MSWD 48	.708753	3	0.46	42.91							
221h	Sr(i) .70734 ± 8	.709727	3	0.95	37.65	.512419	2	4.42	30.54	.087	-1.61	763
221i		.709034	2	0.60	41.45	.512472	2	*4.11	26.55	.090	-0.65	718
Naij Tal												
236a	178 ± 10	.713329	4	1.33	71.52			*3.40	19.70	.100		
236d	(w.r.) 4 pts	.711335	3	0.55	74.90	.512314	1	4.22	26.00	.098	-3.85	1020
236e	MSWD 4	.712520	3	1.04	71.87	.512327	1	3.44	20.04	.104	-3.74	970
236f	Sr(i) .70987 ± 7	.713235	3	1.13	78.46			3.28	25.40			
236g		.712240	3	0.93	72.34							
Wanbaogou												
222a		.750788	4	6.80	127.60			*9.33	44.46			
222b		.756146	4	7.88	118.95							
222c		.752098	4	7.03	128.16							
222d	388 ± 10	.755592	5	7.56	136.19	.512201	2	6.23	31.06	.121	-4.83	1394
222e	(w.r. 8 pts)	.757196	3	7.73	145.63							
222f	MSWD 0.9	.745654	3	5.93	122.95							
222g	Sr(i) .71300 ± 52	.742977	2	5.23	139.86	.512181	2	*9.04	44.48	.123	-5.32	1450
222h		.771679	2	10.63	123.77	.512480	2	18.47	57.37	.187	-2.66	3620
232a		.820012	3	15.51	427.23	.512211	3	4.29	18.21	.143	-5.69	1791
232b		.822157	2	15.45	462.40							
232c		.817643	3	14.04	508.92	.512205	4					

CENTRAL REGION ISOTOPE DATA

Sample	Age	87Sr/86Sr	+/-	87Rb/86Sr	ΣSr	143/144Nd	+/-	Sm	Nd	147Sm/144Nd	Σ Nd	TDM (Ma)
Golmud Hydro Group												
Central Granite												
245a	248 ± 3	.744335	2	9.73	64.69	.512311	7	3.07	12.90	.144	-4.71	1610
245b	(w.r. 4 pts)	.741951	4	9.06	65.97							
245e	MSWD 0.7	.726267	6	4.61	72.52							
245f	Sr(i) .71009 ± 13	.727903	5	5.04	73.60	.512390	3	2.60	12.72	.120	-2.38	1100
Pink Granite												
245c	254 ± 2	.745803	3	9.76	84.60	.512304	4	2.72	12.02	.137	-4.61	1470
244a	(w.r. 6 pts)	.723880	5	3.71	86.48	.512238	2	*3.90	21.60	.109	-5.02	1180
244b	MSWD 0.6	.723774	48	3.71	84.97							
260e	Sr(i) .71050 ± 8	.718490	3	2.21	86.61							
261b		.718621	4	2.08	95.12	.512384	1	*5.20	25.70	.122	-2.59	1100
263	(256 ± 6)	.733204	3	6.30	86.52			*4.37	21.40			
264a	(MSWD 8 on both)	.727216	3	4.67	84.79			4.46	31.50			
Little Granite												
248a	261 ± 56	.722808	2	3.57								
248b	w.r. 4 pts	.723609	2	3.71	77.35	.512301	2	*5.24	22.20	.143	-4.82	1600
248c	MSWD 2	.723088	4	3.60	75.78	.512271	2	*4.98	20.00	.151	-5.70	1900
248d	Sr(i) .70974 ± 140	.721852	3	3.25								
Golmud Junction												
249a	217 ± 20	.721803	7	2.93	118.19							
249b	(w.r. 6pts)	.719040	4	2.06	117.08			*11.1	43.70			
249c	MSWD 38	.719742	3	2.49	107.99	.512300	4	*6.85	37.99	.109	-4.21	1090
249d	Sr(i) .71233 ± 31	.722670	3	3.31	113.98			9.00	62.50			
249e		.715986	2	1.19	111.84	.512314	1	*15.05	61.78	.150	-5.07	1650
238		.723809	4	3.65	114.90			*7.15	33.15			

NORTHERN REGION ISOTOPE DATA

Sample	Age	87Sr/86Sr	+/-	87Rb/86Sr	ΣSr	143/144Nd	+/-	Sm	Nd	147Sm/144Nd	Σ Nd	TDM (Ma)
East Quarry												
246a		.712943	4	0.12	115.18	.512244	2	*2.71	14.80	.111	-4.91	1200
246b	258 ± 3	.712628	3	0.11	111.23							
246c	biotite age	.712840	3	0.10	114.76	.512208	2					
246d	Sr(i) .71242	.712865	2	0.10	115.12							
246e		.712951	3	0.15	113.73	.512181	3	*3.86	24.20	.096	-5.64	1125
246f		.711030	2	0.05	91.67	.512314	2	4.35	18.77	.140	-4.50	1460
Duo Ya He												
266a	382 ± 160	.717309	4	1.22	90.79	.512083	1	5.50	34.84	.096	-5.95	1250
266b	(w.r. 5 pts)	.716661	4	1.07	93.18							
266c	MSWD 11	.717484	3	1.19	95.60	.512146	1	*3.76	24.28	.095		1160
266d	Sr(i) .71078 ± 134	.717279	4	1.22	90.37							
266e		.716822	3	1.10	93.15	.512147	2	4.90	29.00	.102	-5.01	1230
Golmud E												
273a		.711678	4	0.60	73.52							
273b	240 ± 6	.711913	3	0.66	73.95							
273c	(zircon)	.711846	3	0.68	72.03	.512285	1	3.80	26.07	.089	-3.64	940
273d	Sr(i) .7096	.711736	11	0.66	71.44	.512201	1	4.26				
273e		.711825	4	0.69	71.25	.512283	3	3.79				

OTHER ISOTOPE DATA

Sample	Age	87Sr/86Sr	+/-	87Rb/86Sr	ΣSr	143/144Nd	+/-	Sm	Nd	147Sm/144Nd	Σ Nd	TDM (Ma)
Clasts												
242c		.710904	5	0.97		.512361	2	*2.67	18.34	.088		815
242d		.711416	2	1.07		.512381	2					
262a		.739703	10	1.97		.512341	3	*7.55	21.37	.213		
262b		.740127	2	1.54		.512247	5					
262c		.745661	3	2.41		.512282	3					
x69a		.737101	4	1.24		.512234	6	4.63	12.95	.216		
Boulders	267 ± 30											
225a	(w.r. 3 pts)	.721188	3	2.53								
225b	MSWD 22	.715334	10	1.85	55.76	.512341	2	*2.96	18.90	.095	-2.36	910
225c	Sr(i) .70823 ± 67	.725041	3	4.35	58.73	.512296	2					
Schist												
209a		.742395	2	1.77		.511932	6	*7.33	38.1	.116		1740
Diorites												
272b		.712015	2	0.03		.512444	3	*1.29	4.68	.160		2000
Dykes												
272c		.710972	6	0.01								

* analysed by INAA

VOLCANICS ISOTOPE DATA

Lithology	Age	87Sr/86Sr	+/-	87Rb/86Sr	ΣSr	143/144Nd	+/-	Sm	Nd	147Sm/144Nd	ΣNd	TDM (Ma)
Carb volcs												
250a	400 Ma	.717098	3	1.52	59.95	.512232	2	7.90	35.80	.133	-4.71	1546
250b	(assumed)	.714810	2	0.41		.512270	2					
250c		.713046	1	0.71	67.96	.512302	1	6.10	25.10	.147	-4.06	1700
250d		.711516	1	0.24								
250e		.715556	2	0.50								
250f		.708865	2	0.50	25.59	.512448	2	6.40	26.50	.146	-1.16	1345
250g		.710290	1	0.32		.512434	2					
258a		.734532	2	2.60		.512270	6					
Dev volcs												
253h		.709379	2	0.31	48.20	.512513	2	3.10	15.30	.123	1.29	899
253i		.715059	2	1.65	20.47	.512754	1	5.10	19.90	.155	4.36	775
255b		.717570	2	0.60		.512179	2					
Dyke												
253y		.726661	2	3.63	25.03	.512413	1	12.00	51.20	.142	-1.64	1341

KUNLUN BATHOLITH NORMATIVE DATA

Modal wt %	Quartz	Orthoclase	Albite	Anorthite	Hornblende	Biotite	Muscovite	Magnetite	Haematite	Ilmenite	Apatite
Xidatan	Xidatan	Xidatan	Xidatan	Xidatan	Xidatan	Xidatan	Xidatan	Xidatan	Xidatan	Xidatan	Xidatan
206a	35.40	25.40	29.20	4.40	0.00	2.20	3.20	0.00	0.10	0.00	0.10
206b	30.00	16.60	32.40	11.80	0.00	8.40	0.00	0.00	0.30	0.10	0.30
207	31.50	27.60	29.30	6.60	0.00	3.30	1.30	0.00	0.20	0.10	0.20
208	31.00	18.50	32.30	8.90	0.00	7.30	1.20	0.00	0.30	0.10	0.40
x67	23.80	14.20	35.50	15.50	0.00	10.00	0.00	0.40	0.00	0.00	0.50
206c	34.60	26.20	30.10	4.00	0.00	2.20	2.60	0.00	0.10	0.00	0.20
206d	35.20	26.50	30.50	3.90	0.00	2.20	1.50	0.00	0.10	0.00	0.20
206e	33.30	27.30	32.60	4.10	0.00	1.00	0.00	0.00	0.10	1.50	0.10
Yie in Gou	Yie in Gou	Yie in Gou	Yie in Gou	Yie in Gou	Yie in Gou	Yie in Gou	Yie in Gou	Yie in Gou	Yie in Gou	Yie in Gou	Yie in Gou
213a	31.90	23.70	35.70	5.90	0.00	2.50	0.10	0.00	0.20	0.00	0.10
213b	24.80	0.00	25.50	4.30	0.00	28.20	0.00	17.10	0.00	0.00	0.10
214a	29.90	15.00	34.40	12.50	0.00	7.50	0.00	0.00	0.30	0.30	0.20
214b	21.40	17.40	42.00	10.20	4.30	3.80	0.00	0.00	0.20	0.40	0.30
214c	25.90	14.00	38.30	12.20	0.00	8.60	0.00	0.00	0.30	0.20	0.40
221a	24.40	11.20	38.60	14.90	0.00	9.90	0.00	0.00	0.30	0.20	0.50
221b	24.30	5.40	38.90	17.70	0.00	12.50	0.00	0.00	0.40	0.30	0.60
221c	26.00	9.60	38.80	15.50	0.00	9.30	0.00	0.00	0.30	0.20	0.40
221d	24.90	12.50	40.00	13.10	0.00	8.60	0.00	0.00	0.30	0.20	0.40
221e	25.40	11.20	38.20	14.30	0.00	9.80	0.00	0.00	0.40	0.30	0.50
221f	23.80	12.60	39.30	14.50	0.00	8.90	0.00	0.00	0.30	0.20	0.40
221h (enclave)	16.60	11.60	31.10	12.00	6.00	20.30	0.00	1.20	0.00	0.10	1.10
221i	25.90	10.10	38.60	14.60	0.00	9.80	0.00	0.00	0.30	0.20	0.40
Naij Tal	Naij Tal	Naij Tal	Naij Tal	Naij Tal	Naij Tal	Naij Tal	Naij Tal	Naij Tal	Naij Tal	Naij Tal	Naij Tal
236a	32.60	16.30	33.40	11.10	0.00	6.20	0.00	0.10	0.10	0.10	0.20
236d	26.30	10.20	36.40	16.00	1.40	8.80	0.00	0.20	0.10	0.20	0.50
236e	29.10	17.40	34.30	11.60	0.20	6.80	0.00	0.20	0.10	0.10	0.30
236f	26.60	17.70	36.80	11.70	0.00	6.60	0.00	0.00	0.20	0.10	0.30
236g	25.70	15.60	38.00	12.80	0.00	7.40	0.00	0.10	0.10	0.10	0.30
237	30.50	15.60	32.20	11.80	0.00	8.90	0.30	0.10	0.20	0.10	0.30
Wanbaogou	Wanbaogou	Wanbaogou	Wanbaogou	Wanbaogou	Wanbaogou	Wanbaogou	Wanbaogou	Wanbaogou	Wanbaogou	Wanbaogou	Wanbaogou
222a	29.70	21.00	31.60	8.80	0.70	7.30	0.00	0.00	0.50	0.20	0.10
222c	30.00	21.10	31.20	9.30	0.00	7.40	0.00	0.00	0.50	0.10	0.30
222d	28.00	24.20	31.80	8.70	0.00	6.60	0.00	0.00	0.40	0.10	0.10
222e	30.90	23.50	28.80	8.00	0.00	7.60	0.30	0.00	0.50	0.10	0.20
222f	35.50	17.10	29.30	10.20	0.00	7.20	0.00	0.00	0.50	0.20	0.10
222g	26.10	22.70	32.10	9.60	0.00	8.50	0.00	0.00	0.60	0.20	0.20
222h (enclave)	3.90	8.60	44.50	7.00	17.80	13.20	0.00	0.00	1.70	1.20	2.10
232a	32.20	22.80	31.70	2.90	0.00	2.90	6.80	0.00	0.20	0.00	0.40
232b	31.80	23.80	32.00	2.90	0.00	2.90	6.00	0.00	0.20	0.00	0.30
232c	32.50	22.60	30.80	3.30	0.00	3.10	7.10	0.00	0.20	0.00	0.30

KUNLUN BATHOLITH NORMATIVE DATA

Modal wt %	Quartz	Orthoclase	Albite	Anorthite	Hornblende	Biotite	Muscovite	Magnetite	Haematite	Ilmenite	Apatite
Gol Hydro	Gol Hydro	Gol Hydro	Gol Hydro	Gol Hydro	Gol Hydro	Gol Hydro	Gol Hydro	Gol Hydro	Gol Hydro	Gol Hydro	Gol Hydro
245a	34.50	25.00	32.60	3.90	0.00	2.90	0.80	0.00	0.20	0.00	0.10
245b	35.70	23.50	30.10	3.60	0.00	3.10	3.50	0.00	0.20	0.00	0.20
245c	35.00	23.80	32.60	3.80	0.00	2.90	1.60	0.00	0.20	0.00	0.10
245e	34.10	22.60	33.20	5.80	0.00	3.90	0.00	0.00	0.30	0.00	0.10
245f	31.10	22.50	34.90	5.60	0.10	4.00	0.00	0.00	0.30	1.40	0.10
244a	32.30	19.40	33.00	8.30	0.00	6.40	0.00	0.00	0.40	0.00	0.20
244b	32.90	19.30	32.30	8.40	0.00	6.60	0.00	0.00	0.40	0.00	0.10
260	32.90	14.10	30.80	11.70	0.00	9.80	0.00	0.00	0.50	0.00	0.20
261	31.00	12.30	34.80	11.40	0.00	9.80	0.00	0.00	0.50	0.00	0.20
263	31.70	24.80	31.70	6.50	0.00	4.80	0.00	0.00	0.40	0.00	0.10
264	31.40	20.80	33.10	7.90	0.00	6.20	0.00	0.00	0.40	0.00	0.10
248a	29.80	22.90	32.20	8.60	0.00	6.00	0.00	0.00	0.40	0.00	0.10
248b	33.10	22.30	30.80	7.70	0.00	5.50	0.00	0.00	0.40	0.00	0.20
248c	28.70	20.30	32.20	9.60	0.30	8.00	0.00	0.00	0.60	0.00	0.20
248d	29.90	22.90	33.10	7.90	0.00	5.60	0.00	0.00	0.40	0.00	0.10
Gol Junction	Gol Junction	Gol Junction	Gol Junction	Gol Junction	Gol Junction	Gol Junction	Gol Junction	Gol Junction	Gol Junction	Gol Junction	Gol Junction
249a	23.30	25.10	37.20	5.90	7.60	0.00	0.00	0.00	0.40	0.30	0.10
249b	22.50	20.90	33.70	12.20	7.00	2.70	0.00	0.00	0.50	0.50	0.10
249c	25.90	19.20	36.40	10.10	0.00	7.70	0.00	0.00	0.60	0.00	0.10
249d	32.30	21.90	33.30	8.40	0.00	3.70	0.00	0.00	0.30	0.00	0.10
249e	11.60	13.20	36.10	11.90	22.80	1.80	0.00	0.00	0.80	1.10	0.50
238	26.70	19.30	36.30	9.40	0.00	7.70	0.00	0.00	0.60	0.00	0.10

KUNLUN BATHOLITH NORMATIVE DATA

Modal wt %	Quartz	Orthoclase	Albite	Anorthite	Hornblende	Biotite	Muscovite	Magnetite	Haematite	Ilmenite	Apatite
East Quarry	East Quarry	East Quarry	East Quarry	East Quarry	East Quarry	East Quarry	East Quarry	East Quarry	East Quarry	East Quarry	East Quarry
246a	30.70	1.70	37.50	18.90	0.00	10.20	0.00	0.00	0.50	0.00	0.40
246b	29.70	9.00	28.90	18.50	4.20	8.70	0.00	0.00	0.40	0.40	0.20
246c	27.50	4.40	30.40	20.40	4.20	12.00	0.00	0.20	0.40	0.20	0.40
246d	28.70	3.60	31.50	21.20	0.00	14.10	0.00	0.20	0.30	0.10	0.30
246e	25.90	11.90	32.60	16.30	4.10	8.20	0.00	0.00	0.30	0.40	0.30
246f (enclave)	8.10	3.00	27.80	21.20	33.50	3.40	0.00	1.20	0.00	1.10	0.70
246g (pegmatite)	28.50	17.10	45.00	7.20	2.00	0.00	0.00	0.00	0.10	0.00	0.10
Duo Ya He	Duo Ya He	Duo Ya He	Duo Ya He	Duo Ya He	Duo Ya He	Duo Ya He	Duo Ya He	Duo Ya He	Duo Ya He	Duo Ya He	Duo Ya He
266a	35.70	9.80	31.90	13.50	0.00	7.90	0.50	0.00	0.30	0.10	0.30
266b	35.40	13.20	34.50	11.20	1.60	3.60	0.00	0.00	0.20	0.10	0.10
266c	37.90	12.10	30.90	12.00	0.00	5.80	0.90	0.00	0.20	0.00	0.20
266d	36.50	10.30	34.80	12.50	0.00	5.10	0.40	0.00	0.20	0.00	0.10
266e	35.10	11.70	32.80	12.80	0.00	7.10	0.00	0.00	0.20	0.10	0.20
Golmud E	Golmud E	Golmud E	Golmud E	Golmud E	Golmud E	Golmud E	Golmud E	Golmud E	Golmud E	Golmud E	Golmud E
273a	25.90	8.50	31.30	19.60	0.00	13.60	0.00	0.20	0.30	0.10	0.50
273b	25.30	11.60	31.60	17.80	1.00	11.80	0.00	0.20	0.20	0.10	0.50
273c	23.60	13.60	31.80	17.20	4.90	8.20	0.00	0.00	0.40	0.30	0.00
273d	24.70	14.80	31.20	16.00	3.20	9.20	0.00	0.00	0.30	0.30	0.40
273e	24.20	10.10	32.20	17.90	2.50	11.90	0.00	0.20	0.30	0.10	0.50
Clasts	Clasts	Clasts	Clasts	Clasts	Clasts	Clasts	Clasts	Clasts	Clasts	Clasts	Clasts
242b	33.30	22.90	33.90	5.30	2.80	1.50	0.00	0.00	0.00	0.20	0.10
242c	29.60	25.50	33.60	4.40	0.00	0.00	0.00	0.00	0.10	0.30	0.10
242d	30.70	24.50	32.60	4.40	3.60	0.00	0.00	0.00	0.20	0.30	0.20
242f	28.80	2.20	56.40	4.30	3.40	0.00	0.00	0.00	0.20	0.20	0.10
242g	18.50	9.60	7.00	19.30	16.50	25.90	0.00	3.00	0.00	0.00	0.20
262a	33.30	0.20	59.10	3.10	0.00	4.00	0.00	0.00	0.20	0.00	0.10
262b	35.40	0.00	54.60	3.60	0.00	3.20	1.30	2.00	0.00	0.00	0.10
262c	34.20	3.30	49.70	5.00	0.00	6.20	1.20	0.10	0.10	0.00	0.10
x69a	35.20	0.60	53.20	2.30	0.00	0.00	3.90	4.60	0.00	0.10	0.10
x69b	33.60	1.10	56.10	2.40	0.00	0.00	2.30	4.30	0.00	0.10	0.10
Boulders	Boulders	Boulders	Boulders	Boulders	Boulders	Boulders	Boulders	Boulders	Boulders	Boulders	Boulders
225a	34.30	16.10	37.60	7.20	0.00	4.30	0.00	0.00	0.30	0.10	0.10
225b	32.60	13.00	35.40	11.10	0.00	7.50	0.00	0.00	0.30	0.00	0.10
225c	33.60	19.30	34.90	6.30	0.00	5.60	0.00	0.00	0.30	0.00	0.10